ResearchOnline@JCU

JAMES COOK UNIVERSITY AUSTRALIA

This file is part of the following work:

Bruce, Matthew Donald (2007) ***The development and 3D geometry of porphyroblast inclusion trails: significance for the tectonic evolution of the Lebanon Antiformal Syncline, New Hampshire.*** **PhD Thesis, James Cook University.**

Access to this file is available from:

https://doi.org/10.25903/a0r6%2Dvt43

Copyright © 2007 Matthew Donald Bruce

The author has certified to JCU that they have made a reasonable effort to gain permission and acknowledge the owners of any third party copyright material included in this document. If you believe that this is not the case, please email researchonline@jcu.edu.au

The development and 3D geometry of porphyroblast inclusion trails: significance for the tectonic evolution of the Lebanon Antiformal Syncline, New Hampshire

Volume I: Text

Thesis submitted by
Matthew Donald Bruce BSc (Hons)
in July, 2007

for the degree of Doctor of Philosophy
in the School of Earth and Environmental Sciences

James Cook University

STATEMENT OF ACCESS

I, the undersigned, author of this work, understand the James Cook University will make this thesis available for use within the University Library and, via the Australian Digital Thesis network, for use elsewhere.

I understand that, as an unpublished work, a thesis has significant protection under the Copyright Act and I do not wish to place further restriction on access to this work.

_____ _____

Matthew Donald Bruce Date

STATEMENT OF SOURCES

I declare that this thesis is my own work and has not been submitted in any other form for another degree or diploma at any university or other institution of tertiary education. Information derived from published or unpublished work of others has been acknowledged in the text and a list of references is given.

_____ _____

Matthew Donald Bruce Date

Statement on the Contribution of others

Tim Bell developed the technique central to this study. He initiated the project, spent long hours working with me on a dual headed microscope and edited all drafts. Funding for fieldwork and analysis was provided from an ARC Large grant to Tim Bell and a JCU Doctoral Merit Research Scheme grant to Matt Bruce. Stipend support was received from a JCU School of Earth Sciences Scholarship and a JCU Postgraduate Research Scholarship.

Tim Bell is co-author of Sections 2 & 3 and these have been published as papers in the Journal of Structural Geology. Domingo Aerden and Kyuichi Kanagawa provided critical reviews of Section 1 which greatly improved the manuscript. James Lally collected samples TC1365 and TC1365i (Section 2) and brought them to our attention.

Electronic Copy

I, the undersigned, the author of this work, declare that the electronic copy of this thesis provided to the James Cook University Library is an accurate copy of the print thesis submitted, within the limits of the technology available.

_____ _____

Matthew Donald Bruce Date

Acknowledgements

Firstly, I must say a massive thank you to Tim Bell for inviting me to come to Townsville and for all the support during the preparation of this thesis. I've really enjoyed the opportunity to work here in the glorious tropical Queensland climate and to be a part of the SAMRI team. Tim, your boundless energy, unbridled enthusiasm and wicked sense of humour is truly inspirational.

Thanks to all the members of SAMRI, past and present. Special thanks to Afroz, Al, Asghar, Benny, Cam, Chris, Clement, Ioan, Mark, Musti, Sayab and Shyam. I feel privileged to have worked with so many truly excellent people. Thank you all for your friendship, support and for many absorbing discussions. Thanks also to Mike Rubenach for your metamorphic insights and for helping to keep Tim under control.

The task of grinding hundreds of thin sections was made slightly less painful by Darren Richardson's cheerful nature and his ability to keep the petrographic facilities at JCU ticking over. Thanks to the girls in the office for astounding feats of organisation and for the positive way in which they approach every challenge.

I would like to thank the people of Farmington and Rochester and especially Dottie Bean and Freddi Olson for their hospitality during my time in New Hampshire. The assistance of Wally Bothner in allowing me to use the rock saws and storage at the University of New Hampshire is greatly appreciated.

To my Mum and Dad, thanks for your encouragement, support and the copious amounts of newspaper clippings from home. Thank you to my terrific little blokes, Trev and Lachie for making every day fun and for making me laugh when I need it most. Finally, to my wonderful wife, Ann. Thank you for your love, support and for the truest of friendships.

Table of Contents, Volume I

Statement of Access	i
Statement of Sources	ii
Statement of the Contribution of Others	iii
Statement on Electronic Copy	iv
Acknowledgements	v
Table of Contents, Volume I	vi
Table of Contents, Volume II	ix
Introduction and Thesis Outline	x

Section A. Movement directions in porphyroblastic rocks: Evaluation of the "FitPitch" and the "asymmetry" methods.

	Abstract	A-1
1	Introduction	A-1
2	FIA determination	A-4
	2.1 Asymmetry method	A-4
	2.2 The "FitPitch" computer program	A-5
3	Examples from the Lebanon Antiformal Syncline, New Hampshire	A-5
	3.1 Geological setting	A-5
	3.1.1 Tectonic framework	A-5
	3.1.2 The Lebanon Antiformal Syncline	A-6
	3.2 Methodology	A-7
	3.3 Results	A-8
	3.3.1 Sample MB019	A-9
	3.3.2 Sample MB030	A-10
	3.3.3 Sample MB028	A-12
4	Discussion and conclusions	A-13
	4.1 Asymmetry vs. FitPitch	A-13
	4.2 Matrix lineations	A-14
	4.3 Shear sense	A-15
	4.4 Independent tests	A-16
	References	A-17

Section B. The internal inclusion trail geometries preserved within a first phase of porphyroblast growth

	Abstract	B-1
1	Introduction	B-1
2	FIA trend variation within samples from the Tommy Creek Block	B-3
	2.1 The samples	B-3
	2.2 Timing of porphyroblast growth and FIA trend	B-3
	2.3 Interpretation	B-4
3	Inclusion trail geometries in 3-D	B-6
	3.1 Establishing a model porphyroblast	B-7
	3.2 Slicing the model	B-8
	3.3 The cut effect	B-9
	3.4 Variation in FIA trend through the model	B-10
4	Discussion	B-11
	4.1 The early growth of porphyroblasts relative to deformation	B-11
	4.2 Porphyroblast nucleation and initial growth	B-12
	4.3 Significance of foliation curvature towards the vertical or horizontal	B-13
	4.4 Curvature of the intersection or inflexion axis within a porphyroblast	B-14
	4.5 Apparent spiral shaped inclusion trails due to section orientation	B-14
	4.6 Geometry of foliation development against a porphyroblast	B-15
	4.7 The asymmetry method versus the cut effect	B-15
	4.8 Consistency of FIA trends	B-16
	References	B-17

Section C. Progressive deformation partitioning and deformation history: Evidence from millipede structures

	Abstract	C-1
1	Introduction	C-1
2	Deformation history	C-3
	2.1 The non-uniqueness of most structures	C-3

2.2 Are millipede geometries a unique indicator of deformation history? C-4

3 Examples of very coaxial geometries C-5

3.1 Millipede generating fold hinge C-5

3.2 Millipede shaped inclusion trails in porphyroblasts C-7

3.2.1 Interpretation of trend of L^3_3 C-8

3.3 A model millipede C-9

4 Interpretation and discussion C-10

4.1 Deformation history versus geometry C-10

4.2 The progressive development of the fold C-11

4.3 The progressive development of deformation partitioning C-12

4.3.1 Reactivation weakening in fold hinges C-13

4.3.2 Reactivation weakening - a mechanism for crenulation cleavage development and switching off porphyroblast growth C-14

4.4 Millipedes in 3D C-16

4.5 Cut effect millipede-like structures C-16

4.6 Transection of sheath fold hinges C-17

5 Conclusions C-18

References C-19

Section D. Timing nappe development in multiply tectonised rocks: A new approach

Abstract D-1

1 Introduction D-1

2 Geologic setting D-3

2.1 Tectonic framework D-3

2.2 Stratigraphy D-4

2.3 Structure and metamorphism D-4

3 Description of samples D-6

4 Inclusion trail morphology D-6

4.1 Sigmoidal and staircase inclusion trails D-6

4.2 Differentiated crenulation cleavages D-7

5 Methods D-8

5.1 FIA determination D-8
5.1.1 Asymmetry method D-8
5.1.2 The "FitPitch" computer program D-9
5.2 Relative timing criteria and FIA succession D-9
6 Results D-9
6.1 FIA data D-9
6.2 Relative timing of FIAs D-11
6.3 FIA sets D-11
6.4 Asymmetry of inclusion trails D-12
7 Interpretation D-13
7.1 Structural and metamorphic relationships D-13
7.2 Significance of FIA data D-16
7.3 Inclusion trail asymmetry and development of the Lebanon Antiformal Syncline D-16
8 The significance of gravity in orogenesis D-21
9 Discussion and conclusions D-22
References D-24

Conclusions xiv

Table of Contents, Volume II

Table of contents		i
List of tables		ii
List of figures		iii
Section A.	Movement directions in porphyroblastic rocks: Evaluation of the "FitPitch" and the "asymmetry" methods.	A-1
Section B.	The internal inclusion trail geometries preserved within a first phase of porphyroblast growth	B-1
Section C.	Progressive deformation partitioning and deformation history: Evidence from millipede structures	C-1
Section D.	Timing nappe development in multiply tectonised rocks: A new approach	D-1
Appendix A:	FitPitch data	vii
Appendix B:	Sample localities and mineralogical data	xvii
Appendix C:	JCU collection numbers	xx
Appendix D:	Structure and stratigraphy of the Lebanon Antiformal Syncline, New Hampshire, USA	Map
Appendix E:	Electronic supplements	CD
	E01-asymmetry method.mov	
	E02-vertical sigmoid slice 090.mov	
	E03-vertical sigmoid rotate.mov	
	E04-vertical sigmoid slice 000.mov	
	E05-vertical sigmoid slice 010.mov	
	E06-vertical sigmoid slice 030.mov	
	E07-horizontal millipede slice.mov	
	E08-vertical millipede slice 120.mov	
	E09-vertical millipede rotate slice.mov	
	E10-millipede.zip	
	E11-vertical spiral rotate.mov	
	E12-vertical spiral slice 000.mov	
	E13-vertical spiral slice 010.mov	
	E14-vertical spiral slice 030.mov	
	E15-vertical spiral slice 090.mov	

Introduction and Thesis Outline

This thesis investigates the processes of deformation and porphyroblast growth during orogenesis. The primary focus of the thesis is on the development of the New England Appalachian Orogen, USA but some spectacular examples of structures preserved within porphyroblasts from the Tommy Creek Block, Mount Isa Province and the Robertson River metamorphics of Queensland, Australia are also examined. The thesis consists of four sections, each intended for publication in international journals. Sections B and C have already been published in the Journal of Structural Geology (Bell and Bruce, 2006; 2007). The first section (Section A) compares and contrasts two methods for determining the orientation of foliation intersection/inflection axes preserved in porphyroblasts (FIAs). Sections B and C examine the 3-dimensional geometry of structures preserved within porphyroblasts as inclusion trails and their interpretation. Section D is a detailed FIA study, using the orientation and geometry of porphyroblast inclusion trails to determine the timing and mechanism of emplacement of the Blue Hills Nappe and subsequent development of the Lebanon Antiformal Syncline, New Hampshire, USA. This is part of a larger research project in the Appalachians undertaken by the Structural and Metamorphism Research Institute (SAMRI) at James Cook University. Volume I of the thesis contains the text and references, and Volume II contains figures, tables and appendices.

Porphyroblasts provide a unique opportunity to examine the small-scale geometries that form as deformation commences and begins to partition through the rock because these large crystals nucleate and/or grow at this time (Spiess and Bell, 1996). As they grow, porphyroblasts trap and preserve microstructures that are destroyed in the matrix by the same event or during subsequent deformation (e.g., Bell and Johnson, 1989; Bell and Newman, 2006). Examining the geometry of inclusion trails in porphyroblasts and their relationship to the surrounding matrix provides important information on the processes occurring early in the local deformation history of multiply deformed metamorphic terrains and reveals a tectonic record that is commonly more complete than that preserved in the matrix (e.g., Cihan and Parsons, 2005, Rich, 2006).

Section A

Two methods of measuring FIAs are compared and contrasted. FIAs have most commonly been measured using multiple vertical thin sections with different strikes to determine the switch in inclusion trail curvature asymmetry that takes place across the FIA trend. The "FitPitch" computer program is an alternative method to determine FIA orientation via the measurement of apparent dips of foliations defined by inclusion trails from a variety of thin section orientations. The results obtained from both methods are contrasted while the strengths and weaknesses of each approach are highlighted and discussed.

Section B

The geometry of inclusion trails contained within a first phase of porphyroblast growth are compared to those preserved by subsequent porphyroblast enlargement. The variation in inclusion trail geometry and FIA trend within different porphyroblastic phases in the same rock layer, as well as within the same phase in different layers, from two adjacent samples from one outcrop is examined to explore the effect that pre-existing porphyroblasts have on the strain field. A thin section is statistically unlikely to perfectly bisect an individual porphyroblast. The influence this cut-effect has on the geometry of the inclusion trails recorded on a thin section and on the asymmetry method of FIA determination is explored via 3-D computer analysis of sigmoidal inclusion trails obtained from X-ray computed tomography (X-ray CT) of a single garnet porphyroblast. The significance and implications of these phenomena for structural geologists and metamorphic petrologists working with porphyroblastic rocks is discussed.

Section C

Most structures can be produced through different deformation history paths. In particular, structures that result from some form of inhomogeneous shortening can also be produced by some combination of shearing plus rotation of the whole geometry or through overprinting by shearing in another direction. "Millipede" structures (oppositely concave microfolds) preserved in porphyroblasts are interpreted to indicate a deformation history of bulk

inhomogeneous shortening (Bell, 1981). However, Johnson & Bell (1996) suggest that such structures may not be unique because similar geometries have been produced experimentally during modelling of progressive simple shear (Ghosh, 1975). Natural and experimentally derived geometries are re-examined in this section.

Section D

Foliation intersection/inflection axes preserved as inclusion trails in porphyroblasts (FIAs) from the Lebanon Antiformal Syncline of SE New Hampshire, USA, are examined in an attempt to document changes in bulk shortening geometry associated with emplacement and refolding of a large-scale recumbent fold (the Blue Hills Nappe). Overprinting criteria plus inclusion trail composition, texture and orientation are used to establish a paragenesis of FIA trends that developed during Acadian orogenesis. Metamorphic phase relations and pseudosections are used to examine the P-T conditions during deformation and FIA development. Analysis of asymmetries recorded by the inclusion trails is used to determine the dominant sense of shear operating during nappe emplacement that resulted in inversion of the stratigraphic sequence and during refolding of the overturned limb of the nappe to form the Lebanon Antiformal Syncline.

References

Bell, T.H., 1981. Foliation development: the contribution, geometry and significance of progressive bulk inhomogeneous shortening. *Tectonophysics* **75**, 273-296.

Bell, T.H. and Bruce, M.D., 2006. The internal inclusion trail geometries preserved within a first phase of porphyroblast growth. *Journal of Structural Geology* **28**, 236-252.

Bell, T.H. and Bruce, M. D., 2007. Progressive deformation partitioning and deformation history: Evidence from millipede structures. *Journal of Structural Geology* **29**, 18-35.

Bell, T.H. and Johnson, S.E., 1989. Porphyroblast inclusion trails: the key to orogenesis. *Journal of Metamorphic Geology* **7**, 279-310.

Bell, T.H. and Newman, R., 2006. Appalachian orogenesis: the role of repeated gravitational collapse. In Styles of continental compression, R. Butler and S. Mazzoli, (eds.) *Special Papers of the Geological Society of America* **414**, 95-118.

Cihan, M. and Parsons, A., 2005. The use of porphyroblasts to resolve the history of macro-scale structures: an example from the Robertson River Metamorphics, North-Eastern Australia. *Journal of Structural Geology* **27**, 1027-1045.

Ghosh, S.K., 1975. Distortion of planar structures around rigid spherical bodies. *Tectonophysics* **28**, 185-208.

Johnson, S.E. and Bell, T.H., 1996. How useful are "millipede" and other similar porphyroblast microstructures for determining syn-metamorphic deformation histories. *Journal of Metamorphic Geology* **14**, 15-28.

Rich, B.H., 2006. Permian bulk shortening in the Narragansett Basin of southeastern New England, USA. *Journal of Structural Geology* **28**, 682-694.

Spiess, R. and Bell, T.H., 1996. Microstructural controls on sites of metamorphic reaction: a case study of the inter-relationship between deformation and metamorphism. *European Journal of Mineralogy* **8**, 165-186.

Section A:

Movement directions in porphyroblastic rocks:

Evaluation of the "FitPitch" and

the "asymmetry" methods

Abstract

Using mineral elongation lineations for determining movement directions in porphyroblastic rocks is problematic because they are routinely subjected to reorientation due to reactivation of compositional layering during subsequent deformation events. Foliation inflexion or intersection axes preserved within porphyroblasts (FIAs) have been shown by numerous studies to be a consistent and reliable indicator of movement direction in metamorphic terrains that have experienced multiple episodes of bulk shortening. Furthermore, they appear to form orthogonal to the direction of relative plate motion. FIAs have most commonly been measured using multiple vertical thin sections with different strikes to determine the switch in inclusion trail curvature asymmetry that takes place across the FIA trend. An alternative method uses the "FitPitch" computer program to determine FIAs via the measurement of apparent dips of foliations defined by inclusion trails from a variety of thin section orientations. The results obtained from both methods are contrasted while the strengths and weaknesses of each approach are highlighted and discussed. "FitPitch" works best where the inclusion trails are predominately straight, whereas the "asymmetry" method requires that they display some degree of curvature. The two techniques compliment each other by permitting FIAs to be obtained from a larger proportion of samples and they can also be used as independent tests in samples that are suitable for both methods. The sense of shear operating during progressive bulk shortening is indicated by inclusion trail curvature recorded in thin sections cut at a high angle to the FIA. Unlike the "asymmetry" method, "FitPitch" does not give the shear sense directly but can be used to establish the most suitably oriented thin section in which to look for inclusion trail curvature.

Keywords: FitPitch; Porphyroblasts; Inclusion Trails; Lineations

1. Introduction

Linear indicators of movement direction combined with shear sense indicators are important tools used to decipher the kinematics of deformation during orogenesis (e.g., Hobbs *et al.*, 1976). Until recently, relatively little attention has been paid to such structures preserved in

porphyroblasts, or their significance for relative plate motion. This occurred because matrix linear indicators of movement direction in shear zones and thrusts of equivalent age conflict with the direction of relative plate motion determined from magnetic anomaly maps of the sea floor. Platt *et al*. (1989) demonstrated that there appears to be no direct relationship between directions of relative plate motion and linear indicators of movement direction such as stretching lineations, fibres and striations on fault planes, for the Alps. However, the orientation of foliation intersection or inflection axes preserved as inclusion trails in porphyroblasts (FIAs) from the same area have been demonstrated (Bell *et al*., 1995; Bell & Wang, 1999) to reflect successive changes in the direction of bulk shortening associated with relative motion between the African and European plates.

The determination of shear sense along foliations in deformed and metamorphosed rocks is an important part of structural analysis that provides constraints on kinematic and metamorphic paths, during orogenesis. The use of porphyroblasts as shear sense indicators is commonly regarded as controversial because the interpreted movement direction differs depending on whether the porphyroblast is regarded as having rotated or not relative to fixed geographical coordinates during deformation of the surrounding rock mass and the perception that they are re-oriented by younger folding events (e.g., Rosenfeld, 1968; 1970; Vissers & Mancktelow, 1992; Johnson, 1999). In the rotational model, the curved inclusion trails are interpreted as the result of rotation during porphyroblast growth, with respect to a foliation that is parallel to the plane of shear during simple shear or non-coaxial flow (e.g., Rosenfeld, 1970; Schoneveld, 1977; Passchier *et al*., 1992; Williams & Jiang, 1999). Conversely, the non-rotational model involves rotation of the matrix foliation about the growing porphyroblast during multiple foliation-forming events (Ramsay, 1962; Bell *et al*., 1992; Stallard & Hickey, 2001). How inclusion trails are interpreted in micro-structural studies is largely dependant on which of these contradictory models is favoured. If the porphyroblasts were to experience significant rotation and/or translation during deformation, as suggested by the rotation model, their usefulness as kinematic indicators is reduced to near zero. In this case, rotation would be expected to be non-systematic and would result in a wide range of FIA orientations, particularly for those structures that formed early in the tectonic history and had experienced multiple phases of ductile deformation. It has

been suggested (Bell & Johnson, 1990; 1992) that the correct shear sense can generally be inferred if the porphyroblasts did not rotate during growth. Such lack of rotation is supported by a large amount of quantitative data (e.g., Bell & Hickey, 1997; Mares, 1998; Bell *et al*., 1998; 2003; 2004; 2005; Stallard & Hickey, 2001; Bell and Welch, 2002; Ham and Bell, 2004; Bell and Newman, 2006) and can be demonstrated where the distribution of early FIA trends retains a non-random clustering in porphyroblastic metamorphic rocks that have undergone multiple phases of tectonism and porphyroblast growth (Bell & Newman, 2006).

Bell & Johnson (1992) point out that since deformation partitioning controls the development of new foliations in part by rotation of older ones, the geometry developed must reflect the strain field. Therefore, to determine the local shear sense for a particular deformation event, one needs only to distinguish the curvature of an earlier formed foliation into a later one (from zones of low strain to zones of high strain). The curvature of early foliations preserved as inclusion trails in porphyroblasts or in strain shadows of relatively large heterogeneities in the rock allow the determination of local shear senses for early generations of foliations and can potentially reveal a kinematic history much more extensive than that preserved in the matrix.

The analysis and interpretation of FIAs is based on the premise that useful structural information, which may have been obliterated from the matrix during prograde metamorphism and matrix coarsening processes can be preserved by inclusion trails in a wide variety of porphyroblastic mineral phases. Measurement and analysis of FIA orientations (e.g., Hayward, 1990; Bell & Hickey, 1997; Bell *et al*., 2003; 2004; 2005) has lead to the development of a quantitative approach to understanding and integrating structural and metamorphic processes occurring during orogenesis. Provided that no rotation of the porphyroblasts takes place during subsequent ductile deformation events, the orientation of these FIAs and the geometry of the inclusion trails can be used to quantify such processes as the direction of bulk transport and dominant sense of shear during orogenesis (Bell *et al.*, 1998), timing and mechanisms of folding (Bell *et al.*, 2003; 2004) and foliation development during changing metamorphic conditions (Reinhardt & Rubenach, 1989; Williams, 1994).

Figure 1(a) shows a representation of the three-dimensional shape of a doubly-curving foliation surface from a porphyroblast with "simple" sigmoidal inclusion trails. This geometry is described in Johnson (1993) and has been illustrated using high-resolution X-ray computed tomography in the 3-D reconstruction of individual garnet porphyroblasts (e.g., Huddlestone-Holmes & Ketcham, 2005; Bell & Bruce, 2006; thesis Section B). The FIA is the axis of curvature or apparent relative rotation between porphyroblast and matrix. Alternatively, a FIA may be considered to be the intersection between two foliations preserved within a porphyroblast (Fig. 1b).

This paper examines two techniques of FIA determination that may be used to routinely measure these structures. The well established technique developed by Hayward (1990) and Bell *et al*. (1995) requires that inclusion trails be curved and asymmetrical. A new technique, 'FitPitch' (Aerden, 2003), which allows determination of FIA orientations in porphyroblastic rocks previously considered unsuitable for FIA studies, is examined and results compared for samples to which both techniques can be applied.

2. FIA determination

2.1 Asymmetry Method

The trend of the FIA is ascertained by cutting a series of vertical thin-sections with different strikes and examining the geometry of the foliations (S_i) preserved within the porphyroblasts (Hayward, 1990; Bell *et al*., 1995; Bell *et al*., 1998). The FIA is marked by the flip in inclusion trail geometry from "S" to "Z" shape between two closely oriented thin-sections laying either side of the axis (Fig. 2, see also Appendix E: "E01-asymmetry method.mov" for a QuickTime movie that illustrates the basic principles of the asymmetry method). After examining an initial set of six vertical sections oriented at 30^0 intervals (i.e., strikes of 0, 30, 60, 90, 120 and 150 degrees), two additional sections are prepared in order to refine the estimation of the FIA. In the example shown in Figure 2, the flip in asymmetry is seen to occur between 90^0 and 120^0 so two additional sections with strikes of 100^0 and 110^0 are prepared and examined. The flip in

asymmetry is narrowed down to somewhere between 110^0 and 120^0 with the mid-point being recorded as the trend of the FIA (Bell *et al*., 1998). This approach works well where the curvature of the inclusion trails can be easily seen but fails where the inclusions are predominately straight or inconsistent.

2.2 The 'FitPitch' computer program

The 'FitPitch' computer program allows the characterisation of preferred orientations of planar microstructures in a rock from the pitches of their intersection-lines on different sections (Aerden, 2003). A uniformly-dipping plane can be uniquely identified by the pitches (or apparent dips) of this plane measured in several sections of different orientation.

FitPitch takes measured pitch or strike angles of inclusion trails in a set of differently orientated thin sections and compares them to the theoretical intersection lines of one, two or three model planes on the same sections. The best solution is considered to be the one which minimises the deviation between the data and the model planes. The intersection of the best-fit model planes are FIAs. A detailed discussion of the program principles can be found in Aerden (2003).

3. Examples from the Lebanon Antiformal Syncline, New Hampshire

3.1 Geological setting

3.1.1 Tectonic framework

The Appalachians extend for over 3000 km along the east coast of the North American continent from Alabama in the south to Newfoundland in easternmost Canada. Several major periods of orogenesis have been suggested to account for the development of this mountain chain (e.g., Hatcher, 1981; Robinson, 1983). These consist of the Ordovician Taconic, the late

Devonian Acadian and the Carboniferous to Permian Alleghanian events. However, in some sections of the belt, only one or two of these periods of orogenesis are evident.

Eastern New England, including the area which is the subject of this study, is dominated by Acadian age (~423-355 Ma; Eusden *et al*., 2000; Bell & Welch, 2002) structures and metamorphism. The Acadian orogen is thought to be the result of the final closure of the Iapetus Ocean (proto-Atlantic) and the docking of Avalonia and Baltica (ancestral Europe) with Laurentia (Kent & Keppie, 1988) to form Euramerica. The final phase of orogenesis involved a rotation of Gondwana with respect to the Euramerican landmass, culminating in the late Carboniferous/Permian Alleghanian orogeny and resulted in the assembly of the super continent, Pangea (Kent & Keppie, 1988). Rifting and separation of the continents to form the modern Atlantic Ocean commenced at approximately 200Ma.

3.1.2 The Lebanon Antiformal Syncline

The Central Maine Terrane (Fig. 3) is interpreted as a large Silurian to early Devonian depositional basin extending from Connecticut to Maine and bounded by the Bronson Hill Anticlinorium to the west and the Nonesuch River fault zone to the east. The meta-turbidite sequence represents an eastward thickening continental margin deposit that appears to have been deposited before an advancing tectonic front (Osberg, 1988; Bradley *et al*., 1998). The study area (Fig. 4, Appendix D) is centred on the Lebanon Antiformal Syncline on the eastern edge of the Central Maine Terrane. Billings (1956) mapped all the metasedimentary rocks of the Central Maine Terrane as lower Devonian Littleton Formation. Eusden *et al*. (1987) subdivided the sequence observed around the Lebanon Antiformal Syncline into five units and correlated these with the Silurian Rangeley, Perry Mountain, Smalls Falls and Madrid Formations and the Devonian Littleton or Carrabassett Formation in west-central Maine.

The rocks of the Lebanon Antiformal Syncline are located on the overturned limb of a major recumbent fold (Fig. 4), the Blue Hills Nappe (F_1 of Eusden *et al*., 1987). This limb is refolded by tight to open, south-east-verging folds with generally shallow, north-east- or south-

west-plunging axes. These later generation folds (F_2) have a distinctive, spaced axial planar differentiated crenulation cleavage and are seen to fold both S_0 and S_1. The F_2 folds are considered the principal cause of the observed outcrop pattern and the general north-west dip of both S_0 and S_1. F_3 folds are represented by the broad scale change in trend of the F_2 fold axes from E-W in the south-west of the mapped area to nearly N-S in the north-east (Eusden *et al*., 1987; thesis Section D).

3.2 Methodology

The asymmetry method (Hayward, 1990; Bell *et al*., 1995; Bell *et al*., 1998) requires that at least six vertical thin-sections be prepared for each sample. Additional thin-sections are cut in order to refine the orientation of the FIA to within 10°. Horizontal sections were also examined in an endeavour to better understand the three dimensional nature of the microstructures preserved within the porphyroblasts. These same sections were used for analysis with the 'FitPitch' computer program. Samples were divided into those suitable for analysis using the asymmetry approach (i.e., those with clear asymmetric curvature of the inclusion trails), those suitable only for use with 'FitPitch' (i.e., having relatively straight inclusion trails) and samples which could be used with both techniques (i.e., possessing either inclusion trails which are straight with clear curvature at their extremities or a mixture of asymmetrically curved and relatively straight trails).

Measurements were made of all angles between relatively straight inclusion trails in these sections and the thin-section edge, using a rotating stage microscope, and converted to true pitch (vertical sections) or strike angles (horizontal sections), following the procedure of Aerden (2003). Thin-sections were examined by scanning along parallel bands under the microscope and measuring the orientation of inclusion trails in every new porphyroblast that appeared in the field of view. Inclusion trails which lacked straight segments were ignored. 'FitPitch' produces solutions involving one, two or three model planes. It is up to the user to decide which (if any) of these solutions best describes the data and what is observed in the sample.

As discussed in Aerden (2003), the quality of each possible solution can be evaluated by calculating the average deviation between measured and model intersection lines (α_d). This is just the sum of deviations of all data from their nearest model intersection lines divided by the total number of data. The choice of which solution best fits the data can also be based on the relationship between best-fit lines calculated for individual thin sections and best-fit model intersection lines based on all data. One, two or three best-fit lines are calculated for the data of each individual thin-section. The parameter α_m is the average deviation between these lines and the model intersection lines.

A three plane solution will always yield smaller average deviations than a two or one plane solution so the average deviations must be normalised to uniform data to remove the bias towards multiple plane models. This is accomplished by calculating the above parameters for uniform data to give α_u. Two new parameters can be considered:

$$R_d = \alpha_u/\alpha_d$$

provides a measure of the quality or 'tightness' of a best-fit solution and

$$R_m = \alpha_u/\alpha_m$$

gives a measure of the degree of internal consistency of the data set. Both these quantities are calculated by FitPitch and presented in the output of the program. The solution that best fits the data will be the one with the highest R_d and R_m values.

3.3 Results

Three samples, taken from the Perry Mountain Formation, have been selected to demonstrate how 'FitPitch' can be used to compliment the traditional asymmetry method of FIA determination. The Perry Mountain Formation is a well-bedded, meta-turbidite containing abundant garnet porphyroblasts and characterised by stringers or pods of pink garnet and quartz

"coticule" (Thomson, 1992; 2001) parallel to bedding, near the base of many of the metasandstone layers. These three samples are part of a larger data set that is presented in thesis Section D. The accumulated pitch and strike data for each sample was analysed with "FitPitch' and results obtained for one, two and three model plane solutions. These results are presented in Table 1. The pitch measurements from all samples treated with FitPitch are presented in Appendix A. A discussion of three representative samples and implications of the results are presented below.

3.3.1 Sample MB019

MB019 contains abundant small (1-2 mm) garnet porphyroblasts. One horizontal and nine vertical thin-sections prepared from this sample were examined, using both the asymmetry and FitPitch techniques. The pitch data is presented in Figure 5a on a lower-hemisphere equal area stereonet (the data is contoured to emphasize any broad trends) and as an individual rose diagram for each thin-section. The results obtained from FitPitch (Table 1 and Fig. 5b) show that a single plane cannot adequately describe the data and should be rejected in favour of either a two or three model plane solution. In this case a three plane solution is preferred, not just because it has high R_d and R_m values (the two plane solution has a slightly higher R_m value), but also because it best describes what is actually observed in the thin-sections. Many of the garnet porphyroblasts beautifully preserve an early differentiated crenulation cleavage (Fig. 6) which pre-dates the growth of garnet. This structure is similar to that illustrated if Figure 1b. Because this cleavage formed before it was overgrown by garnet, it is called a pseudo-FIA (pFIA). In addition to the two early foliations, most of the garnet porphyroblasts display a clear core and rim texture. The core contains the differentiated crenulation while the rim trails are sub-parallel to the matrix foliation. This is illustrated in a photomicrograph and interpretive sketch of a porphyroblast from the 090^0 section of sample MB019 (Fig. 6a). The data points allocated to each model plane by FitPitch are given different symbols and plotted on an equal area lower hemisphere stereonet along with the three planes (Fig. 6b) and the rose diagram which corresponds to the 090^0 section. The three modal orientation maxima observed in the rose diagram of measured pitch data closely match those that would be expected in the intersection of the vertical thin-section (dashed line)

with the three model planes calculated by FitPitch and also the three different foliations shown in the photomicrograph of the porphyroblast (Fig. 6a).

Three model planes result in three possible FIA (since there are three ways in which three planes can intersect). The orientations of these calculated FIA are presented in Table 2 along with the trends of the FIA established using the asymmetry method. FitPitch calculates both a trend and a plunge for the FIA whereas only a trend has been established using the asymmetry method (it is possible to determine the plunge of the FIA using this approach but this requires that many more thin-sections be prepared and since most FIAs are shallowly plunging, this is not usually done). Both techniques yield remarkably similar results. However, the FIA which results from the curvature of the rim trails into the matrix (established using the asymmetry method) is not accounted for using FitPitch as no measurements of the matrix foliation were used in the calculations. Similarly, FitPitch provides the orientation of a FIA that was never actually observed in the sample (i.e., the lineation formed by the intersection of the earliest core foliation trails and the rim trails). These two FIA orientations are marked with asterisks in Table 2.

3.3.2 Sample MB030

Sample MB030 contains numerous small (mm scale) porphyroblasts, many of which display prominent rims, resulting in a distinctive core and rim texture. The cores have fine, relatively straight inclusion trails, surrounded by an inclusion-free median. The rims have coarser inclusions trails that are straight to gently curving and sub-parallel to the dominant matrix foliation. One horizontal and nine vertical thin-sections of sample MB030 were examined, using both FitPitch and the asymmetry method. Pitch data is presented in Figure 7(a) on a lower-hemisphere equal area stereonet and as an individual rose diagram for each thin-section. A two plane solution emerges as the best candidate when the data is analysed with FitPitch (Table 1 and Fig. 7b) and the results compared with observations.

Figure 8 shows photomicrographs and interpretive sketches of porphyroblasts from the 030^0 and 100^0 sections of sample MB030 along with an equal area lower hemisphere stereonet

plot of pitch measurements and rose diagrams of measured data for the same sections. The intersections between the two vertical thin-sections (dashed lines on stereonet) with the two model planes calculated by FitPitch closely mirror the data presented in the corresponding rose diagrams and what is observed in the thin-sections. The two model planes are close together where they intersect the 030^0 section on the stereonet. This is reflected in the rose diagram, where only one broad modal peak is observed in the data, and in the 030^0 photomicrograph, where the inclusion trails of both the core and rim are very nearly parallel. By contrast, the 100^0 section intersects the model planes on opposite sides of the stereonet, the rose diagram displays two definite modal peaks and the core and rim inclusion trails in the 100^0 photomicrograph are nearly perpendicular to one another.

Further evidence supporting a two plane solution was found by separating the pitch measurements into core and rim data (Fig. 9b). These two data sets were plotted using different symbols on the same stereonet and compared with the two planes defined by FitPitch (Fig. 9a). The core and rim data very closely correspond to the data allocated by FitPitch to Plane A and Plane B respectively. Some confusion arises when allocating data as either core or rim because of cut effects (i.e., not every cut goes through the centre of the porphyroblast).

The two plane solution provided by FitPitch seems to describe the data very well. It would therefore be expected that this answer would agree with that ascertained by the well established asymmetry method. Table 2 shows the results from the two techniques. It can be seen that the two methods provide very different answers. FitPitch suggests a FIA trending approximately towards 017^0 while the asymmetry approach gives a FIA trending towards 115^0. The FIA trends established for the same sample, using the two different techniques are separated by nearly 90^0. Clearly, these results require some explanation. The asymmetry method works by picking the orientation of the axis of curvature of the core foliation (i.e., the curvature of this foliation into the next subsequently formed foliation). FitPitch works by calculating the intersection lineation formed between two foliations. As noted earlier, the majority of the porphyroblasts in sample MB030 possess an inclusion-free median (Fig. 8). It is suggested that the FIA established using the asymmetry method represents the axis of curvature of the core trails

into a foliation developed during the growth of this inclusion-free median. By contrast, the FIA found using FitPitch is the lineation produced by the intersection of the core and rim foliations.

3.3.3 Sample MB028

The Perry Mountain Formation contains numerous stringers or pods of very fine-grained garnet "coticule" (Fig. 10). These distinctive lithologies are of uncertain and controversial origin (Eusden *et al*., 1984; Thomson, 1992; 2001) but possible protoliths include manganiferous chert or Mn-Fe-bearing carbonate concretion. This material was previously considered useless for FIA studies because the tiny (~100 μm) garnet porphyroblasts mostly contain extremely straight trails, meaning that the asymmetry method could not be used. 440 pitch measurements were made from one horizontal and six vertical sections and analysed with FitPitch. The results are presented in Table 1 and Figure 11.

A three plane solution is preferred for this sample based on R_d and R_m values and this is supported by observation. The inclusion trails preserved in the garnet porphyroblasts are mostly straight but Figure 12 shows a rare example of a porphyroblast that has overgrown a differentiated crenulation cleavage. The orientation of the preserved inclusion trails combined with the matrix foliation very closely matches the modal peaks of the pitch data (as shown on the rose diagram) and also mirrors the intersections of the 030^0 section with the model planes calculated by FitPitch. Numerous small porphyroblasts are observed with straight inclusion trails which have the same orientation as either the very early foliation, the differentiated crenulation or the matrix foliation. This may be indicating something about the way that garnets nucleate and grow in the coticule material. Rather than forming overgrowths on previously existing garnets (as observed in samples MB019 and MB030), the majority of the coticule garnets seem to preserve just one foliation as inclusion trails. This suggests that it is easier to nucleate new garnets in this material than continue growing the old and may partly explain the very small size of the porphyroblasts in the coticule.

4. Discussion and Conclusions

4.1 Asymmetry vs. FitPitch

FIA orientations determined using both the traditional asymmetry and "FitPitch" techniques have been compared and contrasted. It has been demonstrated that results obtained from the two techniques can either agree with (sample MB019), or sharply contradict each other (sample MB030). In order to reconcile different results obtained from the two methods, it is important to understand how the two techniques differ and what the resulting FIAs actually relate to. The results from sample MB030 highlight these important differences. The asymmetry method relies on the curvature of one foliation into a subsequently formed foliation. The FIA is found by examining the pattern formed by the intersection of vertical thin-sections of differing strikes with the curved inclusion trails preserved within porphyroblasts and picking the flip from "S" to "Z" shape between two closely oriented sections. FitPitch takes a mathematical approach and attempts to fit one, two or three model planes to pitch data measured in a set of differently oriented thin-sections. The best solution is considered to be the one that minimises the deviation between the data and the model planes. Intersections between these model planes define FIAs.

The dramatically different results obtained for sample MB030, using the two techniques can be explained by the absence of inclusion trails in the median of the porphyroblasts. The garnets in this sample generally display distinct cores and rims, separated by a largely inclusion-free median. Clearly, no pitch data can be obtained from the median so the FIA calculated by FitPitch is the product of the intersection between the core and rim foliations. This virtual FIA is never directly observed in the rock. By contrast, the core FIA established using the traditional asymmetry approach is found by examining the curvature of the core foliation into the median. This effectively gives the intersection lineation between core and median foliations. Therefore, the two procedures measure quite different FIAs.

4.2 Matrix lineations

The usual procedure followed by structural geologists is to prepare and examine P and N sections (i.e., sections cut perpendicular to the dominant matrix foliation and both parallel (P) and normal (N) to the stretching or mineral elongation lineation). In areas that have been multiply deformed and metamorphosed, this approach will commonly result in an incomplete picture of the tectonic history of an area (Cihan, 2004). Stretching and elongation lineations are subject to reorientation during all subsequent episodes of folding, reactivation (Bell, 1986) and/or reuse (Davis & Forde, 1994) of previously developed foliations. They are rotated by the cumulative effects of all successive deformations rather than indicating the direction of movement during the youngest deformation. Accordingly, they should be regarded as products of the cumulative strain and not the instantaneous strain ellipsoid. Furthermore, the mineral elongation lineation on $S_1//S_0$ will commonly be the product of numerous deformations due to the routine reorientation of S_0 (e.g., Bell et al., 2003, 2004, 2005, Ham and Bell, 2004).

The orientation of linear indicators of movement direction on gently dipping planes appears to relate more to topography than relative plate motion. The radiating pattern of linear indicators of movement direction perpendicular to topographic highs (e.g., Platt *et al*., 1989; Bell & Wang, 1999) suggests that body forces associated with gravitational collapse and spreading rather than the effects of relative plate motion are responsible for the development of these structures. Elliot (1976) first proposed the idea that nappes and thrusts could advance by gravitational spreading, while undergoing internal thinning under the weight of overlying rocks. Subsequent work (e.g., Law *et al*., 1986; Merle, 1989; Sandiford, 1989; Northrup, 1996; Aerden & Malavieille, 1999) has found this idea to be in good agreement with the strain patterns and structures observed in some thrust sheets.

FIAs form from the preservation, as inclusion trails, of intersecting successive foliations that develop against the porphyroblast margins. A FIA trend is controlled only by the orientation of steeply dipping foliations and is independent of the movement direction on horizontal planes.

Therefore, the FIA is the only linear indicator of movement direction that consistently reflects the direction of bulk shortening associated with relative motion between plates.

4.3 Shear sense

It is often difficult to ascertain which thin-section orientation is the most suitable for determining sense of shear, particularly when inclusion trails show minimal curvature or where that curvature appears to be inconsistent. The procedure of examining only 'P' and 'N' sections to determine shear sense is inadequate in multiply deformed rocks, and will commonly give misleading or inaccurate results. FIAs develop perpendicular to the direction of bulk horizontal shortening (Bell *et al*., 1992) and therefore, only sections cut at a high angle to the FIA provide an accurate indication of shear sense during ductile deformation. The determination of shear sense is a fundamental part of the traditional approach to FIA determination. The asymmetry of a large number of inclusion trails in a set of differently oriented vertical thin sections is recorded in order to find two closely oriented sections between which the asymmetry flips (i.e., from 'S' to 'Z' shaped). The FIA is interpreted to lie at the midpoint between these two sections. The correct shear sense can be easily resolved by re-examining the data recorded for sections at a high angle to the FIA.

The "FitPitch" computer program does not give the correct sense of shear directly. However, it does provide a method to easily determine the orientation of the FIA, even in samples with negligible inclusion trail curvature. It is then possible to quickly establish which section orientation is most suitable for shear sense determination. As few as three differently oriented thin sections (e.g., Aerden, 2003; two vertical and one horizontal) are needed to give a reasonably good estimate of the FIA trend. Once the orientation of the FIA is determined, shear sense can be ascertained by examination of a section cut perpendicular to the FIA. Even samples with predominantly straight or confusing trails will usually show some amount of curvature at their extremities and FitPitch provides a simple answer to the challenge of deciding which section orientation is most suitable for examination. Differently oriented sections are required for rocks with changing FIA trends from the core to the rim of porphyroblasts.

4.4 Independent tests

FitPitch is a valuable tool which compliments existing methods of FIA determination by providing a check for results obtained from the asymmetry method and by making it possible to get results where the latter method cannot, as demonstrated with sample MB028. Three FIAs were obtained from this sample which was previously considered unsuitable for this type of study. The two techniques take completely different approaches and can be employed as independent tests of one another. The same thin-sections can be used for both techniques but an additional horizontal section helps in gaining a better understanding of the three dimensional microstructures preserved within the porphyroblasts.

Caution needs to be exercised when using FitPitch. It will always provide solutions for one, two and three model planes, even if no planes are present or if more than three planes would better describe the data. It is imperative that the solutions provided by FitPitch be compared and reconciled with the structures observed in the thin-sections.

References

Aerden, D., 2003. Preferred orientation of planar microstructures determined via statistical best-fit of measured intersection-lines: the 'FitPitch' computer program. *Journal of Structural Geology* **25**, 923-934.

Aerden, G.A.M., Malavieille, J., 1999. Origin of a large-scale fold nappe in the Montagne Noire, Variscan belt, France. *Journal of Structural Geology* **21**, 1321-1333.

Bell, T.H., 1986. Foliation development and refraction in metamorphic rocks: reactivation of earlier foliations and decrenulation due to shifting patterns of deformation partitioning. *Journal of Metamorphic Geology* **4**, 421-444.

Bell, T.H. and Bruce, M.D., 2006. The internal inclusion trail geometries preserved within a first phase of porphyroblast growth. *Journal of Structural Geology* **28**, 236-252.

Bell, T.H., Forde, A., Wang, J., 1995. A new indicator of movement direction during orogenesis: measurement technique and application to the Alps. *Terra Nova* **7**, 500-508.

Bell, T.H., Ham, A.P., Hickey, K.A., 2003. Early formed regional antiforms and synforms that fold younger matrix schistosities: their effect on sites of mineral growth. *Tectonophysics* **367**, 253-278.

Bell, T.H., Ham, A.P., Kim, H.S., 2004. Partitioning of deformation along an orogen and its effects on porphyroblast growth during orogenesis. *Journal of Structural Geology* **26**, 825-845.

Bell, T.H., Ham, A.P., Hayward, N., Hickey, K.A., 2005. On the development of gneiss domes. *Australian Journal of Earth Sciences* **52**, 183-204.

Bell, T.H., Hickey, K.A., 1997. Distribution of pre-folding linear indicators of movement direction around the Spring Hill Synform, Vermont: significance for mechanism of folding in this portion of the Appalachians. *Tectonophysics* **274**, 275-294.

Bell, T.H., Hickey, K.A., Upton, G.J.G., 1998. Distinguishing and correlating multiple phases of metamorphism across a multiply deformed region using the axes of spiral, staircase and sigmoidally curved inclusion trails in garnet. *Journal of Metamorphic Geology* **16**, 767-794.

Bell, T.H., Johnson, S.E., 1990. Rotation of rigid objects during ductile deformation: well established fact or intuitive prejudice? *Australian Journal of Earth Sciences* **37**, 441-446.

Bell, T.H., Johnson, S.E., 1992. Shear sense: anew approach that resolves problems between criteria in metamorphic rocks. *Journal of Metamorphic Geology* **10**, 99-124.

Bell, T.H., Johnson, S.E., Davis, B. Forde, A., Hayward, N. and Wilkins, C., 1992. Porphyroblast inclusion-trail orientation data: eppure non son girate! *Journal of Metamorphic Geology* **10**, 295-308.

Bell, T.H. and Newman, R., 2006. Appalachian orogenesis: The role of repeated gravitational collapse. *Geological Society of America Special Paper 414*: *Styles of Continental Contraction*, 95–118.

Bell, T.H., Wang, J., 1999. Linear indicators of movement direction versus foliation intersection axes in porphyroblasts (FIAs) and their relationship to directions of relative plate motion. *Earth Science Frontiers* **6**, 3, 31-47.

Bell, T.H., Welch, P.W., 2002. Prolonged Acadian orogenesis: revelations from foliation intersection axis (FIA) controlled monazite dating of foliations in porphyroblasts and matrix. *American Journal of Science* **302**, 549-581.

Billings, M.P., 1956. The geology of New Hampshire: part II – Bedrock geology: Concord, New Hampshire State Planning and Development Commission.

Bradley, D.C., Tucker, R.D., Lux, D.R., Harris, A.G., McGregor, C.D., 1998. Migration of the Acadian orogen and foreland basin across the northern Appalachians of Maine and adjacent areas, *U.S. Geol. Survey Professional Paper 1624*.

Cihan, M., 2004. The drawbacks of sectioning rocks relative to fabric orientations in the matrix: A case study from the Robertson River Metamorphics (Northern Queensland, Australia). *Journal of Structural Geology* **26**, 2157-2174.

Davis, B.K., Forde, A., 1994. Regional slaty cleavage formation and fold axis rotation by re-use and reactivation of pre-existing foliations: the Fiery Creek Slate Belt, North Queensland. *Tectonophysics* **230**, 161-179.

Elliot, D., 1976. The energy balance and deformation mechanisms of thrust sheets. *Philosophical Transactions of the Royal Society of London* **A283**, 289-312.

Eusden, J.D., Jr., Barreiro, B., 1988. The timing of peak high-grade metamorphism in central-eastern New England. *Maritime Sediments and Atlantic Geology* **24**, 241-255.

Eusden, J.D., Jr., Bothner, W.A. and Hussey, A.M., Laird, J.,1984. Silurian and Devonian rocks in the Alton and Berwick quadrangles, New Hampshire and Maine, In Hanson, L.S. (ed.) *Geology of the coastal lowlands, Boston, MA to Kennebunk, ME: New England Intercollegiate Geologic Conference*, 1984, Trip C5, 325-351.

Eusden, J.D., Jr., Bothner, W.A., Hussey, A.M., 1987. The Kearsarge-Central Maine Synclinorium of southeastern New Hampshire and southwestern Maine: stratigraphic and structural relations of an inverted section. *American Journal of Science* **287**, 242-264.

Ham, A.P. and Bell, T.H., 2004. Recycling of foliations during folding. *Journal of Structural Geology* **26**, 1989-2009.

Hatcher, R.D., 1981. Thrusts and nappes in the North American Appalachian Orogen, In McClay, K.R. and Price, N.J. (eds.) *Thrust and nappe tectonics,* 491-499. Blackwell Scientific Publications.

Hayward, N., 1990. Determination of early fold axis orientations within multiply deformed rocks using porphyroblasts. *Tectonophysics* **179**, 353-369.

Hickey, K.A., Bell, T.H., 1999. Behaviour of rigid objects during deformation and metamorphism: a test using schists from the Bolton Syncline, Connecticut, USA. *Journal of Metamorphic Geology* **17**, 211-228.

Hobbs, B.E., Means, W.D., Williams, F., 1976. An Outline of Structural Geology. Wiley, New York.

Huddlestone-Holmes C.R., Ketcham, R.A., 2005. Getting the inside story: using computed X-ray tomography to study inclusion trails in garnet porphyroblasts, *American Mineralogist* **90**, ea1-ea17.

Johnson, S.E., 1993. Unravelling the spirals: a serial thin-section study and three-dimensional computer-aided reconstruction of spiral-shaped inclusion trails in garnet porphyroblasts. *Journal of Metamorphic Geology* **11**, 621-634.

Kent, D.V. and Keppie, J.D., 1988. Silurian-Permian palaeocontinental reconstructions and circum-Atlantic tectonics, In Harris, A.l., Fettes, D.J. (eds.) The Caledonian-Appalachian Orogen. *Geological Society Special Publication* **38**, 469-480.

Law, R.D., Casey, M., Knipe, R.J., 1986. Kinematic significance of microstructures and crystallographic fabrics within quartz mylonites from the Assynt and Eriboll regions of the Moine thrust zone, NW Scotland. *Transactions of the Royal Society of Edinburgh: Earth Sciences* **77**, 99-125.

Lyons, J.B., Livingston, D.E., 1977, Rb-Sr age of the New Hampshire Plutonic Series, *Geological Society of America Bulletin* **88**, 1808-1812.

Mares, V.M., 1998. The structural development of the Soldiers Cap Group within a portion of the eastern fold belt of the Mount Isa Inlier: a succession of near-horizontal and near-vertical deformation events and large-scale shearing. *Australian Journal of Earth Sciences* **45**, 373-387.

Merle, O., 1989. The building of the Swiss Alps: An experimental approach. *Tectonophysics* **165**, 41-56.

Northrup, C.J., 1996. Structural expressions and tectonic implications of general non-coaxial flow in the midcrust of a collisional orogen: The northern Scandinavian Caledonides. *Tectonics* **15**, 490-505.

Osberg, P.H., 1988. Silurian to lower Carboniferous tectonism in the Appalachians of the USA. In Harris, A. l., Fettes, D.J. (eds.), The Caledonian-Appalachian Orogen, *Geological Society Special Publication* **38**, 449-452.

Passchier, C.W., Trouw, R.A.J., Zwart, H.J., and Vissers, R.L.M., 1992. Porphyroblast rotation: eppur si muove? *Journal of Metamorphic Geology*, **10**, 283–294.

Platt, J.P., Behrmann, J.H., Cunningham, P.C., Dewey, J.F., Helman, M., Parish, M., Shepley, M.G., Wallis, S., Western, P.J., 1989. Kinematics of the Alpine arc and the motion history of Adria. *Nature* **337**, 158-161.

Ramsay, J. G., 1962. The geometry and mechanics of formation of similar type folds. *Journal of Geology,* **70**, 309–327.

Reinhardt, J. and Rubenach, M.J., 1989. Temperature-time relationships across metamorphic. zones: evidence from porphyroblast-matrix relationships in progressively deformed metapelites. *Tectonophysics* **158**, 141-161.

Robin, P.Y.F., and Jowett, E.C. 1986. Computerized density contouring and statistical evaluation of orientation data using counting circles and continuous weighting functions. *Tectonophysics* **121**, 207–223.

Robinson, P., 1983. Realms of regional metamorphism in southern New England, with emphasis on the eastern Acadian metamorphic high. In Schenk, P.E.(ed.), Regional trends in the geology of the Appalachian-Caledonian-Hercynian-Mauritanide orogen. D. Reidel Publishing Company, 249-258.

Rosenfeld, J.L., 1968. Garnet rotations due to major Palaeozoic deformations in southeast Vermont. In Zen *et al*. (eds.), Studies of Appalachian Geology. Wiley Interscience, New York, 185-202.

Rosenfeld, J.L., 1970. Rotated Garnets in Metamorphic Rocks. *Geological Society of America Special Paper,* **129**. Geological Society of America, Boulder, Colorado.

Sandiford, M., 1989. Horizontal structures in deep crustal granulite terrains: a record of mountain building or mountain collapse? *Geology* **17**, 449- 452.

Schoneveld, C., 1977. A study of some typical inclusion patterns in strongly paracrystalline-rotated garnets. *Tectonophysics*, **39**, 453–471.

Stallard, A.R., Hickey, K.H., 2001. Fold mechanisms in the Canton Schist: constraints on the contribution of flexural flow. *Journal of Structural Geology* **23**, 1865-1881.

Steiger, R.H., Jager, E, 1977. Subcommision on Geochronology; convention on decay constants in geo- and cosmochronology. *Earth and Planetary Science Letters* **36**, 359-363.

Thomson, J.A., 1992. A mineralogically and chemically zoned granulite-facies coticule from the lower Silurian Rangeley Formation, south-central Massachusetts. *Canadian Mineralogist* **30**, 393-413.

Thomson, J.A., 2001. Relationships of coticule geochemistry to stratigraphy in the Perry Mountain and Megunticook formations, New England Appalachians. *Canadian Mineralogist* **39**, 1021-1037.

Vissers, P., Mancktelow, N.S., 1992. The rotation of garnet porphyroblasts around a single fold, Lukmanier Pass, Central Alps. *Journal of Structural Geology* **14**, 1193-1202.

Williams, M.L., 1994. Sigmoidal inclusion trails, punctuated fabric development, and interactions between metamorphism and deformation. *Journal of Metamorphic Geology* **12**, 1-21.

Williams, P.F. and Jiang, D., 1999. Rotating garnets. *Journal of Metamorphic Geology*, **17**, 367–378.

Section B:

The internal inclusion trail geometries preserved within a first phase of porphyroblast growth

Abstract

The inclusion trail geometry within a first phase of porphyroblast growth can differ significantly from that preserved by further enlargement because the porphyroblast forms a rigid mass up against which the rock preferentially strains during ensuing events. The geometry of the first overgrown inclusion trails is affected by their primary orientation, including any pre-existing curvature, combined with any heterogeneous rotation of this foliation about the developing stretching lineation. This can impact the apparent timing of foliation intersection/inflection axes preserved within porphyroblasts (FIAs) that nucleated during the development of a sub-horizontal foliation, but is readily resolved. 3-D computer analysis of sigmoidal inclusion trails reveals that the asymmetry method for FIA determination is unaffected by the cut location relative to the porphyroblast core. Significantly, perfect spiral inclusion trail geometries can be produced from a sigmoidal shape in cuts up 30° away from the FIA. Therefore, since FIAs in most porphyroblasts bear no relation to matrix structures, there is a 17% chance that thin-sections cut relative to the foliation lie within 30° of a FIA and could contain such an apparent spiral. FIAs maintain consistent trends for the first phase of porphyroblast growth accompanying horizontal bulk shortening but may vary in plunge. FIAs have sub-horizontal plunges for porphyroblasts nucleating during gravitational collapse, but may vary in trend. For all periods of porphyroblast regrowth the data available indicates that FIAs remain consistently trending and sub-horizontal until the relative direction of plate motion causing orogenesis changes.

Keywords: Porphyroblast nucleation; Porphyroblast growth; Crenulation cleavage; Shear sense

1. Introduction

Over a decade has passed since measurements were first made on the orientation of foliation intersection/inflection axes in porphyroblasts (FIAs). For some years now this data has been providing extended structural histories that have been lost from the matrix due to repeated shearing or reactivation of the bedding (e.g., Ham & Bell, 2004), extended metamorphic P-T-t paths (e.g., Sayab, 2005), quantitative correlation of metamorphic and structural data around

oroclines and along and across orogens (e.g., Aerden, 2004), and a means for dating periods of deformation associated with the successive changes in relative plate motion that accompany extended orogenesis (e.g., Bell & Welch, 2002).

One feature of this data has not received much attention. A first phase of porphyroblast growth does not necessarily behave like the later phases in terms of the internal inclusion trail geometry preserved within. This occurs because once a porphyroblast has grown, it forms a rigid mass against which the rock preferentially deforms during ensuing events, preventing reactivation of the compositional layering as shown in Figure 1. Subsequent porphyroblast growth can entrap the foliations that have formed against the porphyroblast rim and they maintain predominantly sub-vertical and sub-horizontal orientations (e.g., Hayward, 1992). However, the first phase of porphyroblast growth overgrows a crenulation hinge as it begins to develop in a pre-existing foliation; such crenulations or foliation inflections may have a large range of orientations depending on the orientation of this earlier-formed foliation. For example, if the porphyroblast grows in a deformation event that forms a sub-vertical foliation, then the resulting FIA will have a trend consistent with those measured from porphyroblasts that contain earlier formed cores, but a variable plunge (Fig. 2; Bell & Wang, 1999). If the porphyroblast grows in a deformation event that forms a sub-horizontal foliation, then the resulting FIA will have a sub-horizontal plunge but potentially a trend that is not consistent with those measured from porphyroblasts with earlier formed cores (Fig. 3). If there has been a previous crenulation event that was not accompanied by porphyroblast growth, then other geometries are possible.

To demonstrate the geometric consequences and significance of these effects we:-

1. examine the variation in inclusion trail geometry and FIA trend within different porphyroblastic phases in the same layer, as well as within the same phase in different layers, from two adjacent samples from the one outcrop; in these samples there is a remarkable consistency of FIA trends between porphyroblasts showing multiple phases of growth and those that grew during the development of a sub-vertical foliation. This

contrasts dramatically with those that only grew during the development of a sub-horizontal foliation.

2. examine the 3-D geometry of sigmoidally shaped inclusion trails obtained by high-resolution X-ray computed tomography (X-ray CT) of a garnet porphyroblast that reveals significant aspects of the variation of inclusion trails that are possible within a first phase of porphyroblast growth, which need to be taken into account when attempting to time porphyroblasts microstructurally.

3. discuss the significance and implications of these phenomena for structural geologists and metamorphic petrologists working with porphyroblastic rocks.

2. FIA trend variation within samples from the Tommy Creek Block

2.1 The samples

Samples TC1365 and TC1365i were taken from adjacent thin pelitic bands in an outcrop of the Tommy Creek Block, Mount Isa Province of Queensland, Australia (Fig. 4; Lally, 1997). Three different pelitic bands within these samples contain:-

A. garnet porphyroblasts (layer A; sample TC1365i).
B. garnet plus andalusite porphyroblasts (that locally replace staurolite; layer B; sample TC1365i).
C. garnet and staurolite porphyroblasts (layer C; sample TC1365).

2.2 Timing of porphyroblast growth and FIA trend

The FIAs preserved in these porphyroblasts were measured separately for each porphyroblastic phase in each compositional layer. The foliations and phases of growth preserved within these porphyroblasts, plus the FIA trends they define, are as follows:-

1. Layer A - garnet porphyroblasts preserve up to 6 stages of growth (Fig. 5) that occurred during D_2 (S_2 sub-vertical, S_3 sub-horizontal) through D_7 (S_7 sub-horizontal). All have a FIA trending at 350°.

2. Layer B - garnet porphyroblasts in the andalusite bearing layer (Fig. 6a) contain sub-vertical S_4 with a clockwise asymmetry (looking NE) into sub-horizontal S_5 and the FIA trends at 45°. Local relics of staurolite porphyroblasts preserved within masses of andalusite have a very similar inclusion trail geometry to garnet, preserving sub-vertical S_4 with a clockwise asymmetry into sub-horizontal S_5 (Fig. 6b). The FIA was not determined for staurolite because relics of this phase are only present in a few thin sections, but we expect it to be similar to that in garnet. Andalusite porphyroblasts grew early during the development of a matrix crenulation with a sub-vertical axial plane (S_6), and then during the development of another with a sub-horizontal axial plane (S_7); the FIA for andalusite trends at 350°.

3. Layer C - garnet and staurolite porphyroblasts in layer C (Fig. 7c) contain FIA trending at 350° and 45° respectively. Garnet grew predominantly during the development of sub-vertical S_4, with some rim growth during the development of sub-horizontal S_5, whereas staurolite grew predominantly during the development of sub-horizontal S_5 (Fig. 7a).

2.3 Interpretation

Layer A contains garnet porphyroblasts preserving multiple phases of growth that accompanied up to 6 different deformation events. Once garnet had formed, any foliations that developed against its rim were preserved by subsequent phases of growth in the orientation in which they were produced, as shown in Figures 5 and 8b. The FIA trend of 350° is controlled by the strike of the sub-vertical foliation S_2 that predated porphyroblast growth as well as the strike of S_4 and S_6 that accompanied it, independent of any rotational effects or reactivation in the matrix. There was no rotation of L^2_3 towards the stretching lineation L^3_3, such as that shown in Figure 2, prior to porphyroblast nucleation in the very early stages of D_3.

In layer B, garnet only grew during development of sub-horizontal S_5 (Figs. 6a, b and 8d). The regionally coarsely partitioned nature of D_5 (Bell & Hickey, 1998) caused the L^4_5 intersection lineation to rotate towards the W-E trending L^5_5 mineral elongation lineation, such as shown in Fig. 3, at a scale much bigger than a porphyroblast. Where garnet nucleation accompanied reduction in the scale of deformation partitioning, it overgrew portions of rock where L^4_5 had been rotated from 350° towards the L^5_5 stretching lineation to a trend of 45° (Figs. 3 and 8d). Andalusite first nucleated in D_6, which produced sub-vertical S_6 (Fig. 8e). It then grew during development of a weak sub-horizontal S_7. The 350° FIA trend in andalusite is controlled by the 350° striking sub-vertical S_6. This FIA could vary in plunge from the horizontal if rotation of L^5_6 towards the steeply pitching L^6_6 occurred in a similar manner to that which affected L^4_5 (such as shown in Fig. 3); however, such rotation does not affect the primary 350° FIA trend. The weak character of D_7 meant that the 350° FIA was maintained in any andalusite that did not nucleate on previously formed porphyroblasts. Very locally, andalusite has replaced staurolite (Fig. 6c, d) and in these locations could preserve the staurolite FIA trend.

In layer C, where garnet porphyroblasts first grew early during the development of sub-vertical D_4, the 350° FIA trend is controlled by the strike of sub-vertical S_4 (Fig. 8a, c; see also Fig. 2) There was no rotation of S_4 preserved in the strain shadows of the porphyroblasts (Fig. 7d) during minor rim growth that accompanied the development of sub-horizontal S_5 and so the FIA defined by L^4_5 remained at 350°. Staurolite grew predominantly during the development of sub-horizontal D_5, which as described in (2) above, caused rotation of L^4_5 towards L^5_5 prior to porphyroblast nucleation and resulted in the 45° trending FIA (Fig. 8d).

These observations from adjacent layers reveal variation in FIA trend is possible during a single sub-horizontal foliation producing deformation event for a first phase of porphyroblast growth in some layers versus a second or later phase in others. For example, the different FIA trends in garnet porphyroblasts that grew during D_5 in layers A and B can be readily interpreted via the effects that the presence of a porphyroblast has on the development and preservation of foliations in the matrix against it. Furthermore, the parallelism of FIA trends in garnet and

andalusite porphyroblasts that grew for the first time during a sub-vertical foliation producing deformation event, with those in garnet in layer A overgrowing earlier formed cores, has resulted from the only variation that is possible due to heterogeneous strain being in the vertical plane around a steep stretching lineation (Fig. 2).

Thus the variation in FIA trend from phase to phase and layer to layer can be readily interpreted when the timing of porphyroblast development is examined with regards to whether the foliation that accompanied growth developed sub-horizontally or sub-vertically. Where foliations preserved in porphyroblasts are successively sub-vertical and sub-horizontal the FIA trends are controlled by the strike of sub-vertical foliations as shown in Fig. 8a. Once a porphyroblast has formed, sub-vertical foliations that formed against it are preserved in its strain shadow from the effects of rotation due to subsequent deformation or reactivation of bedding. Any foliation pre-dating porphyroblast growth can be rotated by the effects of prior deformation, or locally by that accompanying porphyroblast nucleation.

3. Inclusion trail geometries in 3-D

A significant quantity of data has been published on the measurement and analysis of FIA orientations with the majority of this work carried out using the approach established by Hayward (1990) of cutting multiple vertical thin sections around the compass. This method averages the asymmetry of the inclusion trails in a large population of porphyroblasts from a single rock sample using several differently oriented thin sections. Reconciliation of the structures observed in differently oriented thin sections into a complete three-dimensional presentation of the inclusion trail geometry is generally impractical because each porphyroblast is cut somewhere between its centre and edge. This does not change the inclusion trail asymmetry for one stage of growth but it may change the shape (e.g., compare Fig. 9a, b, c; see also Appendix E: "E02-vertical sigmoid slice 090.mov" a QuickTime movie that shows the range of possible inclusion trail geometries that could be encountered depending on where the 090° section intersects the porphyroblast). In particular, it may reveal curvature of inclusion trails in some porphyroblast

cores that passes towards the horizontal (Fig. 9a, b) or vertical; such curvature has significance (see discussion).

Numerous studies have attempted to predict the geometry of inclusion trails based on the process by which they form (e.g., Schoneveld, 1977; Bell & Johnson, 1989; Masuda & Mochizuki, 1989; Williams & Jiang, 1999), but relatively little data has been presented on the three dimensional geometry of inclusion trails preserved in real rocks. A doubly curving non-cylindrical geometry of "simple" sigmoidal inclusion trails has been described by several studies (e.g., Johnson, 1993) utilising a serial sectioning approach in which the inclusion trails were reconstructed from tracings of several parallel thin sections made through a single large porphyroblast. Marschallinger (1998) employed a precision serial lapping and scanning technique to aid in similar reconstructions.

The advent of high-resolution X-ray CT has permitted the actual three-dimensional geometry of curved inclusion trails in garnet porphyroblasts to be studied in detail for the first time (Ikeda *et al*., 2002; Huddlestone-Holmes & Ketcham, 2005). The combination of attenuation data with thin section and microprobe data allows inclusion phases to be distinguished and separated. The 3-D model of a single garnet porphyroblast produced by Huddlestone-Holmes & Ketcham (2005) provides the actual geometry of a doubly curving single sigmoidal quartz-rich inclusion trail that runs through the centre of the porphyroblast, paralleled by numerous ilmenite inclusions. Their model serves as the template for this study as the geometry of inclusion trails preserved throughout this porphyroblast can be examined and computer derived 2-D cuts made through it in any orientation to quantify and thus understand the significance of inclusion trail cut effects through a single porphyroblast.

3.1 Establishing a model porphyroblast

The 3-D inclusion trail geometry, produced from the high-resolution X-ray CT by Huddlestone-Holmes & Ketcham (2005) on a sample of Cram Hill Formation from south-eastern Vermont, is shown in Figure 10a. This representation was imported into and manipulated in the

3D modelling, animation and rendering package Discreet 3ds Max™. This software allows individual phases (garnet, quartz, ilmenite, etc.) or even individual inclusions to be treated and managed separately. It is possible to turn individual parts of the model on or off to highlight aspects of interest. We stripped away garnet and crack-fill material to reveal the central quartz inclusion trail (light coloured) along with higher attenuation opaques (ilmenite) inclusions (Fig. 10b). For clarity, we removed isolated quartz inclusions around the periphery of the garnet because this study is concerned with structures preserved during the first phase of porphyroblast growth and these inclusions were overgrown very late. The central quartz inclusion trails were traced in three dimensions by adjusting the vertex points of a flat, box-shaped primitive object in 3ds Max. Adjustments were made so that the resultant continuous inclusion trail passes through the centres of the quartz inclusions (Fig. 10c), resulting in a continuous representation of the inclusion trail geometry. Removing the central quartz trails reveals that the dark ilmenite inclusions are parallel to the central continuous trail in Figure 10d. Additional trails were made by extrapolation of the central trail, using the ilmenite inclusions as a guide and adjusting as necessary to create a satisfactory fit (Fig. 10e). We then replaced the garnet around the periphery that was established by the original X-ray CT to produce the final model (Fig. 10f). The inclusion trails in this model offer the advantage that they contain no breaks or gaps. A section cut through the garnet at any orientation or position will always intersect the trails and produce a continuous trace.

3.2 Slicing the model

The trend of the FIA is usually found by looking for the flip in inclusion trail asymmetry in a set of radial vertical thin sections. Figure 11 illustrates the inclusion trail geometries encountered in a set of such radial sections made through the centre of the model porphyroblast (see also D: “D3-vertical sigmoid rotate.mov”). In reality, we need only cut sections at 0°, 30°, 60°, 90°, 120° and 150° to get this information. Sections at 180°, 210°, 240°, 270°, 300° and 330° can be examined simply by reversing the initial set of six sections. It can be seen that the flip in asymmetry from “Z” to “S” shaped occurs at, or very close to 0° (000° or 180° section). Consequently, The FIA for this sample is oriented approximately N-S. The trend of the FIA can

be further constrained by cutting additional sections close to 000° (Fig. 12). These additional sections confirm that the flip in asymmetry occurs very close (+/- 5°) to 0°.

Figure 11 shows that the sections cut perpendicular to the FIA (090° and 270°) display the least apparent curvature of the trails. These sections, passing through the centre of the porphyroblast provide true profiles of the inclusion trail geometry. Sections cut in the remaining orientations display an increase in the apparent curvature, appearing more spiral like, culminating in the closed loop structures of sections cut parallel to the FIA (000° and 180°). Structures observed in sections cut very close to the axis of curvature (e.g., the 010°, 020° and 350° sections of Figure 12) exhibit almost 180° of apparent rotation from the centre to the margin of the porphyroblast. A comparison of sections made through the trails of the schematic model and the original model of Huddlestone-Holmes & Ketcham (2005) is presented in Figure 12. The sections through the schematic model clearly reflect the geometry represented by the central quartz inclusions of the original model but the schematic model has the advantage that it is unaffected by the paucity of inclusions, particularly opaques/ ilmenite.

3.3 The cut effect

All sections pass through the centre of the porphyroblast in Figure 11. However, it is unlikely that any particular porphyroblast will be perfectly bisected by a thin section. Consequently, the inclusion trails observed usually vary from central cuts as shown for a set of radial thin sections in Figure 13 (the numbers in parenthesis are those section orientations that can be obtained simply by flipping the original section over; 210° is equivalent to 030° viewed from the opposite direction). Significantly, the flip in asymmetry occurs very close to 0° regardless of whether the sections utilised pass through the centre or the closer to the edge of the porphyroblast for one phase of porphyroblast growth. That is, the asymmetry method for determination of the axis of curvature is unaffected by cut effects. However, the doubly curving, non-cylindrical nature of the inclusion trails results in a significant decrease in the apparent curvature of the inclusion trails from the centre to the outer margin of the porphyroblast. This is especially apparent in sections cut nearly orthogonal to the FIA (e.g., at 090°). While this can

potentially make determination of asymmetry difficult, these effects can be overcome by examining a large enough population of porphyroblasts.

Another aspect to cut effects is the orientation of a section relative to the FIA. Structures observed in sections cut within 30° of the axis of curvature (Fig. 11 and the 010°, 020° and 350° sections of Fig. 12) exhibit almost 180° of apparent rotation from the centre to the margin of the porphyroblast and would be called spiral inclusion trails as opposed to sigmoidal if viewed in isolation through cutting just one or two thin sections from this sample. Different sets of FIAs can show a large range of trends relative to the matrix foliation (e.g., Ham & Bell, 2004). Therefore, thin sections cut perpendicular to the matrix foliation and perpendicular or parallel to a lineation, may cut through a porphyroblast where the FIA lies at 30° or less to the section plane. Such thin sections may show perfect spiral shaped inclusion trails in porphyroblasts where the actual geometry is a sigmoid (e.g., Fig. 11) and would be interpreted by many today as a product of intense local shear zone development (e.g., Williams & Jiang, 1999). Appendix E: E02-D06 contains several QuickTime movies that illustrate the range of possible inclusion trail geometries that could be encountered by vertical thin sections with different strikes intersecting the model porphyroblast at a range of distances between its centre and its edge.

3.4 Variation in FIA trend through the model

Figure 14a shows three horizontal cuts through the inclusion trail geometry. The variation in the orientation of the intersection of the inclusion trails with the horizontal cut that passes through the porphyroblast centre potentially defines the maximum variation in trend of a FIA that could be recorded by the growth of a single porphyroblast that grew in this event. The intersection of this foliation with the horizontal cut varies through a maximum of 60°. Huddlestone-Holmes & Ketcham (2005) measured the FIAs separately in 58 porphyroblasts using X-ray CT on 5 cylinders cored from different portions of this sample and found a maximum variation of 30° around the mean FIA trend giving a total variation of 60°. Therefore, the question to be resolved is how much of this variation predated or was synchronous with porphyroblast growth. This is particularly pertinent with this sample because, as mentioned

above, it contains evidence of a foliation inflection through the vertical that strongly suggests the foliation either initially had a sub-horizontal orientation (Fig. 14b (i)) or was a reactivated oblique moderately east dipping foliation sub-parallel to compositional layering (Fig. 14b (ii) or was a pre-existing crenulation about a steep axial plane (Fig. 14b (iii)). This foliation in Figure 14b (i) was initially rotated by a deformation with a sub-vertical axial plane to the steep east dip or started in this orientation prior to the deformation with the sub-horizontal axial plane that accompanied porphyroblast growth. It was then overprinted by the crenulation with the sub-horizontal axial plane that accompanied porphyroblast growth. If the porphyroblast did not overgrow the centre of a partially decrenulated pre-existing hinge (Fig. 14c (i)), but instead was centred above that as shown in Figure 14c (ii), then the resulting foliation through the centre of the porphyroblast would look like Figure 14a (ii) with the actual geometry that should have been preserved in the porphyroblast centre looking like that in Figure 14a (i). Therefore, we conclude that the bulk of the variation occurred prior to development of the sub-horizontal foliation in this sample.

4. Discussion

4.1 The early growth of porphyroblasts relative to deformation

Porphyroblast growth during regional metamorphism commences very early during a deformation event (Bell *et al*., 2003) and ceases once a differentiated crenulation cleavage begins to form in the immediate vicinity (Fig. 15; Bell & Hayward, 1991). Nucleation of a porphyroblastic phase for the first time at a particular site requires irregular partitioning of the deformation into progressive shearing and shortening components on the scale of a porphyroblast (e.g., Fig. 15a), which generally involves relatively coaxial strain to enhance microfracture along pre-existing foliations (e.g., Bell *et al*., 2004). This means that the first phase of porphyroblast growth generally preserves simple trails that commonly have a very similar orientation across a thin section (Ramsay, 1962), fold or region (Fyson, 1980; Aerden, 2004). However, deformation may locally commence and be distributed very homogeneously on a scale much larger than a porphyroblast. For example, if reactivation of the pre-existing foliation is possible or becomes

possible, then the foliation can rotate without crenulations developing at the scale of a porphyroblast (e.g., Bell *et al*., 2003). If this occurs, porphyroblasts will not nucleate unless the deformation begins to partition into progressive shearing and shortening components at the scale of a porphyroblast. Consequently, the foliation preserved as inclusion trails within such porphyroblasts could vary significantly from its orientation prior to the commencement of that deformation event. However, it is significant that in many examples this is not the case.

Foliations that have been folded several times before porphyroblast growth begins should show a large range of variation in orientation when preserved as inclusion trails. It is intriguing how uncommon this appears to be at the scale of several outcrops (Steinhardt, 1989; Aerden, 1995), shear zone (Jung *et al*., 1999), or region (Fyson, 1980). Possible reasons for this are:-

1. Such variation is less interesting than consistency and has not been recorded; consequently, it is less well represented in the literature.

2. Foliations lying parallel to bedding are crenulated at a coarser scale than recently developed axial planar ones causing porphyroblasts to preferentially nucleate in the latter.

A significant factor that would promote the situation described in 2 is that compositional layering always will reactivate if the geometry is appropriate and this reduces the number of sites available for porphyroblast growth (Bell *et al*., 2003).

4.2 Porphyroblast nucleation and initial growth

As a result of the early commencement of porphyroblast growth relative to deformation in the vicinity, the most common inclusion trail geometry preserved is one of straight inclusion trails that are slightly curved at the porphyroblast edges (Fig. 15c). Porphyroblast growth ceases once inclusion trail curvature becomes significant because the progressive shearing causing foliation curvature also causes a differentiated crenulation cleavage to begin to develop. The dissolution and solution transfer associated with this process stops further porphyroblast growth

(Fig. 15d, e, f; Bell & Hayward, 1991). Consequently, porphyroblasts will generally not nucleate over a foliation lying at a low angle to that which is newly developing as such foliations will reactivate antithetically as shown in Figure 1 (e.g., Bell *et al*., 2003) or be reused synthetically (e.g., Davis & Forde, 1994). The next most common inclusion trail geometry is one of sigmoidal inclusion trails that are slightly more curved at the porphyroblast edges than towards the core. Such trails commonly result from the overprint of a pre-existing crenulation hinge by a younger event as shown in Figure 14b (iii). Their development is very similar to that just described except that relics of an early crenulation are present providing more curvature of the inclusion trails.

4.3 Significance of foliation curvature towards the vertical or horizontal

Multiple thin sectioning of samples commonly reveals in some porphyroblasts inflections towards the vertical or horizontal for the earliest observable portion of the inclusion trail as shown in Figure 16. These inflections have significance if inclusion trails result from the development of successive sub-vertical and sub-horizontal foliations as first argued by Bell & Johnson (1989). They can form in one of 3 ways.

1. They reflect the remains of an older crenulation that predates porphyroblast growth as shown in Figure 14b (iii).

2. They reflect the remains of a reactivated foliation that lay oblique to the horizontal or vertical (Fig. 14b (ii)).

3. They result from relatively coaxial deformation occurring early during the deformation that occurred prior to the first phase of porphyroblast growth (Fig. 15a-c; Bell & Bruce, 2007; thesis Section C).

If they result from nucleation on an older crenulation then one would expect that X-ray CT scans of 3D inclusion trail geometries from many porphyroblasts in the same sample would reveal such geometries in a lot of them. This could also apply if the foliation was the remains of

an oblique reactivated one. Indeed this is the situation recorded by Huddlestone-Holmes & Ketcham (2005). If, however, they formed by early coaxial deformation one would expect that the variation in geometry from porphyroblast to porphyroblast would be very large (e.g., Bell & Bruce 2007; thesis Section 3). If such changes occurred at a much larger scale than a porphyroblast then no porphyroblast would tend to nucleate. However, if repartitioning of the deformation occurred at a finer scale through the outcrop, any porphyroblasts that nucleated would overgrow the previously rotated foliation and perhaps have a similar geometry to that described for 1 and 2 above. At a larger scale this might not be the case and the inclusion trail geometry could vary significantly from porphyroblast to porphyroblast.

4.4 Curvature of the intersection or inflexion axis within a porphyroblast

When a porphyroblast first nucleates the FIA could show considerable curvature in 3-D (Fig. 10) causing a change in trend in a horizontal plane in Figure 14a (i-iii) and plunge in a vertical plane in Fig. 14b. This variation can be recorded using X-ray CT methods within individual porphyroblasts as shown in Figure 10. However, the method of measurement used to record the FIA and described by Hayward (1990) records the FIA for a sample and not for an individual porphyroblast. The effects of such primary variation within a porphyroblast are eliminated.

4.5 Apparent spiral shaped inclusion trails due to section orientation

The 3-D geometry of inclusion trails in the garnet porphyroblast revealed by X-ray CT shows that some section orientations in space contain spiral shaped inclusion trail geometries even though the inclusion trails are sigmoidal in 3-D (e.g., the 030° and 150° sections in Fig. 11). This possibility will be recognized by anyone who works extensively with multiple thin sections around the compass but will not be known by most metamorphic and structural geologists because they have not done this type of work. Consequently, where thin sections are cut either randomly or relative to the matrix microstructures (where the porphyroblast is truncated by the schistosity), they may show spiral shaped inclusion trails when in fact only sigmoidal ones are

present in 3-D. This could dramatically influence interpretation of the structural history of the region, depending on whether one interpreted that the inclusion trails had formed by porphyroblast rotation or non-rotation. Wherever spiral shaped inclusion trails are seen in thin section showing a maximum of 180° of curvature, extra thin sections in other orientations should be cut to check whether true spirals or just sigmoidal trails are present.

4.6 Geometry of foliation development against a porphyroblast

Once a porphyroblast has formed it provides a rigid or competent object against which the shearing component of the deformation in the matrix tends to nucleate soon after the commencement of deformation. The large amount of quantitative data available on the orientation of foliations forming after an initial stage of porphyroblast growth suggests that they form predominantly sub-vertically or sub-horizontally (Fig. 17, modified from Gavin 2004; see also fig. 10 in Hayward, 1992). This is confirmed by the shallow plunges of FIAs in the terrains where these have been measured (Fig. 18 from data in fig. 9d in Bell & Hickey, 1997; table 1 in Bell & Wang, 1999; fig. 9 in Hickey & Bell, 1999; and Bell & Newman, 2006). FIAs resulting from successive steep foliations would have plunges ranging from mainly very steep to locally very gentle (Fig. 19), which is not what is observed where porphyroblasts have grown for a second or subsequent time. The only way to achieve plunges less than 30° during every phase of porphyroblast growth after the first is for the FIAs to result from the intersection of successively preserved sub-vertical and sub-horizontal foliations. Such sub-horizontal plunges are independent of whether a sub-horizontal foliation overprints a sub-vertical foliation or a sub-vertical foliation overprints a sub-horizontal foliation.

4.7 The asymmetry method versus the cut effect

The asymmetry method of FIA determination uses the curvature of inclusion trails in all porphyroblasts present in a thin section. Therefore, it uses all cuts through a porphyroblast from the core to the rim, in at least 8 different orientations around the compass. Conceptually, all slices through one period of growth of the porphyroblast should preserve the asymmetry and the above

method should be independent of any cut effect, but it is clearly important to test this. Figure 13 shows that this is the case. Therefore, the asymmetry method provides an excellent procedure for measuring foliation inflection/intersection axes preserved in the porphyroblasts within a sample that is independent of any cut effect on the inclusion trail geometry through a porphyroblast.

4.8 Consistency of FIA trends

Where FIAs have been measured regionally they maintain remarkably consistent successions of trends for large distances (e.g., Aerden, 2003; Bell *et al*., 2004). In a range of locations, individual FIAs result from successions of up to 7 foliations intersecting in the one axis requiring that directions of relative bulk shortening remain constant for significant periods of time. Bell & Welch (2002) suggest that these periods are around 10 to 30 million years in length. Layer A in sample TC1365i contains garnet porphyroblasts preserving evidence for 5 foliations plus a crenulation axial plane in the matrix that intersect in the one axis at 350°. Variation from this trend only occurs in samples where there is one phase of growth that occurred during the development of a horizontal foliation. Such samples can be readily eliminated from a regional analysis if anomalies relative to multiple FIA samples are recorded.

References

Aerden, D., 1995. Porphyroblast non-rotation during crustal extension in the Variscan Lys-Caillaouas Massif, Pyrenees. *Journal of Structural Geology* **17**, 709-725.

Aerden, D., 2004. Correlating deformation in Variscan NW-Iberia using porphyroblasts; implications for the Ibero-Armorican Arc. *Journal of Structural Geology* **26**, 177-196.

Bell, T.H. and Bruce, M. D., 2007. Progressive deformation partitioning and deformation history: Evidence from millipede structures. *Journal of Structural Geology* **29**, 18-35.

Bell, T.H. and Hayward, N., 1991. Episodic metamorphic reactions during orogenesis: The control of deformation partitioning on reaction sites and duration. J*ournal of Metamorphic Geology* **9**, 619-640.

Bell, T.H. and Hickey, K.A., 1997. Distribution of pre-folding linear movement indicators around the Spring Hill Synform, Vermont: significance for mechanism of folding in this portion of the Appalachians. *Tectonophysics* **274**, 275-294.

Bell, T.H. and Hickey, K.A., 1998. Multiple deformations with successive sub-vertical and sub-horizontal axial planes: their impact on geometric development and significance for mineralization and exploration in the Mount Isa region. *Economic Geology* **93**, 1369-1389.

Bell, T.H. and Johnson, S.E., 1989. Porphyroblast inclusion trails: the key to orogenesis. *Journal of Metamorphic Geology* **7**, 279-310.

Bell, T.H. and Newman, R., 2006. Appalachian orogenesis: The role of repeated gravitational collapse. *Geological Society of America Special Paper 414*: *Styles of Continental Contraction*, 95–118.

Bell, T.H. and Wang, J., 1999. Linear indicators of movement direction versus foliation intersection axes in porphyroblasts (FIAs) and their relationship to directions of relative plate motion. *Earth Science Frontiers* **6**, 31-46.

Bell, T.H. and Welch, P.W., 2002. Prolonged Acadian orogenesis: revelations from foliation intersection axis (FIA) controlled monazite dating of foliations in porphyroblasts and matrix. *American Journal of Science* **302**, 549-581.

Bell, T.H., Ham, A.P. and Hickey, K.A., 2003. Early formed regional antiforms and synforms that fold younger matrix schistosities: their effect on sites of mineral growth. *Tectonophysics* **367**, 253-278.

Bell, T.H., Ham, A.P. and Kim H.S., 2004. Partitioning of deformation along an orogen and its effects on porphyroblast growth during orogenesis. *Journal of Structural Geology* **26**, 825-845.

Davis, B.K. and Forde, A., 1994. Regional slaty cleavage formation and fold axis rotation by reuse and reactivation of pre-existing foliations: the Fiery Creek Slate Belt, north Queensland. *Tectonophysics* **230**, 161-179.

Fyson, W.K., 1980. Fold fabrics and emplacement of an Archean granitoid pluton, Cleft Lake, Northwest Territories. *Canadian Journal of Earth Sciences* **17**, 325-332.

Gavin B., 2004. The microstructural and metamorphic history preserved within garnet porphyroblasts from southern Vermont and northwestern Massachusetts. Unpublished PhD thesis, James Cook University, 184p.

Ham, A.P. and Bell, T.H., 2004, Recycling of foliations during folding: *Journal of Structural Geology* **26**, 1989-2009.

Hayward, N. 1990. Determination of early fold axis orientations within multiply deformed rocks using porphyroblasts. *Tectonophysics* **179**, 353-369.

Hayward, N., 1992. Microstructural analysis of the classic snowball garnets of southeast Vermont. Evidence for non-rotation. *Journal of Metamorphic Geology* **10**, 567-587.

Hickey, K. and Bell, T.H., 1999. Behaviour of rigid objects during deformation and metamorphism. a test using schists from the Bolton Synform, Connecticut. *Journal of Metamorphic Geology* **17**, 211-228.

Huddlestone-Holmes C.R. and Ketcham, R.A., 2005. Getting the inside story: using computed X-ray tomography to study inclusion trails in garnet porphyroblasts, *American Mineralogist* **90**, ea1-ea17.

Ikeda, T., Shimobayashi, N., Wallis, S. R. and Tsuchiyama, A. 2002. Crystallographic orientation, chemical composition and three dimensional geometry of sigmoidal garnet: evidence for rotation. *Journal of Structural Geology* **24**, 1633-1646.

Johnson, S.E., 1993. Unraveling the spirals: A serial thin section study and three-dimensional computer-aided reconstruction of spiral-shaped inclusion trails in garnet porphyroblasts. *Journal of Metamorphic Geology* **11**, 621-634.

Jung W.S., Ree, J.H. and Park, Y., 1999. Non-rotation of garnet porphyroblasts and 3-D inclusion trails data – an example from the Imjingang Belt, South Korea. *Tectonophysics* **307**, 381-395.

Lally, J.H., 1997. The structural history of the central eastern fold belt, Mount Isa Inlier, Northwest Queensland, Australia., Unpublished PhD thesis, James Cook University, 214p.

Marschallinger, R., 1998. Three-dimensional reconstruction and modelling of microstructures and microchemistry in geological materials. *Scanning* **20**, 65-73.

Masuda, T. and Mochizuki, S., 1989. Development of snowball structure: numerical simulation of inclusion trails during synkinematic porphyroblast growth in metamorphic rocks. *Tectonophysics* **170**, 141-150.

Ramsay, J.G., 1962. The geometry and mechanics of formation of similar type folds. *Journal of Geology* **70**, 309-327.

Sayab, M., 2005. Microstructural evidence for N-S shortening in the Mount Isa Inlier (NW Queensland, Australia): the preservation of early W-E trending foliations in porphyroblasts revealed by independent 3D measurement techniques. *Journal of Structural Geology* **27**, 1445-1468.

Schoneveld, C, 1977. A study of some typical inclusion patterns in strongly paracrystalline rotated garnets. *Tectonophysics* **39**, 453-471.

Steinhardt, C.K., 1989. Lack of porphyroblast rotation in non-coaxially deformed schists from Petrel Cove, South Australia, and its implications. *Tectonophysics* **158**, 127-144.

Williams, P.F. and Jiang, D., 1999. Rotating garnets. *Journal of Metamorphic Geology* **17**, 367-378.

Section C:

Progressive deformation partitioning and deformation history:

Evidence from millipede structures

Abstract

The progressive development and migration of patterns of deformation partitioning at all scales through the rock matrix commonly destroys any record of the ductile history associated with previous events making the problem of similar structures developing through multiple pathways generally intractable. However, records of the small-scale geometries that form as deformation commences and begins to partition through a rock are routinely trapped and protected by porphyroblasts because these large crystals nucleate and/or grow at this time. This allows examination of the geometry of microstructures formed at the start of deformation partitioning that were destroyed by the same event in the matrix, or which formed during an event prior to any preserved in the matrix. Porphyroblasts locally preserve oppositely concave microfolds ("millipedes"), which, in all examples that we have found, exclusively indicate a deformation history of bulk inhomogeneous shortening. Very similar structures have been formed experimentally during inhomogeneous simple shear but can readily be distinguished from those trapped in porphyroblasts that form during progressive bulk inhomogeneous shortening. Oppositely concave microfolds in some porphyroblasts reveal that deformation near orthogonal to a previously developed foliation occurred by axial plane shear driven rotation that led to rapid reactivational "card-deck-like" collapse of the pre-existing foliation. Differentiated crenulation cleavages may result from the same process providing yet another reason for the cessation of porphyroblast growth at the start of differentiation.

Keywords: Progressive bulk inhomogeneous shortening; Shear sense; porphyroblast nucleation; porphyroblast growth; coaxial deformation; crenulation cleavage development

1. Introduction

Deformation partitioning (illustrated in Fig. 1) plays a significant role in numerous processes that accompany tectonism (Siame *et al*., 2005). These include the development of foliations of all types other than bedding (Bell, 1981; Davis, 1995), porphyroblast nucleation and growth within a sample (Hayward, 1992), sites of recrystallization during mylonitization (Bell &

Johnson, 1989), dissolution and solution transfer (Stewart, 1997), crystal-plasticity versus solution-transfer (Lagoeiro *et al*., 2003), the leaching and transport of metals from low concentration environments to ones where orebodies develop (Davis, 2004), the development of meso and microstructures used for shear sense determinations (Bell & Johnson, 1992), and sites for the formation of metamorphogenic ore bodies (Aerden, 1991). The effects of deformation partitioning are obvious in the case of localization of shearing on the boundary of more competent rocks such as a granite pluton, where the rheological contrasts between the intrusion and the country rocks provide a ready explanation for the geometry observed. However, the effects and role of deformation partitioning are much less certain in the development of crenulation cleavages in massive slates and schists or anastomosing shear zones in granitoids and amphibolites, where the rock was more homogeneous to start with. Little is known about the progressive development of this phenomenon in tectonized rocks because the distribution of zones of progressive shearing and shortening (that is the pattern of partitioning; e.g., Figs. 1 and 2a, b) changes as the deformation proceeds and early stages are obliterated by the overprinting effects of later stages in the same event, as well as by subsequent events.

How inclusion trails are interpreted in micro-structural studies is largely dependant on whether the porphyroblast is regarded as having rotated or not relative to fixed geographical coordinates during deformation of the surrounding rock mass. If the porphyroblasts were to experience significant rotation and/or translation during deformation their usefulness as kinematic indicators is reduced to near zero. In this case, rotation would be expected to be non-systematic and would result in a wide range of FIA orientations, particularly for those structures that formed early in the tectonic history and had experienced multiple phases of ductile deformation. It has been suggested (Bell and Johnson, 1990; 1992) that the correct shear sense can generally be inferred if the porphyroblasts did not rotate during growth. Such lack of rotation is supported by a large amount of quantitative data (e.g., Bell and Hickey, 1997; Mares, 1998; Bell *et al*., 1998; 2003; 2004; 2005; Stallard and Hickey, 2001; Bell and Welch, 2002; Ham and Bell, 2004; Bell and Newman, 2006) and can be demonstrated where the distribution of early FIA trends retains a non-random clustering in porphyroblastic metamorphic rocks that have undergone multiple phases of tectonism and porphyroblast growth (Bell and Newman, 2006).

Quantitative structural studies of porphyroblasts involving the routine measurement of inclusion trail geometries, have provided substantial evidence that these large crystals preserve considerable data on the history of the progressive role of deformation partitioning in the surrounding rocks (e.g., Bell *et al*., 2004; Cihan & Parsons, 2005; Sayab, 2005). Once the P, T and bulk composition are appropriate, porphyroblasts grow in zones of progressive shortening that result from deformation partitioning at a scale similar to the their maximum size and cease growth once a pattern of non-coaxial deformation is established and differentiation begins. For porphyroblasts to nucleate or regrow in these zones a pre-existing foliation lying at a high angle to any newly developing one must be present and there should be limited or no reactivation of the compositional layering (Bell *et al*., 2003).

Oppositely concave microfolds preserved in porphyroblasts (millipedes; Fig. 2a, b) potentially provide a geometry that contains unique evidence of the deformation history that a rock has been through (Bell, 1981). Some results from experimental models produced in the seventies appear to suggest that this might not be the case (Ghosh, 1975). We re-examine natural and experimentally derived geometries and conclude that all oppositely concave microfolds that we have examined in rocks provide a unique insight into at least a portion of the deformation history that the host rocks have undergone. This insight leads to revelations on the role of near orthogonal foliations in crenulation cleavage development and the cessation of porphyroblast growth.

2. Deformation history

2.1 The non-uniqueness of most structures

Most structures can be produced through different deformation history paths. In particular, structures that result from some form of inhomogeneous shortening (e.g., Fig. 1) can also be produced by some combination of shearing plus rotation of the whole geometry or through overprinting by shearing in another direction. The simplest example of this is progressive pure shear versus progressive simple shear where the strain geometry produced by simple shear

in Figure 2c, d is produced by pure shear plus a rotation in Figure 2e, f, g. Folds preserved in porphyroblasts that are oppositely concave along their axial plane with the transition containing straight layers as shown in Figure 2a, b (millipede geometry) appeared to be uniquely a product of progressive bulk inhomogeneous shortening. However, Johnson & Bell (1996) suggested that such structures may not be unique because similar ones had been produced experimentally during modelling of progressive simple shear (Ghosh, 1975). This possibility is re-examined below.

2.2 Are millipede geometries a unique indicator of deformation history?

Ghosh (1975) reported experiments in which silicone putty containing rigid wood cylinders was deformed by progressive simple shear (Figs. 3 and 4). He marked each experimental run with a passive marker from which an estimate of the resultant 2-D strain field geometry can be determined. He marked some with indented circles, which on deformation became strain ellipses, allowing an estimate of the foliation generated by the deformation to be determined. His starting configuration in Figure 3a shows a rigid circular central cylinder, plus lines in grey (the marker) and the circles in light grey that were indented into on the silicone putty matrix (which define strain ellipses after deformation has been imposed). The final strain state in Figure 3b shows the effects of anticlockwise progressive simple shear on rotation of the rigid cylinder, the markers and the indented circles; the latter become ellipses. Significantly, heterogeneities that develop in the silicone putty with deformation follow the strain ellipses and can be used to define the "foliation" that develops during the experimental deformation. These matrix silicone putty "foliations" were drawn on the photo in fig. 10 from Ghosh (1975) after it had been reproduced at high magnification on a computer. Where the markers lie at a high angle to the newly developing foliation, as shown in Figure 3, a shear zone-type geometry forms. Where they lie at a moderate angle and dip in the direction of relative shear, a millipede-like geometry can be formed (Fig. 4).

Figure 4 shows the pre-deformation, intermediate and final states of strain for the same experiment as in Figure 3 (figs. 11, 12b and 13 respectively in Ghosh, 1975) but where the markers lay at 45° to the shear plane, oriented so that during anticlockwise progressive shearing it would initially undergo shortening (compare Fig. 4a with 4b). The "foliation" developing as a result of this deformation, which is defined by the matrix silicone putty strain lines that were

drawn on the photo at high magnification, is shown in Figure 4b, c. As described by Johnson & Bell (1996), the grey lines defining the initial "foliation" are deformed into millipede-like shapes in Figure 4b, c. However, when one compares these shapes (Fig. 5a, b) with the newly developed "foliation" the difference between this geometry and the natural millipede shown in Figure 5c is apparent around the porphyroblast margins that lie parallel to the newly developed foliation. In natural millipedes, the newly developed foliation follows the hinge line from one direction of curvature to the opposite as seen in Figure 5c around the porphyroblast rim. For millipede-like shapes formed during a history of progressive simple shear, this is not the case. The foliation that developed during deformation cuts across the axial planes defined by the millipede-like shapes. Beaumont-Smith (2001) suggested that millipede geometries might result from conjugate crenulations forming around a porphyroblast that were then overgrown by the porphyroblast rim. However, his "conjugate" crenulations are simply the anastomosing crenulation geometries that develop during the early coaxial stages prior to the development of a differentiated crenulation cleavage (Fig. 6a-f) and no different to the geometries that we describe (e.g., Bell *et al*., 2004).

3. Examples of very coaxial geometries

3.1 Millipede generating fold hinge

Figures 7 and 8 show a D_3 fold hinge (Sample H20C) from an amphibolite facies outcrop of a muscovite and quartz rich schist containing numerous plagioclase porphyroblasts in the Robertson River metamorphics where the first millipede microstructures were recognized (Bell & Rubenach, 1980). This sample contains 3 foliations that can be readily observed under the microscope. The axial plane structure is a differentiated crenulation cleavage called S_3 (Fig. 9). The folded foliation (Figs. 7 to 9), which is crenulated microscopically to form S_3 seams (Fig. 9c, d, e), is also a differentiated crenulation cleavage called S_2 (Fig. 9a). Between the S_2 cleavage seams a crenulated cleavage called S_1 is preserved (Figs. 9a, c and 10a, b). Attempts at modelling the progressive development of the millipede microstructures in this outcrop resulted in the strain field geometry shown in Figures 1 and 2a, b and the concepts on the role of deformation partitioning in its development that were described by Bell (1981). This fold hinge formed during the same deformation event that developed the millipede microstructures.

The asymmetry of curvature of a crenulated cleavage into an overprinting differentiated crenulation cleavage (Fig. 6d, e, f), called the differentiation asymmetry (which is clockwise in the matrix in Fig. 6d, e, f), does not necessarily change across a fold hinge (compare figs. 2b and 2d in Bell *et al*., 2003). In the case of the fold shown in Figures 7 and 8 the asymmetry of curvature of crenulated S_2 into differentiated crenulation cleavage S_3 remains clockwise on both limbs in the matrix away from porphyroblasts. This differs from the foliation/foliation asymmetry of S_2 relative to S_3 across the fold, which switches from limb to limb (e.g., Bell *et al*, 2003). This fold contains numerous plagioclase porphyroblasts, all of which preserve superb millipede-shaped quartz inclusion trail geometries with the example shown in Figure 9 containing the most oblique relationship between S_2 and S_3 that was found. Generally it is only in regions adjacent to these porphyroblasts that local anticlockwise curvature of S_2 into S_3 is preserved. One thin section was cut from each of the lower and upper limbs and the hinge of 4 separate profile plane slabs of this fold as shown in Figure 8a, b; the profile plane dips 80° S, strikes at 120° and the fold was cylindrical on the scale of the outcrop. Thin sections were also cut from the lower and upper limbs plus hinges in 4 slabs cut parallel to L^2_3 and perpendicular to S_3, as shown in Figure 8a, c.

All porphyroblasts present in each of the 12 thin sections from the profile plane of the fold (Fig. 8b) contain millipede inclusion trail geometries. The straight foliation defined by the bulk of the inclusion trails across the core of all the porphyroblasts on the lower limb of the fold (the location of the thin section blocks are shown in Figure 8b) pitches SE. It is significant (see below) that in the hinge and upper limb this foliation pitches both SE and NE; therefore, this data is distinguished in Table 1, as are the widths of the zones of partitioned strain that contain the porphyroblasts in Table 2. A photo of the porphyroblast in the hinge region that contains inclusion trails pitching at the lowest angle (45° SE) is shown in Figure 9a (see below).

We measured the width perpendicular to S_3 across the widest part of each porphyroblast (W in Fig. 9a) in the 12 profile plane thin sections mentioned above as well as 12 thin sections cut from 4 vertical slabs (using the thin section blocks shown in Fig. 8c). We did this to provide a measure of the width of the millipede shaped zone of deformation partitioning within which the

porphyroblast grew to see if any differences related to the variation in inclusion trail pitch for the lower limb versus the hinge and upper limb were observable (Table 2). Such measurements are completely dependent on where the thin section cuts through each porphyroblast measured. However, sufficient porphyroblasts were found in each limb for the average width obtained to have some significance. The average width of this zone in the lower limb, where all the porphyroblasts contain inclusions dipping towards the SE in 3-D, is 6.00mm (Table 2). The average width of this zone for porphyroblasts containing inclusion trails that do not have the lower limb dip direction is 2.63mm in the hinge and 3.73mm in the upper limb. Averaging the data for all porphyroblasts containing inclusion trails that do not have the lower limb dip direction gives 3.29mm. Thus the zones of progressive shortening strain that contain porphyroblasts with inclusion trails dipping in the opposite direction to those in the lower limb are 54.8%, on average, the width of those in the lower limb.

3.2 Millipede shaped inclusion trails in porphyroblasts

Figure 9 shows the foliation relationships preserved in and around a porphyroblast from the hinge of the fold in Figure 7, where S_2 in the matrix lies at a high angle to the sub-horizontal axial plane S_3, but where S_2 preserved as inclusion trails lies at a quite oblique angle. There is a spectacular increase in the separation of S_2 foliation planes as they exit into the matrix (shown in Fig. 9a, b) with the distance parallel to S_3 increasing 1.83 times from inside to outside the porphyroblast. At high magnification, the matrix above and below the porphyroblast is dominated by a clockwise asymmetry of curvature of crenulated S_2 into sub-horizontal differentiated crenulation cleavage S_3 (Fig. 9d, e). This differentiation asymmetry is opposite to the anticlockwise shear required if the porphyroblast had been rotated to this orientation after or while it grew. However, in the strain shadow regions to the immediate left and right of the porphyroblast (Figs. 9 and 10) the differentiation asymmetry of S_2 into S_3 is anticlockwise (Fig. 10b, c), which is the shear sense required to rotate the S_2 foliation prior to it being overgrown by the porphyroblast. The pattern of S_1 and S_2 preserved within the strain shadows can be used to test this (Fig. 10). S_2 is a differentiated crenulation cleavage with an anticlockwise differentiation asymmetry due to the curvature of S_1 into S_2 (outside of the strain shadow in Fig. 10b). In Figure

10b, the triangular shaped portion of S_2 in the strain shadow to the right of the porphyroblast is bounded by S_3 on its upper and lower margin with an anticlockwise differentiation asymmetry of S_2 into S_3. This differs from the clockwise differentiation asymmetry that dominates the matrix above and below. Within this triangular portion, as well as within the region now overgrown by the porphyroblast, if clockwise reactivation of S_2 occurred during D_3 rather than development of an S_3 axial plane cleavage (Bell, 1986), this would have resulted in the primary anticlockwise S_1/S_2 differentiation asymmetry being switched to clockwise and produce the geometry shown in Figure 10a, b. Figure 10c shows the rotational effect that such a process would have on S_2 within an ellipsoidal pod of partitioned strain prior to porphyroblast growth.

Figure 10a, b shows that the crenulated cleavage S_1 can be seen between differentiated S_2 seams in the matrix but not in the porphyroblast in a profile plane section (Fig. 8a, b) cut perpendicular to L^2_3. This occurs for all 12-profile plane sections that we cut. All sections cut perpendicular to S_3 and parallel to L^2_3 (Fig. 8a, c) show crenulated S_1 in the porphyroblasts between differentiated S_2 seams but not in the matrix. Therefore, L^1_2 lies sub-parallel to L^2_3 in the matrix but sub-perpendicular to it in the porphyroblasts. Furthermore, L^2_3 changes from porphyroblasts to matrix in sections cut parallel to S_3 as shown in Figure 8a.

3.2.1 Interpretation of trend of L^3_3

The above combination of facts allow us to derive the orientation of the stretching lineation L^3_3, within the axial plane structure S_3 even though we cannot observe it directly because of the seamy nature of S_3. The S_3 seams developed post porphyroblast growth. Therefore, L^1_2 was rotated during D_3 in the matrix but not in the porphyroblasts. Such rotation in more highly strained portions of rock always occurs towards the developing stretching lineation L^3_3 (e.g., Alsop & Holdsworth, 2004). Therefore, L^3_3 must trend at a low angle to the matrix intersection lineation L^2_3 as shown in Figure 8a. A significant result of the low angle between L^2_3 and L^3_3 is that the displacement of S_2 across S_3 differentiated crenulation cleavage seams is minimalized in sections parallel to the profile plane (e.g., Fig. 9b, c, d, e), enhancing the coaxial nature of the resulting matrix geometry and possibly the millipedes.

3.3 A model millipede

Johnson & Moore (1996) used the computer program Mathematica® to produce a three-dimensional representation of a millipede porphyroblast microstructure from one of our samples of Robertson River Metamorphics, Australia collected from the same location as that shown in Figures 5c through 11. Foliations and porphyroblast outlines in a set of 12 closely spaced parallel thin sections were scanned and traced before being imported into Mathematica. The foliation surfaces and porphyroblasts were then reconstructed by redefining the traced curves as functions with a fitting algorithm. The 3D surfaces were then defined using a second set of functions using the techniques in Johnson & Moore (1993, 1996) and Moore & Johnson (1993, 2001). While the results obtained from Mathematica show the major features of the structure quite well, the fitting routines significantly simplify and smooth the final result. The scope for exploring the 3D nature of the structure in Mathematica is also extremely limited. We present a different version of the same millipede structure, reconstructed with the 3D modelling, animation and rendering package Discreet 3D Studio Max™.

The 12 traced sections (from fig. 9 in Johnson & Moore, 1996) were digitized and imported into 3ds Max, where they were scaled and positioned using a vertical spacing of 1.5 mm (Fig. 12a). Once in position, the foliation and porphyroblast surfaces were reconstructed by stretching "U-loft" surfaces between the traced curves. This is akin to stretching a skin over a set of ribs and is demonstrated in Figures 12b and c. These show the 12 curves that define one of the foliation surfaces (Fig. 12b) and the resulting surface created between the curves (Fig. 12c). The final model (Fig. 12d) is composed of the 5 individual foliation surfaces (light grey) and 3 plagioclase porphyroblasts (dark grey).

The geometry of foliation surfaces can be now examined and computer derived 2-D cuts made at any orientation. Horizontal and vertical slices through the model are presented in Figures 13, 14 and 15 (see also Appendix E: E07-E09). The oppositely concave nature of the foliation surfaces is readily apparent in nearly all sections made through these models and reflect the structures observed in thin sections cut horizontally (Fig. 11) and vertically (Fig. 9) through

sample H20C from the Robertson River Metamorphics. The millipede structures preserved in this sample can essentially be described as oppositely facing irregular cup shaped folds where they pass into the matrix and this is best seen by accessing the 3-D VRML model that can be accessed at http://www.es.jcu.edu.au/research/SAMRI/millipede.zip (also presented in Appendix E :"E10-millipede.zip"). Sections cut at almost any orientation (Fig. 15, Appendix E: E09) will display spectacular oppositely concave folds. The only sections that do not consistently display millipede shaped inclusion trail geometries are those cut sub-vertical but perpendicular to the fold profile plane.

4. Interpretation and discussion

4.1 Deformation history versus geometry

When first discovered, the millipede geometry appeared to provide a unique example of a structure that could only be produced by a history of progressive bulk inhomogeneous shortening (Bell & Rubenach, 1980). Recognition that a similar geometry could be produced experimentally during progressive inhomogeneous shearing (Fig. 4b, c) appeared to change this (Johnson & Bell, 1996). However, millipede-like shapes developed in the foliation being folded experimentally during bulk shear are only superficially similar to those that form in and around actual porphyroblasts (compare Figs. 5a, b and c). In examples of millipedes preserved by porphyroblasts, the matrix foliation follows the axial plane of the folds to either side of the central core structure. These are shown by the two lines of hinges marked with heavier black lines in Figure 5c. The matrix "foliation" in the models produced experimentally by inhomogeneous simple shear does not follow the axial plane of the folds to either side of the central core structure. Instead, this foliation cuts across the millipede-like structure into the "porphyroblast" (Fig. 5a, b). This simple test is readily applied to naturally occurring millipedes allowing them to be used to distinguish the deformation history. This is a significant breakthrough because millipede geometries around porphyroblasts are found relatively commonly when vertical thin sections are cut around the compass rather than oriented relative to the matrix foliation.

4.2 The progressive development of the fold

To understand how this fold developed (Fig. 16) we have to be able to explain why the straight portion of S_2 inclusion trails that dominates all porphyroblasts pitches only SE (Table 1) on the lower limb of the fold (Figs. 7 and 8), but both SE and NW in the hinge and upper limb (Table 1). We also have to be able to explain why all porphyroblasts, independent of whether their S_2 inclusion trails pitch SE or NW, contain millipede inclusion trail geometries on their rims that developed during the same deformation that produced the fold.

The curvature of crenulated S_2 into differentiated S_3 (called the S_3 differentiation asymmetry) is dominantly clockwise in the matrix away from the porphyroblasts on both limbs of the fold. Therefore, shear on S_3, once differentiation became significant, was predominantly clockwise, or top to the SE in Figures 7 and 8 (shown schematically in Fig. 6d, e, f) and could rotate S_2 from SE pitches to NE pitches but not vice versa (Fig. 16a, b, c). However, the millipede geometries trapped within the porphyroblasts reveal that they all grew during coaxial bulk shortening. Consequently, those with SE pitching S_2 inclusion trails on the hinge upper limb probably grew before the fold developed as shown in Figure 16d. Those with NW pitching S_2 inclusion trail in the hinge and upper limb porphyroblasts (Fig. 16f) would have grown after the upper NW dipping limb began to form (Fig. 16e) when these portions of the fold contained NW pitching S_2 and the lower limb did not. This interpretation of the history of fold development is supported by the change in width of the zones of progressive shortening shown in Table 2, which for NW pitches decreases to 54.8% the width of the zones with SE pitches in the lower limb, suggesting that progressive shearing repartitioned at a finer scale in these regions to develop the upper limb of the fold as shown in Figure 16f.

We interpret that the fold formed by progressive bulk inhomogeneous shortening with a component of top to the SE shear (e.g., Bell & Hickey, 1997; Ham & Bell, 2004). However, if only clockwise shear occurred on developing S_3, an enormous amount of bulk shortening would have been required to rotate S_2 in the lower limb to its lowest local pitch of 20°. This is shown in Figure 16 where 100% homogeneous bulk shortening of Figure 16b produced SE pitches only as

low as 45° in Figure 16c. This suggests there was some local top to the NW or anticlockwise shear on the lower limb. Detailed examination of the location where the lower limb locally pitches 20° SE revealed that an anticlockwise differentiation asymmetry on S_3 is very locally present.

Of course local components of clockwise and anticlockwise shear (Fig. 2a, b) must have been present to form the millipede geometries; rotation of S_2 occurred in opposite directions along the same S_3 axial plane during the early stages of D_3 (e.g., Fig. 6a, b, c) as can be seen in Figure 9a, b. Therefore, during porphyroblast growth (e.g., Fig. 6a to 6c) no pattern of non-coaxiality had developed and crenulations with both asymmetries developed. However, the final dominance in the matrix of a clockwise differentiation asymmetry for S_3 across the fold suggests that from the commencement of progressive bulk inhomogeneous shortening during D_3, although the deformation was essentially coaxial, there was a small component of top to the SE displacement. This rotated S_2 into steeper orientations until it dipped NW and started to form alternate folds limbs (e.g., Fig. 16e). This explains the preservation of porphyroblasts with inclusion trails pitching SE on both limbs in profile plane thin sections (Fig. 16d). Those porphyroblasts in the hinge and on the upper fold limb containing inclusion trails that vary through the vertical to pitching steeply NW lie in domains wrapped by S_3 that are 54.8% on average shorter in width than those containing porphyroblasts in the lower limb where all the inclusion trails pitch SE (Fig. 16f). This suggests that the deformation during D_3 repartitioned at a smaller scale in the zones that became hinges and NW dipping limbs (compare Fig. 16e and f). This repartitioning resulted in the nucleation and growth of more porphyroblasts that have smaller widths perpendicular to S_3, but which preserve millipede shaped inclusion trails because the deformation was still dominantly coaxial.

4.3 The progressive development of deformation partitioning

Large-scale orogenesis can be a response to crustal shortening, or gravitational collapse of an over thickened orogen; collapse can result from over thickening due to excessive crustal shortening or from extension due to roll back (e.g., fig. 14 in Bell & Newman, 2006). Such large-

scale modes of deformation occur by a general history of progressive bulk inhomogeneous shortening at a low angle to σ_1. Within the orogen, the deformation partitions into portions where a large component of progressive bulk shortening accompanies and even results in the development of significant zones of progressive shearing such as mylonite zones on major thrusts (e.g., fig. 18 in Bell & Newman, 2006). Zones of progressive inhomogeneous shear (i.e., where there is no component of bulk shortening across the shear zone) tend to be restricted to vertical transform or transfer faults where, geometrically, there is no role for bulk shortening. Determining the progressive development of deformation partitioning has generally been an unresolved problem in orogenic belts because the deformation repartitions through the rocks at finer and finer scales as it intensifies. Porphyroblasts provide the best evidence for the role of partitioning in deformation history because they preserve the microstructures that they overgrow from obliteration as the deformation intensifies. Indeed, they provide the only source of data on what took place geometrically in a rock prior to the intensification of the matrix foliation. Porphyroblasts always nucleate and grow prior to the commencement of differentiated crenulation cleavage development (e.g., Spiess & Bell, 1996; fig. 1 in Bell *et al*., 2004). Consequently, for any deformation event that was very intense, they preserve evidence of the character of the deformation partitioning at the initial stages of impact of that event on the rock (e.g., Fig. 6a, b, c); they cease to grow once the deformation intensifies to such a level that a differentiated crenulation cleavage begins to form in their immediate vicinity (Fig. 6d, e, f; Bell *et al*., 2004).

4.3.1 Reactivation weakening in fold hinges

The fold hinge in Figure 7a preserves other intriguing information on the role of deformation partitioning in these rocks during the early stages of deformation. Sub-horizontal S_3, which accompanied the development of this fold, is dominated by a clockwise differentiation asymmetry on both limbs and the hinge (Fig. 9d,e). This indicates that top to the SE shear accompanied bulk shortening as this foliation and the fold developed (Bell & Johnson, 1992). Of course the opposite (anticlockwise) asymmetry is preserved in the rims of all porphyroblasts and in the strain shadows of some (e.g., Fig. 10b), as millipede geometries could not develop without

both shear senses occurring at the same time (e.g., Fig. 2a,b). Furthermore, in one location where the limb pitch in the profile plane on the lower limb locally reduces to 20°, an anticlockwise differentiation asymmetry is very locally preserved.

S_2 preserved as inclusion trails in porphyroblasts on the lower limb always pitches in the one direction averaging around 70° to the SE (Table 1). Similarly pitching S_2 trails in the hinge and upper limb, as well as others that pitch NW (Table 1), plus the dominant top to the south SE shear on S_3, suggests that S_2 dipped 70° to the SE in the early stages of D_3 as shown in Figure 16d and discussed earlier. However, due to the effects of early reversals in shear that predated the final all pervasive clockwise shear that dominates the matrix, S_2 was locally rotated anticlockwise as shown in Figures 9 and 10. This rotation took place without the pervasive development of a differentiated S_3 by antithetic shear on S_2 (Fig. 10c) after it had rotated sufficiently from a high angle to the newly developing D_3 axial plane to be reactivated (Bell, 1986). Furthermore, the amount of anticlockwise rotation of S_2 was large (Figs. 9 and 10); this is particularly significant because this rotation occurred in a local and isolated ellipsoidal zone (Fig. 10c) within the fold hinge where S_3 was developing near orthogonal to S_2 (Fig. 9a, b, c). This extraordinary setting for such an anomalous amount of rotation of the foliation being folded strongly suggests that the interaction of synthetic shear on a newly developing axial plane structure and antithetic shear on a well developed foliation that is being folded can have runaway effects in terms of the amount of strain that can be locally accumulated over a short period of the deformation history. It suggests that if the circumstances are right, after some critical amount of rotation, such a geometry can literally collapse like a pack of cards as shown in Figure 10c, but by a completely ductile process. The critical amount of rotation of a pre-existing foliation away from orthogonal to the newly developing one lies somewhere between 20° and 40°.

4.3.2 Reactivation weakening - a mechanism for crenulation cleavage development and switching off porphyroblast growth

The anomalous rotation of S_2 prior to porphyroblast growth (Fig. 10) in the hinge of the fold in Figure 7 has implications for the mechanism of differentiated crenulation cleavage

development and the switching off of porphyroblast growth that takes place as differentiation begins (e.g., Bell *et al*., 2004). Crenulation cleavage development during the 1960's and 1970's was considered to be a product of buckling and dissolution of the long limb through a mechanism of pressure solution involving the effect of stress differentials on chemical potential (e.g., Gray & Durney, 1979). However, stress differentials around a grain do not accumulate as the deformation continues; they vary as deformation occurs and remain small making it difficult to accept them as a significant driving force for the slow process of dissolution and solution transfer.

An alternative mechanism was proposed in the 1980's involving the effects of deformation partitioning. This mechanism suggests differentiated crenulation cleavage seams form along zones of progressive shearing (e.g., Fig. 1; Bell 1981). When a zone of progressive shearing begins to form, dislocation densities accumulate in non platy minerals within this zone; this increases chemical potential gradients from the rim to core causing dissolution and removal of the rim and eventually of the whole. This brings together platy minerals, which do not accumulate dislocations, into differentiated crenulation cleavage seams (Fig. 6d, e, f; Bell & Cuff, 1989). After initiation of the zone of progressive shearing, non platy minerals on the margins of these zones are progressively strained increasing chemical potential gradients from rim to core these grains and causing their dissolution and removal. The platy (and locally some fibrous) minerals are left behind as cleavage seams that widen the more shear strain that has occurred along the zone of progressive shearing (Bell & Cuff, 1989). In this model, bulk shear operates along the crenulation cleavage seam, as shown in Figures 1 and 6d, e, and equates with that acting along S_3 in Figures 7 to 9.

In the early stages of crenulation development, once some rotation of the crenulated cleavage has occurred, reactivational shear along this cleavage (S_2 in the case described herein) can occur. If rapid collapse of this zone occurred, similar to that discussed in the previous section, then differentiated cleavage development may occur through the same reactivational weakening process. This could go a long way to help explaining the link between the cessation of porphyroblast growth and the commencement of this stage of crenulation cleavage development that has been observed and pondered over for 2 decades (e.g., Spiess & Bell, 1996).

4.4 Millipedes in 3D

Figures 13, 14 and 15 show that millipede geometries can be seen in most thin section orientations within porphyroblasts (see also Appendix E: E07-E09). This is not the case for cut effect millipede-like geometries that are common in thin sections cut sub-parallel to foliation intersection/inflection axes preserved in porphyroblasts (FIAs) containing spiral shaped inclusion trails. As shown in Figures 13, 14 and 15, where the inclusion trails are continuous with the matrix foliation millipede geometries can be seen in almost all thin sections orientations. The only orientation where they tend be uncommon is for thin sections cut parallel to the L^2_3 and perpendicular to S_3 such as the 030° section in Figure 15. This has considerable significance because even where porphyroblasts pre-date the matrix foliation and are completely truncated by it, millipede geometries will be preserved in most thin section orientations within the porphyroblasts and revealed in spite of cutting sections relative to the matrix microstructures. Therefore, if two or more differently oriented sections are cut relative to geographic coordinates, and the porphyroblasts contain millipede microstructures, these will be revealed in at least one of these sections. For the discerning reader we have constructed a virtual reality model (VRML), which can be accessed on the world wide web at the URL http://www.es.jcu.edu.au/research/SAMRI/millipede.zip (Appendix E: E10-millipede.zip). This model allows the reader to examine the millipede geometry in Figures 13 to 15 in full colour in 3-D and rotate it for observation from any direction. At the push of a button the model will split along the planes shown in Figure 14.

4.5 Cut effect millipede-like structures

Stallard *et al*. (2002) make the assertion that millipede microstructures may simply represent a peculiar 2-D slice through a 3-D spiral. Certainly, as mentioned above, cut effect millipede-like structures appear when thin sections are cut parallel to the FIA through natural spiral inclusion trails preserved in porphyroblasts. We compared several computer-derived slices through a simple model spiral, constructed using the “soft selection” tool in 3d Studio Max with slices through an actual millipede. A rotation of 270° was applied to the central vertex of a model

composed of seven parallel sheets, each defined by 100 x 100 x 5 vertices. The effect produced was that the central part of the model was rotated 270° with a decreasing amount of rotation with distance away from the central vertex. A cut-away view of the model spiral is shown in Figure 17a. The separated elements of the spiral in Figure 17a compare favourably with those produced by Stallard *et al*. (2002). Sections cut parallel to the axis of rotation show oppositely curved or closed-loop structures (000° in Fig. 17b). These structures may exhibit a resemblance to sections through genuine millipedes. However, the opposite extremities of the curving inclusion trails tend to start to bend back towards each other, in some cases making a closed loop (compare Figs. 17b and 15), in complete contrast with true millipedes, which never have this character. We have also shown that sections of almost any orientation through genuine millipede structures will display oppositely curving foliation traces. The converse is true for sections through spirals. Only sections cut very close to the axis of rotation will display such structures. The vast majority of sections will display either spirals or simple sigmoidal foliation traces (Fig. 17b; see also Appendix E: E11-E15). Therefore, it is relatively easy to distinguish cut effect millipede-like structures from true millipedes. One simply needs to cut a thin section striking at 45° to the one in which the millipede-like geometry appeared. If spiral inclusion trails are revealed, then the geometry was produced by a cut effect.

4.6 Transection of sheath fold hinges

Alsop & Holdsworth (2004, p. 1578) described natural sheath folds where the intersection lineation of the foliation being generated transects the hinge line. Alsop & Holdsworth (unpublished data) have been exploring ways of discriminating zones of high strain containing sheath folds resulting from a deformation history of inhomogeneous simple shear from those that formed during bulk inhomogeneous shortening. If transection occurs in samples where the deformation history was of the former type (Alsop, G.I. pers. comm. 2006), but not in those where it was the latter, this would be of considerable interest. It might reflect the transection of fold axial plane geometries resulting from the inhomogeneous simple shear experiments discussed herein and eventually provide a quantifiable discriminator of deformation history for sheath fold development. One would have to be certain that the sheath folds formed at the same

time as the cleavage rather than being overprinted by it because it is now apparent that the latter history is common in regional folds (Ham & Bell, 2004; Bell *et al*., 2005).

5. Conclusions

Millipede structures with an axial plane foliation can only form by progressive bulk inhomogeneous shortening.

Millipede-like shapes transected by a foliation that accompanied their development form during progressive inhomogeneous simple shear.

References

Aerden D.G.A.M., 1991. Foliation-boudinage control on the formation of the Rosebery Pb-Zn orebody, Tasmania. *Journal of Structural Geology* **13**, 759-775.

Alsop, G.I. and Holdsworth R.E., 2004. The geometry and topology of natural sheath folds: a new tool for structural analysis. *Journal of Structural Geology* **26**, 1561–1589.

Beaumont-Smith, C.J., 2001. The role of conjugate crenulation cleavage in the development of 'millipede' microstructures. *Journal of Structural Geology* **23**, 973-978.

Bell, T.H., 1981. Foliation development: the contribution, geometry and significance of progressive bulk inhomogeneous shortening. *Tectonophysics* **75**, 273-296.

Bell, T.H., 1986. Foliation development and refraction in metamorphic rocks: reactivation of earlier foliations and decrenulation due to shifting patterns of deformation partitioning. *Journal of Metamorphic Geology* **4**, 421-444.

Bell, T.H. and Cuff, C., 1989. Dissolution, solution transfer, diffusion versus fluid flow and volume loss during deformation/metamorphism. *Journal of Metamorphic Geology* **7**, 425-448.

Bell, T.H. and Hickey, K.A., 1997. Distribution of pre-folding linear movement indicators around the Spring Hill Synform, Vermont: significance for mechanism of folding in this portion of the Appalachians. *Tectonophysics* **274**, 275-294.

Bell, T.H. and Johnson, S.E., 1989. The role of deformation partitioning in the deformation and recrystallization of plagioclase, orthoclase and microcline in the Woodroffe Thrust Mylonite Zone. *Journal of Metamorphic Geology* **7**, 151-168.

Bell, T.H., Johnson, S.E., 1990. Rotation of rigid objects during ductile deformation: well established fact or intuitive prejudice? *Australian Journal of Earth Sciences* **37**, 441-446.

Bell, T.H. and Johnson, S.E., 1992. Shear sense: a new approach that resolves problems between criteria in metamorphic rocks. *Journal of Metamorphic Geology* **10**, 99-124.

Bell, T.H. and Newman, R., 2006. Appalachian orogenesis: the role of repeated gravitational collapse. In Styles of continental compression, R. Butler and S. Mazzoli, (eds.) *Special Papers of the Geological Society of America* **414**, 95-118.

Bell, T.H. and Rubenach, M.J., 1980. Crenulation cleavage development - evidence for progressive bulk inhomogeneous shortening from "millipede" microstructures in the Robertson River Metamorphics. *Tectonophysics* **68**, T9-T15.

Bell, T.H. and Welch, P.W., 2002. Prolonged Acadian orogenesis: revelations from foliation intersection axis (FIA) controlled monazite dating of foliations in porphyroblasts and matrix. *American Journal of Science* **302**, 549-581.

Bell, T.H., Hickey, K.A., Upton, G.J.G., 1998. Distinguishing and correlating multiple phases of metamorphism across a multiply deformed region using the axes of spiral, staircase and sigmoidally curved inclusion trails in garnet. *Journal of Metamorphic Geology* **16**, 767-794.

Bell, T.H., Ham, A.P. and Hickey, K.A., 2003. Early formed regional antiforms and synforms that fold younger matrix schistosities: their effect on sites of mineral growth. *Tectonophysics* **367**, 253-278.

Bell, T.H., Ham, A.P. and Kim H.S., 2004. Partitioning of deformation along an orogen and its effects on porphyroblast growth during orogenesis. *Journal of Structural Geology* **26**, 825-845.

Bell, T.H., Ham, A.P., Hayward, N. and Hickey, K.A., 2005. On the development of gneiss domes. *Australian Journal of Earth Sciences* **52**, 183-204.

Cihan, M. and Parsons, A., 2005. The use of porphyroblasts to resolve the history of macro-scale structures: an example from the Robertson River Metamorphics, North-Eastern Australia. *Journal of Structural Geology* **27**, 1027-1045.

Davis, B.K., 1995. Regional-scale foliation reactivation and reuse during formation of a macroscopic fold in the Robertson River metamorphics, North Queensland, Australia. *Tectonophysics* **242**, 293-311.

Davis, T.P., 2004. Mine-scale structural controls on the mount Isa Zn-Pb-Ag and Cu orebodies. *Economic Geology* **99**, 543-559.

Ghosh, S.K., 1975. Distortion of planar structures around rigid spherical bodies. *Tectonophysics* **28**, 185-208.

Gray, D.R. and Durney D.W., 1979. Crenulation cleavage differentiation - implications of solution-deposition processes. *Journal of Structural Geology* **1**, 73-80.

Ham, A.P. and Bell, T.H., 2004, Recycling of foliations during folding: *Journal of Structural Geology* **26**, 1989-2009.

Hayward, N., 1992. Microstructural analysis of the classic snowball garnets of southeast Vermont. Evidence for non-rotation. *Journal of Metamorphic Geology* **10**, 567-587.

Johnson, S.E. and Bell, T.H., 1996. How useful are “millipede” and other similar porphyroblast microstructures for determining syn-metamorphic deformation histories. *Journal of Metamorphic Geology* **14**, 15-28.

Johnson S.E. and Moore, R.R., 1993. Surface reconstruction from parallel serial sections using the program Mathematica: example and source code. *Computers and Geosciences* **19**, 1023-1032.

Johnson, S.E. and Moore, R.R., 1996. De-bugging the 'millipede' porphyroblast microstructure: a serial thin-section study and 3-D computer animation. *Journal of Metamorphic Geology* **14**, 3-14.

Lagoeiro, L. and Hippertt, J., Lana, C., 2003. Deformation partitioning during folding and transposition of quartz layers. *Tectonophysics* **361**, 171-186.

Mares, V.M., 1998. The structural development of the Soldiers Cap Group within a portion of the eastern fold belt of the Mount Isa Inlier: a succession of near-horizontal and near-vertical deformation events and large-scale shearing. *Australian Journal of Earth Sciences* **45**, 373-387.

Moore, R.R. and Johnson, S.E., 1993. Reconstruction of inclusion surfaces within metamorphic garnet crystals. *Mathematica Journal* **3**, 70-75.

Moore, R.R. and Johnson, S.E., 2001. Three dimensional reconstruction and analysis of complexly folded surfaces using Mathematica. *Computers and Geosciences* **27**, 401-418.

Sayab, M., 2005. N-S shortening during orogenesis within the Mt Isa Inlier (NW Queensland, Australia): the preservation of early W-E trending foliations in porphyroblasts revealed by independent 3D measurement techniques. *Journal of Structural Geology* **27**, 1445-1468.

Siame, L.L, Bellier, O., Sebrier, M. and Araujo, M. 2005. Deformation partitioning in flat subduction setting: Case of the Andean foreland of western Argentina (28 degrees S-33 degrees S). *Tectonics* **24**, TC5003.

Spiess, R. and Bell, T.H., 1996. Microstructural controls on sites of metamorphic reaction: a case study of the inter-relationship between deformation and metamorphism. *European Journal of Mineralogy* **8**, 165-186.

Stallard, A.R., Hickey, K.H., 2001. Fold mechanisms in the Canton Schist: constraints on the contribution of flexural flow. *Journal of Structural Geology* **23**, 1865-1881.

Stallard, A., Ikei, H. and Masuda, T. 2002. QuickTime movies of 3D spiral inclusion trail development**.** In Bobyarchick, A. (ed.). Visualisation, Teaching and Learning in Structural Geology. *Journal of the Virtual Explorer* **9**, 17-30.

Stewart, L.K., 1997. Crenulation cleavage development by partitioning of deformation into zones of progressive shearing (combined shearing, shortening and volume loss) and progressive shortening (no volume loss): quantification of solution shortening and intermicrolithon-movement. *Tectonophysics* **281**, 125-140

Section D:

Timing nappe development in multiply tectonised rocks:

A new approach

Abstract

The succession of foliation intersection/inflection axes preserved as inclusion trails in porphyroblasts (FIAs) from the Lebanon Antiformal Syncline of SE New Hampshire, USA, document changes in bulk shortening geometry associated with emplacement and refolding of a large-scale recumbent fold (the Blue Hills Nappe). A sequence of four FIAs trending NW-SE, NE-SW, E-W and NNW-SSE has been distinguished based upon overprinting criteria plus inclusion trail composition, texture and orientation. This succession indicates a general clockwise rotation in the direction of horizontal bulk shortening during Acadian orogenesis. Metamorphic phase relations and pseudosections used to examine the P-T conditions during deformation and FIA development indicate an increase in both pressure and temperature associated with inversion of the stratigraphic sequence. Analysis of asymmetries recorded by the inclusion trails reveals a spectacular dominance of top to the south-east directed, non-coaxial horizontal shear during nappe emplacement and subsequent refolding that is attributed to repeated episodes of gravitational collapse in the orogen core to the west that progressively rotated, translated and amplified originally sub-vertical folds and foliations into sub-horizontal orientations.

Keywords: Lebanon Antiformal Syncline; Blue Hills Nappe; shear sense; non-coaxial deformation; FIA; porphyroblasts; inclusion trails; deformation partitioning; reactivation

1. Introduction

Inclusion trails in porphyroblasts in tectonised metamorphic rocks contain a wealth of information regarding metamorphism and deformation that occurred during orogenesis (Sayab, 2005). Correlation between the progressive development of micro-structural features, porphyroblastic mineral growth and large-scale bulk movement directions is made possible using a technique for measuring the orientation of Foliation Inflexion/ Intersection Axes within porphyroblasts (FIA) preserved as inclusion trails (Hayward, 1990; Bell *et al*., 1995) combined with a detailed study of inclusion trail asymmetries (e.g., Bell & Hickey, 1997; Bell *et al*., 2003). Consistent trends of FIA for large distances along orogens (e.g., Bell & Mares, 1999; Bell &

Newman, 2006) suggest that changes in bulk movement direction, and hence relative plate motion (Bell & Wang, 1999), during orogenesis are reflected in changes in the orientation of successive sets of FIA. If a consistent distribution pattern and succession of FIA trends can be established, there is potential to distinguish and correlate multiple phases of metamorphism and tectonism, many of which predate matrix microstructures (Ham & Bell, 2004).

Matrix foliations in metamorphic rocks that have undergone multiple phases of tectonism are commonly composite fabrics that have been re-used, re-oriented and reactivated since their formation (Davis, 1995). Reactivation of the matrix foliation or bedding tends to obscure or destroy early formed microstructures, except in porphyroblasts where these subtle effects may be preserved. Even a relatively minor deformation event will commonly produce a foliation against a rigid object such as a porphyroblast but may have a lesser effect in the matrix and on larger macroscopic structures. As a porphyroblast grows during the early stages of deformation, it preserves the foliation that develops up against its edge (Bell & Bruce, 2006; thesis Section B). The matrix foliation intensifies against the porphyroblast rim because the rigid porphyroblast takes up no strain. The most pronounced foliation development occurs against the margins of any rigid bodies in the rock because these cannot take up any strain internally, and appears to form perpendicular to the direction of bulk shortening (Bell & Mares, 1999; Bell & Wang, 1999).

The curvature of inclusion trails preserved within porphyroblasts provides vital information on the dominant sense of shear operating during metamorphism and deformation. Previous studies (e.g., Bell *et al*., 2003; Ham & Bell, 2004; Cihan & Parsons, 2005) indicate that most of the deformation taking place during the development of both sub-vertical and sub-horizontal foliations is relatively coaxial on the bulk scale. This occurs even though the development of the foliations themselves involves heterogeneous non-coaxial strain (Bell, 1981; Bell & Newman, 2006). This study utilises inclusion trails preserved within garnet, andalusite and staurolite porphyroblasts to reveal a remarkable and enduring dominance of top to the south east shear that provides evidence for the timing and mechanism of emplacement of a regional-scale recumbent fold (the Blue Hills Nappe) and the processes operating during refolding of the overturned limb to form the Lebanon Antiformal Syncline of SE New Hampshire.

2. Geologic setting

2.1 Tectonic framework

The Appalachians extend for over 3000 km along the east coast of the North American continent from Alabama in the south to Newfoundland in easternmost Canada. Several major periods of orogenesis have been suggested to account for the development of this mountain chain (e.g., Hatcher, 1981; Robinson, 1983). These consist of the Ordovician Taconic, the late Devonian Acadian and the Carboniferous to Permian Alleghanian events. However, in some sections of the belt, only one or two of these periods of orogenesis are evident.

Eastern New England, including the area which is the subject of this study, is dominated by Acadian age (~423-355 Ma?; Eusden *et al*., 2000; Bell & Welch, 2002) structures and metamorphism. The Acadian orogen is thought to be the result of the final closure of the Iapetus Ocean (proto-Atlantic) and the docking of Avalonia and Baltica (ancestral Europe) with Laurentia (Kent & Keppie, 1988) to form Euramerica. The final phase of orogenesis involved a rotation of Gondwana with respect to the Euramerican landmass, culminating in the late Carboniferous/Permian Alleghanian orogeny and resulted in the assembly of the super continent, Pangea (Kent & Keppie, 1988). Rifting and separation of the continents to form the modern Atlantic Ocean commenced at approximately 200Ma.

The Taconic, Acadian and Alleghanian phases of Appalachian tectonism are usually regarded as separate and distinct orogenic events, with episodes of deformation being punctuated by periods of quiescence (e.g., Osberg, 1983; Rodgers, 1970). This tends to imply a stop-and-start nature to the motion of the tectonic plates. Recent work (Bell & Welch, 2002; Lisowiec, 2005; Rich, 2005; Bell & Newman, 2006) using U-Th-Pb techniques to date individual monazites in porphyroblasts, suggests that deformation and metamorphism was continuous for most of the history of the Appalachian orogen. It seems likely that deformation continued as the plates converged, with peaks in the intensity of deformation and metamorphism corresponding to times of continent/continent or continent/micro-continent collision.

2.2 Stratigraphy

The Central Maine Terrane (Fig. 1) is interpreted as a large Silurian to early Devonian depositional basin extending from Connecticut to Maine and bounded by the Bronson Hill Anticlinorium to the west and the Nonesuch River fault zone to the east. The meta-turbidite sequence represents an eastward thickening continental margin deposit that appears to have been deposited before an advancing tectonic front (Osberg, 1988; Bradley *et al*., 1998).

Billings (1956) mapped all the metasedimentary rocks of the Central Maine Terrane as lower Devonian Littleton Formation. Eusden *et al*. (1987) subdivided the sequence observed around the Lebanon Antiformal Syncline into five units and correlated these with the Silurian Rangeley, Perry Mountain, Smalls Falls and Madrid Formations and the Devonian Littleton or Carrabassett Formation in west-central Maine. The age of the Carrabassett formation is constrained by shelly fossils found in correlatives at three localities in New Hampshire as late Llandoverian or pre 438 Ma (Moench *et al*., 1995). Well preserved graded bedding indicates that the majority of the rock strata in the study area are inverted.

2.3 Structure and metamorphism

The Lebanon Antiformal Syncline (Fig. 2, Appendix D) is situated on the eastern edge of the meta-turbidite sequences of the Central Maine Terrain that were multiply deformed and metamorphosed during the Acadian and possibly the Alleghanian orogenies (Eusden *et al*., 1987). Early low P/ intermediate T metamorphism involved the development of strong axial planar cleavages and the growth of Buchan facies zone minerals. This was followed by high T metamorphism associated with the intrusion of Acadian plutons (Eusden *et al*., 1984). A final stage of retrogressive metamorphism, M_4, is characterised by sericitisation of alumininosilicates and chlorite pseudomorphs of biotite and garnet.

The rocks of the Lebanon Antiformal Syncline are located on the overturned limb of a major recumbent fold (Fig. 3), the Blue Hills Nappe (F_1 of Eusden *et al*., 1987). This limb is

refolded by tight to open, south-east-verging folds with generally shallow, north-east- or south-west-plunging axes. These later generation folds (F_2) have a distinctive, spaced axial planar differentiated crenulation cleavage and are seen to fold both S_0 and S_1. The F_2 folds are considered the principal cause of the observed outcrop pattern and the general north-west dip of both S_0 and S_1. F_3 folds are represented by the broad scale change in trend of the F_2 fold axes from E-W in the south-west of the mapped area to nearly N-S in the north-east (Eusden *et al*., 1987).

A feedback mechanism between crustal anatexis and contractional deformation has been proposed for adjacent west-central Maine (Solar *et al*., 1998; Solar and Brown, 1999, 2000; Johnson *et al*., 2003) that is supported by U-Pb zircon and monazite ages for granite crystallisation that coincide with ages of syntectonic metamorphism in the same area (Smith and Barreiro, 1990). This model, in which granite ascent, metamorphic mineral growth and deformation are focused in zones of high strain (Solar and Brown, 2001) contrasts with an alternate view (e.g., Gudotti, 2000) that regional metamorphism in this part of the Central Maine Terrain was primarily the result of advective heat flow associated with the emplacement of "post-tectonic" granites.

Dates of 377±? and 363±? Ma have been established for late syn- and post-tectonic two-mica granites that cross-cut the sequence that forms the Lebanon Antiformal Syncline (Eusden & Barriero, 1988) using U/Pb in monazite techniques. Elongate quartz diorite bodies that intrude the sequence are most likely correlatives of the lithologically similar Winnipesaukee and Spaulding quartz diorites, dated at 393±5 Ma by Rb/Sr whole rock techniques (Lyons & Livingston, 1977 and recalculated by Steiger & Jager, 1977). The Nonesuch River fault system cuts off earlier formed structures, resulting in the juxtaposition of the Silurian and Devonian rocks of the Lebanon Antiformal Syncline against the Precambrian and/or Ordovician (Lyons *et al*., 1982; Olszewski, 1984) Merrimack Group rocks to the south-east.

3. Description of samples

104 spatially oriented samples were taken from road cuttings and isolated outcrops across the Lebanon Antiformal Syncline and surrounding areas. 751 vertical and horizontal thin sections were prepared from these samples and provided the foundation for the microstructural analysis. 55 of these samples contain porphyroblasts with well preserved inclusion trails. These samples consist of rusty sulphidic and non-rusty pelitic and carbonaceous schists of predominantly staurolite to lower sillimanite grade. The porphyroblastic phases present are garnet, andalusite and staurolite. The matrix contains a well developed schistosity (S_m), defined by preferentially aligned muscovite, elongate quartz grains and graphite, that is parallel to the original bedding (S_0), and a distinctive spaced crenulation cleavage (S_2) defined by reoriented muscovite and quartz. Additional matrix forming minerals locally include plagioclase, chlorite, ilmenite, sillimanite, tourmaline and pyrite. Sillimanite occurs both as fibrolite in radiating clusters, knots or mats and as prismatic crystals. Porphyroblasts of biotite with quartz strain shadows are common. Chlorite occurs as large, well developed crystals that cross cut the matrix foliation and as a retrograde alteration product of biotite, muscovite, garnet and sillimanite. The alteration of garnet commonly resulted in a core surrounded by chlorite that retains the original euhedral shape of the garnet porphyroblast, similar to those described by Guidotti & Johnson (2002).

4. Inclusion trail morphology

4.1 Sigmoidal and staircase inclusion trails

Williams (1994) defined sigmoidal inclusion trail geometries as those that exhibit less than 90^0 of internal foliation (S_i) curvature within the porphyroblast (Fig. 4a). These are the most common geometries encountered in samples from the Lebanon Antiformal Syncline and are interpreted to be the result of porphyroblast growth during a single episode of deformation. Sigmoidal inclusion trails are preserved in garnet, andalusite and staurolite. Common inclusions are quartz, graphite and ilmenite with minor biotite and tourmaline. Several samples contain

partial or complete pseudomorphs of coarse grained muscovite after andalusite and retain the original sigmoidal geometry of opaque inclusion trails.

Staircase shaped inclusion trail geometries (Fig. 4b) consist of more than one S_i antiform/ synform pair and are interpreted to be the result of multiple episodes of syntectonic porphyroblast growth. Many of the samples studied contain garnet porphyroblasts that preserve fine grained sigmoidal trails in their cores truncated by coarser sigmoidal trails in their rims. The trails in the garnet rims are commonly continuous with the matrix foliation (e.g., Fig. 5a, b). These core/ rim trails are useful for relative timing. Alternatively, well defined sigmoidal core trails may be separated from the matrix by an inclusion-free rim.

4.2 Differentiated crenulation cleavages

Several samples contain garnet that overgrew a differentiated crenulation cleavage that developed in the matrix prior to porphyroblast growth (Fig. 4c). Fine, elongate quartz and ilmenite grains define an early formed foliation that has been overprinted by a crenulation cleavage at stage 4 of development (Bell & Rubenach, 1983). The inclusion free zones separating the folded quartz grains preserve the remains of mica seams that have been entirely replaced by garnet. Measurements of these structures allow the determination of pseudo-FIAs or pFIAs (see below, Bell & Newman, 2006), so called because they predate porphyroblast growth. They are interpreted as asymmetric matrix microstructures that were overgrown in contrast to true FIAs that are matrix foliations incorporated as inclusion trails in the early stages of the same deformation that crenulated them. They are preserved in numerous garnet cores in several of the samples studied. In some cases, curvature of their axial planes can be noted and used to determine a true FIA (e.g., Bell *et al*., 1998) for that sample which can be different from the pFIA.

5. Methods

5.1 FIA determination

5.1.1 Asymmetry method

The mean trend of the FIA for a given sample is ascertained by cutting a series of at least eight differently oriented vertical thin sections and examining the geometry of the inclusion trails (S_i) preserved within the porphyroblasts (Hayward, 1990; Bell *et al*., 1995; Bell *et al*., 1998). The trend of the FIA is found by initially preparing a set of six vertical sections, cut at 30^0 intervals from an oriented horizontal slab (i.e., trends of 0, 30, 60, 90, 120 and 150 degrees). The blocks are marked and cut in such a way that the final thin sections have their strike parallel to their long edge. Each section is examined from the same direction around the compass under a petrological microscope and the geometry of the inclusion trails is recorded. A FIA determined within a 10° range can be measured by preparing two additional sections covering the 30° interval over which the flip in asymmetry is observed. This is seen to occur between 90^0 and 120^0 for the model shown in Fig. 6. In this example, two sections with strikes of 100^0 and 110^0 are prepared and examined. The change from "S" shaped to "Z" shaped inclusion trails is now constrained to between 110^0 and 120^0 with the mid-point being recorded as the trend of the FIA (Bell *et al*., 1998). The FIA trend for a single sample is the mean for the total population of porphyroblasts present in the thin sections analysed. See also Appendix E: "E01-asymmetry method.mov" for a QuickTime movie that illustrates the basic principles of the asymmetry method.

Figure 6 shows that the amount of curvature of individual inclusion trails in a given thin section may vary significantly depending on what part of the three dimensional structure intersects the plane of the section. This "cut effect" is most apparent in sections cut close to the FIA and can cause confusion when apparent spiral shaped inclusion trails are encountered where only simple sigmoidal trails are expected (Bell & Bruce, 2006; thesis Section B). The asymmetry approach works well where the curvature of the inclusion trails can be easily seen but fails where the inclusions are predominately straight or inconsistent.

5.1.2 The "FitPitch" computer program

An alternative method of FIA measurement has been developed by Domingo Aerden of the University of Grenada, Spain (Aerden, 2003). Planar microstructures with preferred orientations in a rock can be characterised by the pitches of their intersection-lines on different sections. A uniformly-dipping plane can be uniquely identified by the pitches (or apparent dips) of this plane measured in several sections of different orientation. The 'FitPitch' computer program takes measured pitch or strike angles of inclusion trails in a set of differently orientated thin sections and compares them to the theoretical intersection lines of one, two or three model planes on the same sections. The best solution is considered to be the one which minimises the deviation between the data and the model planes. The intersection of the best-fit model planes are FIAs. A detailed discussion of the program principles can be found in Aerden (2003) and thesis Section A.

5.2 Relative timing criteria and FIA succession

Different porphyroblastic phases that grew during progressive metamorphism in a single sample can preserve different portions of the deformation history (Bell & Hickey, 1999). Changes in FIA orientation can also occur within an individual porphyroblast. For example, porphyroblasts that have undergone multiple episodes of growth may contain different FIAs in the core and rim (e.g., Fig. 5a, b). A FIA succession for a multi-FIA sample can be determined by utilising established concepts of overprinting. If a consistent succession is observed, the data from all samples can be combined to derive the relative timing of each FIA (Bell *et al*., 1998).

6. Results

6.1 FIA data

The orientations of ninety eight FIAs (Table 1, Fig. 7a) were measured using porphyroblasts within fifty five spatially oriented samples collected from the Lebanon Antiformal

Syncline. Sixty five of these were measured using garnet porphyroblasts. Thirty four samples contain a single garnet FIA and fifteen preserve multiple garnet FIAs including three that contain pFIAs (the result of porphyroblast growth over a pre-existing crenulation cleavage) in addition to a true FIA formed from the curvature of that cleavage (samples MB019, MB023 and MB042). Ten preserve core and rim FIAs (samples MB010, MB019, MB030, MB035, MB063, MB074, MB076, MB080, MB090 and MB095). Seven garnet FIAs were calculated using the FitPitch computer program. Twenty three FIAs were measured from samples containing andalusite. Six samples preserve only a single andalusite FIA; thirteen contain an andalusite FIA in addition to a single garnet FIA; three preserve an andalusite FIA plus garnet core and rim FIAs (samples MB063, MB074 and MB080) and three contain andalusite, garnet and staurolite FIAs (samples MB063, MB066 and MB107). Ten staurolite FIAs were obtained from eight samples. Two samples preserve multiple generations of staurolite FIAs (samples MB042 and MB066). Sample MB063 contains andalusite and staurolite FIAs in addition to garnet core and rim FIAs.

Figure 7a shows all FIA trends measured whereas Figs. 7b, c and d show the data separated for garnet, staurolite and andalusite. The total FIA data (Fig. 7a) shows three modal peaks at 40-60°, 70-90° and 140-170°. This distribution is similar to that for the garnet FIAs (Fig. 7b). Staurolite FIAs (Fig. 7c) display two dominant trends at 60-100° and 140-170°. Andalusite FIAs (Fig. 7d) show a remarkably consistent trend of between 40° and 70°. Andalusite commonly occurs as large (up to several cm) porphyroblasts with high aspect ratios. These crystals are randomly oriented mostly within the plane of foliation (i.e., they tend to have their long axis sub-parallel to bedding (S_0) and the bedding parallel foliation). This implies either that rotation of the andalusite into parallelism with the foliation occurred due to layer flattening during the development of S_1 or that the andalusite preferentially grew sub-parallel to S_0 and S_1. Any significant amount of rotation after their growth would result in a wide range of andalusite FIA orientations. The tight distribution of FIA trends suggests that the degree of rotation during the development of S_1 (or subsequent foliations) was negligible and that the porphyroblasts nucleated preferentially with their long axis sub-parallel to S_0 and the developing foliation (S_1) either because of bulk compositional variation related to the primary layering or in response to the accumulation of strain associated with S_1 development.

6.2 Relative timing of FIAs

A paragenesis of FIA development can be built up by examining overprinting criteria, metamorphic phase relations and textural characteristics of inclusion trails. Core/rim textures were used to establish the relative timing of FIAs since a foliation preserved in the core of a porphyroblast must be older than that in the rim. Samples containing multiple porphyroblastic phases allowed the relative timing of FIAs to be established where it could be determined that growth of one mineral preceded the other. Textural characteristics and the degree of continuity between the internal foliation (S_i) and the matrix foliation (S_e) were used to correlate single FIA samples with the succession determined from the multi-FIA samples. Several samples contain more than one generation of the same porphyroblastic mineral phase. Separate generations were distinguished by the size, shape and composition of their inclusions and whether or not the internal foliation shows continuity with the matrix foliation. For example, early formed garnet porphyroblasts typically have inclusions dominated by very fine quartz grains that are truncated by the matrix foliation. Later generations have coarse inclusions that may include quartz, ilmenite, biotite, tourmaline and staurolite and show varying degrees of continuity with the matrix foliation.

6.3 FIA sets

Relative timing criteria separate the data into four FIA groups (Fig. 8). The earliest formed group (FIA set 0; NW-SE) includes garnet pFIAs, garnet core and single garnet FIAs that pre-date andalusite growth and have inclusion trails that are discontinuous with the matrix foliation. FIA set 1 (NE-SW) is made up of andalusite, garnet core and single garnet FIAs that have inclusion trails consisting of fine grained quartz and showing varying degrees of continuity between their internal foliations and the matrix; they are commonly truncated. One garnet rim FIA (sample MB076) is present in set 1 and it has same trend as that preserved in the core. FIA set 2 (E-W) is largely made up of garnet rim, single garnet and staurolite FIAs. The inclusion trails of set 2 are generally continuous with the matrix foliation and are composed of coarse grained quartz, ilmenite, biotite and tourmaline. FIA set 3 (NNW-SSE) has a similar orientation

to set 0 but is made up of staurolite, single garnet and garnet rim FIAs all of which show continuity between their inclusion trails and the matrix foliation. Fibrolite is commonly present in the rims of garnet and staurolite porphyroblasts that preserve FIA set 3. Garnet grew during all prograde metamorphic episodes and consequently preserves all four FIA sets. The majority of the andalusite FIAs belong to set 1. Staurolite preserves FIA sets 2 and 3.

6.4 Asymmetry of inclusion trails

Deformation partitioning controls the development of new foliations in part by rotation of older ones so the geometry developed must reflect the strain field (Bell & Johnson, 1992). To determine the local shear sense for a particular deformation event, one needs only to distinguish the curvature of an earlier formed foliation into a later one (from zones of low strain to zones of high strain). The curvature of early foliations preserved as inclusion trails in porphyroblasts or in strain shadows of relatively large heterogeneities in the rock, allows the determination of local shear sense for early generations of foliations and reveals a kinematic history much more extensive than that preserved in the matrix.

The asymmetry of inclusion trail curvature for FIA sets 1 and 2 was recorded looking north-east in a section at a high angle to the FIA trend (e.g., for set 1 FIAs trending at 40-70°, the curvature of the inclusion trails was recorded by looking at vertical thin sections striking 130-160° and looking NE). The curvature of FIA set 0 and 3 inclusion trails was recorded looking north-west in sections perpendicular to the FIA trend. The cumulative frequency plot of asymmetry data (Fig. 9) shows that most of the porphyroblast growth occurred during the development of shallow dipping foliations (i.e., the recorded asymmetry is a sub-vertical foliation curving into a shallow dipping foliation). This is strikingly clear for FIA sets 1 and 2, both of which show a spectacular dominance of clockwise (top to the south east) asymmetries that developed during vertical shortening. FIA set 0 shows a high proportion of porphyroblast growth during vertical shortening with slightly more anticlockwise (top to the south west) asymmetries. An overall north-east side up and top to the south-west sense of shear is indicated by the clockwise asymmetries commonly recorded by FIA set 3.

7. Interpretation

7.1 Structural and metamorphic relationships

The polytectonic history of the Lebanon Antiformal Syncline involves at least four phases, of orogenesis. A block diagram (Fig. 10) illustrates the major structural and stratigraphic features. The metamorphic grade generally increases towards the north-west but this distribution is complicated by higher pressure/ lower temperature rocks in the core of the antiform as indicated by the isograds in Figure 2.

An early phase of deformation and metamorphism ($M_{<1}$), represented by small garnet porphyroblasts preserved entirely within andalusite porphyroblasts and by large randomly oriented biotite inclusions in both andalusite and garnet, pre-dates all major structures in the area. Biotite inclusions, which are common in andalusite, are elongate parallel to the dominant foliation where they also lie within the matrix. Differentiated crenulation cleavages, locally preserved as inclusion trails in the cores of matrix garnet porphyroblasts, are attributed to an early phase of tectonism ($D_{<1}$) that pre-dates the bulk of the growth of that mineral.

The earliest major phase of metamorphism (M_1) is a low pressure, regional event recognised throughout the Central Maine Terrane (Robinson *et al*., 1988; Eusden *et al*., 1987; Eusden, 1988) and is characterised by well-developed andalusite porphyroblasts and minor garnet growth. This is interpreted herein as accompanying nappe emplacement (see below). A ubiquitous bedding parallel foliation ($S_{m;}$ S_1 of Eusden *et al*., 1984; 1987) defined by elongate quartz grains and preferentially aligned muscovite and biotite is also inferred to have originally developed during D_1.

M_2 is a progressive event that marks a significant increase in pressure associated with refolding of the Blue Hills Nappe into F_2 folds with a well developed, spaced axial planar crenulation cleavage. The waning stages of D_2 involved a significant heat (and fluid?) pulse that accompanied the intrusion of several large granitic plutons. Extensive garnet growth and the

development of spectacular complete or partial pseudomorphs of andalusite by coarse-grained muscovite and idioblastic to subidioblastic staurolite with quartz-rich symplectitic cores (Fig. 11a) are attributed to M_2. Staurolite replacing andalusite commonly extends into the matrix, overgrowing the earlier foliation developed against the andalusite rim (Fig. 11b) and locally inheriting its inclusion trails (Fig. 12a).

Areas of abundant fibrolitic and prismatic sillimanite are associated with an increase in mineral grain size and are representative of the late D_2 high temperature contact metamorphic event. Paramorphic replacement of andalusite by sillimanite is common (Fig. 12a). Garnet is typically zoned, with earlier formed cores, rich in fine-grained inclusions, overgrown by rims that are inclusion-free or that contain only a few coarse inclusions (Fig. 5a, b). Small quantities of tourmaline are present in most samples and are commonly found as inclusions in the rims of garnet (Fig. 5a, b) and in late (M_3) staurolite. Matrix tourmaline is preferentially distributed along cleavage seams, suggesting that boron may have been derived from crystallising granitic plutons or melts within the migmatites. This influx may have also been partially responsible for the alteration of andalusite to coarse muscovite, similar to such pseudomorphs in west-central Maine (Solar & Brown, 1999; 2000).

Three metamorphic zones (Fig. 2) have been mapped based on the presence of M_2 sillimanite and staurolite in each sample. The isograds mark the appearance or disappearance of each mineral. The sillimanite and staurolite zones are separated by a transition zone that contains both minerals. Pseudosections in the MnKFMASH system were constructed for several representative samples with THERMOCALC 3.21 (Powell & Holland, 1998; Powell *et al.*, 1998), using the dataset of Holland & Powell (1990). Quartz and muscovite were assumed to be in excess and water activity was assumed to be unity. The rock composition (Table 2) was obtained by XRF analysis of 50 mg rock powder from homogeneous 150-250 gram pulverized rock samples using the analytical facilities at James Cook University. Given the inhomogeneous nature of the metaturbidite rock samples, care was taken to analyse the same rock layers from which the thin sections were prepared. Two pseudosections constructed in this manner are presented in Figure 13.

The P-T paths depicted on the pseudosections illustrate differing conditions in the transition (Fig. 13a) and sillimanite zones (Fig. 13b) as M_2 progressed. The stable M_2 mineral assemblage is governed by the pressure and temperature conditions relative to the g-bi-st-sill divariant field shown on the pseudosections. Transition zone rocks display metamorphic textures that permit the relationship between staurolite and sillimanite to be examined in detail. Early M_2 metamorphism involved an increase in pressure and temperature that allowed staurolite to grow at the expense of andalusite (Figs. 11, 12). A thermal pulse associated with emplacement of Acadian granites during the waning stages of D_2 resulted in staurolite becoming unstable and the growth of both fibrolitic and prismatic sillimanite (Fig. 12a, b, c). The staurolite in Fig. 12b shows euhedral crystal faces only where it is protected by andalusite. Rocks in the sillimanite zone (Fig. 13b) never reached the pressure required for the growth of staurolite and M_2 is represented only by the growth of garnet, fibrolite and by the replacement of andalusite by prismatic sillimanite. The majority of rocks containing staurolite in this metamorphic zone are similar in composition to sample MB063. An approximate P-T path for these rocks has been added to the MB063 pseudosection (dotted line; Fig. 13a) to explain the absence of sillimanite in the core of the D_2 antiform. The positive slope of the staurolite/ sillimanite reaction boundary reflects the condition that at elevated pressure, a higher temperature is required for sillimanite to be stable. These rocks experienced the highest pressures and, since they are furthest from granites, they also experienced the lowest peak temperatures. The temperature necessary for sillimanite growth was never attained at the elevated pressure that occurred in the core of the antiform.

M_3 metamorphism is represented by prograde chlorite that cuts across the matrix foliation and the growth of staurolite and minor quantities of garnet. The age of this event remains uncertain. It may be associated with movement on the Nonesuch River Fault system or the broad scale folds (F_3) that result in a change of orientation of the F_2 fold axes from E-W in the south-west of the mapped area to nearly N-S in the north-east (Fig 2; Eusden *et al.*, 1987). A matrix crenulation cleavage (S_3) is preserved locally. Retrogressive metamorphism, M_4, is characterised by sericitisation of alumininosilicates and chlorite pseudomorphs of biotite and garnet.

7.2 Significance of FIA data

The orientation of foliation intersection or inflection axes preserved as inclusion trails in porphyroblasts (FIAs) reflect successive changes in the direction of bulk shortening that occurred synchronous with metamorphism. FIAs appear to form perpendicular to the direction of relative plate motion, their trend being governed by the strike of steeply dipping foliations that form during horizontal bulk shortening (Bell & Wang, 1999; Bell *et al*., 2004). A single FIA trend may be the result of multiple phases of tectonism that produced several overprinting steep and shallow dipping foliations provided the direction of bulk horizontal shortening remained the same. A change in the direction of relative plate motion results in the development of new sub-vertical foliations with a different orientation. Porphyroblasts that overgrow this new foliation record a change in the trend of the FIA (e.g., Bell & Newman, 2006).

The distribution and relative timing of FIA sets (Figs. 7, 8) provides a means to define the succession of bulk movement directions during orogenesis in this part of the Central Maine Terrane. Microstructural and petrographic examination of the schists of the Lebanon Antiformal Syncline indicates a tectonic history involving 4 shifts in the direction of relative plate motion. FIA set 0 (Fig. 8a) is preserved locally and comprises a NW-SE trend that suggests a phase of NE-SW directed bulk shortening that predates all the major structures of the area. FIA set 1 (Fig. 8b) records a considerable NW-SE directed bulk shortening event that accompanied the growth of garnet and andalusite. FIA set 2 (Fig. 8c) is preserved in garnet and staurolite and trends approximately E-W, suggesting a significant phase of N-S directed horizontal bulk shortening that coincided with a major phase of prograde metamorphism (M_2). FIA set 3 (Fig. 8d) represents a late phase of ENE-WSW directed horizontal bulk shortening. The succession of FIA trends indicates a general clockwise rotation in the direction of relative plate motion with time.

7.3 Inclusion trail asymmetry and development of the Lebanon Antiformal Syncline

The dominant sense of shear for each FIA set can be determined by examining the curvature of inclusion trails preserved within porphyroblasts in sections at a high angle to the

FIA. The asymmetry data (Fig. 9) indicates that the majority of porphyroblast growth occurred early during the development of flat-lying foliations. The generation of multiply repeated sub-horizontal foliations suggests that gravitational collapse, initiated either by collapse of an over-thickened orogen (Bell & Johnson, 1989, 1992) or as a result of trench rollback (Meulenkamp *et al*., 1988; Boronkay & Doutsos, 1994) played a major role in Appalachian orogenesis (Bell & Newman, 2006).

FIA set 0 pre-dates all the major structures of the area and records an early phase of tectonism involving predominantly SW side up and top to the SW directed shear (Fig. 9). FIA set 0 is preserved in only a few samples, suggesting that nucleation and growth of porphyroblastic phases at this time was governed by a coarsely partitioned pattern of foliation development that was not conducive to abundant porphyroblast growth. The dominance of a top to the SW differentiation asymmetry suggests that this was the dominant shear sense operating during horizontal foliation development but this interpretation is considered uncertain due to the scarcity of FIA set 0 data.

FIA set 1 formed during NW-SE directed bulk shortening that resulted in a pervasive foliation (S_1) that is preserved in a sub-vertical orientation in the centres of andalusite and garnet porphyroblasts. FIA set 1 is dominated by inclusion trails that display a clockwise (looking NE) steep-to-flat geometry (i.e., the majority of porphyroblast growth occurred during the development of a sub-horizontal foliation and the prevailing sense of shear was top to the SE). The distribution of FIA set 1 asymmetries can be best understood if garnet and andalusite porphyroblasts are considered separately (Fig. 14a). Garnet porphyroblasts display generally equal numbers of clockwise and anticlockwise asymmetries that developed during both horizontal and vertical bulk shortening. By contrast, andalusite shows exclusively clockwise steep-to-flat asymmetry. Two porphyroblastic phases preserving the same FIA trend can only display such contrasting asymmetry distributions if they formed at different times during this period of NW-SE directed bulk shortening.

At the commencement of successive periods of bulk shortening, newly developing crenulations initially overprint the earlier formed foliation relatively coaxially (e.g., Bell *et al*., 2004, Ham & Bell, 2004, Bell & Newman, 2006). For the deformation to intensify significantly, the strain path must become non-coaxial (Bell, 1981, Bell & Bruce, 2006; thesis Section B). Porphyroblast nucleation and growth during regional metamorphism commences very early in a deformation event (Bell *et al*., 2003) and ceases once a differentiated crenulation cleavage begins to develop in the adjacent domains (Bell & Hayward, 1991). FIA set 1 garnet porphyroblasts grew during horizontal bulk shortening displaying roughly equal numbers of clockwise and anticlockwise inclusion trail asymmetries (Fig. 14a). These porphyroblasts are interpreted to have grown early during a deformation that eventually developed a steep crenulation cleavage, while the strain path was coaxial at the bulk scale. As the strain increased and became non-coaxial, garnet growth ceased and the crust thickened. Garnet porphyroblasts that grew during intervening periods of collapse that accompanied the development of flat lying foliations show slightly more clockwise than anticlockwise asymmetries but the distribution is relatively coaxial in comparison to that preserved by andalusite (Fig 14a).

The abundance of porphyroblasts that preserve FIA set 1 indicates that deformation was regionally penetrative at the scale of a porphyroblast at this time and resulted in a sub-vertical foliation (S_1) that was associated with a period of upright folding prior to nappe emplacement. The exclusively clockwise inclusion trail asymmetry of andalusite porphyroblasts preserving FIA set 1 suggests that the growth of this mineral occurred during strong, top to the SE directed shear. The sequence of differentiation asymmetries that formed during the development of FIA set 1 (from coaxial horizontal bulk shortening, weakly non-coaxial vertical shortening and finally, strongly non-coaxial vertical shortening with a top to the south-east sense of shear) preserves the changes in strain path that were responsible for emplacement of the Blue Hills Nappe. The early stage of vertical foliation (S_1) development and upright folding resulted in considerable thickening of the orogenic wedge. Subsequent gravitationally induced spreading of the orogen, at first relatively coaxially at the bulk scale but becoming strongly non-coaxial, resulted in the rotation, translation and amplification of the originally upright fold structure into a sub-horizontally orientated recumbent fold. Bell & Newman (2006) showed how the degree of

shearing increases from the core to the margins of an orogen during gravitational collapse and spreading when partitioning of the amount of bulk shortening occurs vertically through the crust (Fig. 15). The change in asymmetry distribution during the formation of shallow-dipping foliations may be due to a shift in the orogen core towards the NW or may simply be a result of garnet growing very early during the process of vertical bulk shortening, before one asymmetry became dominant.

The distribution of FIA set 2 asymmetries shows some similarities to that of FIA set 1 (Fig. 9), with a clear dominance of porphyroblast growth during the formation of shallow-dipping foliations with a top to the south sense of shear. Garnet and staurolite porphyroblasts have nearly identical asymmetry distributions (Fig. 14b). The timing of FIA set 2 relative to the Lebanon Antiformal Syncline can be demonstrated by dividing the asymmetry data into that obtained from the northern limb (Fig. 16a) and southern limb (Fig. 16b) of the major fold and also by comparing the combined data from all of the northern limbs (Fig. 16c) to the combined data from all of the southern limbs (Fig. 16d) of the second order parasitic antiforms. The data from the northern limb of the Lebanon Antiformal Syncline (Fig. 16a) shows only anticlockwise asymmetries and the southern limb (Fig. 16b) shows a greater proportion of clockwise asymmetries during the formation of sub-vertical foliations for FIA set 2. This observation suggests that the development of FIA set 2 coincided with refolding of the overturned limb of the nappe to form the Lebanon Antiformal Syncline. Interestingly, this is not the case for the parasitic antiforms (Fig. 16c, d). The cumulative data for the northern limbs of the parasitic antiforms show equal numbers of clockwise and anticlockwise asymmetries for the shallow-to-steep geometries and the southern limbs show more anticlockwise than clockwise asymmetries. If porphyroblast growth accompanied formation of the folds, the asymmetries that should occur are anticlockwise on the northern limbs and clockwise on the southern limbs where the trails switch from flat in the core to steep in the rim. This discrepancy suggests that either the parasitic folds formed before the Lebanon Antiformal Syncline and that they predate the majority of FIA set 2 porphyroblast growth or that reactivation of bedding or the bedding parallel foliation occurred on the limbs of the parasitic folds, resulting in more of the opposite asymmetry than that which would be expected.

The dominance of top to the south shear recorded by FIA set 2 (Figs. 9, 14, 16) indicates that gravitational collapse away from the orogen core was an ongoing process. Most of the porphyroblast growth occurred on the southern limbs of both the Lebanon Antiformal Syncline and the smaller scale parasitic antiforms during horizontal bulk shortening (Fig. 16). The geometry of the northern limbs was such that horizontal shortening could be accommodated by the reactivation of bedding and/or the bedding parallel foliation (Fig. 17). Reactivation of an older foliation on the limb of a fold occurs when synthetic shear operating on a newly developing foliation switches to antithetic shear on the older foliation (Bell *et al.*, 2003). This process reduces the number of potential porphyroblast growth sites, since porphyroblasts tend to nucleate in zones of progressive shortening (Bell *et al.*, 1986). The southern limbs could not reactivate during top to the south shear and deformed through the development of a new crenulation cleavage (Fig. 17) that was conducive to porphyroblast nucleation and growth. Collapse and gravitational spreading away from the orogen core resulted in the earlier formed upright structures being reoriented into moderately inclined folds and foliations.

FIA set 3 (Fig. 9) is preserved within garnet and staurolite porphyroblasts. The few samples that were found to preserve this FIA set were collected close to axes of the gentle folds (F_3) that result in a broad scale change in trend of the F_2 fold axes from E-W in the south-west of the mapped area to nearly N-S in the north-east (Fig. 18), where the weak S_3 crenulation is best developed. The curvature of the inclusion trails in porphyroblasts that grew during the formation of the steeply dipping crenulation cleavage are exclusively clockwise on the north-eastern limbs and exclusively anticlockwise on the south-western limbs of F_3 antiforms (Fig. 18). The relationship between inclusion trail asymmetries preserved by porphyroblasts containing FIA set 3 and the F_3 folds suggests that the change in orientation of the F_2 fold axes was caused by ENE-WSW directed bulk shortening during the latest major phase of tectonism that accompanied metamorphism.

8. The significance of gravity in orogenesis

The Lebanon Antiformal Syncline developed through a process of repeated cycles of horizontal bulk shortening, punctuated by gravitational collapse and the formation of flat lying foliations. It has long been recognised (e.g., Jeffreys, 1931; Bucher, 1956; Mudge, 1970; Price, 1971; Elliot, 1976a, b; Ramberg, 1981; Liu, 2001; Bell & Newman, 2006) that gravity has a profound influence on the development of the orogenic wedge in that thickened crustal material has a propensity to collapse and spread laterally under its own weight. Bell & Johnson (1989) proposed a model of orogenesis (Fig. 19), involving bulk orogenic shortening alternating with gravitational collapse that was based on analysis of inclusion trail geometries from different orogenic belts. During the horizontal bulk shortening phase, the crust is thickened as material is effectively forced upwards in the core of the orogenic belt (Fig. 19a). As the orogenic core collapses on itself (Fig. 19b), thrust faults are initiated toward the margin of the orogen and ductile horizontal shear takes place in the lower part. If a cross section of the orogen is divided into four quadrants, the sense of shear in the upper right quadrant is anti-clockwise while a clockwise sense of shear occurs in the lower right quadrant. Shear sense in the other half of the orogen is a mirror image of that in the right. Aerden (1998) refined the model and showed that extension and compression could operate simultaneously in different parts of an orogenic belt. This allows for continued convergent plate motion, with periodic collapse of parts of the orogen as the gravitational potential energy exceeds that which can be supported by the strength of the lithosphere.

Elliot (1976a, 1976b) asserted that thrust nappes can only advance large (up to 100 km) distances as a result of gravitational spreading from areas of high potential energy that are undergoing internal thinning under the weight of overlying rocks. Subsequent work (e.g., Law *et al*., 1986; Merle, 1989; Sandiford, 1989; Northrup, 1996; Aerden & Malavieille, 1999) has supported this concept through the strain patterns and structures observed in some thrust sheets. Gravitational collapse causes pre-existing steeply dipping structures in the ductile levels of the crust to be rotated into sub-horizontal orientations and results in the development of flat-lying foliations. It seems that nappes are most likely to develop where gravitational collapse and

spreading of the orogen play a dominant role in crustal deformation. This process permits the re-use of shallow-dipping foliations during successive periods of gravitational collapse and can potentially produce enough horizontal shear to facilitate the formation of enormous nappe structures.

9. Discussion and conclusions

The development of the Lebanon Antiformal Syncline involved at least four major phases of tectonism and metamorphism (Fig. 20). An early period of NE-SW directed horizontal bulk shortening predates all major structures and matrix foliations but evidence for this event is preserved as inclusion trails in porphyroblasts. The strong, steeply dipping foliation (S_1) that is preserved as inclusion trails in the cores of numerous porphyroblasts and the exclusively clockwise inclusion trail asymmetries contained within andalusite porphyroblasts that grew during the vertical collapse stage of the development of FIA set 1 indicate that the Blue Hills Nappe formed from the horizontal shearing of an originally upright fold. Gravitational spreading during crustal collapse resulted in sub-horizontal, non-coaxial (top to the south-east) flow that progressively rotated, translated and amplified the original upright structure into a sub-horizontal recumbent fold. The dominant matrix fabric (S_m) is a composite foliation that is the result of the re-orientation and reactivation of bedding (S_0) or the bedding-parallel foliation (S_1) during the gravitational collapse stage and subsequent tectonic events.

Eusden *et al*. (1987) proposed that the Central New Hampshire Anticlinorium (Fig. 1) acts as a "dorsal zone," splitting the Central Maine Terrane into two distinct structural styles. West of the "dorsal zone" the early nappes verge west only, while nappes to the east verge east only. The Central New Hampshire Anticlinorium is marked by the oldest formation in the Central Maine Terrane, the lower Rangeley Formation and by the highest grade of metamorphism (Lyons *et al*., 1997). The high grade metamorphic zone that corresponds to the Central New Hampshire Anticlinorium is interpreted to represent the core of the Acadian orogen. The bipolar symmetry of structures on either side of this zone may reflect gravitational collapse away from an area of maximum topography and gravitational potential energy.

The development of FIA set 2 marks a significant increase in pressure that is interpreted to be the result of the folding and inversion of strata on the overturned limb of the nappe and possibly loading by allochthonous material spreading away from the orogen core. This major metamorphic event (M_2) could potentially be considered as two discrete phases. The first of these involves the growth of garnet, staurolite and sillimanite at elevated pressures (Fig. 13). The later phase involves a significant fluid pulse and temperature increase associated with the intrusion of granitic melts. However, while it is considered reasonable to make some broad statements about the relative timing of these minerals in the different metamorphic zones, difficulties arise in differentiating and correlating these phases between outcrops. This is primarily due to the pressure and temperature conditions being very close to the g-bi-st-sill divariant during M_2 (Fig. 13). Slight variations in bulk rock chemistry and the variable activity of the fluid phase means that the growth of sillimanite, staurolite or both could start, stop and restart during M_2. For this reason, M_2 has been treated as a single metamorphic event in this study.

The broad change in orientation of the F_2 fold axes has previously been presented as anecdotal evidence for a late stage of tectonism affecting the Lebanon Antiformal Syncline (Eusden, *et al*., 1987). The measurement of a locally preserved crenulation cleavage axial planar to the F_3 folds and the excellent fit of FIA set 3 asymmetry data to the development of those folds are considered strong supporting evidence for a late stage of ENE-WSW directed bulk shortening.

References

Aerden, D, 1998. Tectonic evolution of the Montagne Noir and a possible orogenic model for syncollisional exhumation of deep rocks, Variscan belt, France. *Tectonics* **17**, 62-79.

Aerden, D. and Malavieille, J, 1999. Origin of a large-scale fold nappe in the Montagne Noire, Variscan belt, France. *Journal of Structural Geology* **21**, 1321-1333.

Aerden, D., 2003. Preferred orientation of planar microstructures determined via statistical best-fit of measured intersection-lines: the 'FitPitch' computer program. *Journal of Structural Geology* **25**, 923-934.

Bell, T.H., 1981. Foliation development – the contribution, geometry and significance of progressive, bulk, inhomogeneous shortening. *Tectonophysics* **75**, 273-296.

Bell, T.H. and Bruce, M.D., 2006. The internal inclusion trail geometries preserved within a first phase of porphyroblast growth. *Journal of Structural Geology* **28**, 236-252.

Bell, T.H., Fleming, P.D. and Rubenach, M.J., 1986. Porphyroblast nucleation, growth and dissolution in regional metamorphic rocks as a function of deformation partitioning during foliation development. *Journal of Metamorphic Geology* **4**, 37-67.

Bell, T.H., Forde, A. and Wang, J., 1995. A new indicator of movement direction during orogenesis: measurement technique and application to the Alps. *Terra Nova* **7**, 500-508.

Bell, T.H., Ham, A.P., Hickey, K.A., 2003. Early formed regional antiforms and synforms that fold younger matrix schistosities: their effect on sites of mineral growth. *Tectonophysics* **367**, 253-278.

Bell, T.H., Ham, A.P., Kim, H.S., 2004. Partitioning of deformation along an orogen and its effects on porphyroblast growth during orogenesis. *Journal of Structural Geology* **26**, 825-845.

Bell, T.H. and Hayward, N., 1991. Episodic metamorphic reactions during orogenesis: the control of deformation partitioning on reaction sites and duration. *Journal of Metamorphic Geology* **9**, 619-640.

Bell, T.H. and Hickey, K.A., 1997. Distribution of pre-folding linear indicators of movement direction around the Spring Hill Synform, Vermont: significance for mechanism of folding in this portion of the Appalachians. *Tectonophysics* **274**, 275-294.

Bell, T.H., Hickey, K.A. and Upton, G. J. G., 1998. Distinguishing and correlating multiple phases of metamorphism across a multiply deformed region using the axes of spiral, staircase and sigmoidally curved inclusion trails in garnet. *Journal of Metamorphic Geology* **16**, 767 - 794.

Bell, T.H. and Hickey, K.A., 1999. Complex microstructures preserved in rocks with a simple matrix: significance for deformation and metamorphic processes. *Journal of Metamorphic Geology* **17**, 521-536.

Bell, T.H. and Johnson, S.E., 1989. Porphyroblast inclusion trails: The key to orogenesis. *Journal of Metamorphic Geology* **7**, 279-310.

Bell, T.H. and Johnson, S.E., 1992. Shear sense: anew approach that resolves problems between criteria in metamorphic rocks. *Journal of Metamorphic Geology* **10**, 99-124.

Bell, T.H. and Mares, V.M., 1999. Correlating deformation and metamorphism around orogenic arcs. *American Mineralogist* **84**, 1727-1740.

Bell, T.H. and Newman, R., 2006. Appalachian orogenesis: The role of repeated gravitational collapse. *Geological Society of America Special Paper 414*: *Styles of Continental Contraction*, 95–118.

Bell, T.H. and Rubenach, M.J., 1982. Sequential porphyroblast growth and crenulation cleavage development during progressive deformation. *Tectonophysics* **92**, 171-194.

Bell, T.H. and Wang, J., 1999. Linear indicators of movement direction versus foliation intersection axes in porphyroblasts (FIAs) and their relationship to directions of relative plate motion. *Earth Science Frontiers* **6**, 3, 31-47.

Bell, T.H. and Welch, P.W., 2002. Prolonged Acadian orogenesis: revelations from foliation intersection axis (FIA) controlled monazite dating of foliations in porphyroblasts and matrix. *American Journal of Science* **302**, 549-581.

Billings, M.P., 1956. The geology of New Hampshire: part II – Bedrock geology: Concord, *New Hampshire State Planning and Development Commission*, 203 p.

Boronkay, K. and Doutsos, T., 1994. Transpression and transtension within different structural levels in the central Aegean region. *Journal of Structural Geology* **16**, 1555-1573.

Bradley, D.C., Tucker, R.D., Lux, D.R., Harris, A.G. and McGregor, C.D., 1998. Migration of the Acadian orogen and foreland basin across the northern Appalachians of Maine and adjacent areas, *U.S. Geol. Survey Professional Paper* 1624.

Cihan, M. and Parsons, A., 2005. The use of porphyroblasts to resolve the history of macro-scale structures: an example from the Robertson River Metamorphics, North-Eastern Australia. *Journal of Structural Geology* **27**, 1027-1045.

Davis, B.K., 1995. Regional-scale foliation reactivation and re-use during formation of a macroscopic fold in the Robertson River metamorphics, north Queensland, Australia. *Tectonophysics* **242**, 293-311.

Elliott, D., 1976a. The motion of thrust sheets. *Journal of Geophysical Research* **81**, 949-963.

Elliott, D., 1976b. The energy balance and deformation mechanisms of thrust sheets: *Philosophical Transactions Royal Astronomical Society* **A-283**, 289-312.

Eusden, J.D., Jr., 1988, Stratigraphy, structure and metamorphism of the "dorsal zone", central New Hampshire. In Bothner, W.A. (ed.) *New England Intercollegiate Geological Conference, 80th annual meeting*; Guidebook to field trips in southwestern New Hampshire, southeastern Vermont and north-central Massachusetts: Durham, University of New Hampshire, 40-59.

Eusden, J.D., Jr. and Barreiro, B., 1989. The timing of peak high-grade metamorphism in central-eastern New England. *Maritime Sediments and Atlantic Geology* **24**, 241-255.

Eusden, J.D., Jr., Bothner, W.A. and Hussey, A.M., Laird, J.,1984. Silurian and Devonian rocks in the Alton and Berwick quadrangles, New Hampshire and Maine, In Hanson, L.S. (ed.) *Geology of the coastal lowlands, Boston, MA to Kennebunk, ME: New England Intercollegiate Geologic Conference*, 1984, Trip C5, 325-351.

Eusden, J.D., Jr., Bothner, W.A. and Hussey, A.M., 1987. The Kearsarge-Central Maine Synclinorium of southeastern New Hampshire and southwestern Maine: stratigraphic and structural relations of an inverted section, *American Journal of Science* **287**, 242-264.

Eusden, J.D., Jr., Guzofski, C.A., Robinson, A.C. and Tucker, R.D., 2000. Timing of the Acadian Orogeny in Northern New Hampshire, *The Journal of Geology* **108**, 219-232.

Guidotti, C.V., 2000. The classic high-T – low-P metamorphism of west-central Maine: Is it post-tectonic or syntectonic? Evidence from porphyroblast – matrix relations: Discussion. *The Canadian Mineralogist* **38**, 1007-1026.

Guidotti, C.V. and Johnson, S.E., 2002. Pseudomorphs and associated microstructures of western Maine, USA, *Journal of Structural Geology* **24**, 1139-1156.

Ham, A.P. and Bell, T.H., 2004. Recycling of foliations during folding. *Journal of Structural Geology* **26**, 1989-2009.

Hatcher, R.D., 1981. Thrusts and nappes in the North American Appalachian Orogen, In McClay, K.R. and Price, N.J. (eds.) *Thrust and nappe tectonics,* 491-499. Blackwell Scientific Publications.

Hayward, N., 1990. Determination of early fold axis orientations within multiply deformed rocks using porphyroblasts. *Tectonophysics* **179**, 353-369.

Holdaway, M.J., 1971. Stability of andalusite and Al2SiO5 phase diagram. *American Journal of Science* **271**, 97–131.

Holland, T.J.B. and Powell, R., 1990. An enlarged and updated internally consistent thermodynamic dataset with uncertainties and correlations; the system K_2O-Na_2O-CaO-MgO-MnO-FeO-Fe_2O_3-Al_2O_3-TiO_2-SiO_2-C-H_2-O_2. *Journal of Metamorphic Geology* **8**, 89-124.

Johnson, T.E., Brown, M. and Solar, G.S., 2003. Low-pressure subsolidus phase equilibria in the MnNCKFMASH system: Constraints on conditions of regional metamorphism in western Maine, northern Appalachians. *American Mineralogist* **88**, 624-638.

Kent, D.V. and Keppie, J.D., 1988. Silurian-Permian palaeocontinental reconstructions and circum-Atlantic tectonics, In Harris, A.l. and Fettes, D.J. (eds.) *The Caledonian-Appalachian Orogen*, *Geological Society Special Publication* No. **38**, 469-480.

Law, R.D., Casey, M. and Knipe, R.J., 1986. Kinematic and tectonic significance of microstructures and crystallographic fabrics within quartz mylonites from the Assynt and Eriboll regions of the Moine thrust zone, NW Scotland. *Transactions of the Royal Society of Edinburgh: Earth Sciences* **77**, 99-126.

Lisowiec, N., 2005. Combining microstructural analysis with EPMA monazite geochronology to constrain progressive stages of orogenesis in the Appalachians. Unpublished PhD thesis, James Cook University, 199p.

Lyons, J.B., Boudette, E.L. and Aleinikoff, J.N., 1982. The Avalon and Gander zones in central eastern New England, In St.-Julien, P. and Beland, J. (eds.) *Major structural zones and faults of the northern Appalachians. Geological Association of Canada Special Paper* **24**, 43-66.

Lyons, J.B., Bothner, W.A., Moench, R.H., and Thompson, J.B., Jr., 1997, Bedrock geologic map of New Hampshire: *U.S. Geological Survey State Geologic Map*, scale 1: 250,000 and 1:500,000, 2 sheets.

Lyons, J.B. and Livingston, D.E., 1977, Rb-Sr age of the New Hampshire Plutonic Series, *Geological Society of America Bulletin* **88**, 1808-1812.

Merle, O., 1989. Strain models within spreading nappes. *Tectonophysics* **165**, 57–71.

Meulenkamp, J.E., Wortel, M.J.R., van Wamel, W.A., Spakman, W. and Hoogerduyn Strating, E., 1988. On the Hellenic subduction zone and the geodynamic evolution of Crete since the late Middle Miocene. *Tectonophysics* **146**, 203-215.

Moench, R.H., Boone, G.M., Bothner, W.A., Boudette, E.L., Hatch, N.L., Jr., Hussey II, A.M., and Marvinney, R.G., 1995. Geologic map of the Sherbrooke-Lewiston Area, Maine, New Hampshire, and Vermont, United States, and Quebec, Canada. *U.S. Geological Survey Miscellaneous Investigations-Series* Map I-1898-D.

Northrup, C.J., 1996. Structural expressions and tectonic implications of general non-coaxial flow in the midcrust of a collisional orogen: the northern Scandinavian Caledonides. *Tectonics* **15**, 490-505.

Olszewski, W.J. Jr., Gaudette, H.E., Bothner, W.A., Laird, J. and Cheatham, M.M., 1984. The Precambrian (?) rocks of southwestern New Hampshire. *Geological Society of America, Abstracts with Programs* **16**, 54.

Osberg, P.H., 1988. Silurian to lower Carboniferous tectonism in the Appalachians of the USA, In Harris, A.l. and Fettes, D.J. (eds.) *The Caledonian-Appalachian Orogen*, *Geological Society Special Publication* No. **38**, 449-452.

Pattison, D.R.M., 1992. Stability of andalusite and sillimanite and the Al2SiO5 triple point: constraints from the Ballachulish aureole, Scotland. *Journal of Geology* **100**, 423–446.

Powell, R. and Holland, T., 1988. An internally consistent dataset with uncertainties and correlations. 3. Applications to geobarometry, worked examples and a computer program. *Journal of Metamorphic Geology* **6**, 173-204.

Powell, R., Holland, T., and Worley, B., 1998. Calculating phase diagrams involving solid solutions via non-linear equations, with examples using THERMOCALC. *Journal of Metamorphic Geology* **16**, 577-588.

Rich, B., 2005. Microstructural insights into the tectonic history of the south-eastern New England Appalachians in Connecticut and Rhode Island. Unpublished PhD thesis, James Cook University, 184p.

Robinson, P., Tracy, R.J., Santallier, D.S., Andreasson, P.G. and Gil-Ibarguchi, J.I., 1988, In Harris, A.I. and Fettes, D.J. (eds.) *The Caledonian-Appalachian Orogen*, *Geological Society Special Publication* No. **38**, 453-467.

Rodgers J., 1970. *The tectonics of the Appalachians*, L.U. De Sitter (ed.), Wiley-interscience.

Sandiford, M., 1989. Horizontal structures in deep crustal granulite terrains: a record of mountain building or mountain collapse? *Geology* **17**, 449 - 452.

Sayab, M., 2005. Microstructural evidence for N–S shortening in the Mount Isa Inlier (NW Queensland, Australia): the preservation of early W–E-trending foliations in porphyroblasts revealed by independent 3D measurement techniques. *Journal of Structural Geology* **27**, 1445 – 1468.

Smith, H.A. and Barreiro, B., 1990. Monazite U-Pb dating of staurolite grade metamorphism in pelitic schists. *Contributions to Mineralogy and Petrology* **105**, 602-615.

Solar, G.S. and Brown, M., 1999. The classic high-T – low-P metamorphism of west-central Maine: Is it post-tectonic or syntectonic? Evidence from porphyroblast – matrix relations. *The Canadian Mineralogist* **37**, 311-333.

Solar, G.S. and Brown, M., 2000. The classic high-T – low-P metamorphism of west-central Maine: Is it post-tectonic or syntectonic? Evidence from porphyroblast – matrix relations: Reply. *The Canadian Mineralogist* **38**, 1007-1026.

Solar, G.S. and Brown, M., 2001. Deformation partitioning during transpression in response to Early Devonian oblique convergence, northern Appalachian Orogen, USA. *Journal of Structural Geology* **23**, 1043-1065.

Solar, G.S., Pressley, R.A., Brown, M. and Tucker, R.D., 1998. Granite ascent in convergent orogenic belts: Testing a model. *Geology* **26**, 711-714.

Steiger, R.H. and Jager, E, 1977, Subcommision on Geochronology; convention on decay constants in geo- and cosmochronology, *Earth and Planetary Science Letters* **36**, 359-363.

Williams, M.L., 1994. Sigmoidal inclusion trails, punctuated fabric development, and interactions between metamorphism and deformation. *Journal of Metamorphic Geology* **12**, 1-21.

Conclusions

This study has demonstrated that inclusion trails within porphyroblasts can preserve a wealth of local tectonic and metamorphic history, much of which is routinely destroyed in the matrix by later deformation events. The unique time-capsule character of porphyroblasts makes it possible to reconstruct the deformation and metamorphic history of multiply deformed metamorphic terrains in unparalleled detail. The principal conclusions of each section are summarised below:

Section A

The asymmetry and FitPitch methods for determining the orientation of foliation intersection/inflection axes preserved in porphyroblasts (FIAs) use very different approaches. The asymmetry method relies on the curvature of one foliation into a subsequently formed foliation. The FIA is found by examining the pattern formed by the intersection of vertical thin-sections of differing strikes with the curved inclusion trails preserved within porphyroblasts and picking the flip from "S" to "Z" shape between two closely oriented sections. FitPitch works best where the inclusion trails are predominately straight and uses a mathematical approach to fit one, two or three model planes to pitch data measured in a set of differently oriented thin-sections. The best solution is considered to be the one that minimises the deviation between the data and the model planes. Intersections between these model planes define FIAs. The two techniques compliment each other by permitting FIAs to be obtained from a larger proportion of samples and they can also be used as independent tests in samples that are suitable for both methods. The sense of shear operating during progressive bulk shortening is indicated by inclusion trail curvature recorded in thin sections cut at a high angle to the FIA. Unlike the "asymmetry" method, "FitPitch" does not give the shear sense directly but can be used to establish the most suitably oriented thin section in which to look for inclusion trail curvature.

FIAs form from the preservation, as inclusion trails, of intersecting successive foliations that develop against the porphyroblast margins. A FIA trend is controlled only by the orientation

of steeply dipping foliations and is independent of the movement direction on horizontal planes. Therefore, the FIA is the only linear indicator of movement direction that consistently reflects the direction of bulk shortening associated with relative motion between plates.

Section B

The geometry of inclusion trails contained within a first phase of porphyroblast growth can show significant differences to those preserved by subsequent enlargement because of the influence a pre-existing porphyroblast has on the strain field. The porphyroblast acts as a rigid mass up against which the rock preferentially strains during ensuing events. The variation in inclusion trail geometry and FIA trend within different porphyroblastic phases in the same rock layer, as well as within the same phase in different layers, from two adjacent samples from one outcrop show a remarkable consistency of FIA trends between porphyroblasts showing multiple phases of growth and those that grew during the development of a sub-vertical foliation. This contrasts dramatically with those that only grew during the development of a sub-horizontal foliation. The foliation preserved as inclusion trails within a first phase of porphyroblast growth can potentially vary significantly from its orientation prior to the commencement of that deformation event. However, it is significant that in many examples this is not the case.

The 3-D geometry of sigmoidally shaped inclusion trails obtained by high-resolution X-ray computed tomography (X-ray CT) of a garnet porphyroblast reveals significant aspects of the variation of inclusion trails that are possible within a first phase of porphyroblast growth. 3-D computer analysis of sigmoidal inclusion trails reveals that the asymmetry method for FIA determinations is unaffected by the cut location relative to the porphyroblast core. Significantly, perfect spiral inclusion trail geometries can be produced from a sigmoidal shape in cuts up 30° away from the FIA. This could dramatically influence interpretation of the structural history of the region, depending on whether one interpreted that the inclusion trails had formed by porphyroblast rotation or non-rotation. Wherever spiral shaped inclusion trails are seen in thin section showing a maximum of 180° of curvature, extra thin sections in other orientations should be cut to check whether true spirals or just sigmoidal trails are present.

Section C

Porphyroblasts locally preserve oppositely concave microfolds ("millipedes"), which, in all examples that we have found, exclusively indicate a deformation history of bulk inhomogeneous shortening. Very similar structures have been formed experimentally during inhomogeneous simple shear but are distinguished from those trapped in porphyroblasts that form during progressive bulk inhomogeneous shortening. Millipede structures with an axial plane foliation can only form by progressive bulk inhomogeneous shortening while millipede-like shapes transected by a foliation that accompanied their development form during progressive inhomogeneous simple shear. Oppositely concave microfolds in some porphyroblasts reveal that deformation near orthogonal to a previously developed foliation occurred by axial plane shear driven rotation that led to rapid reactivational "card-deck-like" collapse of the pre-existing foliation. Differentiated crenulation cleavages may result from a similar process, involving the development of near orthogonal foliations and leading to the cessation of porphyroblast growth.

Section D

The succession of foliation intersection/inflection axes preserved as inclusion trails in porphyroblasts (FIAs) from the Lebanon Antiformal Syncline of SE New Hampshire, USA, document changes in bulk shortening geometry associated with emplacement and refolding of a large-scale recumbent fold (the Blue Hills Nappe). A sequence of four FIAs trending NW-SE, NE-SW, E-W and NNW-SSE has been distinguished based upon overprinting criteria plus inclusion trail composition, texture and orientation. This succession indicates a general clockwise rotation in the direction of horizontal bulk shortening during Acadian orogenesis. Metamorphic phase relations indicate an increase in both pressure and temperature associated with inversion of the stratigraphic sequence. Analysis of asymmetries recorded by the inclusion trails reveals a spectacular dominance of top to the south-east directed, non-coaxial horizontal shear during nappe emplacement and subsequent refolding that is attributed to repeated episodes of gravitational collapse in the orogen core to the west that progressively rotated, translated and

amplified originally sub-vertical folds and foliations into sub-horizontal orientations. The broad change in orientation of the F_2 fold axes that has previously been presented as anecdotal evidence for a late stage of tectonism affecting the Lebanon Antiformal Syncline is attributed to ENE-WSW directed bulk shortening, represented by a locally preserved crenulation cleavage axial planar to the F_3 folds and by the youngest FIA set.

Recommendations for further investigation

FIAs have been used to distinguish a succession of four periods of metamorphism and foliation development in the region of the Lebanon Antiformal Syncline. The consistent succession of FIAs from sample to sample is considered to reflect periods of time over which the relative plate motion was constantly directed before shifting to another trend. Assigning absolute ages to the development of the FIAs may be possible by mapping and analysis of monazite inclusions in porphyroblasts with an electron microprobe, using the U-Th-total Pb technique (Montel *et al*., 1996; Williams *et al*., 1999; Lisowiec, 2006a). Samples with core-rim FIA relationships could potentially be used to test whether the monazite ages are consistent with the FIA succession determined by this study. This would permit the correlation of the FIA data with previous studies undertaken in the New England Appalachians (e.g., Bell and Welch, 2002; Rich, 2005, Lisowiec, 2006b). It is envisaged that this work will be carried out as part of a future project to establish the ages of, and correlate FIAs across the New England Appalachians.

References

Bell, T.H. and Welch, P.W., 2002. Prolonged Acadian orogenesis: revelations from foliation intersection axis (FIA) controlled monazite dating of foliations in porphyroblasts and matrix. *American Journal of Science* **302**, 549-581.

Lisowiec, N., 2006a. Precision estimation in electron microprobe monazite dating: Repeated measurements versus statistical (Poisson) based calculations. *Chemical Geology* **234**, 223-235.

Lisowiec, N., 2006b. Combining microstructural analysis with EPMA monazite geochronology to constrain progressive stages of orogenesis in the Appalachians. Unpublished PhD thesis, James Cook University, 199p.

Montel, J.M., Foret, S., Veschambre, M., Nichollet, C.H. and Provost, A., 1996. Electron microprobe dating of monazite. *Chemical Geology* **131**, 37-53.

Rich, B., 2005. Microstructural insights into the tectonic history of the south-eastern New England Appalachians in Connecticut and Rhode Island. Unpublished PhD thesis, James Cook University, 184p.

Williams, M.L., Jercinovic, M.J. and Terry, M.P.,1999. Age mapping and chemical dating of monazite using the electron microprobe: Deconvoluting multistage tectonic histories. *Geology* **27**, 1023-1026.

The development and 3D geometry of porphyroblast inclusion trails: significance for the tectonic evolution of the Lebanon Antiformal Syncline, New Hampshire

Volume II: Figures, Tables and Appendices

Thesis submitted by
Matthew Donald Bruce BSc (Hons)
in July, 2007

for the degree of Doctor of Philosophy
in the School of Earth and Environmental Sciences

Table of Contents, Volume II

Table of contents		i
List of tables		ii
List of figures		iii
Section A	Movement directions in porphyroblastic rocks: Evaluation of the “FitPitch” and the “asymmetry” methods.	A-1
Section B	The internal inclusion trail geometries preserved within a first phase of porphyroblast growth	B-1
Section C	Progressive deformation partitioning and deformation history: Evidence from millipede structures	C-1
Section D	Timing nappe development in multiply tectonised rocks: A new approach	D-1
Appendix A:	FitPitch data	vii
Appendix B:	Sample localities and mineralogical data	xvii
Appendix C:	JCU collection numbers	xx
Appendix D:	Structure and stratigraphy of the Lebanon Antiformal Syncline, New Hampshire, USA	Map
Appendix E:	Electronic supplements	CD
	E01-asymmetry method.mov	
	E02-vertical sigmoid slice 090.mov	
	E03-vertical sigmoid rotate.mov	
	E04-vertical sigmoid slice 000.mov	
	E05-vertical sigmoid slice 010.mov	
	E06-vertical sigmoid slice 030.mov	
	E07-horizontal millipede slice.mov	
	E08-vertical millipede slice 120.mov	
	E09-vertical millipede rotate slice.mov	
	E10-millipede.zip	
	E11-vertical spiral rotate.mov	
	E12-vertical spiral slice 000.mov	
	E13-vertical spiral slice 010.mov	
	E14-vertical spiral slice 030.mov	
	E15-vertical spiral slice 090.mov	

List of Tables

Section A

Table 1	FitPitch results for samples MB019, MB028 and MB030	A-5
Table 2	FIA orientations calculated with the FitPitch computer program versus the asymmetry method	A-8

Section C

Table 1	Pitch of S_2 preserved as inclusion trials in plagioclase porphyroblasts in the hinge plus lower and upper limbs of the fold	C-11
Table 2	Width between S_3 seams measured across porphyroblasts	C-12

Section D

Table 1	FIA data from the Lebanon Antiformal Syncline separated into that from andalusite, staurolite and garnet porphyroblasts	D-8
Table 2	Major element analyses (shown as weight % oxide) of bulk compositions used in the calculation of pseudosections.	D-15

List of Figures

Section A

Figure 1.	Representation of Foliation Inflection/ Intersection Axes (FIAs)	A-1
Figure 2.	3D model demonstrating the asymmetry method for establishing the FIA trend for a sample containing simple sigmoid inclusion trails	A-2
Figure 3.	Major structural features of New Hampshire	A-3
Figure 4.	Map of the study area showing major structural features and sample localities	A-4
Figure 5.	Pitch data for sample MB019	A-6
Figure 6.	Photomicrograph of a porphyroblast from sample MB019 plus plot of pitch measurements	A-7
Figure 7.	Pitch data for sample MB030	A-9
Figure 8.	Photomicrographs of porphyroblasts from sample MB030 plus plot of pitch measurements	A-11
Figure 9.	Separation of MB030 pitch data into two planes according to FitPitch and core and rim data plotted separately.	A-12
Figure 10.	Hand specimen of sample MB028 and photomicrograph of coticule	A-13
Figure 11.	Pitch data for sample MB028	A-14
Figure 12.	Photomicrograph of a porphyroblast from sample MB028 plus plot of pitch measurements	A-15

Section B

Figure 1.	Vertical cross-section through a porphyroblast within an obliquely dipping foliated matrix	B-1
Figure 2.	3-D sketch showing porphyroblasts that grew in crenulation hinges during a deformation event that formed a sub-vertical foliation	B-2
Figure 3.	3-D sketch showing porphyroblasts that grew in crenulation hinges during a deformation event that formed a sub-horizontal foliation	B-3
Figure 4.	Location map of samples TC1365 and TC1365i	B-4
Figure 5.	Spiral-shaped inclusion trails and associated line diagram	B-5
Figure 6.	Slightly sigmoidal shaped inclusion trails in garnet porphyroblasts	B-6

Figure 7.	Photomicrographs of staurolite and garnet in sample TC1365	B-7
Figure 8.	Skeletal inclusion trail geometries drawn as vertical cross-sections for each porphyroblast phase in each layer	B-8
Figure 9.	Series of parallel vertical cuts through a model porphyroblast	B-9
Figure 10.	Sequence showing creation of the model porphyroblast	B-11
Figure 11.	Set of radial sections made through the centre of the 3-D porphyroblast	B-12
Figure 12.	Sections made through the schematic inclusion trails and original model	B-13
Figure 13.	Range of inclusion trail patterns made by taking sections through the schematic model porphyroblast at different orientations and at various distances from the centre	B-14
Figure 14.	Inclusion trail geometry in three different horizontal cuts through the porphyroblast	B-15
Figure 15.	Porphyroblast growth ceases once a differentiated crenulation cleavage begins to form in the immediate vicinity	B-16
Figure 16.	Skeletal diagrams of vertical cross-sections through spiral-shaped inclusion trails in porphyroblasts	B-17
Figure 17.	Equal area rose diagrams showing the pitch of truncational discontinuities preserved as inclusion trails	B-18
Figure 18.	Stereonets of FIA plunges and histograms of angle of plunge data	B-19
Figure 19.	Stereonet showing how the intersection of a sub-horizontal plane with any other steeply dipping plane has a gentle plunge	B-20

Section C

Figure 1.	Partitioning of deformation	C-1
Figure 2.	Millipede shaped geometry of the strain field that results from coaxial progressive bulk inhomogeneous shortening	C-2
Figure 3.	Accurately reproduced line diagram from fig. 8 in Ghosh (1975)	C-3
Figure 4.	Accurately reproduced line diagram from fig. 11 in Ghosh (1975)	C-4
Figure 5.	Millipede like geometries produced experimentally	C-5
Figure 6.	Line diagrams show how the core of a porphyroblast may preserve a coaxial millipede geometry and difference between differentiation and vergence asymmetry	C-6
Figure 7.	Millipede structures preserved in fold hinge	C-7

Figure 8.	Fold hinge showing the relative orientation and locations of blocks from which thin sections were cut	C-8
Figure 9.	Plagioclase porphyroblast containing highly oblique millipede-shaped trails	C-10
Figure 10.	Photographic detail of right hand millipede end	C-13
Figure 11.	Millipede plagioclase porphyroblast in a sub horizontal section	C-14
Figure 12.	Reconstruction of millipede structure	C-15
Figure 13.	Two horizontal slices cut through the millipede model	C-16
Figure 14.	Vertical millipede sections	C-17
Figure 15.	Radial sections through the millipede model	C-18
Figure 16.	Sketches showing changing scales of deformation partitioning	C-19
Figure 17.	Cut-away profile view of a model spiral and the range of inclusion trail geometries radial thin sections through spiral porphyroblast	C-20

Section D

Figure 1.	Location map showing the major fold structures	D-1
Figure 2.	Detailed map of the study area	D-2
Figure 3.	Schematic section showing the position of the Lebanon Antiformal Syncline on the overturned limb of the refolded Blue Hills Nappe	D-3
Figure 4.	Photomicrographs showing inclusion trail geometries preserved in garnet porphyroblasts	D-5
Figure 5.	Photomicrographs of garnet porphyroblasts from sample MB030	D-6
Figure 6.	3D model demonstrating the asymmetry method for establishing the FIA trend for a sample containing simple sigmoid inclusion trails	D-7
Figure 7.	Equal area rose diagrams of FIA trends	D-9
Figure 8.	Maps and equal area rose diagrams of the 4 successive FIA sets	D-10
Figure 9.	Histograms showing the asymmetry of inclusion trails	D-11
Figure 10.	Block diagram illustrating the major structural and stratigraphic features of the Lebanon Antiformal Syncline	D-12
Figure 11.	Photomicrographs of pseudomorphs of staurolite and muscovite after andalusite	D-13
Figure 12.	Photomicrographs illustrating the relationship between andalusite, staurolite and sillimanite	D-14

Figure 13.	Pseudosections showing approximate P-T paths for rocks in the transition zone, staurolite zone and sillimanite zone	D-16
Figure 14.	Histograms showing the relative frequency of inclusion trail asymmetries	D-17
Figure 15.	Accumulation of displacement during gravitational collapse	D-18
Figure 16.	Inclusion trail asymmetries divided into FIA sets and plotted separately for the northern and southern limb of the Lebanon Antiformal Syncline and the northern and the southern limbs of the second order antiforms	D-19
Figure 17.	Schematic sketch showing the effects of a developing sub-horizontal foliation with a clockwise differentiation asymmetry on each limb of an upright fold	D-20
Figure 18.	Map showing the distribution of samples containing FIA set 3	D-21
Figure 19.	Schematic representation of the upper 50-60 km of the lithosphere during uplift and gravity induced collapse phases of orogenesis	D-22
Figure 20.	Schematic diagram showing the relationship between deformation, metamorphism and porphyroblast growth	D-23

Section A:

Movement directions in porphyroblastic rocks:

Evaluation of the "FitPitch" and

the "asymmetry" methods

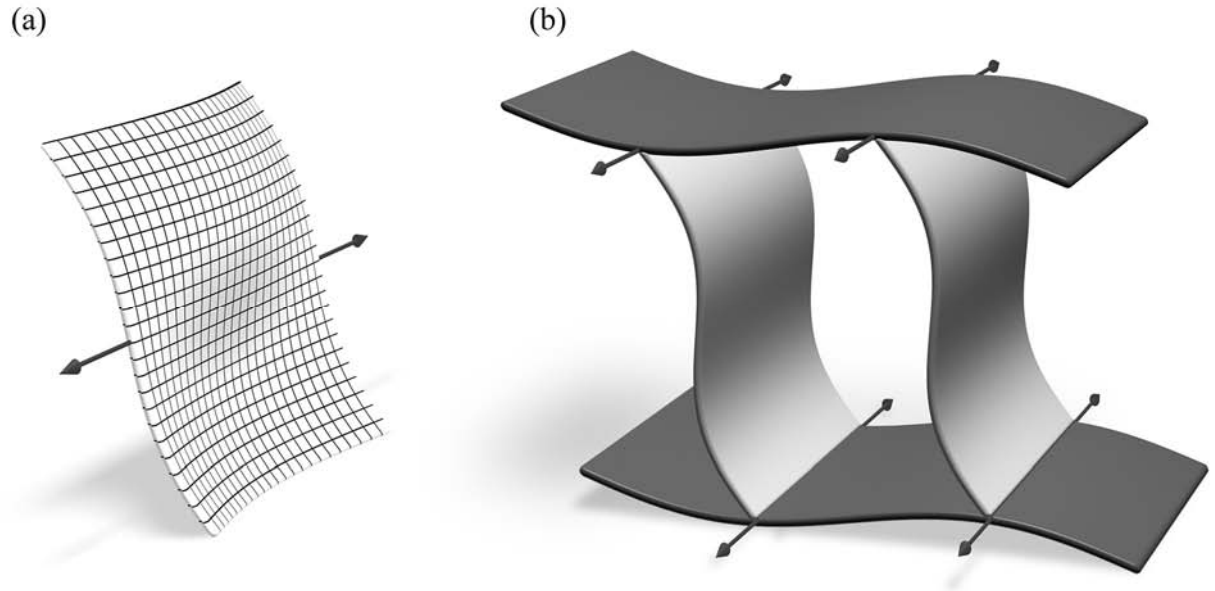

Figure 1. The Foliation Inflexion Axis (FIA), indicted by an arrow, is the axis of zero curvature in the doubly-curving inclusion trails (a). A FIA may also take the form of the intersection lineation (Foliation Intersection Axis) between two foliations preserved within a porphyroblast (b).

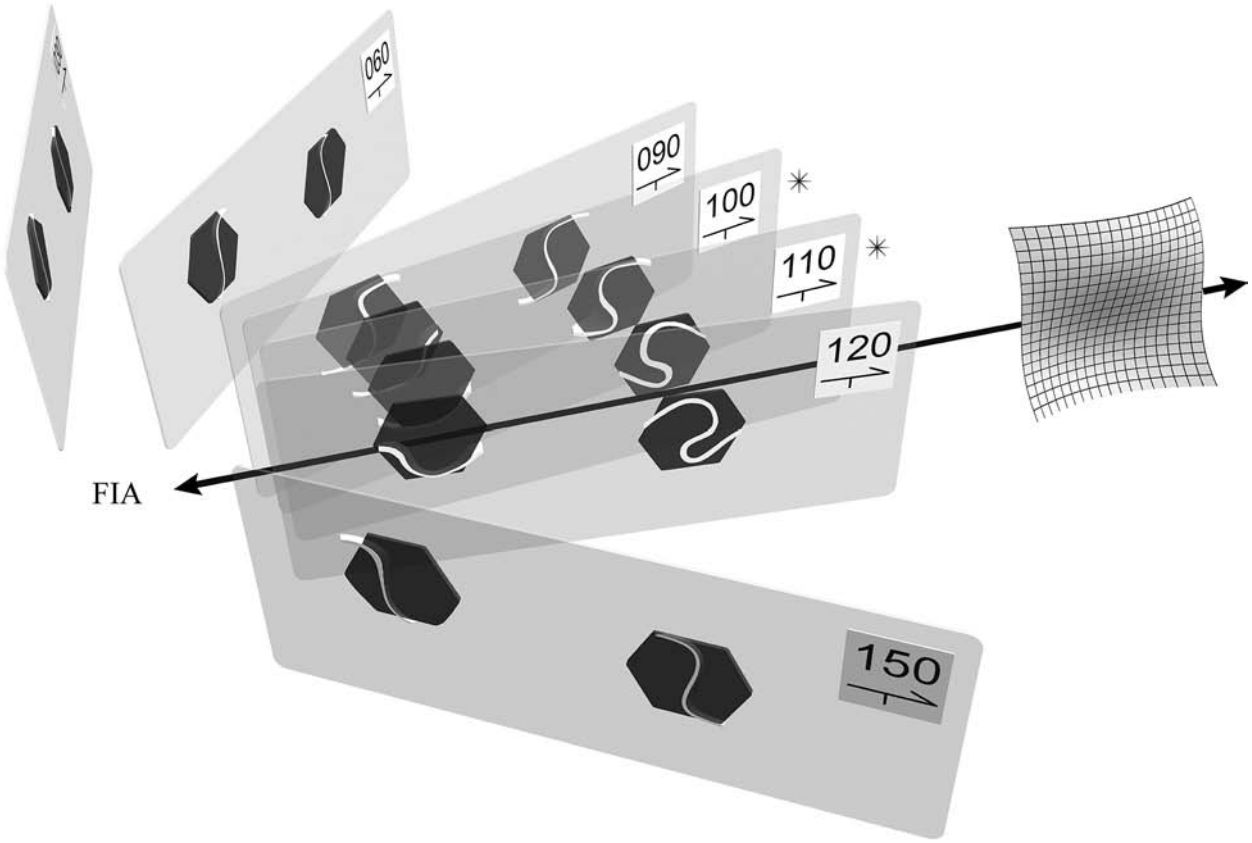

Figure 2. 3D model demonstrating the asymmetry method for establishing the FIA trend for a sample containing simple sigmoid inclusion trails similar to those depicted in Figure 1a. Initially, six vertical thin sections, cut at 30^0 intervals from an oriented horizontal slab (i.e., trends of 0, 30, 60, 90, 120 and 150 degrees) are examined from the same direction around the compass and the geometry of the inclusion trails in all the porphyroblasts is recorded. The FIA trend can be refined to within a 10° range by preparing two additional sections (marked with an asterisk) covering the 30° interval over which the flip in asymmetry is observed. This is seen to occur between 90^0 and 120^0 for the model shown. In this example, two sections with strikes of 100^0 and 110^0 are prepared and examined. The change from "S" shaped to "Z" shaped inclusion trails is now constrained to between 110^0 and 120^0 with the mid-point (115°) being recorded as the trend of the FIA. See also Appendix E: "E01-asymmetry method.mov".

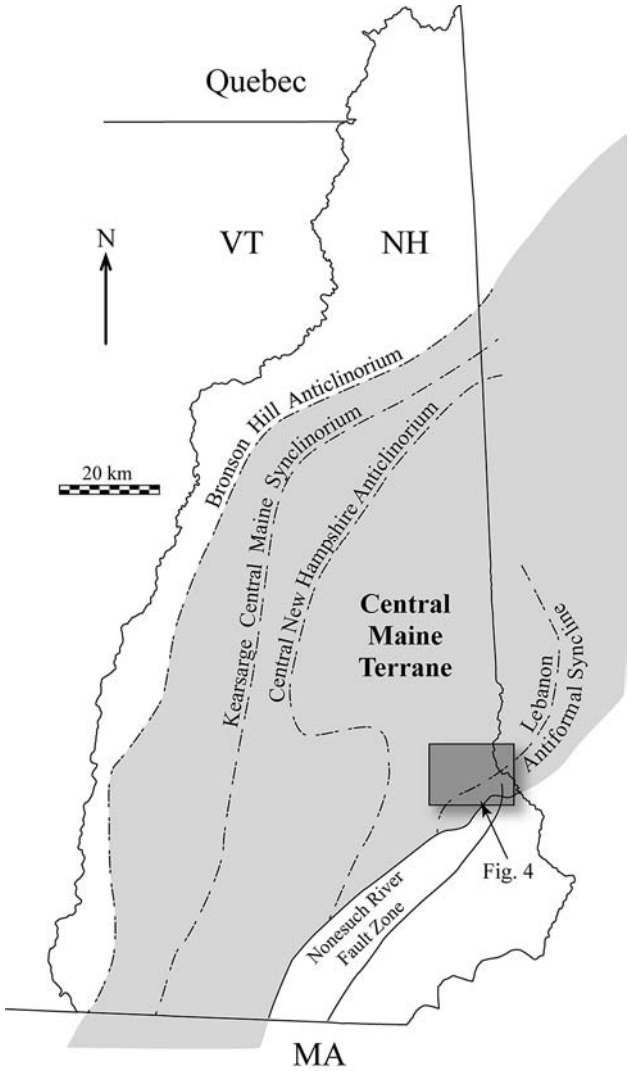

Figure 3. Major structural features of New Hampshire. The Central Maine Terrane (CMT) is interpreted as a large Silurian to early Devonian depositional basin that was multiply deformed and metamorphosed during the Acadian and Alleghanian orogenies. (Modified after Eusden, 1988). The inset box highlights the area shown in Figure 4.

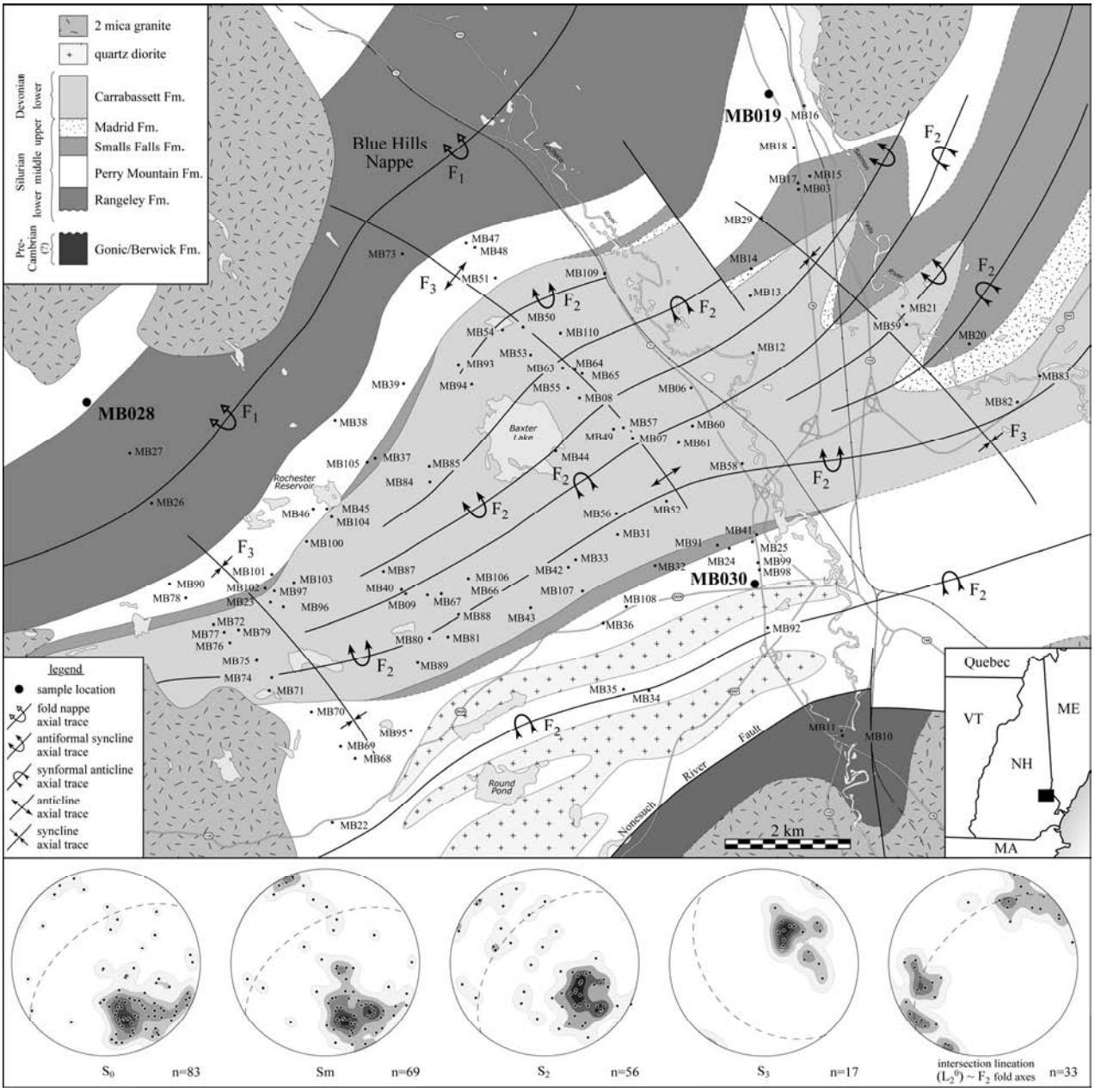

Figure 4. Map of the study area showing major structural features and sample localities. Samples referred to in the text are highlighted in bold. Base map after Eusden *et al*., 1984.

Sample	No. of model planes	α_d	α_m	R_d	R_m	Best fit planes (dip/dip-direction)
MB019	1	26.6	24.9	1.692	1.809	70/272
n=122	2	7.9	3.1	3.318	8.295	60/043; 69/274
Sections: 10	**3**	4.4	4.1	4.944	5.380	60/043; 58/279; 74/266
MB028	1	27.4	26.6	1.642	1.693	67/031
n=440	2	13.5	11.8	1.980	2.269	58/027; 71/245
Sections: 7	**3**	8.3	5.2	2.757	4.415	74/043; 54/024; 71/245
MB030	1	22.6	21.2	1.987	2.125	39/350
n=161	**2**	8.6	4.2	3.268	6.655	42/344; 55/106
Sections: 10	3	6.8	13.1	3.805	1.965	46/346; 55/106; 28/319

Table 1. FitPitch data for the three porphyroblastic samples. The number of data collected is given for each sample, along with the results from FitPitch for one, two and three model planes. The value α_d is the average angular deviation between measured and model intersection-lines (i.e., the sum of deviations of all data from their nearest model intersection lines divided by the total number of data). α_m is the average deviation between best-fit lines calculated for individual thin sections and best-fit model intersection lines based on all data. R_d and R_m are the corresponding values normalised by uniform data to remove the bias towards multiple plane models. The choice of which solution best describes the data (bold type) is based, largely on which solution has the highest R_d and R_m values.

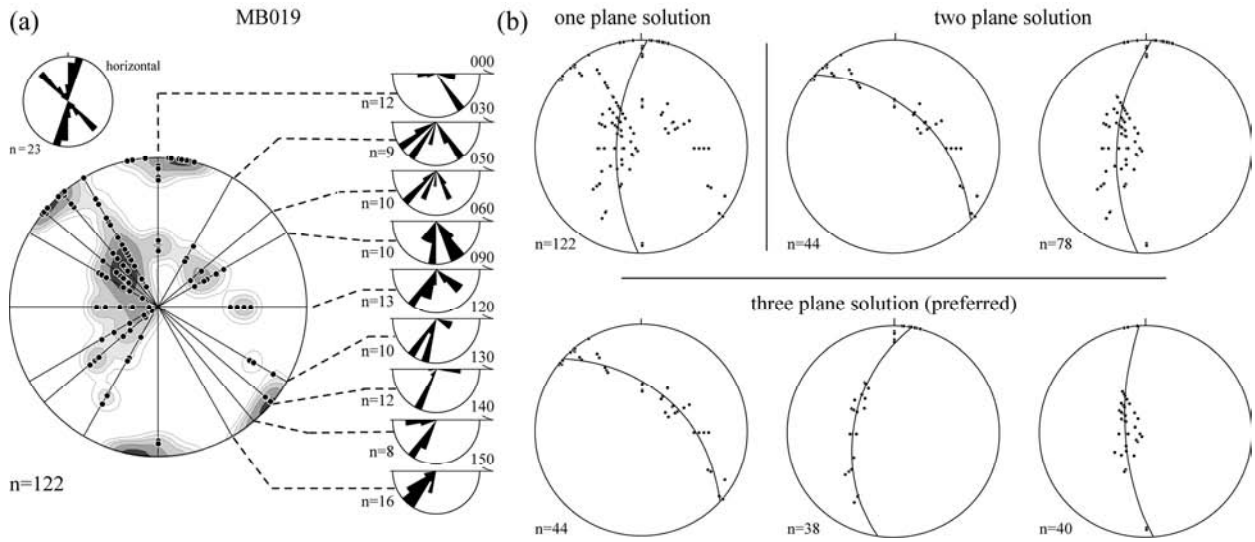

Figure 5. (a) Pitch data for sample MB019 as measured in nine vertical thin-sections, shown as contoured scatter on a lower-hemisphere equal area stereonet (Gaussian contours with k=100 calculated after Robin and Jowett; 1986) and as rose diagrams for each section with 10^0 sector size. (b) Best fit solutions for one, two and three model planes. A three plane solution is preferred as explained in the text.

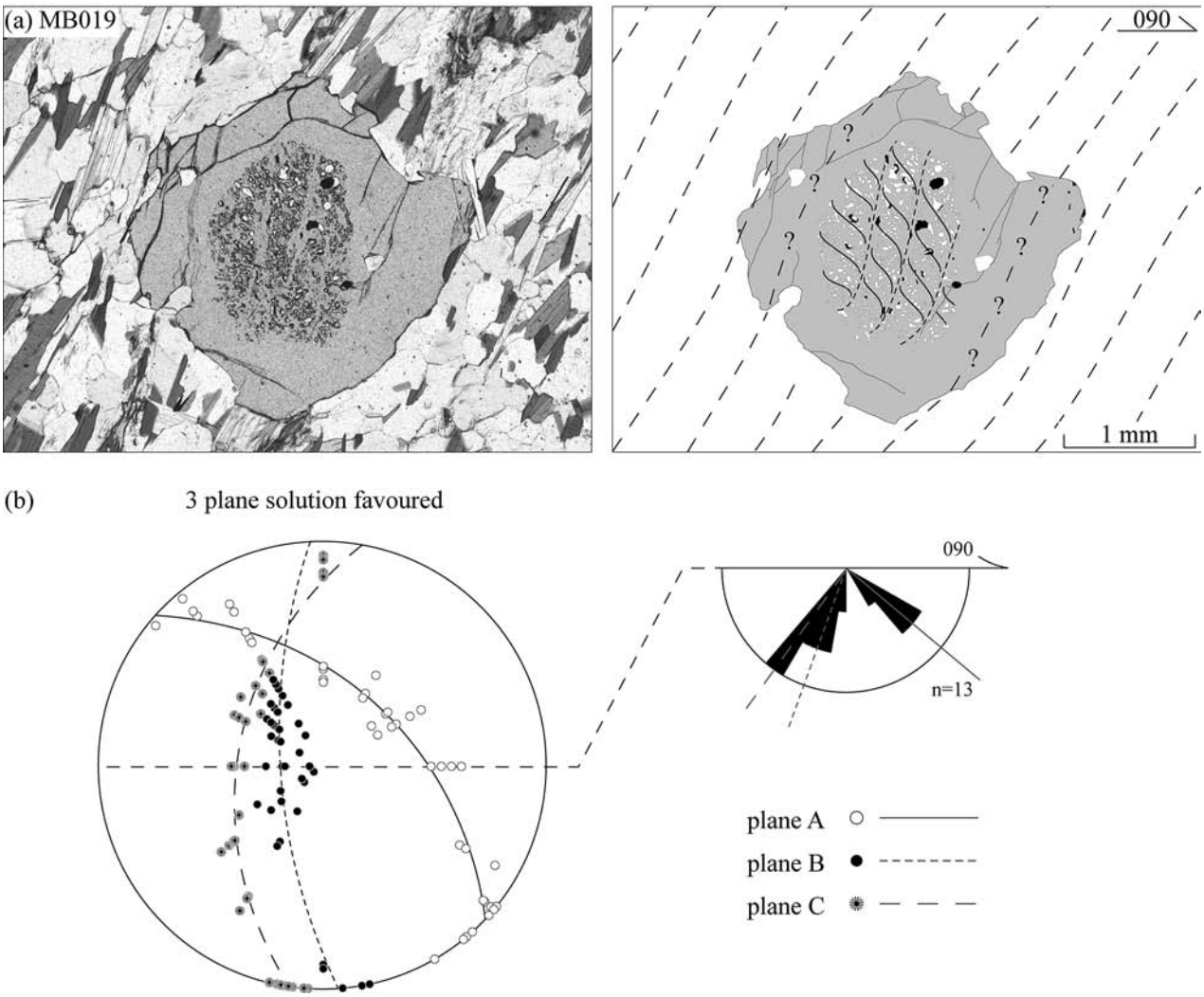

Figure 6. (a) Photomicrograph and interpretive sketch of a porphyroblast from the 090^0 section of sample MB019. (b) Equal area lower hemisphere stereonet plot of pitch measurements and rose diagram of measured data for the 090^0 section from sample MB019. Data points allocated to each model plane by FitPitch are given different symbols on the stereonet. This diagram illustrates the closeness of fit between the three modal orientation maxima observed in the rose diagram, the three different foliations preserved in the porphyroblast and the orientation of the intersection lines between the vertical thin-section (dashed line) and the three model planes.

Sample	Resultant FIA		
	FitPitch (dip/dip direction)	Asymmetry method	
MB019	38/339	155 (335)	pFIA
	41/342	155 (335)	curvature of diff. cren.
	* 31/347 *	* 175 (355) *	rim to matrix
MB028	35/325	-	
	31/323	-	
	33/322	-	
MB030	37/017	115 (295)	core to median ?

Table 2. FIA orientations calculated with the FitPitch computer program versus FIA orientations established for the same samples using the asymmetry method. See text for discussion of the similarities and differences between results obtained by the two different techniques.

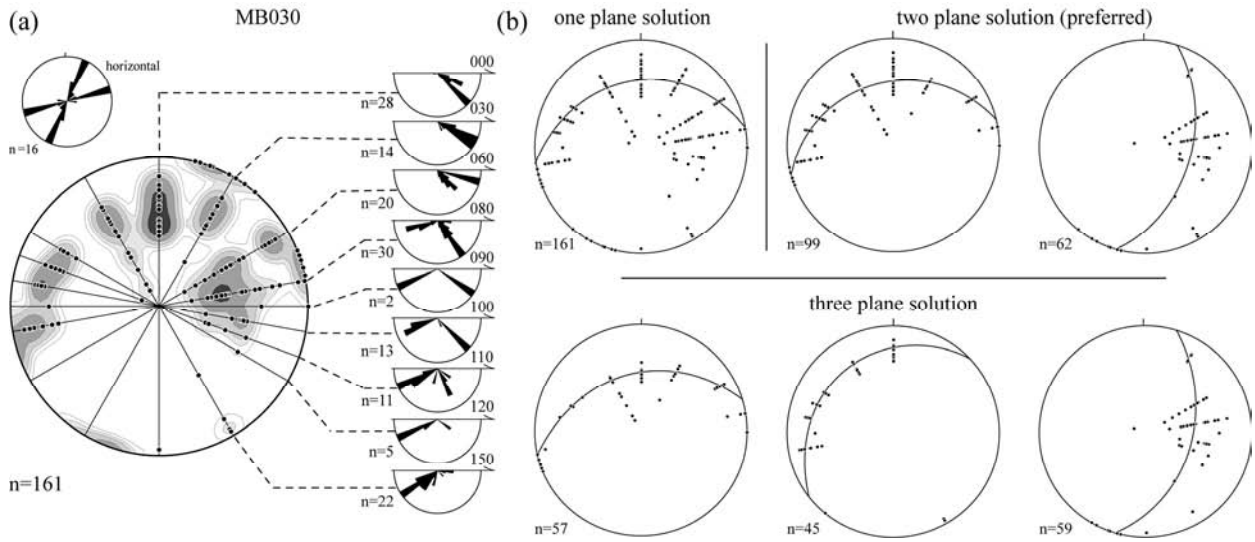

Figure 7. (a) Pitch data for sample MB030 as measured in nine vertical thin-sections, shown as contoured scatter on a lower-hemisphere equal area stereonet (Gaussian contours with k=100 calculated after Robin and Jowett; 1986) and as rose diagrams for each section with 10^0 sector size. (b) Best fit solutions for one, two and three model planes. A two plane solution is preferred as explained in the text.

Figure 8. (a) and (c) Photomicrographs and interpretive sketches of porphyroblasts from the 030^0 and 100^0 sections of sample MB030. (b) Equal area lower hemisphere stereonet plot of pitch measurements and rose diagrams of measured data for the same sections. Data points allocated to each model plane by FitPitch are given different symbols on the stereonet. The intersections between the two vertical thin-sections (dashed lines on stereonet) with the two model planes calculated with FitPitch closely mirror the data presented in the corresponding rose diagrams and what is observed in the thin-sections.

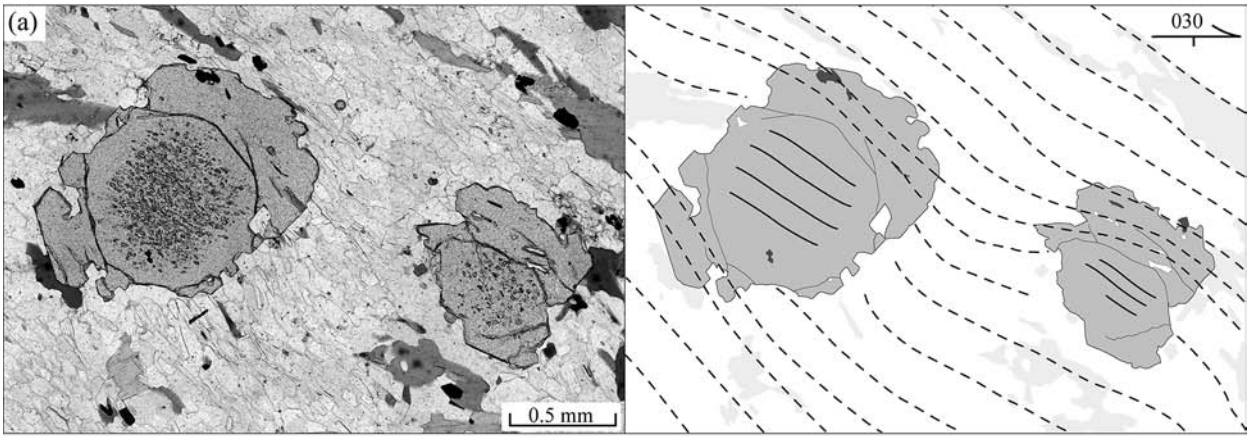
(a)
0.5 mm
030

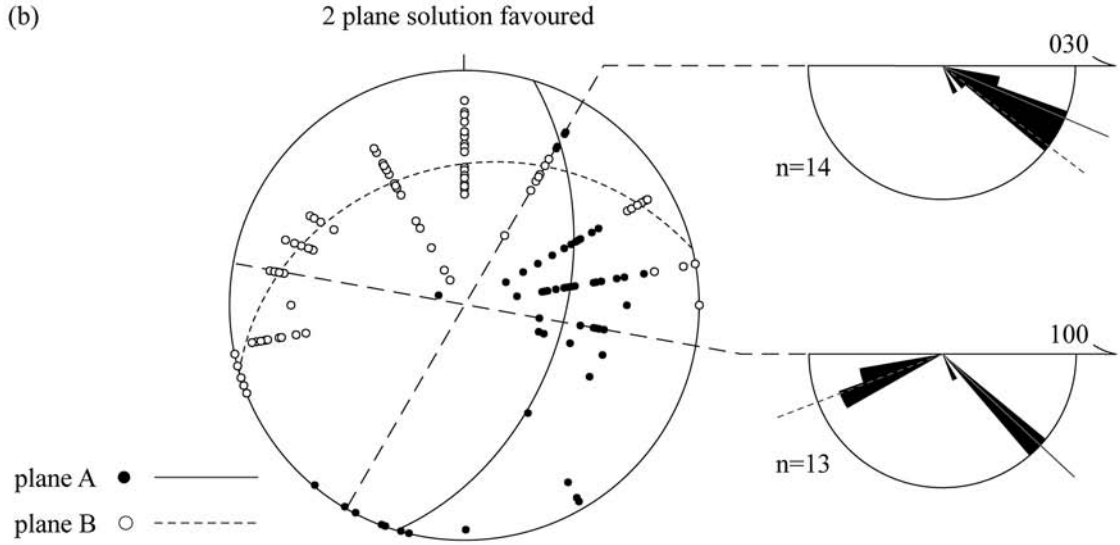
(b)
2 plane solution favoured
030
n=14
100
n=13
plane A
plane B

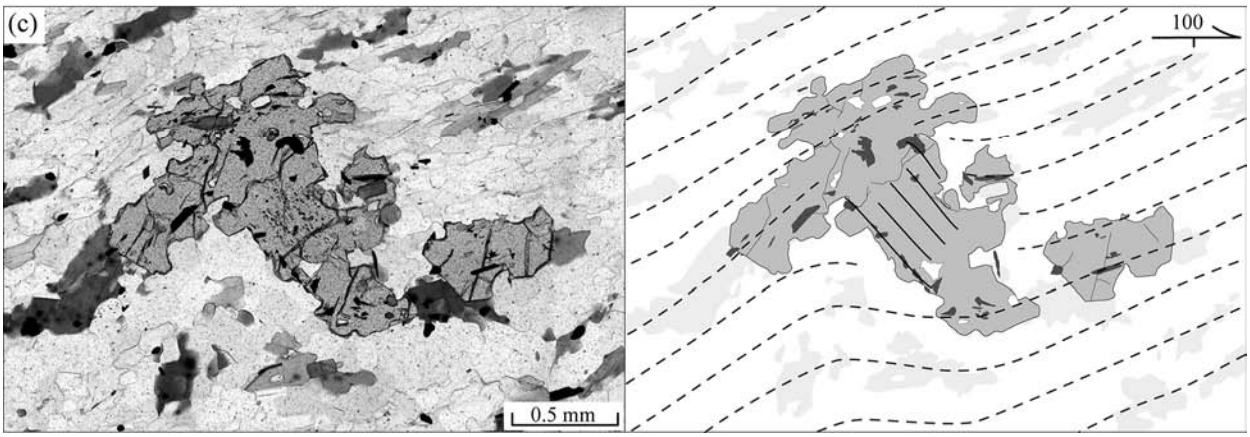
(c)
0.5 mm
100

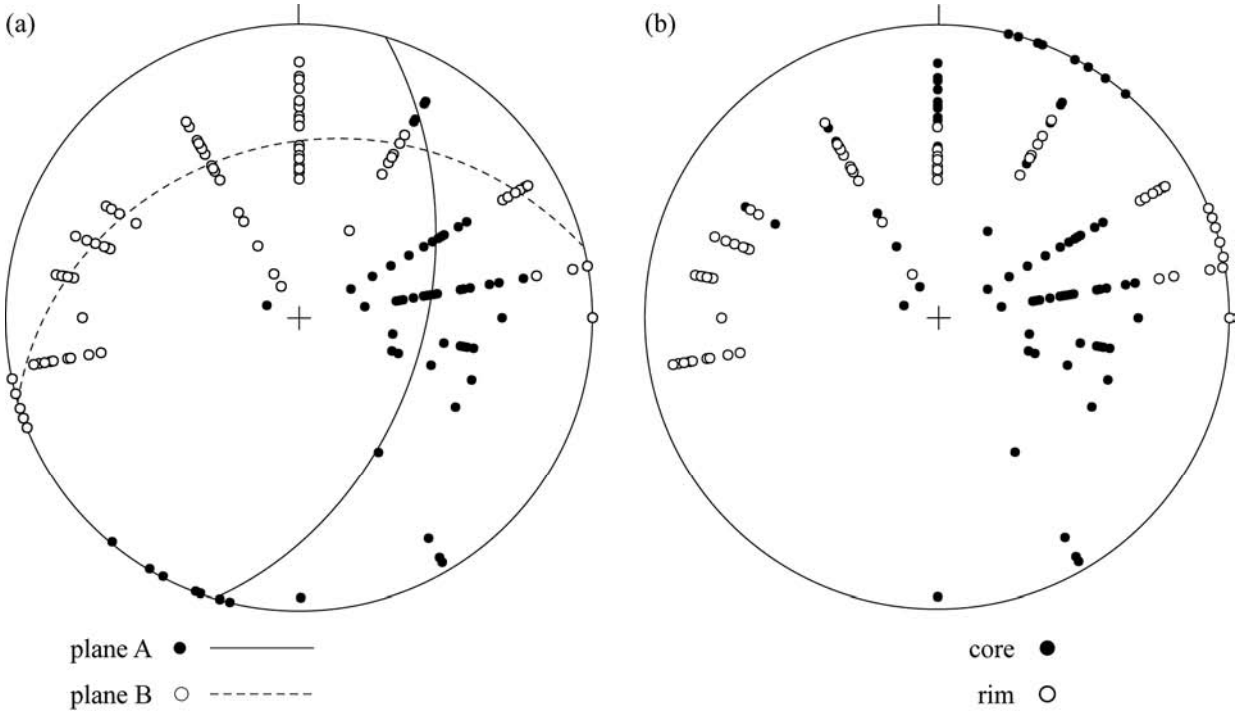

Figure 9. (a) Separation of MB030 pitch data into two planes according to FitPitch and (b) core and rim data plotted separately.

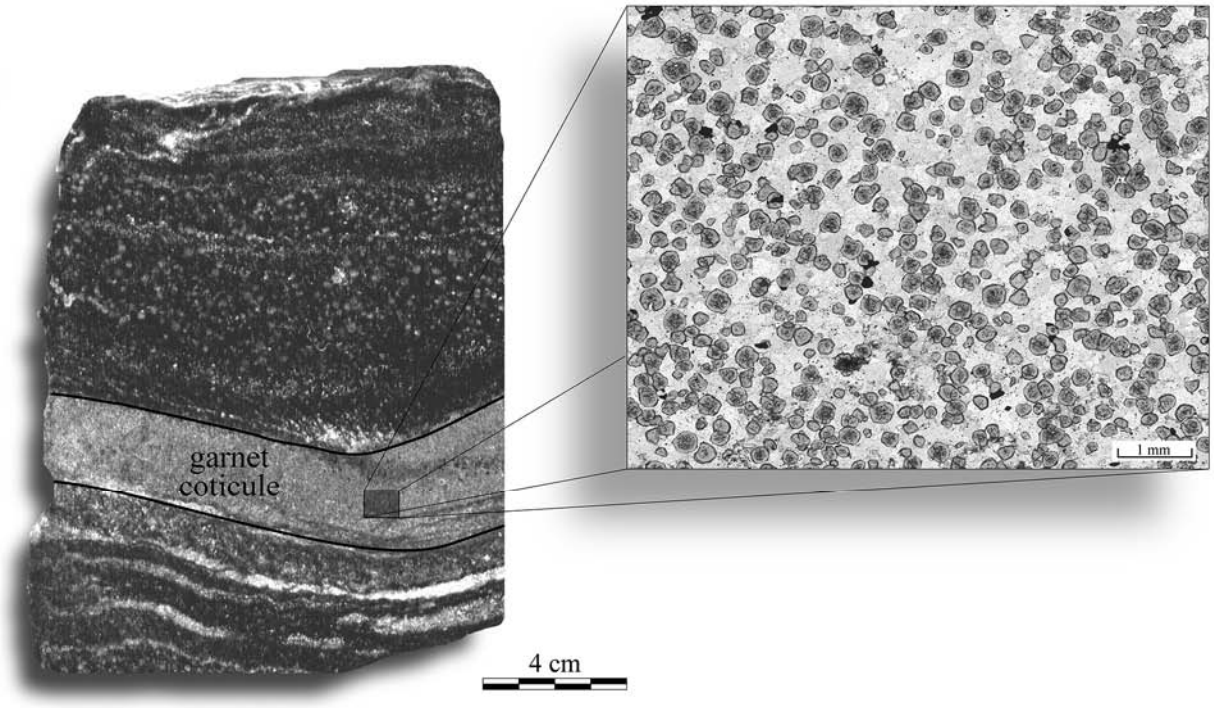

Figure 10. The Perry Mountain Formation is characterised by stringers or pods of garnet "coticule" as shown in this hand specimen of sample MB028. The photomicrograph shows the fine-grained nature of the garnet porphyroblasts which give the coticule its distinctive pink colour.

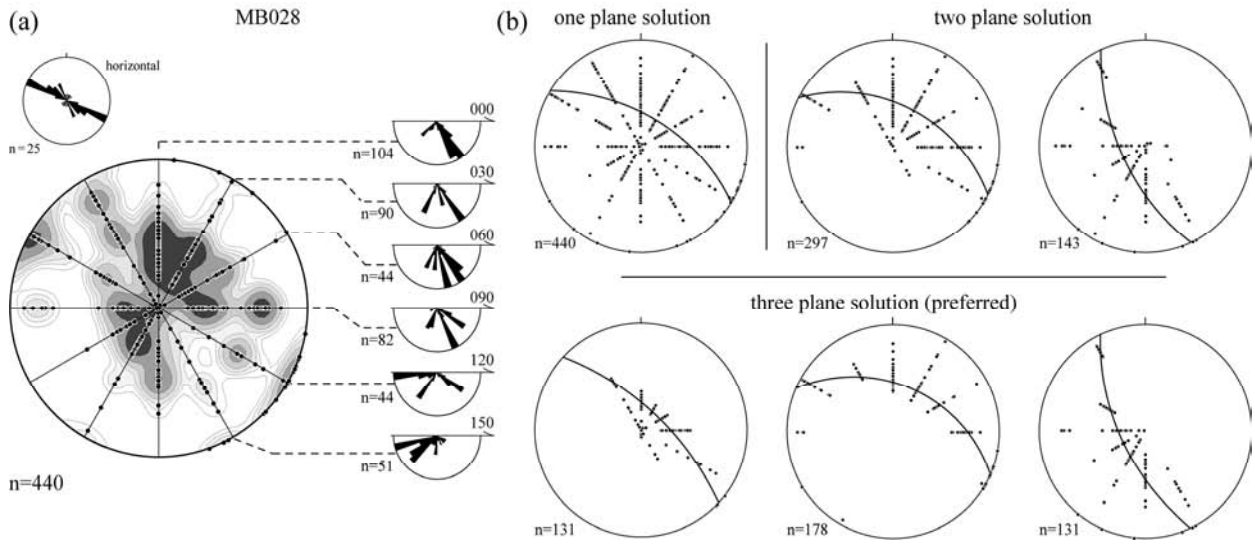

Figure 11. Pitch data for sample MB028 measured in one horizontal and six vertical thin-sections shown as contoured scatter on a lower-hemisphere equal area stereonet (Gaussian contours with k=100 calculated after Robin and Jowett; 1986) and as rose diagrams for each section with 10^0 sector size. (b) Best fit solutions for one, two and three model planes. A three plane solution is preferred as explained in the text.

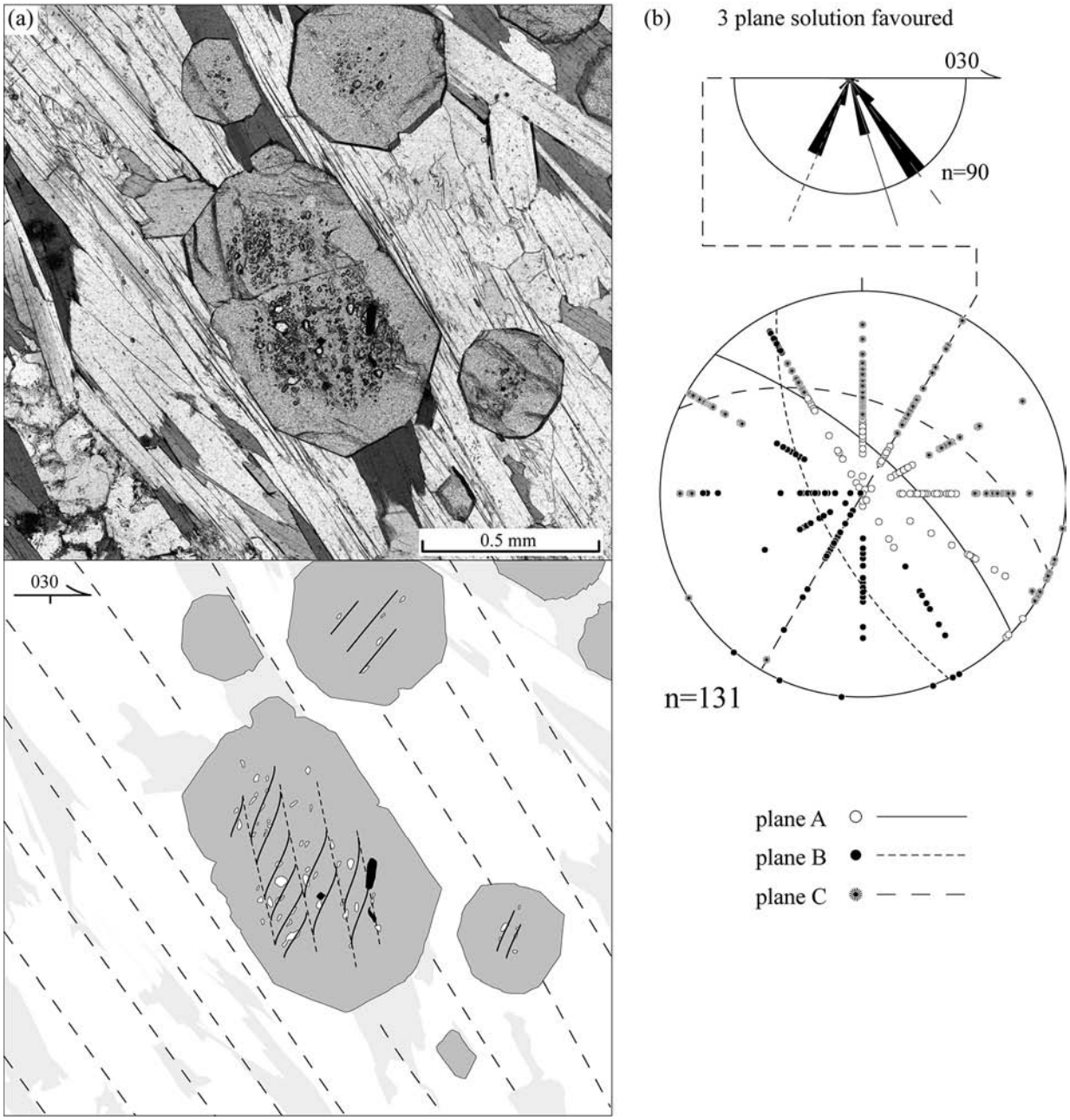

Figure 12. (a) Photomicrograph and interpretive sketch of a porphyroblast from the 030^0 section of sample MB028 which has overgrown a differentiated crenulation cleavage. (b) Equal area lower hemisphere stereonet plot of pitch measurements and rose diagram of measured data for the 030^0 section. Data points allocated to each model plane by FitPitch are given different symbols on the stereonet. The rose diagram clearly displays three modal peaks which correspond to the intersections of the vertical 030^0 section (dashed line) with the three model planes on the stereonet and also with the orientations of the foliations preserved in the core of the garnet porphyroblast and the matrix.

Section B:

The internal inclusion trail geometries preserved within a first phase of porphyroblast growth

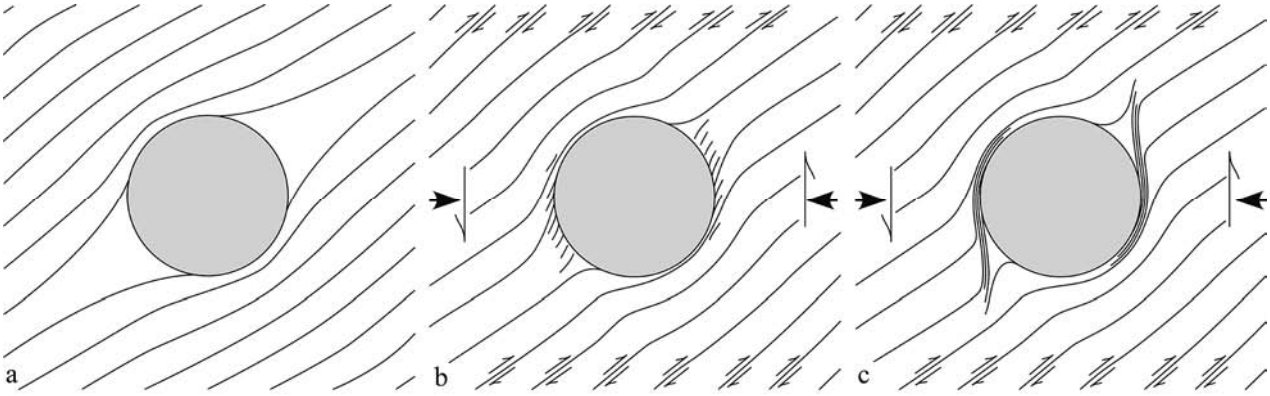

Figure 1. (a) Vertical cross-section through a porphyroblast within an obliquely dipping foliated matrix. (b) Progressive bulk inhomogeneous shortening involving a component of anticlockwise shear causes antithetic (clockwise shear) on the oblique foliation. The presence of the rigid porphyroblast causes synthetic clockwise axial plane shear to localize against its margins. (c) Clockwise synthetic shear develops a differentiated foliation against the porphyroblast margin.

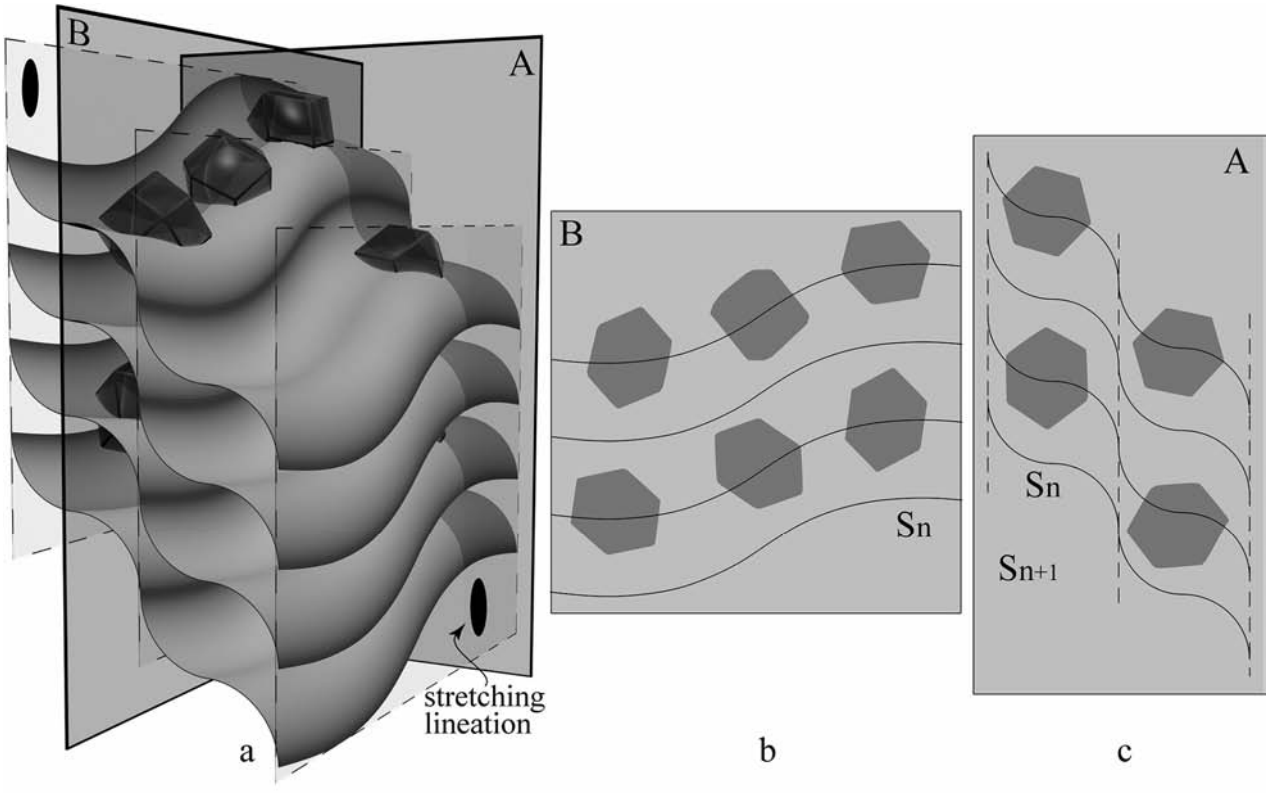

Figure 2. (a) 3-D sketch showing the location of the 2-D longitudinal section (b) and cross section (c). Porphyroblasts that grew in crenulation hinges during a deformation event that formed a sub-vertical foliation S_{n+1} (a, c) contain FIAs with the same trend but variable plunges (a, b).

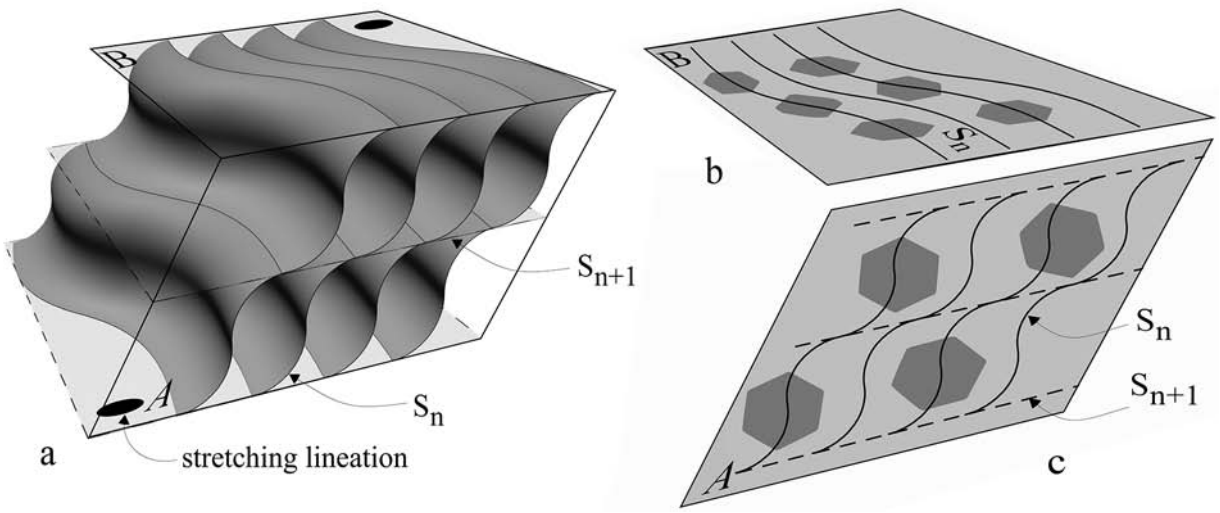

Figure 3. (a) 3-D sketch showing the location of the 2-D horizontal section (b) and cross section (c). Porphyroblasts that grew in crenulation hinges during a deformation event that formed a sub-horizontal foliation S_{n+1} (a, c) contain FIAs with the same plunge but variable trends (a, b).

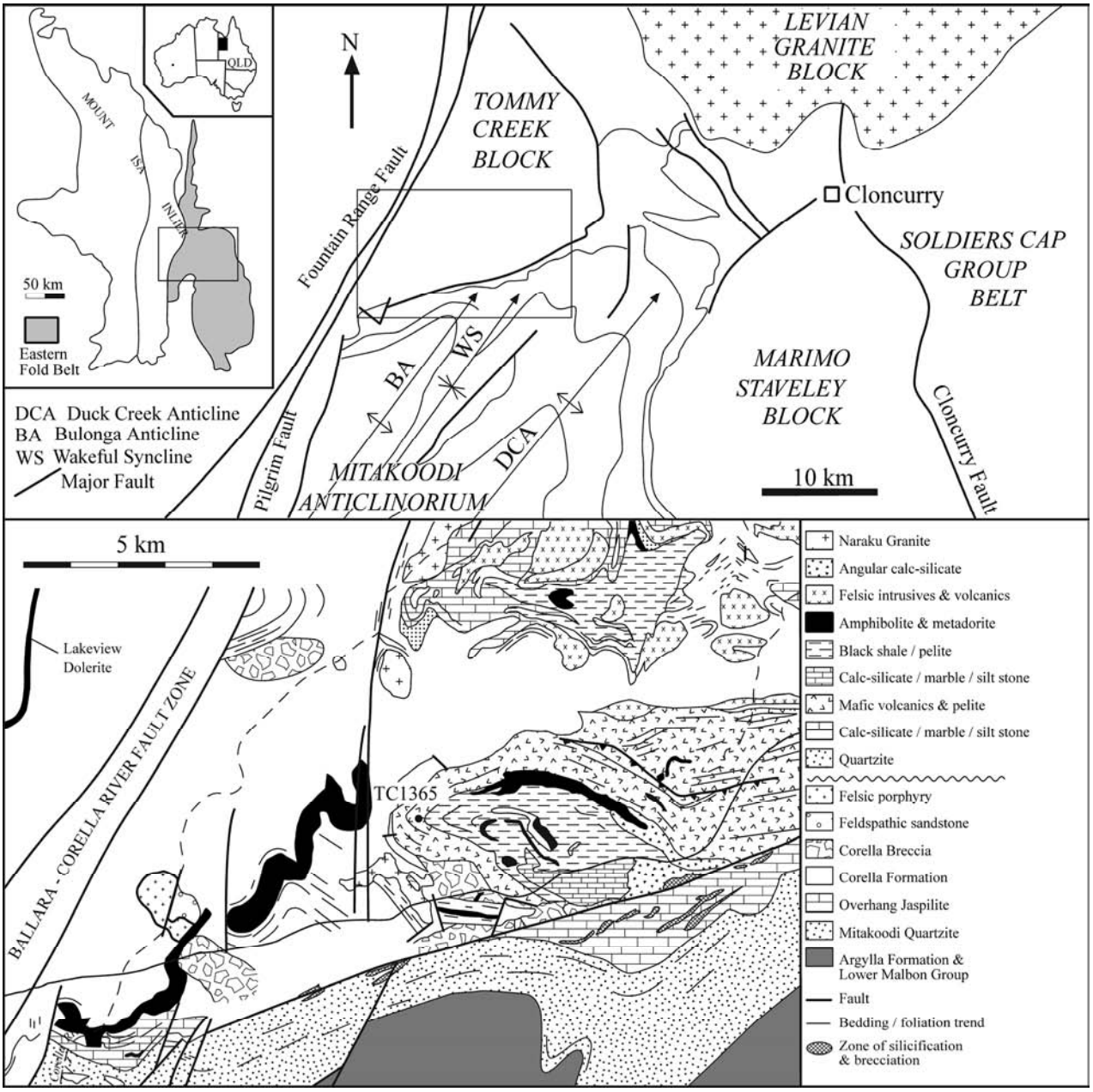

Figure 4. Location of samples TC1365 and TC1365i from adjacent thin pelitic bands in the Tommy Creek Block of the Mount Isa Province of Queensland, Australia.

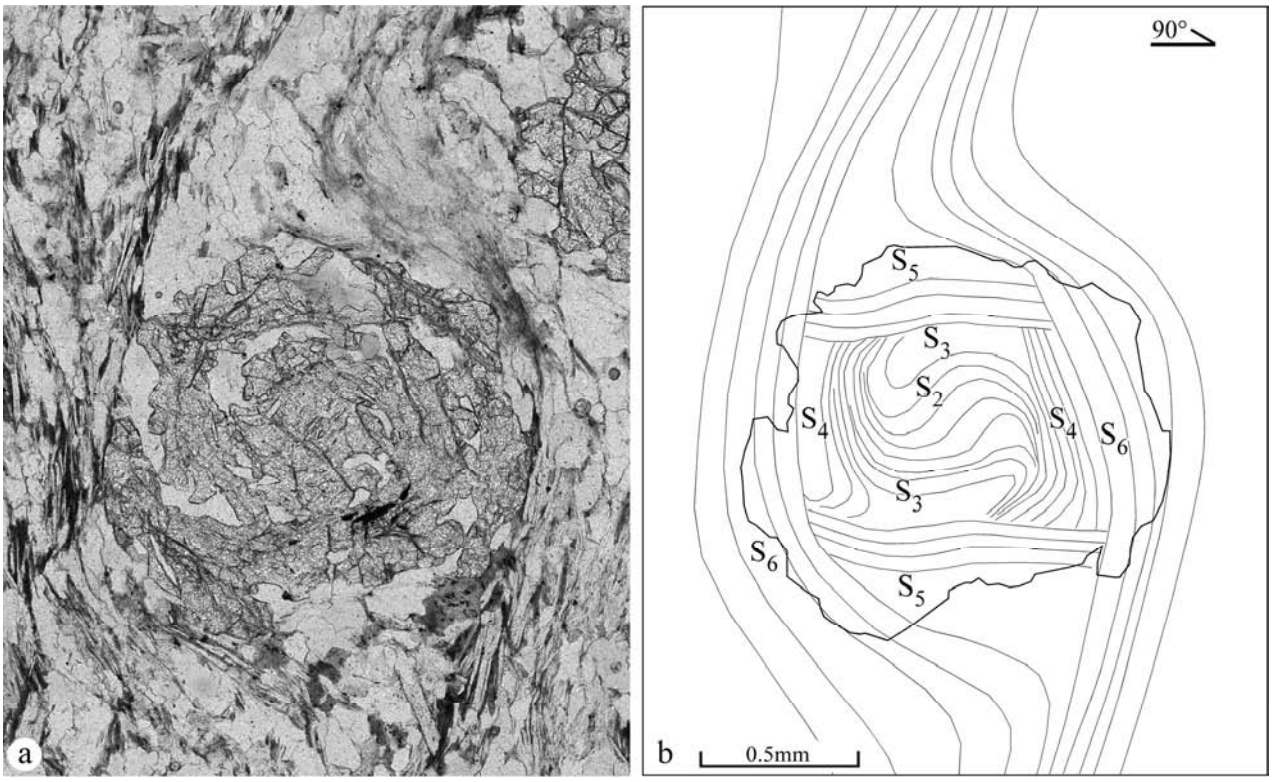

Figure 5. Spiral-shaped inclusion trails (a) and line diagram (b) of a garnet porphyroblast from Layer A in sample TC1365i. Vertical section strikes 90° with single barbed arrow showing strike and way up. The relics of 4 foliations are preserved with the fifth (S_6) being continuous with the matrix foliation. Note the truncational character of S_4, S_5 and S_6. Plane polarized light.

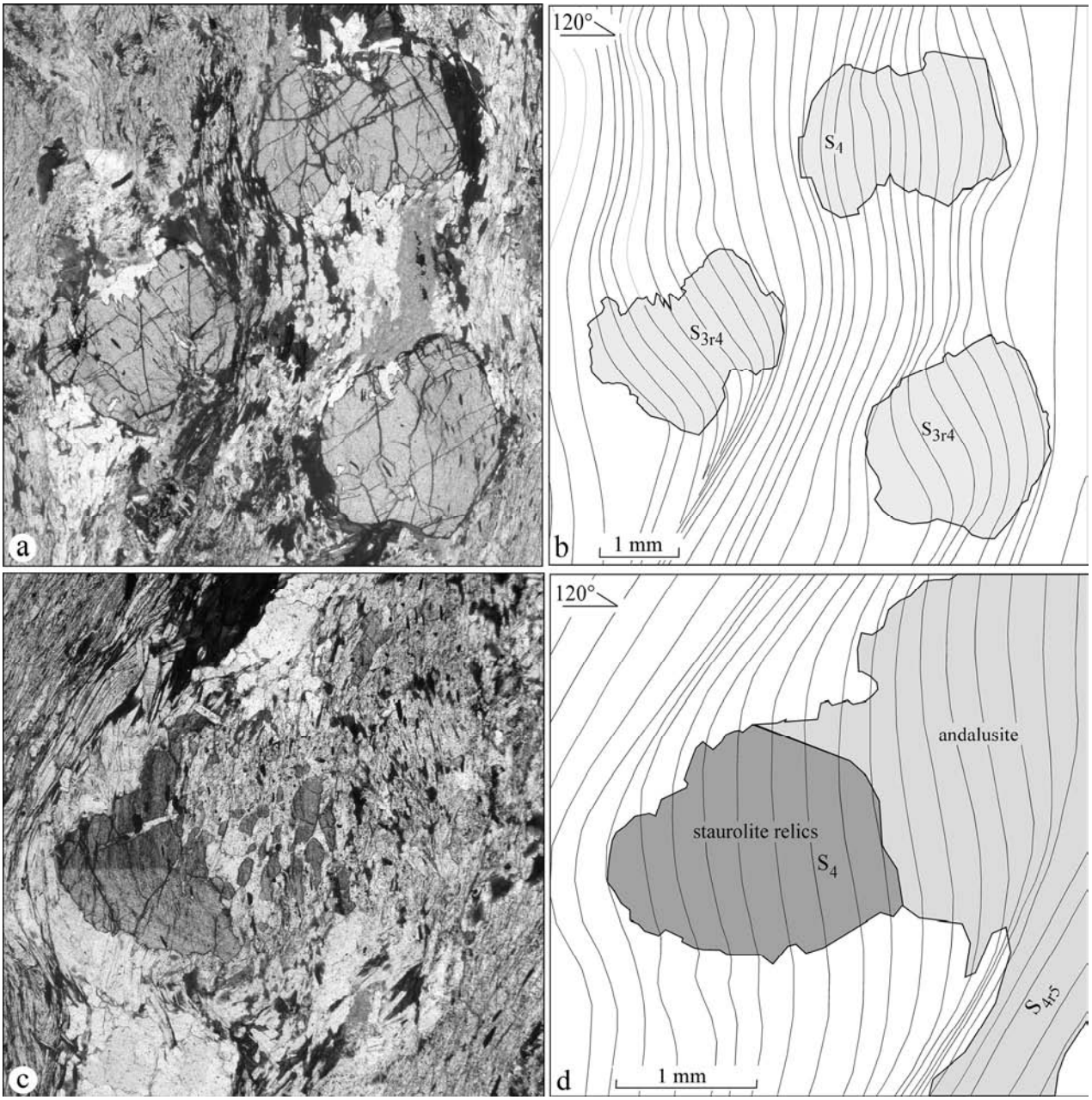

Figure 6. (a, b) Shows straight to slightly sigmoidal shaped inclusion trails in garnet porphyroblasts that grew during the development of a crenulation with a sub-horizontal axial plane S_5 in layer B in sample TC1365i. Vertical section strikes 120° with single barbed arrow showing strike and way up. Plane polarized light. (c, d) Shows a staurolite porphyroblast that grew during the development of a crenulation with a sub-horizontal axial plane S_5 in layer B in sample TC1365i. The staurolite was partially replaced by andalusite in a younger steep event S_6. Partial evidence for this are the remains of S_4, reactivated during D_5, preserved in the andalusite extremities. Vertical section strikes 120° with single barbed arrow showing strike and way up. Plane polarized light.

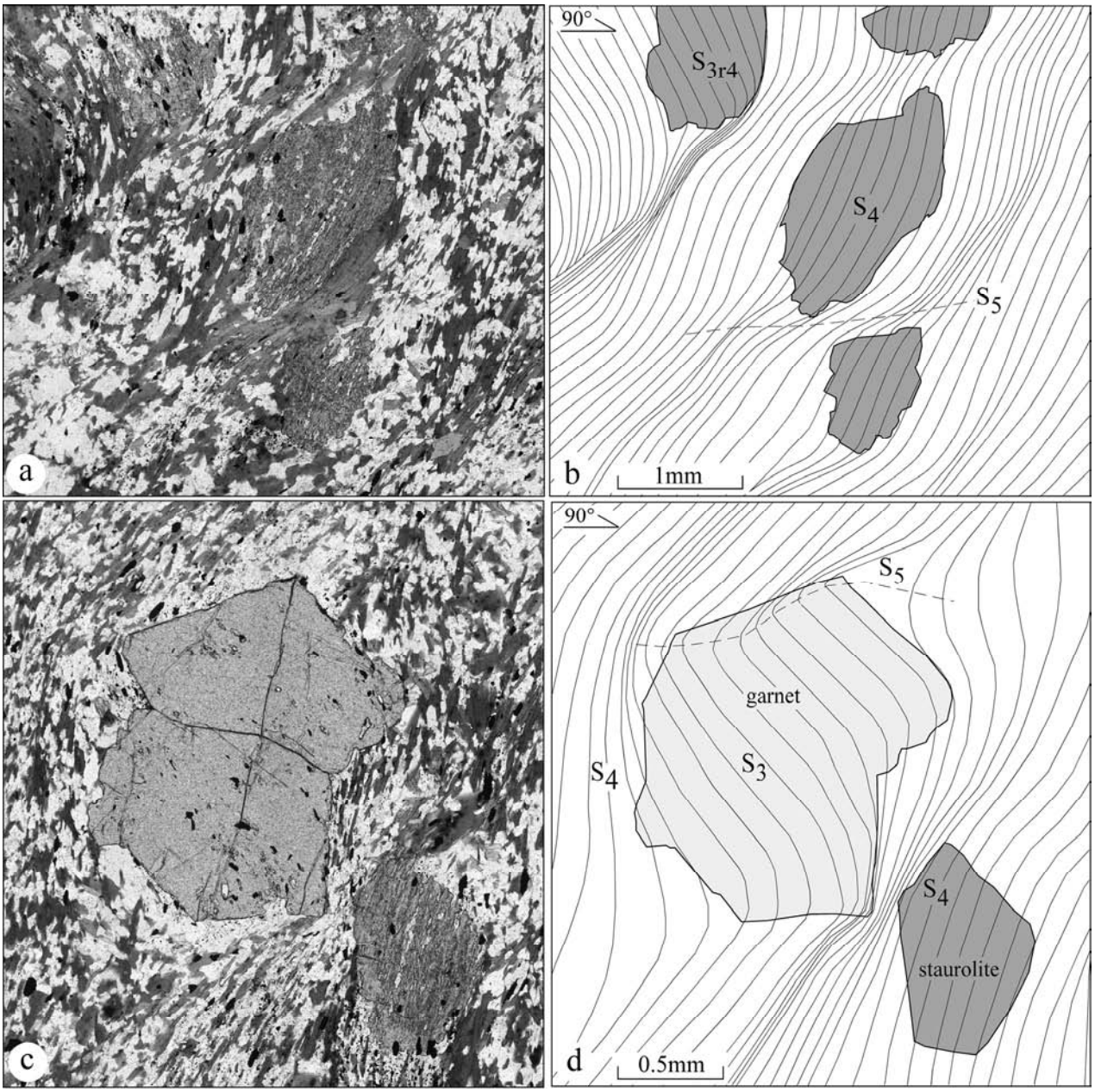

Figure 7. (a, b) Staurolite grown in steep event layer C in sample TC1365. Vertical section strikes 90° with single barbed arrow showing strike and way up. Plane polarized light. (c, d) Bulk of garnet overgrew S_3 in steep D_4 event in layer C in sample TC1365 (vertical S_4 intensifies at garnet rim within lower RH rim). Upper and lower garnet rims grew in D_5. Vertical section strikes 90° with single barbed arrow showing strike and way up. Plane polarized light.

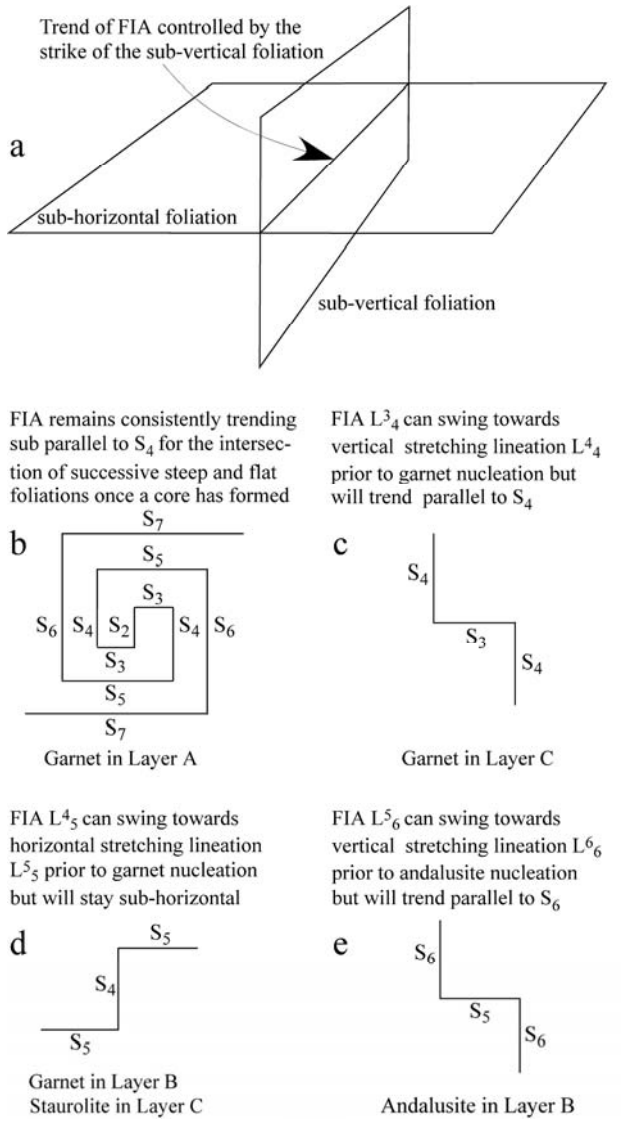

Figure 8. (a) Shows how FIA trend is controlled by the strike of the sub-vertical foliation. (b-e) skeletal inclusion trail geometries drawn as vertical cross-sections for each porphyroblast phase in each layer. The foliations represent those preserved within the porphyroblasts and can be correlated from layer to layer. (b) The FIA defined by L^3_4, L^4_5, L^5_6 and L^6_7 in the garnet from layer A remain consistently oriented throughout porphyroblast growth at 170°. (c) The FIA defined by L^3_4 in garnet from layer C formed during the development of a sub-vertical foliation and trend at 170°. (d) The FIA defined by the L^4_5 intersection lineation were rotated towards L^5_5 during the development of sub-horizontal S_5 in garnet and staurolite in layers B and C respectively and trend at 45°. (e) The FIA defined by the L^5_6 intersection lineation in andalusite in layer B may have been rotated towards the steeply plunging L^6_6 during the development of the sub-vertical S_6 but their trend remains at 170°.

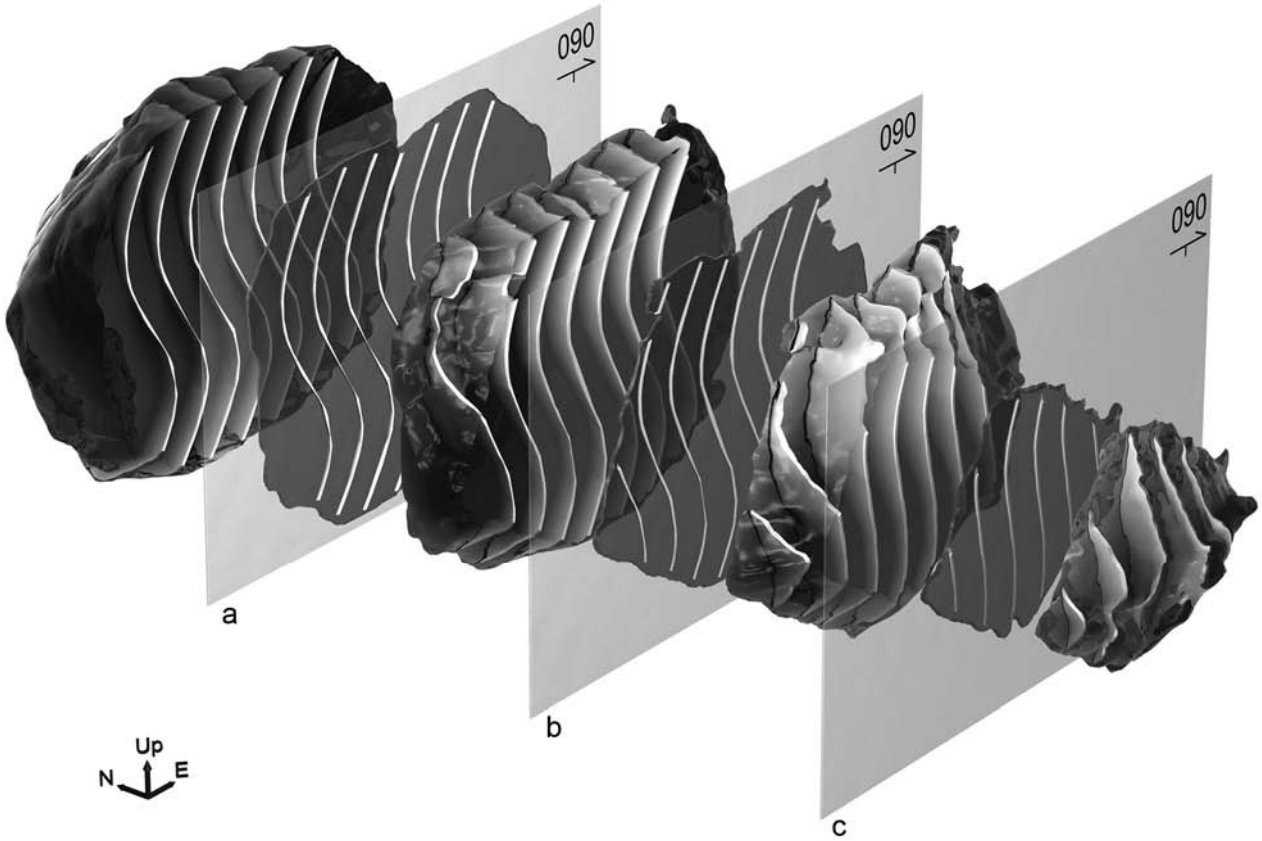

Figure 9. Shows how reconciliation of the structures observed in differently located thin sections into a complete three-dimensional presentation of the inclusion trail geometry is impractical because thin sections commonly cut each porphyroblast represented somewhere between its centre and edge.

Figure 10. (a) The 3-D inclusion trail geometry, produced from the high-resolution X-ray CT by Huddlestone-Holmes and Ketcham (2005) on a sample of Cram Hill Formation from south-eastern Vermont (Sample V209 in Bell et al., 1998). (b) Shows garnet and crack-fill material stripped away to reveal the central quartz inclusion trail (light coloured) along with higher attenuation opaques (ilmenite) inclusions. (c) 3-D inclusion surface drawn to pass through the centre of the quartz inclusions. (d) The dark ilmenite inclusions are parallel to the central surface drawn with the quartz inclusions removed. (e) Additional inclusion surfaces were made by extrapolation of the central trail, using the ilmenite inclusions as a guide and adjusting to create a satisfactory fit. (f). Shows garnet, as established from the original X-ray CT, resulting in the final model.

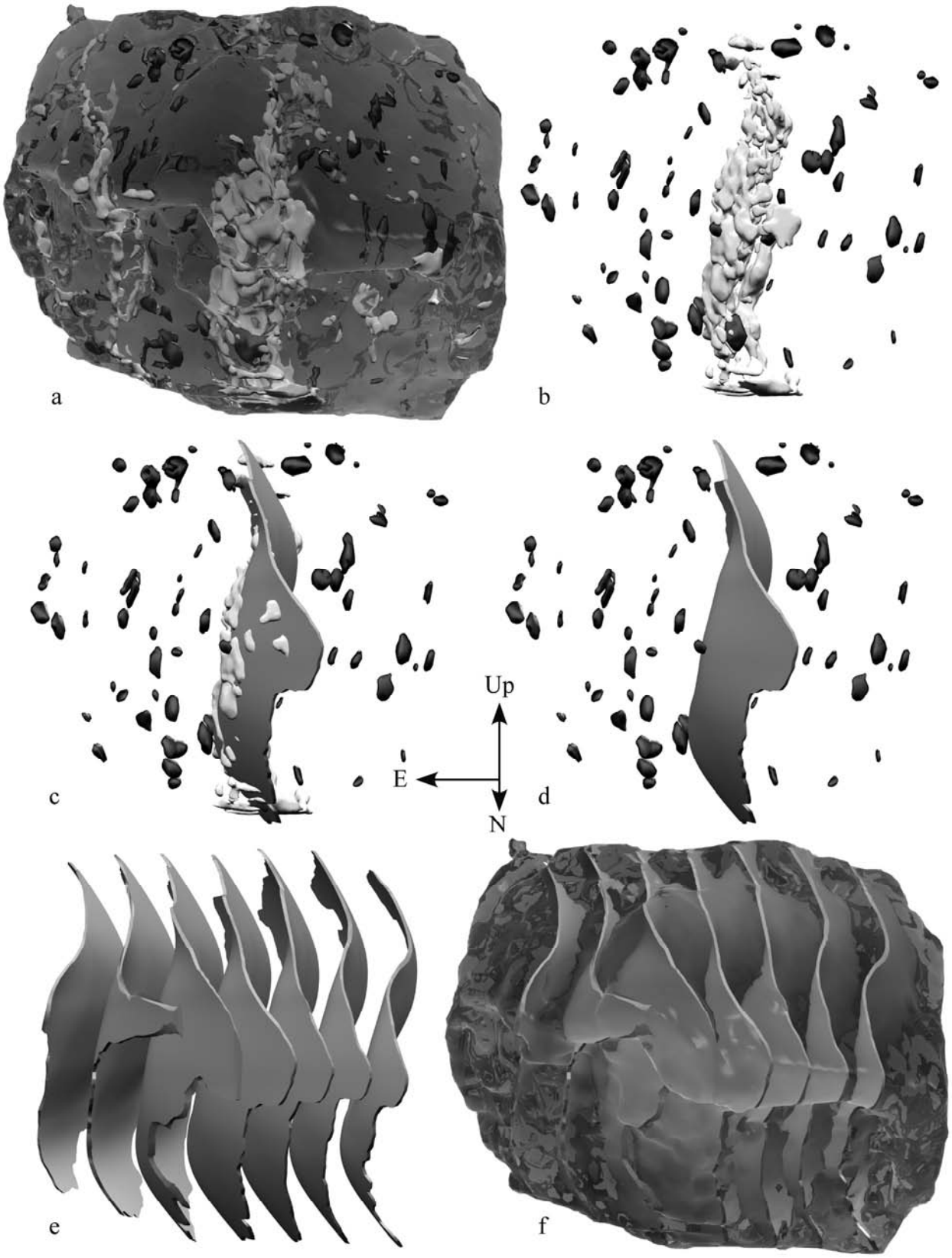
a
b
c
d
Up
E
N
e
f

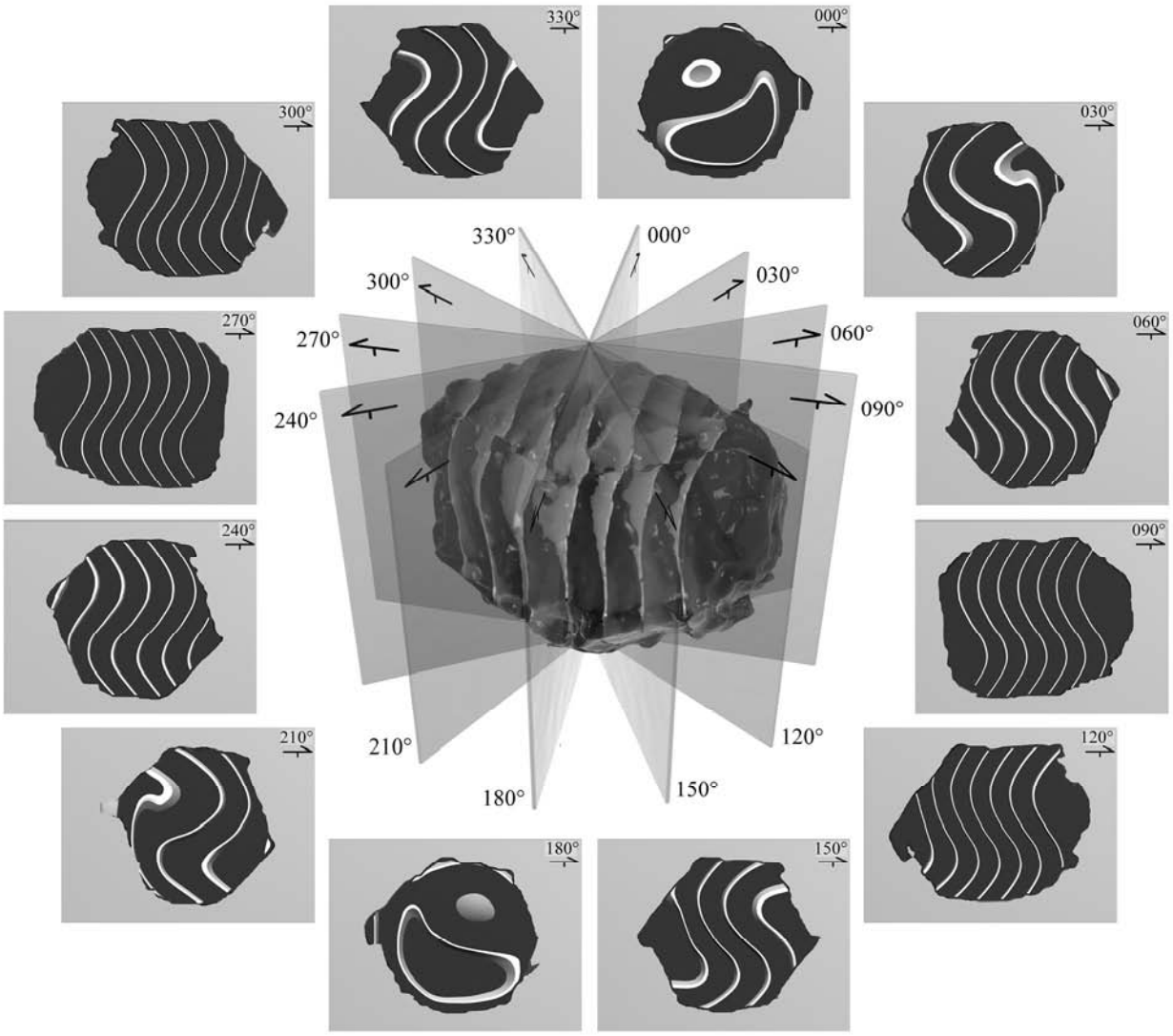

Figure 11. Shows the inclusion trail geometries encountered in a set of radial sections made through the centre of the 3-D porphyroblast constructed in Fig. 10. In reality, we need only cut sections at 0°, 30°, 60°, 90°, 120° and 150° to get this information. Sections cut perpendicular to the FIA (090° and 270°) display the least apparent curvature of the trails. These sections, passing through the centre of the porphyroblast and cut perpendicular to the FIA can be considered true profiles of the inclusion trails. See also Appendix E: "E03-vertical sigmoid rotate.mov".

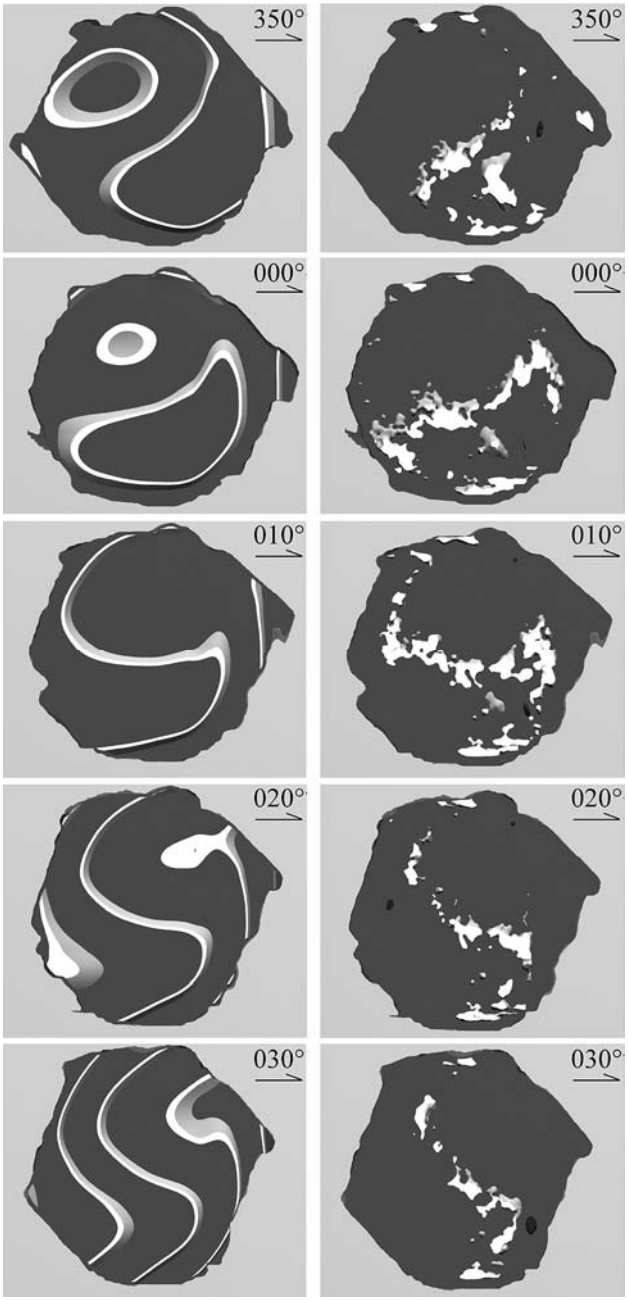

Figure 12. The trend of the FIA can be further constrained by cutting additional sections close to 000°. Sections made through the schematic inclusion trails are compared to sections made through the original model of Huddlestone-Holmes and Ketcham (2005).

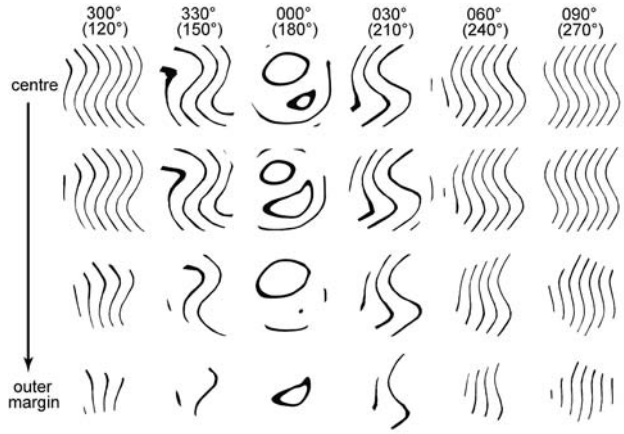

Figure 13. Shows the range of potential inclusion trail patterns made by taking sections through the schematic model porphyroblast at different orientations and at various distances from the centre. It is statistically unlikely that a particular porphyroblast will be perfectly bisected by a thin section. The inclusion trails observed are more commonly variations on these perfect delineations, as illustrated here. See also Appendix E: E02-E06.

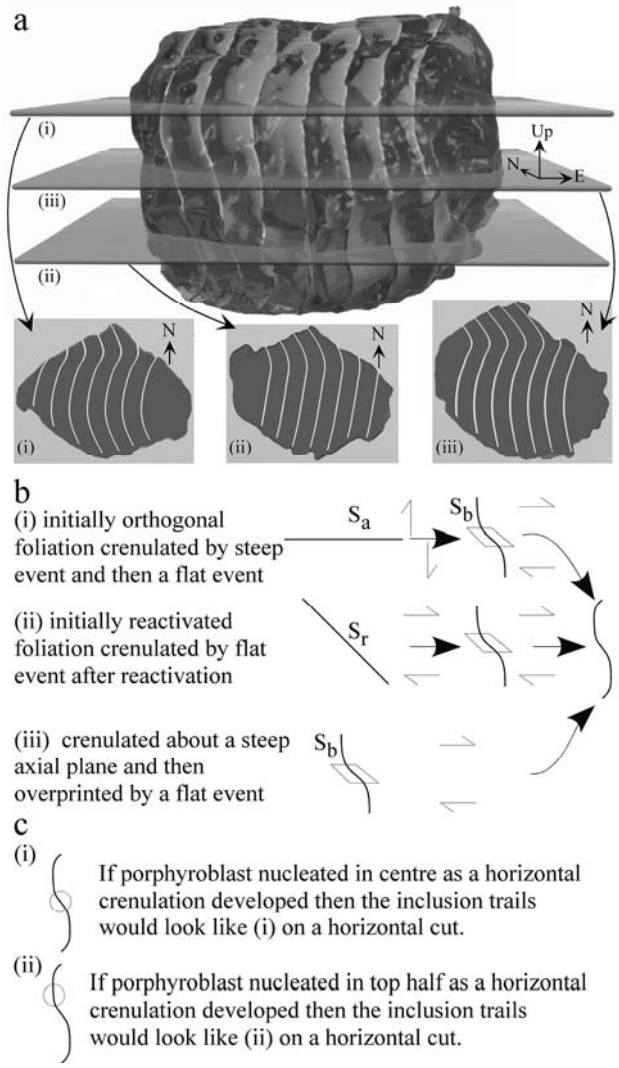

Figure 14. (a) Shows the inclusion trail geometry in three different horizontal cuts through the porphyroblast. (b) The inflection through the vertical shown in (a) can be explained by overprinting during a deformation that develops a sub-horizontal axial plane shown in a vertical cross-section through (i) a foliation that was initially flat lying but which had been overprinted by an earlier steep event, (ii) a foliation that was reactivated and dipping right, or (iii) a pre-existing crenulation. (c) Shows (i) a porphyroblast nucleating in the centre of inflection described in (b) and (ii) a porphyroblast nucleating in the upper part of the same inflection.

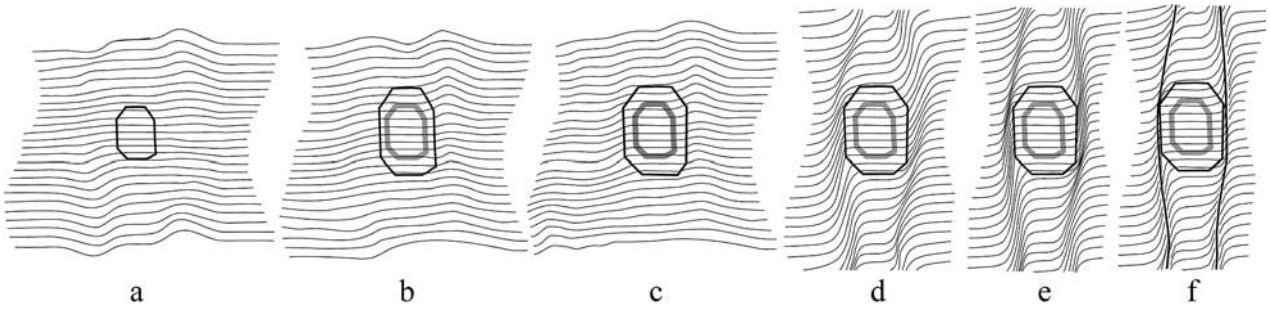

Figure 15. Shows how porphyroblast growth that has commenced very early during a deformation event (a-c) ceases once a differentiated crenulation cleavage begins to form in the immediate vicinity (d-f). Also shows how nucleation of a porphyroblastic phase for the first time at a particular site requires partitioning of the deformation into progressive shearing and shortening components on the scale of a porphyroblast through that location.

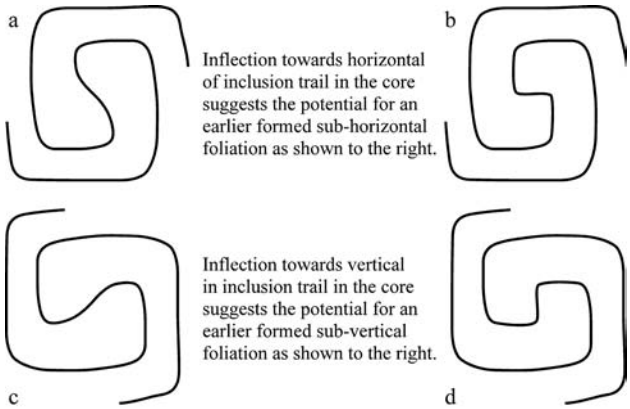

Figure 16. Skeletal diagrams of vertical cross-sections through spiral-shaped inclusion trails in porphyroblasts. Curvature towards horizontal of the central inclusion trail in (a) suggests the presence of an earlier formed sub-horizontal foliation as shown in (b). Curvature towards vertical of the central inclusion trail in (c) suggests the presence of an earlier formed sub-vertical foliation as shown in (d).

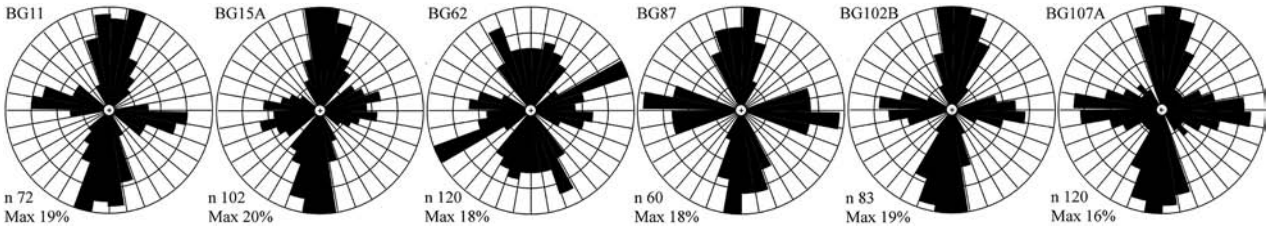

Figure 17. Equal area rose diagrams showing the pitch of truncational discontinuities preserved as inclusion trails measured from between 8 and 12 vertical thin sections with different strikes per sample (from Gavin, 2004).

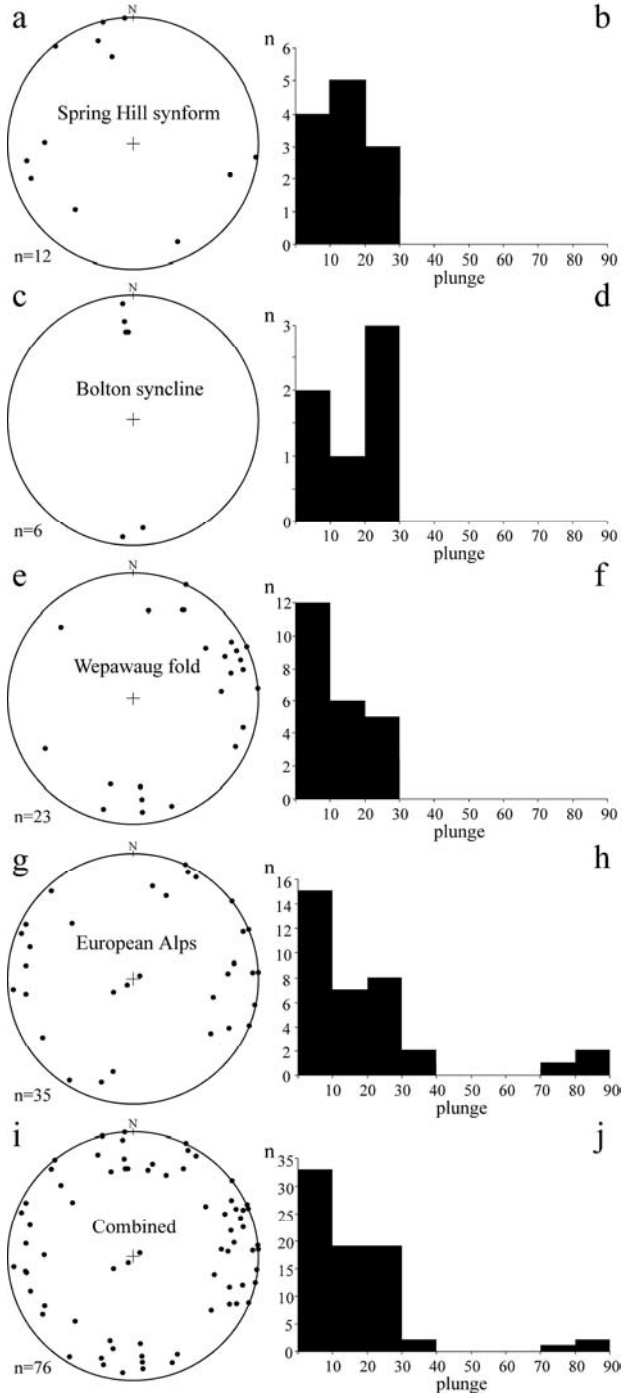

Figure 18. Stereonets of FIA plunges and histograms of angle of plunge data from (a, b) the Spring Hill syncline (Bell and Hickey, 1997), (c, d) the Bolton syncline (Hickey and Bell, 1999), (e, f) the Wepawaug fold (Bell and Newman, unpublished data), (g, h) the European Alps (Bell and Wang, 1999) and (i, j) these four regions all combined into one plot. The plunges are predominantly sub-horizontal ranging up to 30°. The three steep plunges recorded in the Alps all occur in samples where the porphyroblasts grew for the first time during the development of a sub-vertical foliation.

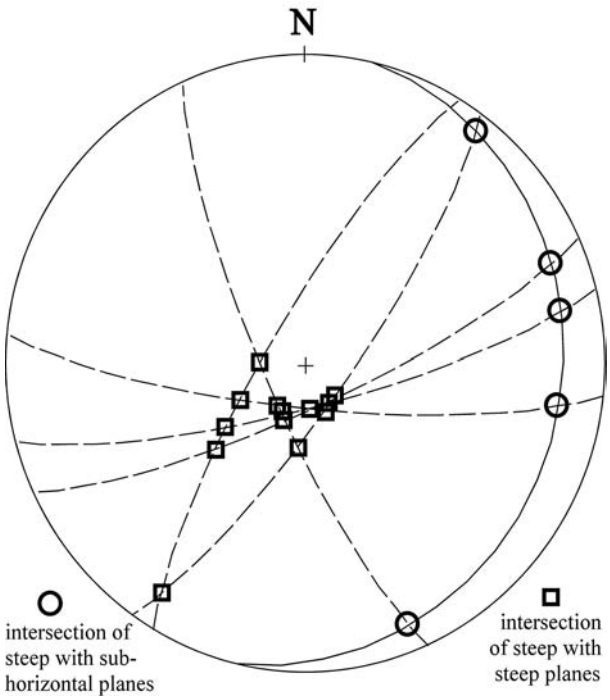

Figure 19. Stereonet showing how the intersection of a sub-horizontal plane with any other steeply dipping plane has a gentle plunge (circles). It also shows how the intersections of steeply dipping planes have mainly steep plunges. They only range to gentle plunges when the intersecting steeply dipping planes are very close in strike, and mainly have opposite dips.

Section C:

Progressive deformation partitioning and deformation history:

Evidence from millipede structures

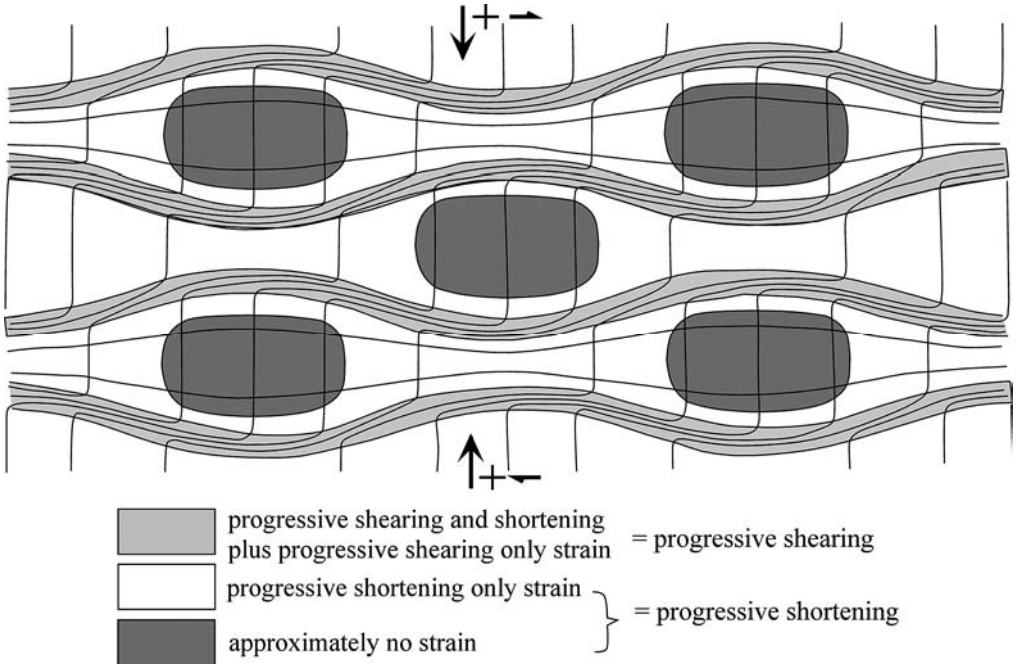

Figure 1. Shows the partitioning of deformation into zones of no strain, progressive shortening strain, progressive shearing plus shortening strain, and progressive shearing only strain that results from a history of deformation involving progressive bulk inhomogeneous shortening (thick arrows) with a component of anticlockwise shear (thin single barbed arrows; after Bell, 1981). For discussion we group the zones of no strain and progressive shortening only strain and call them progressive shortening. We group the zones of progressive shortening plus shearing and progressive shearing strain and call them zones of progressive shearing.

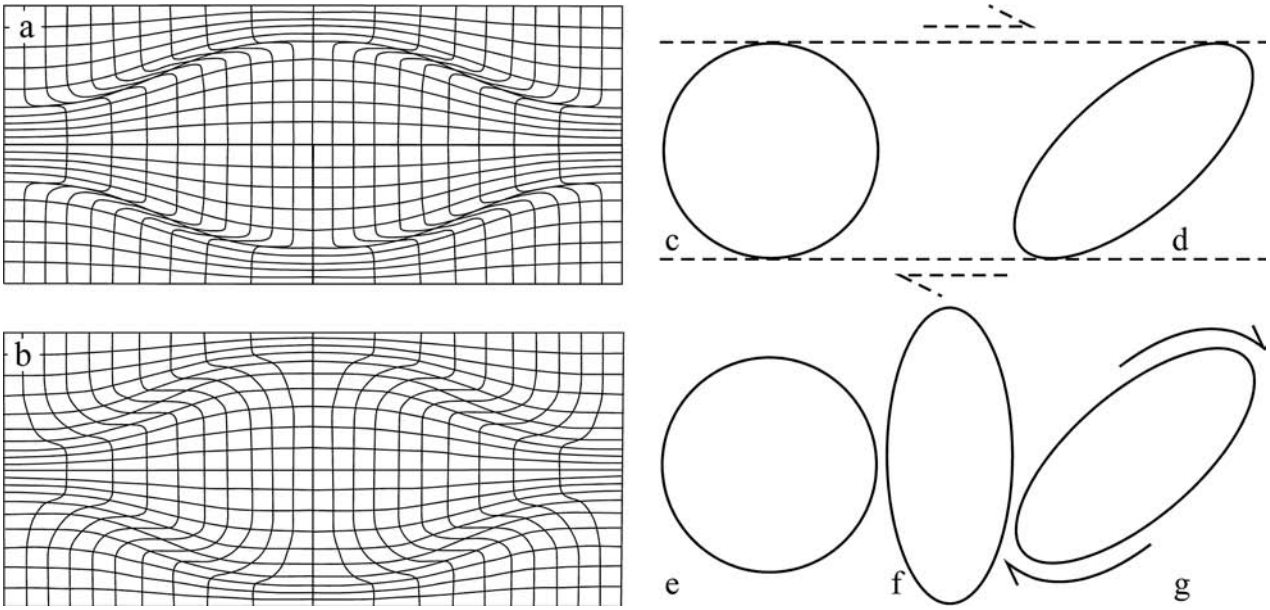

Figure 2. (a, b) The millipede shaped geometry of the strain field that results from coaxial progressive bulk inhomogeneous shortening. The progressive shearing component of the deformation is more confined in (a) than in (b). (c, d) Schematic representation of the transformation of a sphere (c) by progressive simple shear to an ellipsoid. (e-g) Schematic representation of the transformation of a sphere (e) by progressive homogenous shortening (progressive pure shear; f), plus a rotation (g), to the same end product as in (d).

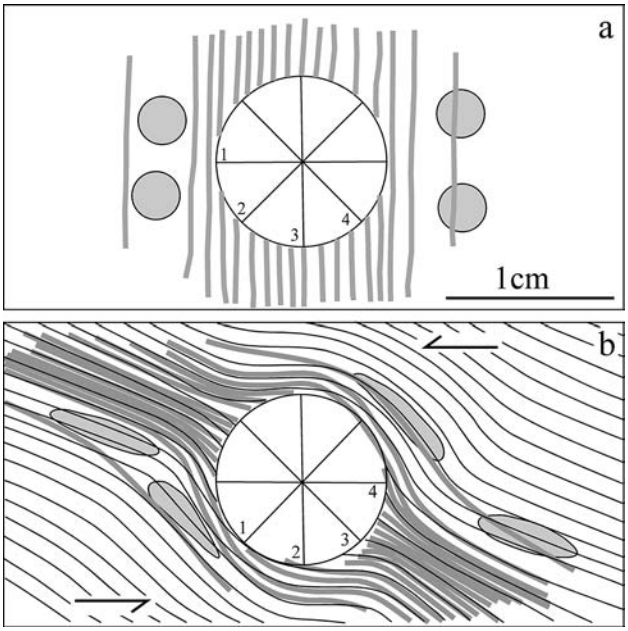

Figure 3. (a) Accurately reproduced line diagram from fig. 8 in Ghosh (1975) of rigid cylinder in silicone putty at start of an experimental run involving top to left (anticlockwise) shear. Prior to commencement of the experiment the grey lines were marked and the grey in filled circles were inscribed (as circles) into the model; they become strain markers. (b) Accurately reproduced line diagram from fig. 10 in Ghosh (1975) at the end of the experimental run involving anticlockwise progressive simple shear. The finer lines are strain lines developed in the silicon putty were drawn onto the image at very high magnification. They lie parallel to the strain ellipsoids. Single barbed arrows show direction of shear applied to produce this geometry.

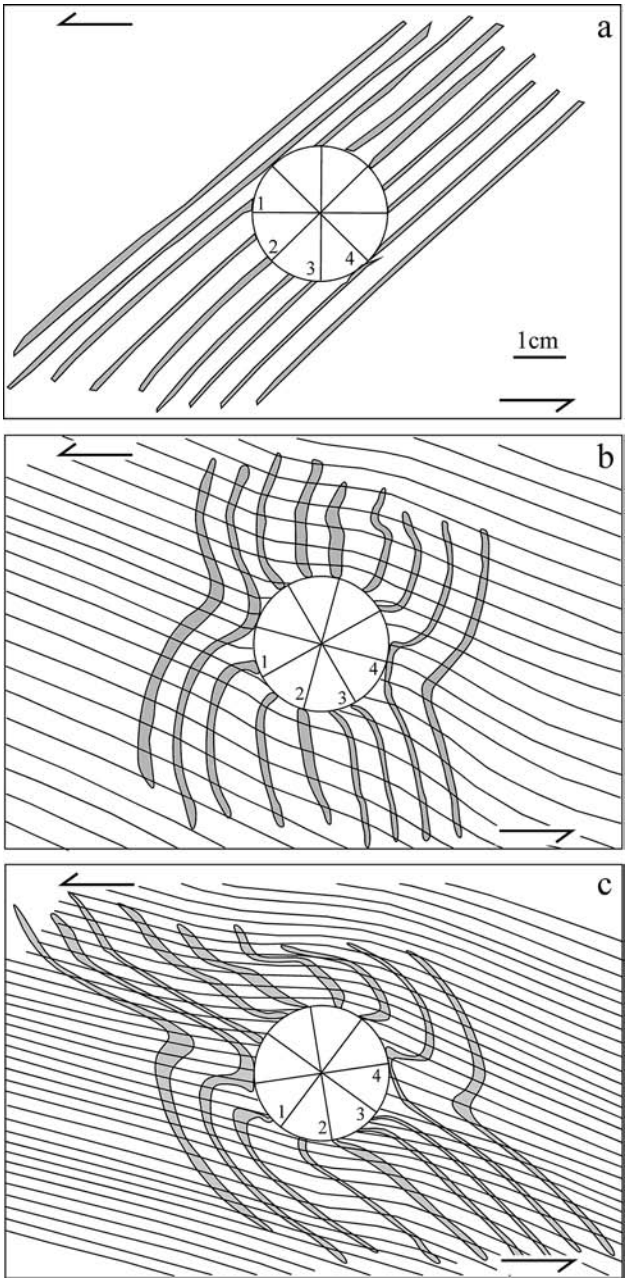

Figure 4. (a) Accurately reproduced line diagram from fig. 11 in Ghosh (1975) of rigid cylinder in silicone putty at start of an experimental run involving top to left (anticlockwise) shear (shown by arrows). The grey lines become strain markers. (b) Accurately reproduced line diagram from fig. 12b in Ghosh (1975) part way through experimental run involving progressive simple shear. The finer lines are strain lines developed in the silicon putty were drawn onto the image at very high magnification. They lie parallel to the strain ellipsoid and define a foliation. (c) As for (b) except at higher strain at the end of the experimental run. Single barbed arrows show direction of shear applied to produce these geometries.

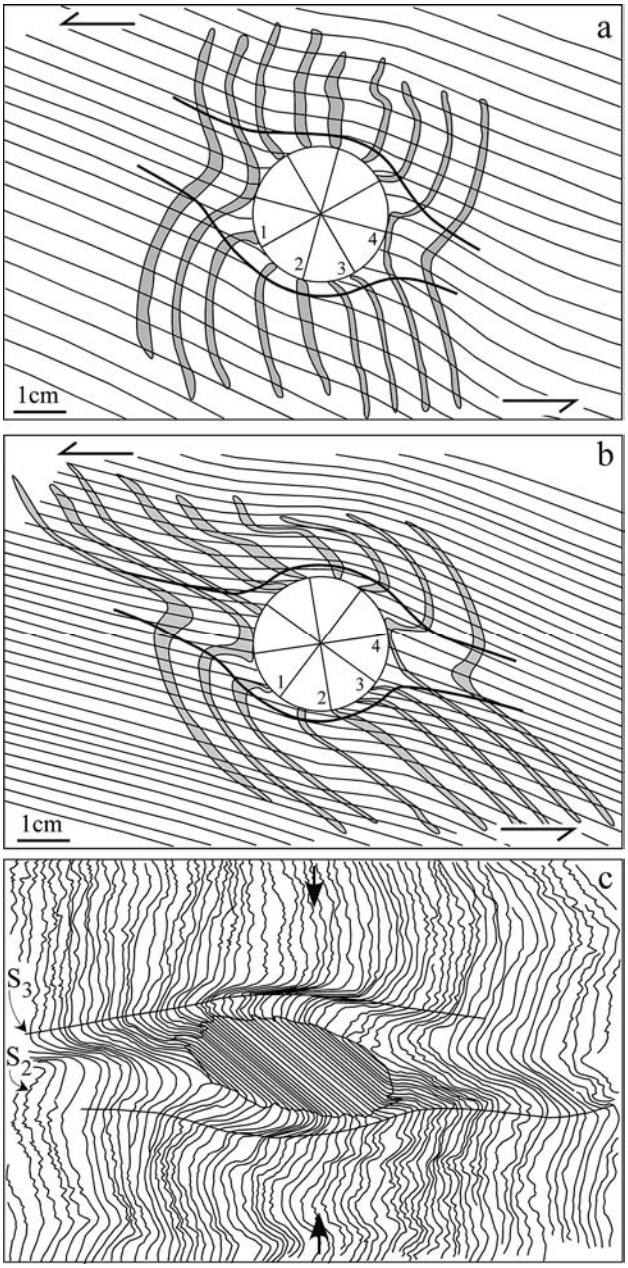

Figure 5. (a, b) Shows millipede like geometries (oppositely concave folds) produced experimentally by progressive simple shear. The foliation (thin lines) cuts across the millipede fold axial planes to either side of the core structure (thicker lines). Single barbed arrows show direction of shear applied to produce this geometry. (c) Shows a natural millipede geometry within a porphyroblast produced by progressive bulk inhomogeneous shortening. The differentiated crenulation cleavage (foliation) produced during the millipede event follows the axial planes of the folds to either side of the core structure (thick lines). Arrows show the inferred direction of bulk shortening that produced this geometry.

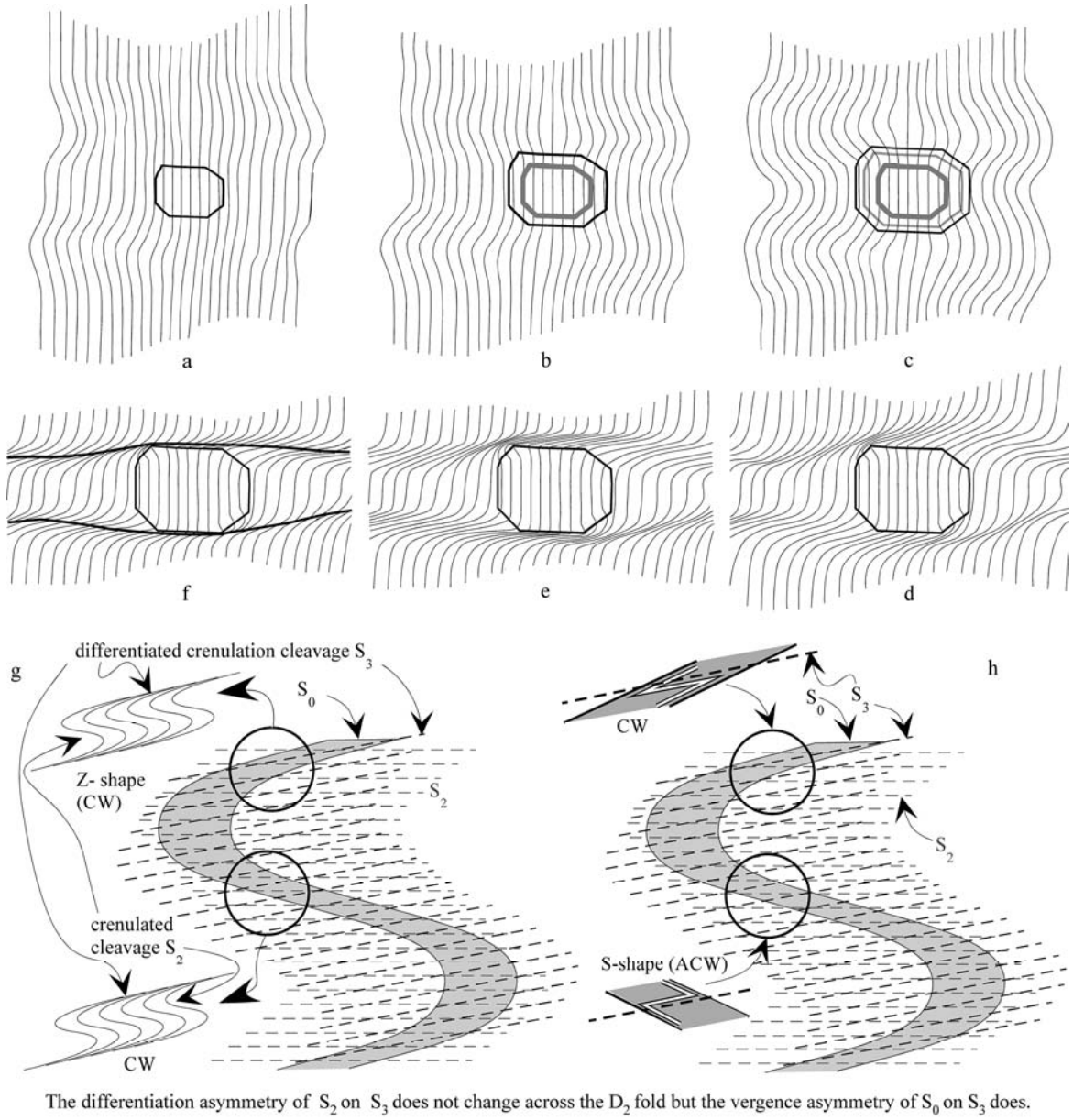

Figure 6. Shows how porphyroblast growth that has commenced very early during a deformation event (a-c) ceases once a differentiated crenulation cleavage begins to form in the immediate vicinity (d-f). The progression shows how the core may preserve a coaxial millipede geometry (a-c), but the more developed matrix contains a consistent clockwise non-coaxial asymmetry at stages (d-f). This figure also shows how nucleation of a porphyroblastic phase for the first time at a particular site requires partitioning of the deformation into progressive shearing and shortening components on the scale of a porphyroblast through that location. The differentiation asymmetry (g), which in this example is the curvature of S_2 into differentiated S_3 (see Bell et al., 2003), is clockwise and does not change across the fold although the vergence asymmetry (h) of S_0 relative to S_3 does. The foliation/foliation asymmetry of S_2 relative to S_3 does not change either.

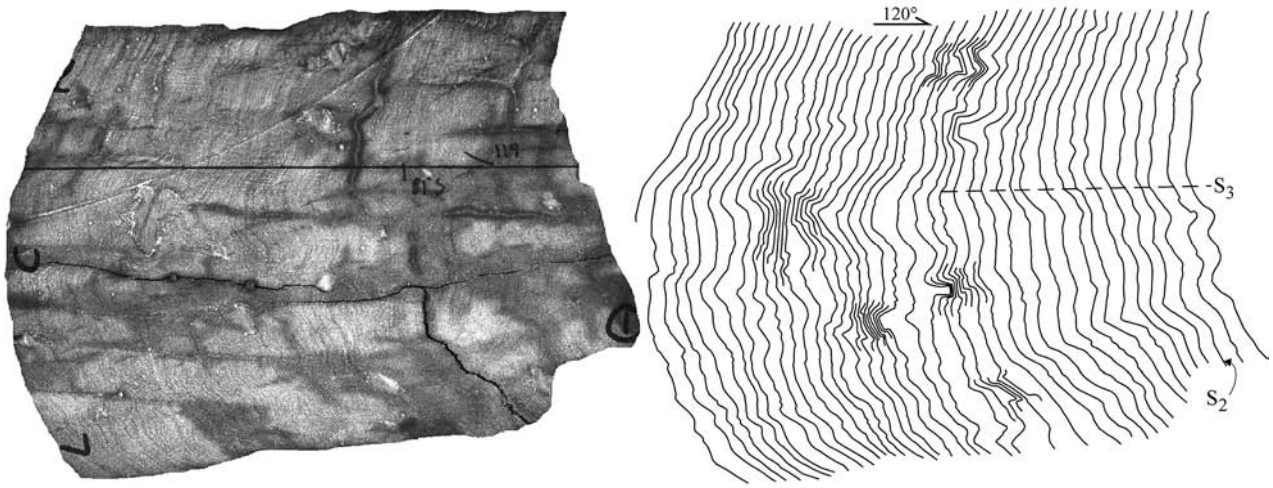

Figure 7. Fold hinge from outcrop containing numerous plagioclase porphyroblasts all of which examined in thin section contain millipede microstructure. The axial plane structure is readily apparent in thin sections and is called S_3. The folded foliation is called S_2. The differentiation asymmetry of S_2 into S_3 in the matrix on both limbs is predominantly clockwise looking in the direction shown (that is, it looks the same as that shown in Fig. 6d-f on a microscope). The single barbed arrow shows the strike of the sub-vertical profile plane. Width perpendicular to axial plane is 10 cm.

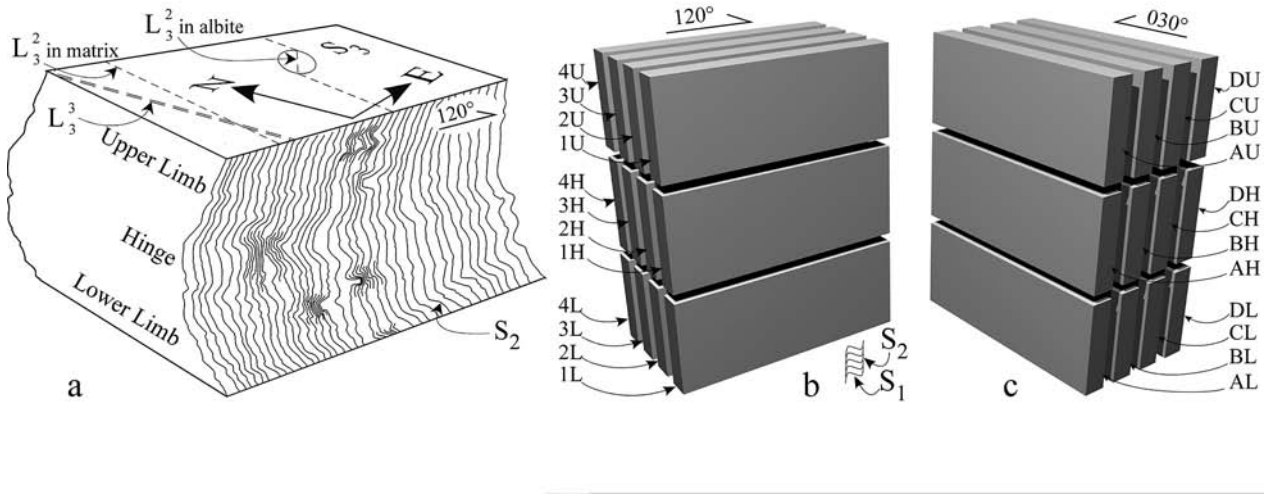

Figure 8. Fold hinge (a) showing the relative orientation and locations of blocks from which thin sections were cut in the profile plane (width perpendicular to axial plane is 10 cm). (b) and parallel to the F^2_3 fold axis but perpendicular to the S_3 axial plane (c). The differentiation asymmetry due to the curvature of crenulated S_1 into the differentiated crenulation cleavage S_2 that is folded around the fold is also shown as it appears in the profile plane.

Figure 9. (a) Plagioclase porphyroblast containing highly oblique millipede-shaped trails from the hinge of the fold in Fig. 7 (vertical width is 2.5 cm). (b) Shows the S_2 foliation, which predates porphyroblast growth, and which was accurately drawn onto the image in (a) at very high magnification. Note the spectacular increase in width parallel to the axial plane S_3 between S_2 planes, from inside to outside the porphyroblast (1.83 times). This is best observed using the two S_2 traces outlined with heavy black lines as they pass out of either end of the porphyroblast and is due the effects of bulk shortening near orthogonal to S_3. (c) Shows changes in crenulated cleavage S_1 as S_2 passes through the porphyroblast strain shadow. Also shows local more intense zones of sub-horizontal differentiated crenulation cleavage S_3 adjacent to the porphyroblast. (d) Detail of boxed area marked d in (a) showing clockwise differentiation asymmetry of S_2 into S_3. (e) Detail of boxed area marked e in (a) showing clockwise differentiation asymmetry of S_2 into S_3.

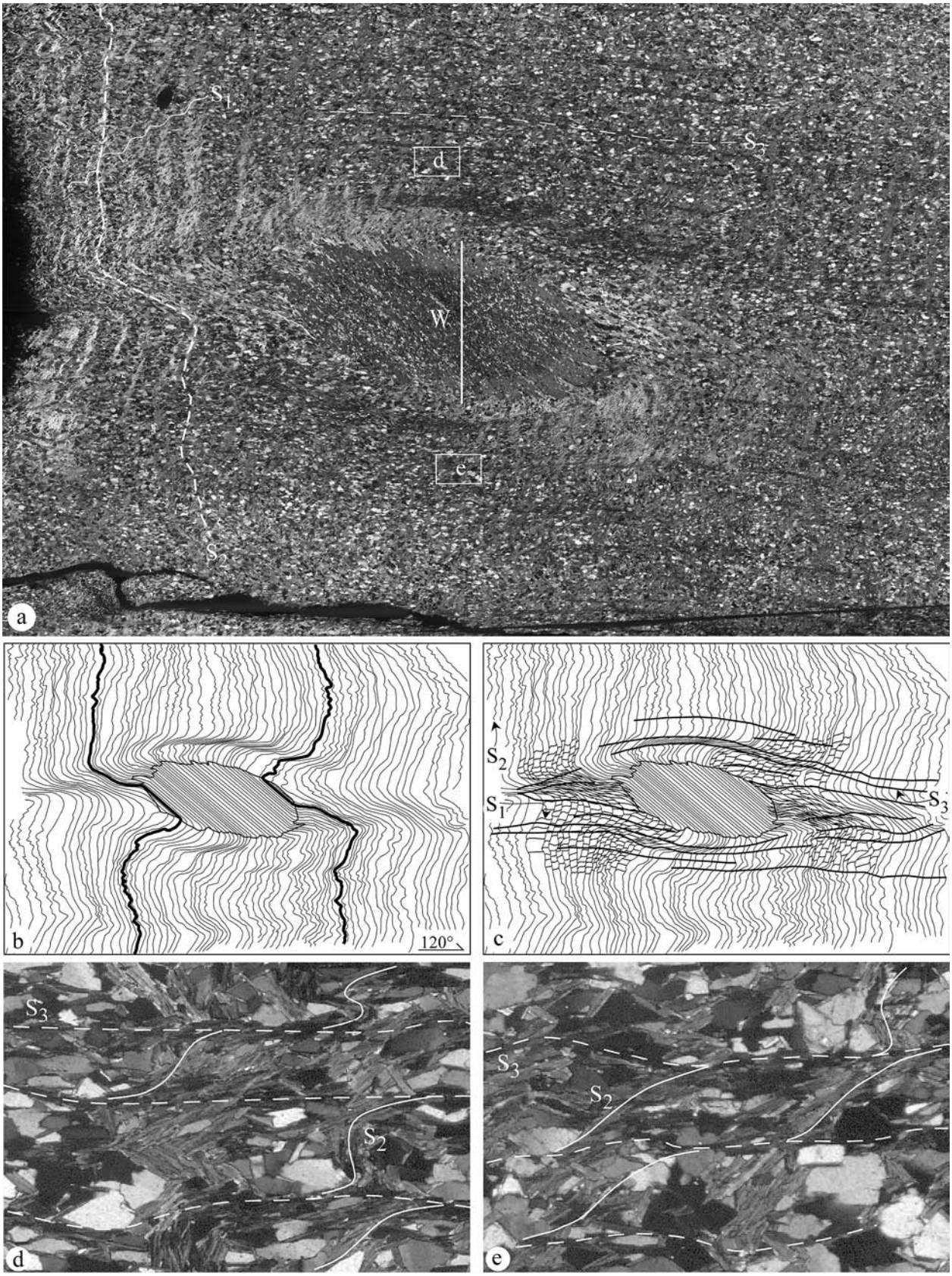
S1
S3
d
W
e
S2
a
b
120°
c
S2
S1
S3
S3
S2
d
S3
S2
e

Location	S_2 pitch SE in degrees	S_2 pitch NW in degrees
Upper Limb	80	65
	82	80
	76	72
		75
		65
		72
Average	79.33	71.50
Hinge of Fold	45	75
	89	88
	50	81
	77	80
	75	82
		75
Average	67.2	80.12
Lower Limb	71	
	60	
	70	
	89	
	51	
	74	
Average	69.17	

Table 1. Shows the pitch of S_2 preserved as inclusion trials in plagioclase porphyroblasts in the hinge plus lower and upper limbs of the fold shown in Fig. 8. The pitches were measured from the 12 thin sections taken from the fold profile plane shown in Fig. 8b. Note how only SE pitches are present in the lower limb.

Location	Width between S_3 for SE pitch in mm	Width between S_3 for NW pitch in mm
Upper	2.7	1.00
Limb	7.7	4.00
	6.75	5.00
	2.45	8.45
	3.80	3.85
	3.25	3.55
	4.10	3.70
	9.25	2.40
		1.60
Average	5.00	3.73
Hinge	4.25	3.85
of Fold	4.60	1.90
	4.45	2.30
	4.00	0.85
	4.25	2.30
	2.70	4.60
	1.90	
	8.60	
Average	4.34	2.63
Lower	0.60	
Limb	9.25	
	8.30	
	4.15	
	6.90	
	3.10	
	10.35	
	5.40	
	4.60	
	7.30	
Average	6.00	

Table 2. Shows the width between S_3 seams measured across porphyroblasts along the line W shown in Fig. 9a separated according to whether the S_2 inclusion trails dip SE or NW in 3-D plus whether the sections were cut from the hinge or lower and upper limbs of the blocks shown in Fig. 8b, c. The dimension W defines the width of the zone of partitioned shortening strain that contains a porphyroblast.

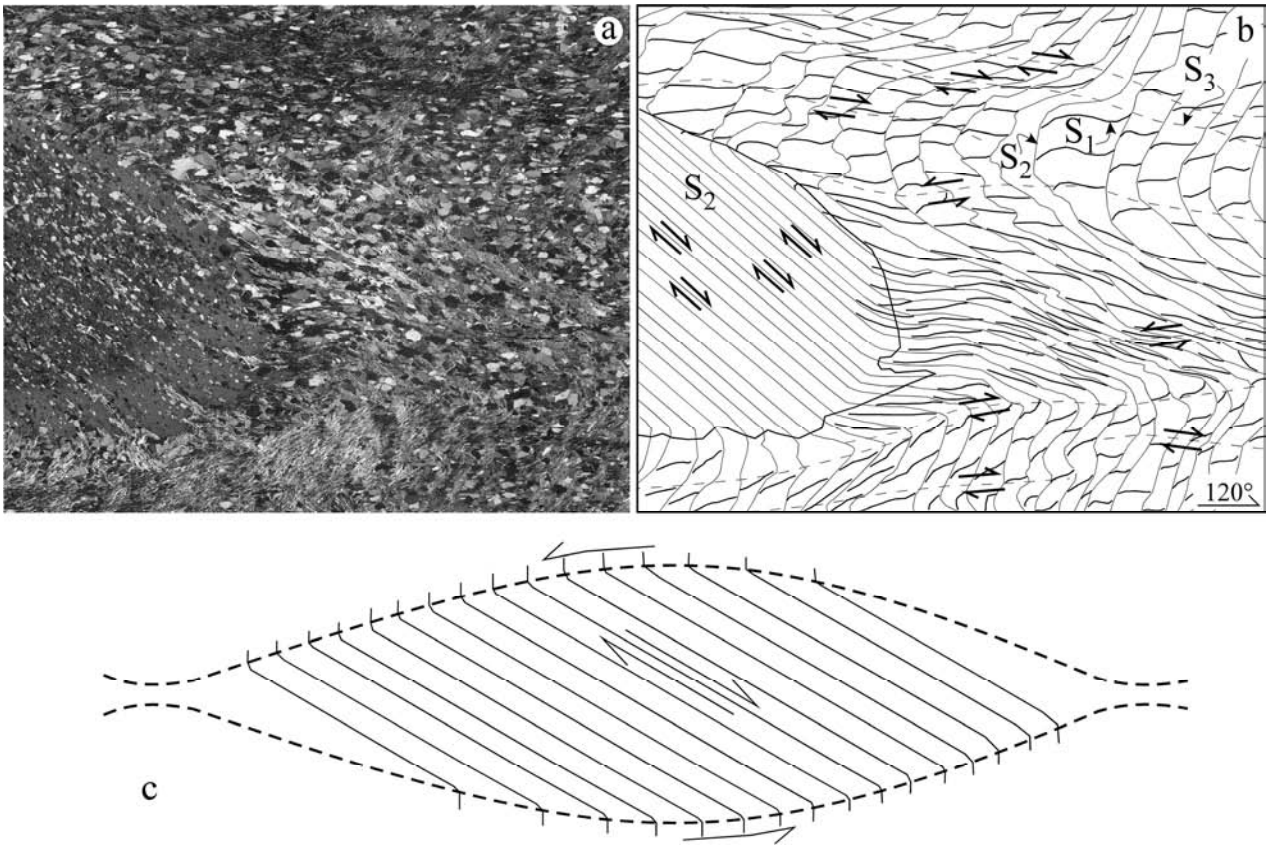

Figure 10. (a) Photographic detail of right hand millipede end. (b) Shows S_1, S_2 and S_3. Note that S_1 inside and outside the triangular shaped strain shadow on the right side of the porphyroblast does not cut across S_2. Shear on S_3 in the matrix switches from clockwise (3 heavy short arrows above and 3 below) in the matrix to anticlockwise (2 heavy short arrows to right of albite) on the S_3 bounding the strain shadow. The S_1 into S_2 differentiation asymmetry outside the porphyroblast strain shadow is anticlockwise. Inside the strain shadow it is clockwise. This resulted from the clockwise reactivation of S_2 early during D_3 that switched the primary anticlockwise differentiation asymmetry of S_1 into S_2 outside of the porphyroblast strain shadow to clockwise within the strain shadow. (c) Schematically summarizes the clockwise reactivation of S_2 that took place within an ellipsoidal pod of partitioned D_3 strain, which rotated S_2 prior to growth of the porphyroblast. The porphyroblast and its strain shadow fill this pod although modification of the strain shadow occurred as D_3 intensified. This pulled S_2 seams apart and elongated relic S_1 lying between them as can be seen in (b).

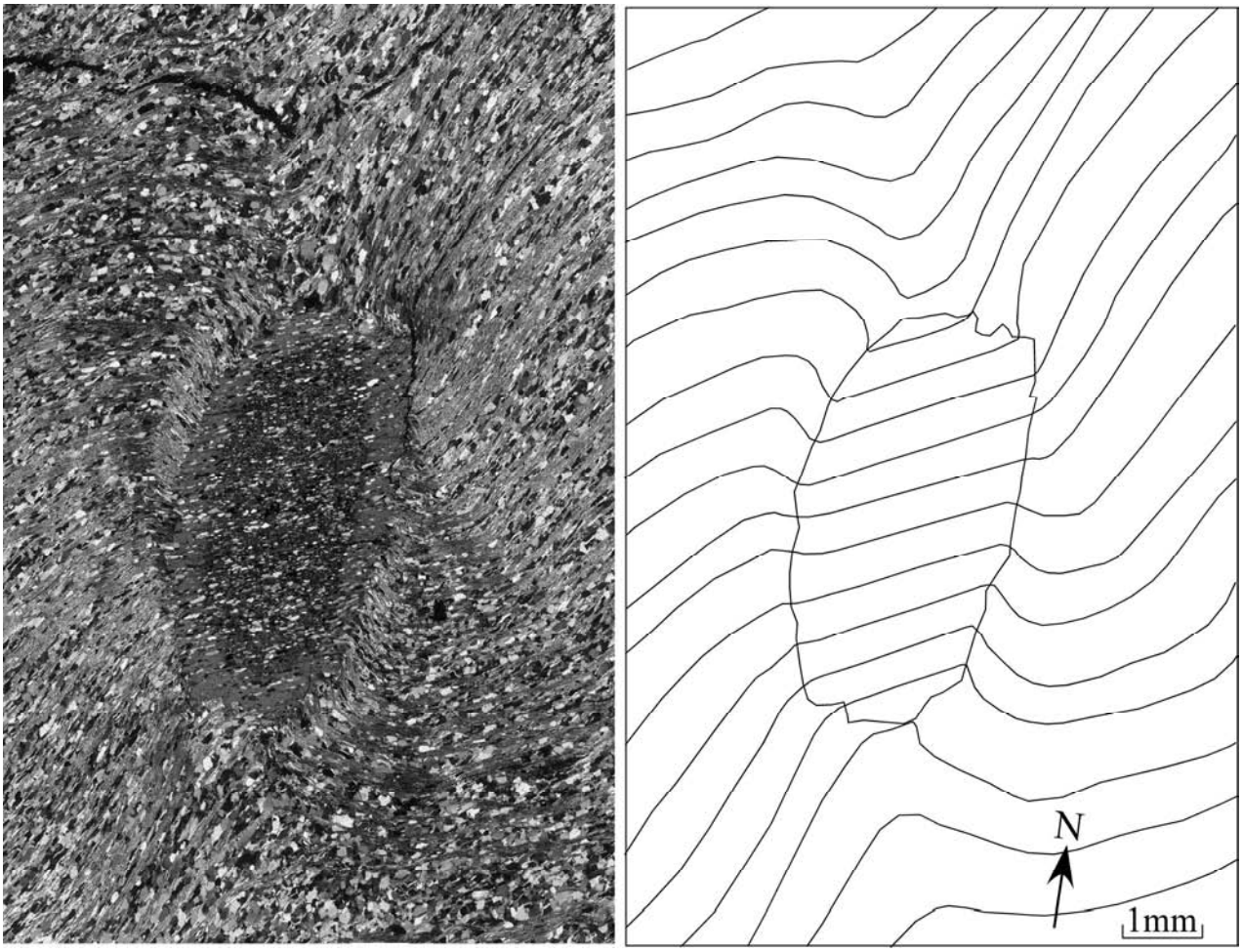

Figure 11. Millipede plagioclase porphyroblast in a sub horizontal section cut parallel to the axial plane structure (S_3) of the F^2_3 fold that generated the millipede geometry. North is marked so that the structures preserved can be related to those in Fig. 8a. Crossed polars.

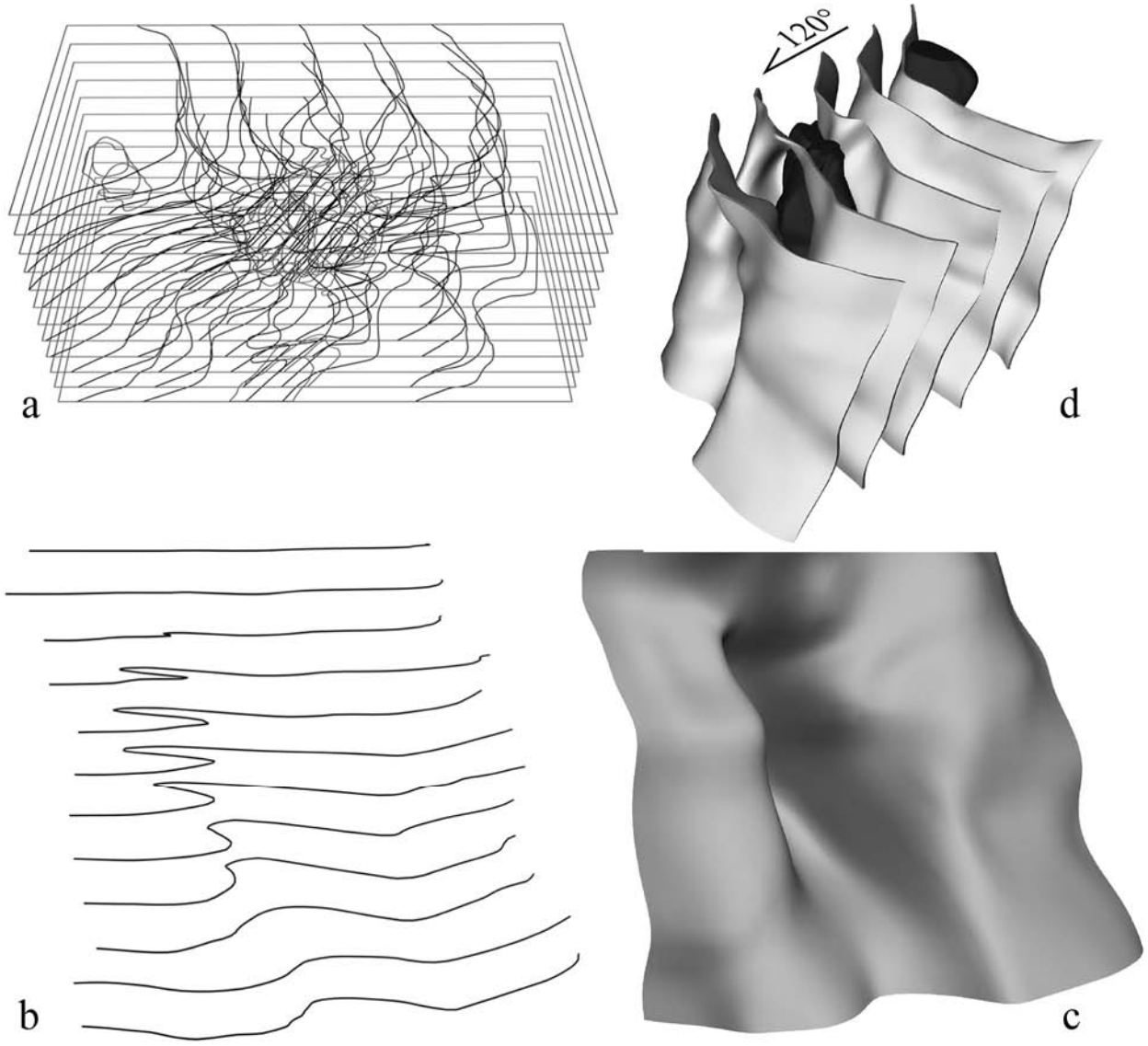

Figure 12. Reconstruction of millipede structure after Johnson and Moore (1996). (a) Digitized and scaled tracings of 12 thin sections positioned with a spacing of 1.5 mm. (b) 12 curves define a single foliation surface. (c) "U-loft" surface created by stretching a skin over the curves. (d) Complete millipede model composed of five foliation surfaces (light grey) and three plagioclase porphyroblasts (dark grey). The single barbed arrow shows the strike and orientation of a face that is vertical when the sample is spatially oriented.

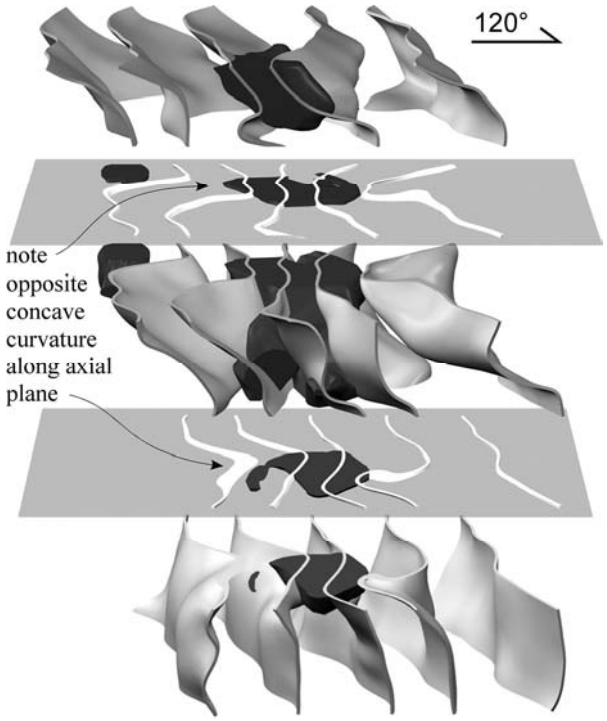

Figure 13. Two horizontal slices cut through the millipede model displaying oppositely concave foliation traces. The single barbed arrow shows the strike of the vertical face on the front of the structure. See also Appendix E: “E07-horizontal millipede slice.mov”.

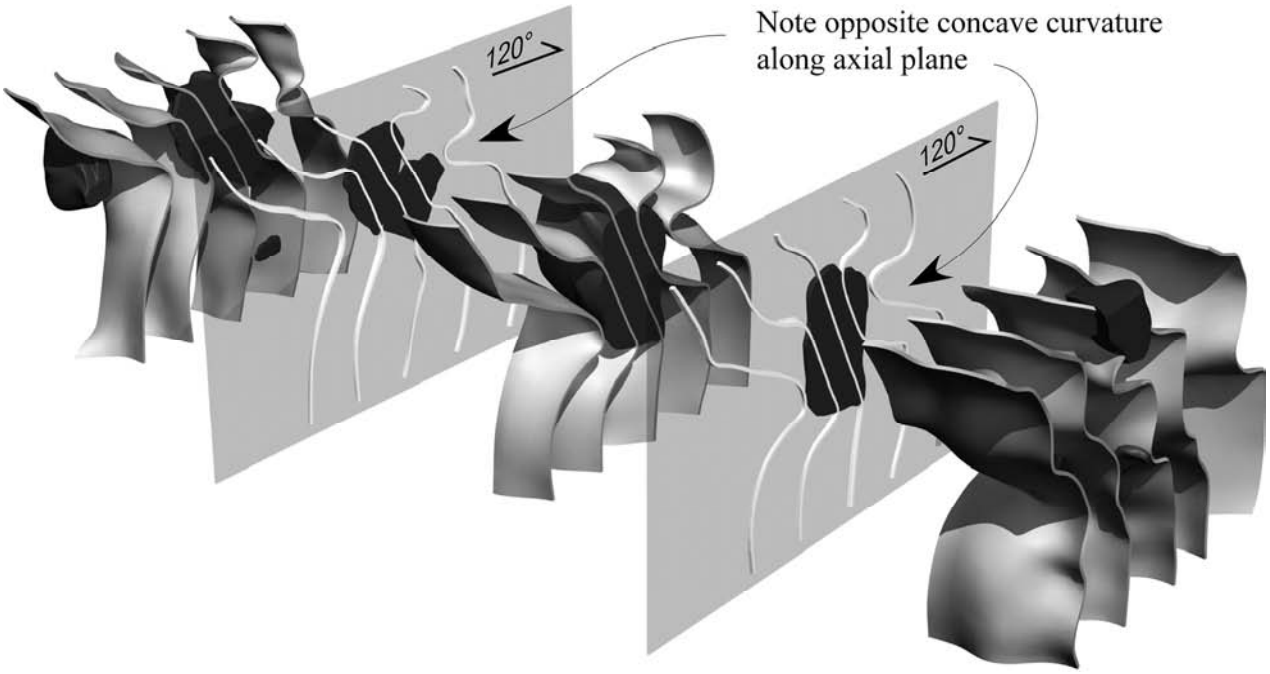

Figure 14. Vertical millipede sections displaying oppositely concave foliation traces. The single barbed arrows show the strike of vertical cuts through the structure. See also Appendix E: "E08-vertical millipede slice 120.mov" and "E10-millipede.zip".

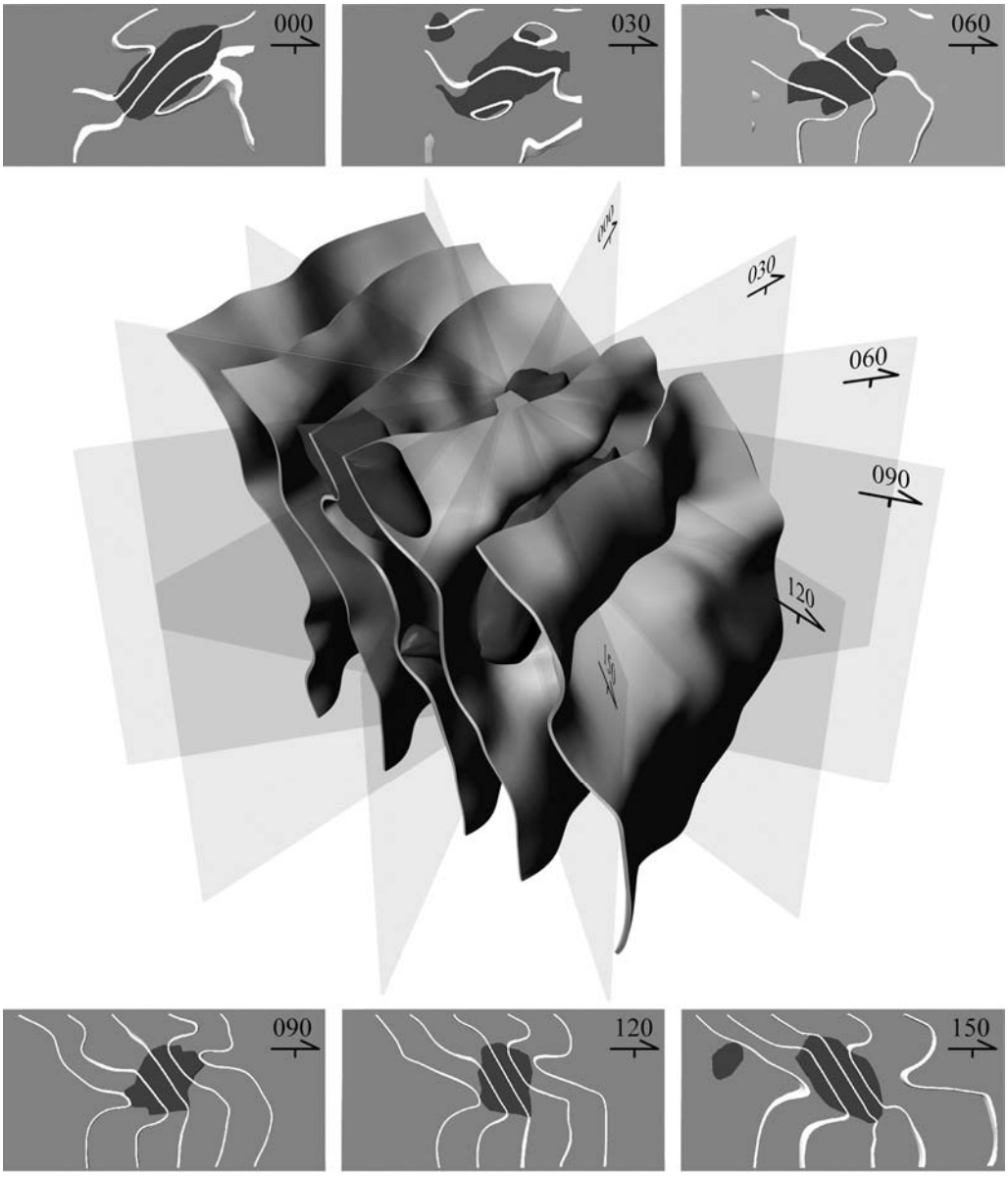

Figure 15. Radial sections through the millipede model display spectacular oppositely curving foliation traces in section of almost any orientation. The single barbed arrows show the strike of successive vertical cuts. See also Appendix E: "E09-vertical millipede rotate slice.mov"

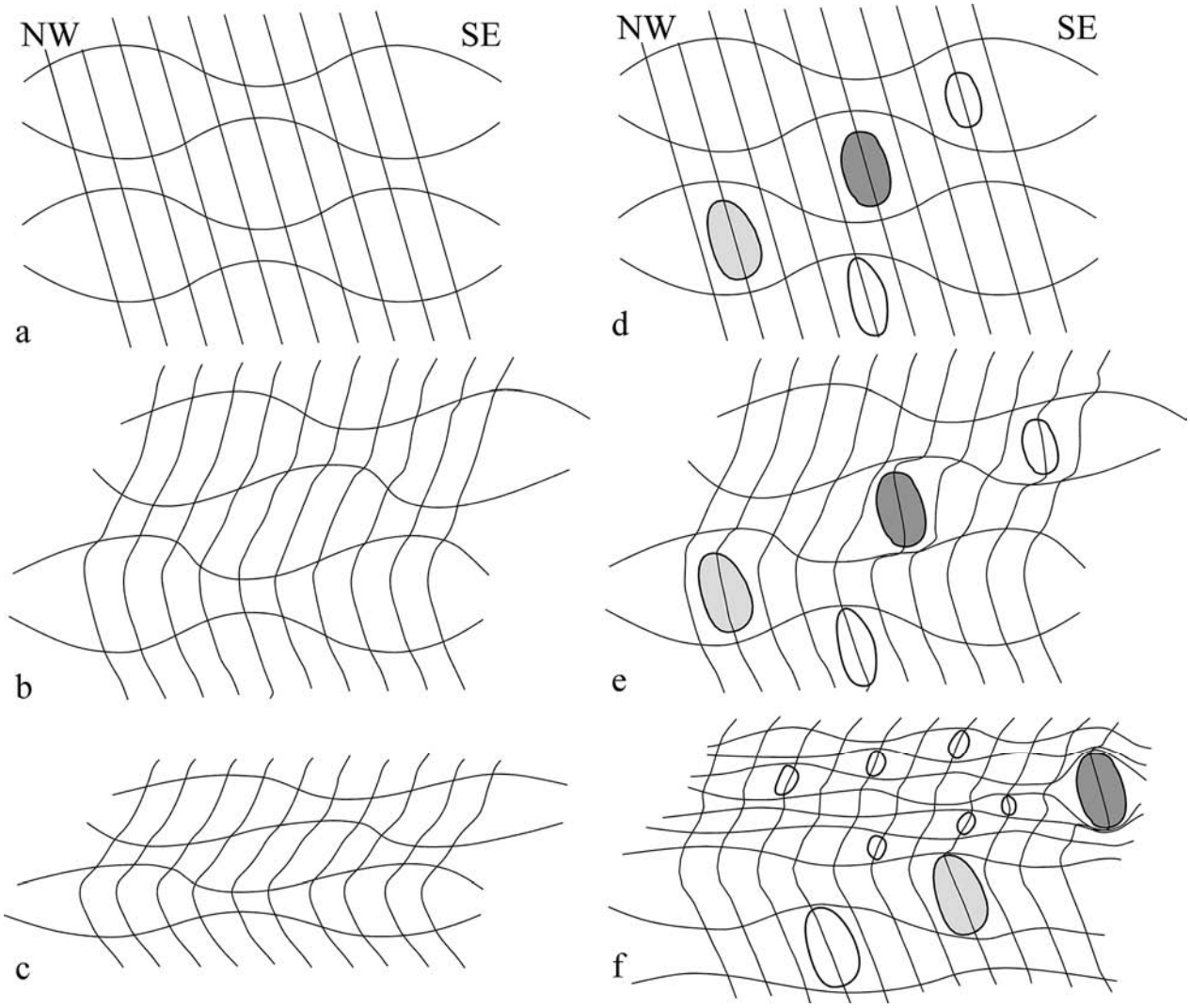

Figure 16. Sketches showing how bulk shortening of an initially 70° SE dipping S_2 foliation (a) and only clockwise shear on the sub-horizontal axial plane differentiated crenulation cleavage S_3 (b) cannot produce the lowest angles (locally as low as 20° to the horizontal) of limb dip on lower limb (c) seen in the fold in Fig. 7. Therefore, early during the deformation history there must have been some anticlockwise shear on the lower limb. (d) porphyroblast growth early in the history of bulk shortening preserves inclusion trails with the initial orientation after folding has commenced. (e) and (f) shows the effects of a reduction in the scale of partitioning on the upper limb of a fold as the deformation intensified. Newly grown porphyroblasts in the progressive shortening domains after repartitioning occurred have smaller dimensions perpendicular to the axial plane.

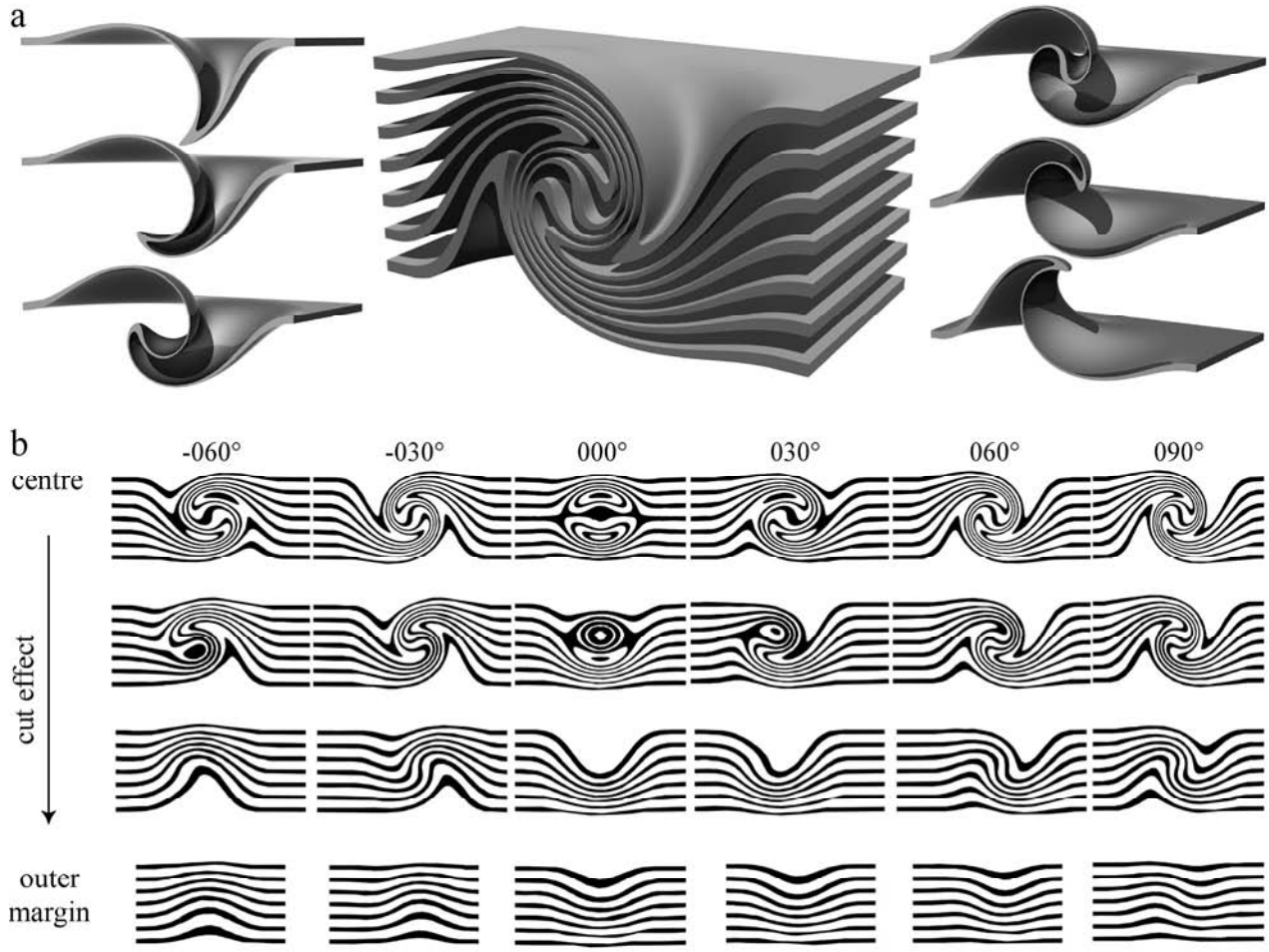

Figure 17. (a) Cut-away profile view of a model spiral structure with the elements of this model separated to either side (*c.f.* Stallard *et al.*; 2002). Shows the range of inclusion trail geometries expected in a series of radial thin sections through a sample containing spiral porphyroblasts. (b) Sections in the top row pass through the centre of the model; those in the bottom row intersect the outer edge. Orientations are given relative to the axis of apparent rotation. Only sections cut parallel to the axis of rotation display foliation traces that could be mistaken for millipede structures, all others show spirals or sigmoids. See also Appendix E: E11-E15.

Section D:

Timing nappe development in multiply tectonised rocks:

A new approach

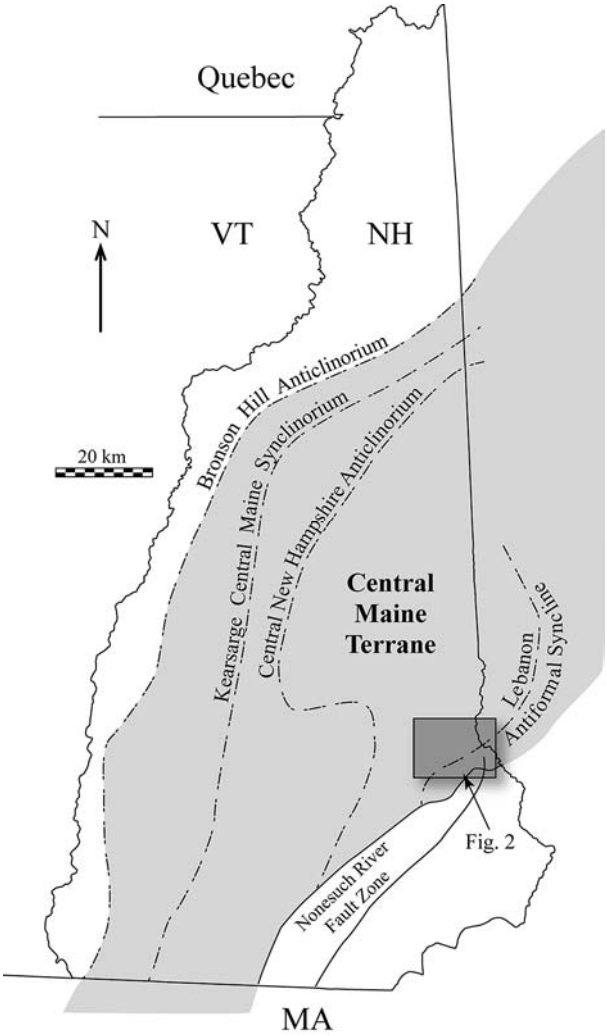

Figure 1. Location map showing the major fold structures of the Central Maine Terrane (Modified after Eusden, 1988). The inset box highlights the area shown in Figure 2.

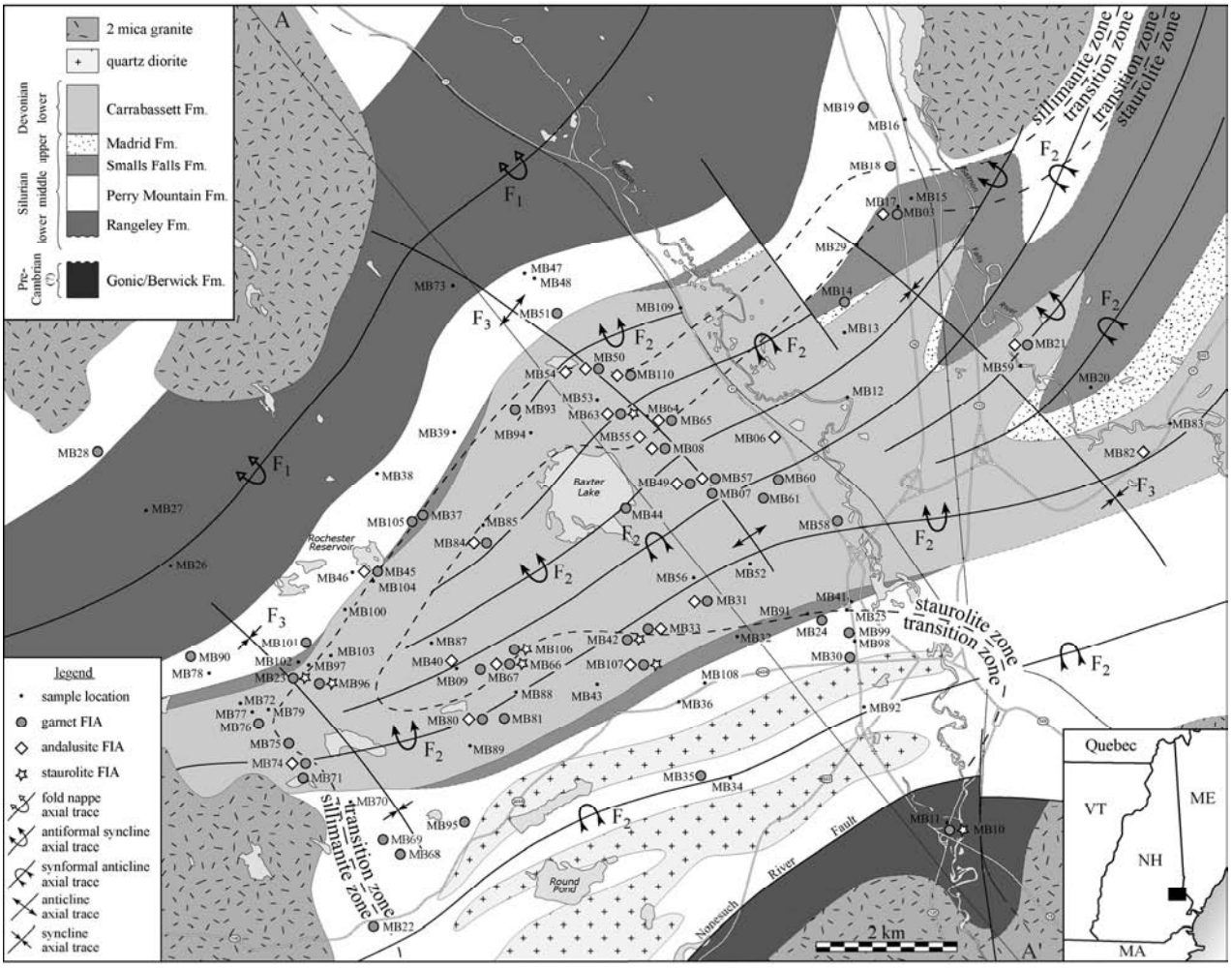

Figure 2. Detailed map of the study area showing the major structural features and sample locations. Samples from which FIAs were measured in garnet, staurolite or andalusite porphyroblasts are also shown. The line A-A' marks the position of the section shown in Figure 10. Base map after Eusden *et al*., 1984. See also Appendix D.

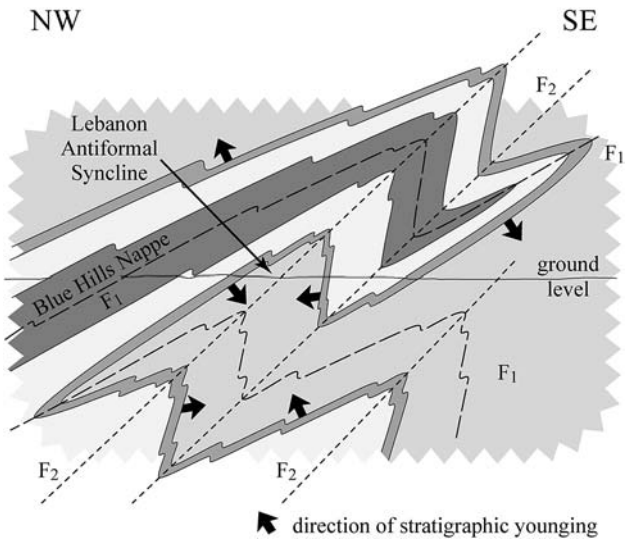

Figure 3. Schematic section showing the position of the Lebanon Antiformal Syncline on the overturned limb of the refolded Blue Hills Nappe, prior to faulting and plutonism. A detailed cross section through the Lebanon Antiformal Syncline is shown in Figure 10.

Figure 4. Photomicrographs and associated line diagrams illustrating inclusion trail (S_i) geometries preserved in garnet porphyroblasts from the Lebanon Antiformal Syncline. Strike of vertical thin section shown by single barbed arrow in upper right corner. Scale bar in lower right corner. (a) Sigmoidal inclusion trail geometry. Sample MB081. Plane polarized light. (b) Staircase inclusion trail geometry. Sample MB090. Plane polarized light. (c) Pseudo-FIA (pFIA). Inclusion trails define a differentiated crenulation cleavage that predates porphyroblast growth. Sample MB019. Plane polarized light.

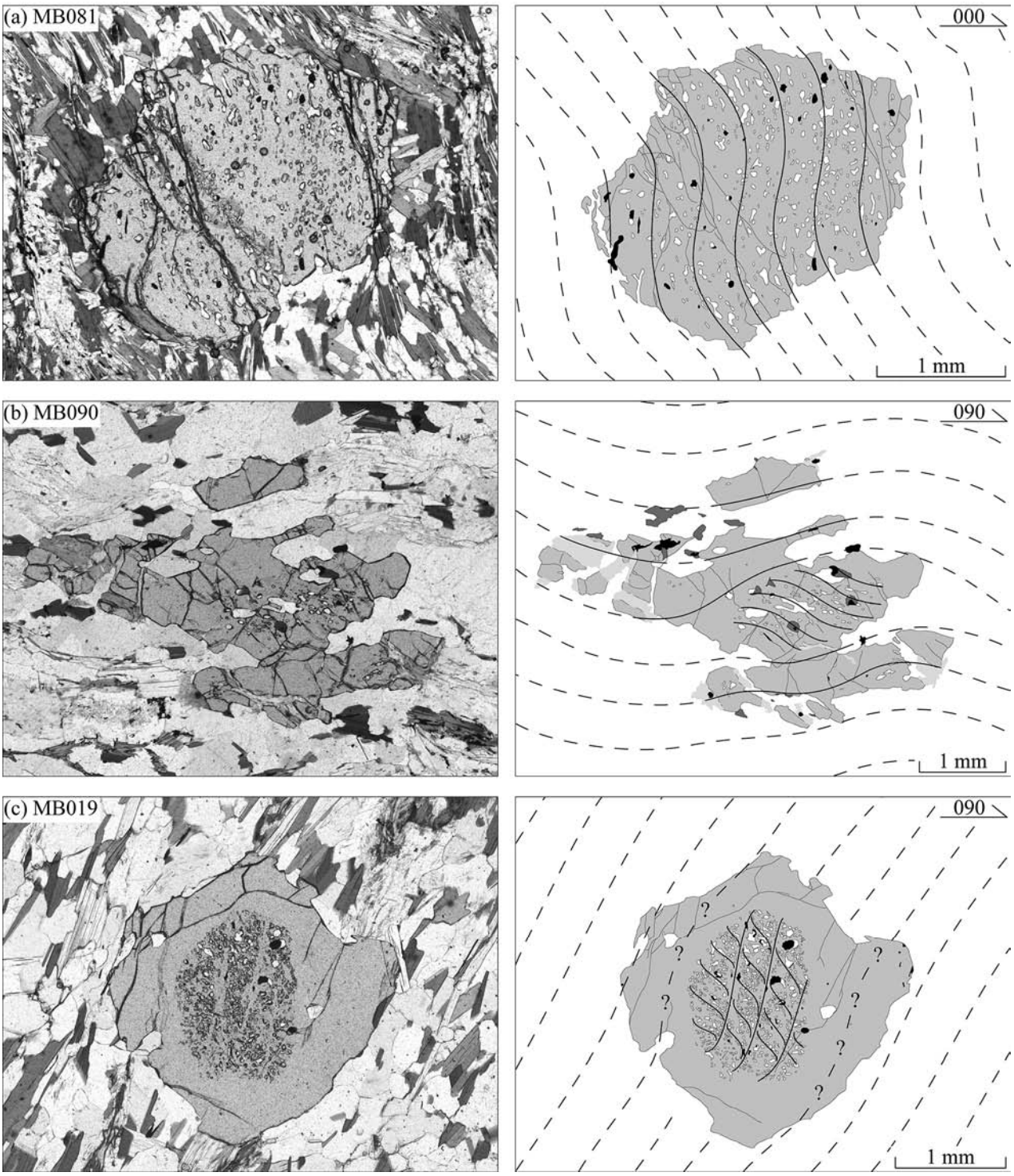
(a) MB081
000
1 mm
(b) MB090
090
1 mm
(c) MB019
090
1 mm

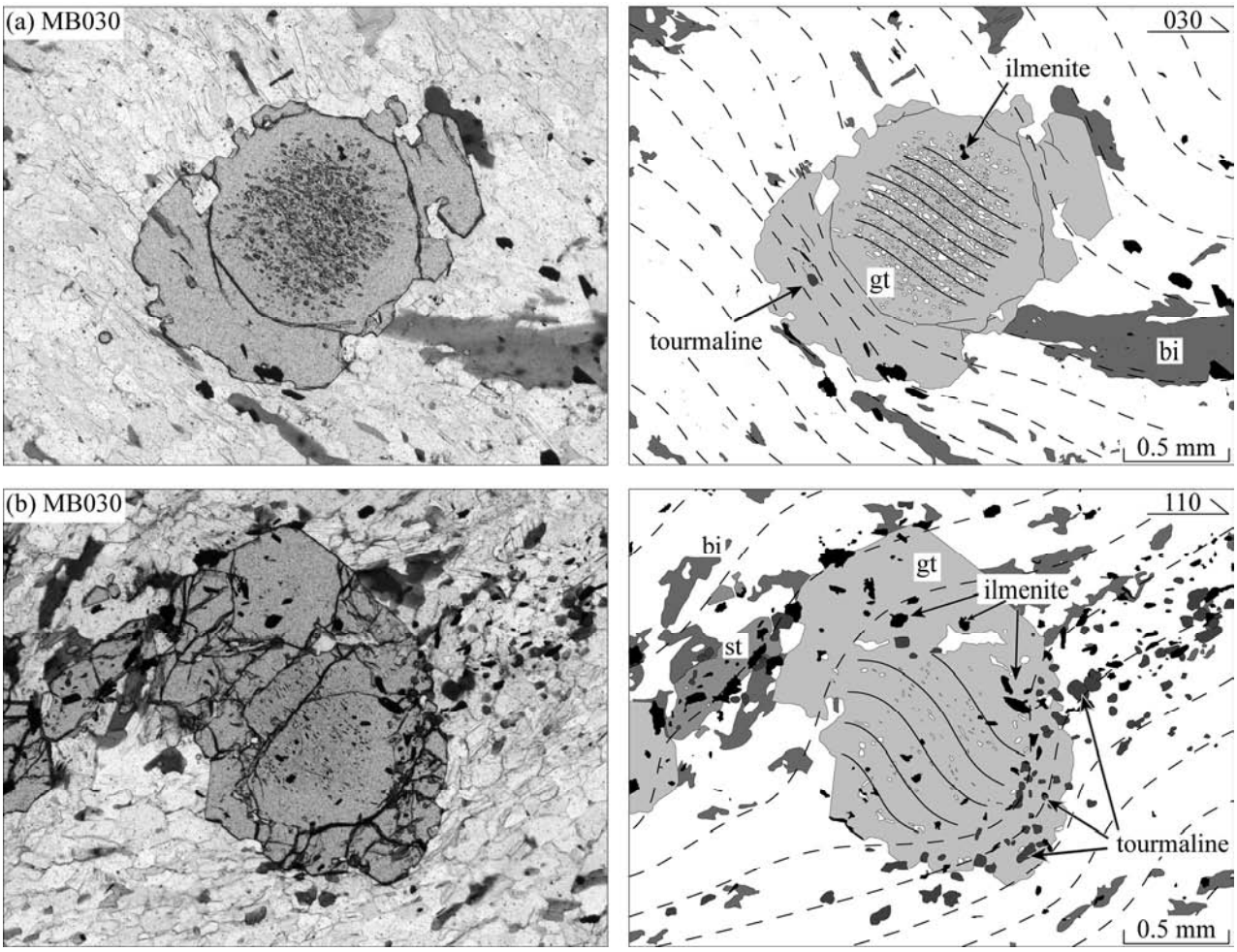

Figure 5. Photomicrographs and associated line diagrams of garnet porphyroblasts in differently oriented thin sections cut from a single sample (MB030) illustrating how variations in composition and morphology can be used to distinguish and correlate different generations of inclusion trails (S_i). These garnet porphyroblasts show a distinct textural zonation with core inclusions of fine grained quartz and ilmenite being truncated by the foliation preserved in the rim. The rim trails are continuous with the matrix foliation and have inclusions of coarse grained quartz, ilmenite and tourmaline. Scale bar in lower right corner. (a) Vertical section striking 030°. Plane polarized light. (b) Vertical section striking 110°. Plane polarized light.

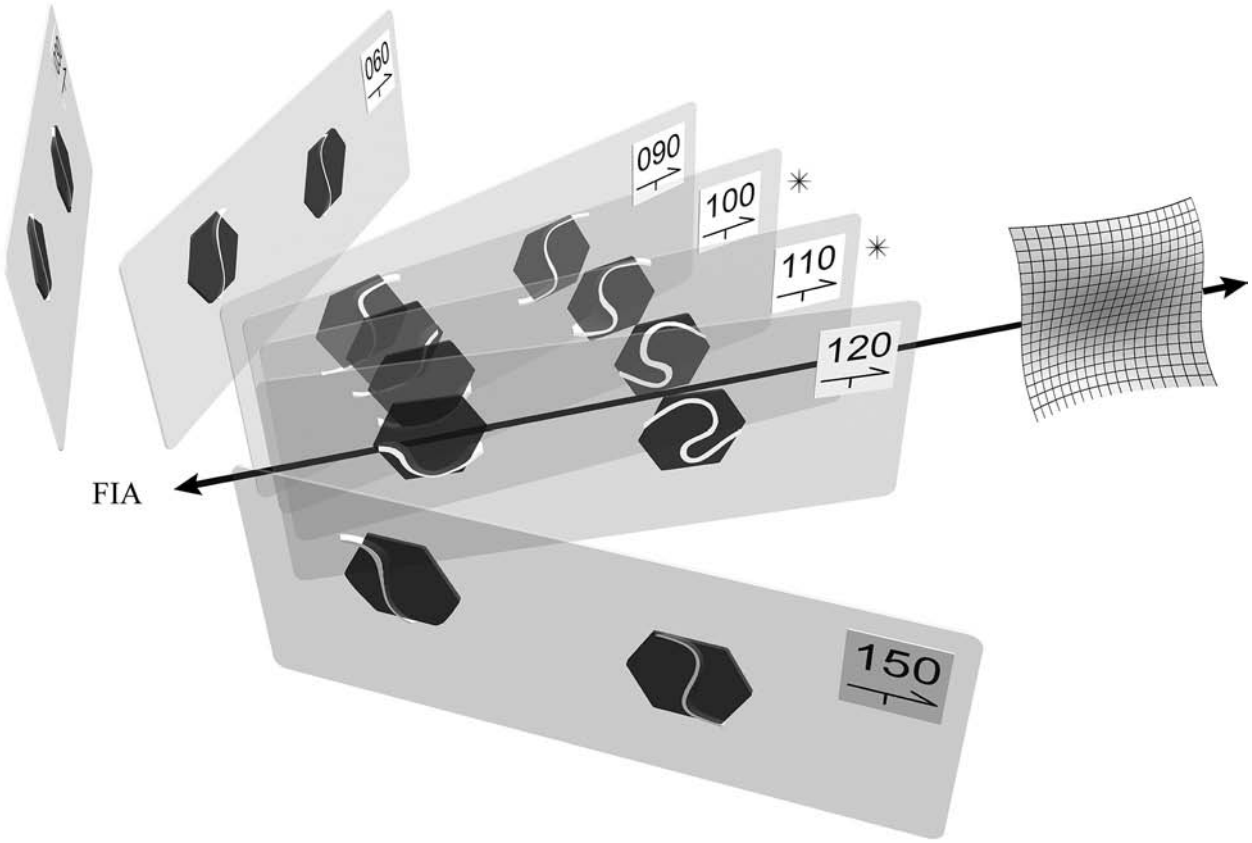

Figure 6. 3D model demonstrating the asymmetry method for establishing the FIA trend for a sample containing simple sigmoid inclusion trails. Initially, six vertical thin sections, cut at 30^0 intervals from an oriented horizontal slab (i.e., trends of 0, 30, 60, 90, 120 and 150 degrees) are examined from the same direction around the compass and the geometry of the inclusion trails in all the porphyroblasts is recorded. The FIA trend can be refined to within a 10° range by preparing two additional sections (marked with an asterisk) covering the 30° interval over which the flip in asymmetry is observed. This is seen to occur between 90^0 and 120^0 for the model shown. In this example, two sections with strikes of 100^0 and 110^0 are prepared and examined. The change from "S" shaped to "Z" shaped inclusion trails is now constrained to between 110^0 and 120^0 with the mid-point (115°) being recorded as the trend of the FIA. See also Appendix E: "E01-asymmetry method.mov".

Sample	garnet					andalusite	staurolite
	pFIA	single FIA	core	rim	FitPitch		
MB003		150				060	
MB006						085	
MB007		085					
MB008		175				055	
MB010			020	065			160
MB014		130					
MB018					038		
MB019	155		155	175			
MB021		045				055	
MB022		080			009		
MB023	130		050				165
MB024		040					
MB028					145, 143		
MB030			120	070			
MB031		085				055	
MB033		120				045	
MB035			045	075			
MB037		075					
MB040						055	
MB042	145		155				085, 080
MB044		085					
MB045		085				045	
MB049		045				060	
MB050		085				055	
MB051					070, 084		
MB054						045	
MB055						045	
MB057		085				075	
MB058		130					
MB060		130					
MB061		155					
MB063			040	090		025	165
MB065		040				045	
MB066		080				065	85, 145
MB067		040					
MB068				085			
MB069				085			
MB071		040					
MB074			050	070		050	
MB075		155					
MB076			050	050			
MB080			075	075		045	
MB081		070					
MB082						115	
MB084		085				055	
MB090			160	155			
MB093						065	
MB095			045	140			
MB096		085					065
MB099		050					
MB101		040					
MB106		155					090
MB105					076		
MB107				075		065	085
MB110		075				035	

Table 1. FIA data from the Lebanon Antiformal Syncline separated into that from andalusite, staurolite and garnet porphyroblasts. Garnet FIAs are subdivided into pFIA, single FIA, core, rim and FitPitch data.

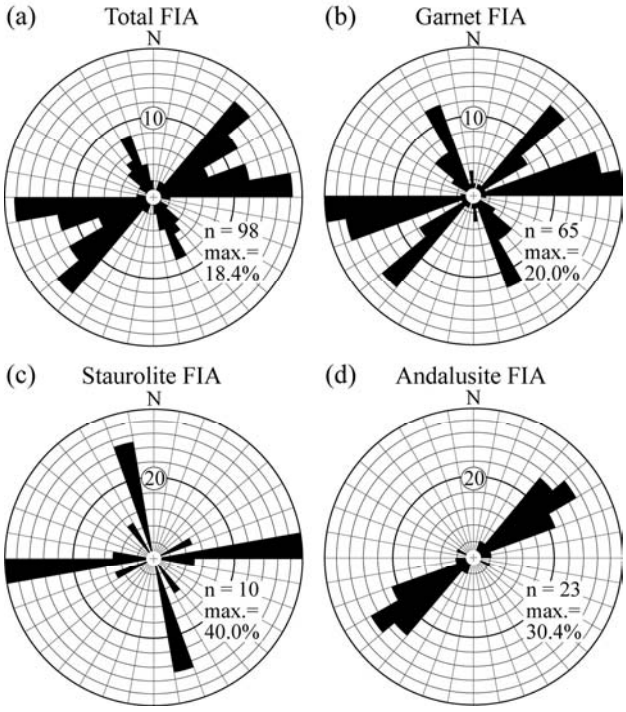

Figure 7. Equal area rose diagrams of FIA trends. (a) The plot of total data shows three modal peaks at 40-60°, 70-90° and 140-170° that are also reflected in the garnet data (b). The distribution of staurolite FIAs (c) displays two dominant peaks at approximately 60-100° and 140-170° and andalusite shows one dominant trend of between 40° and 70°.

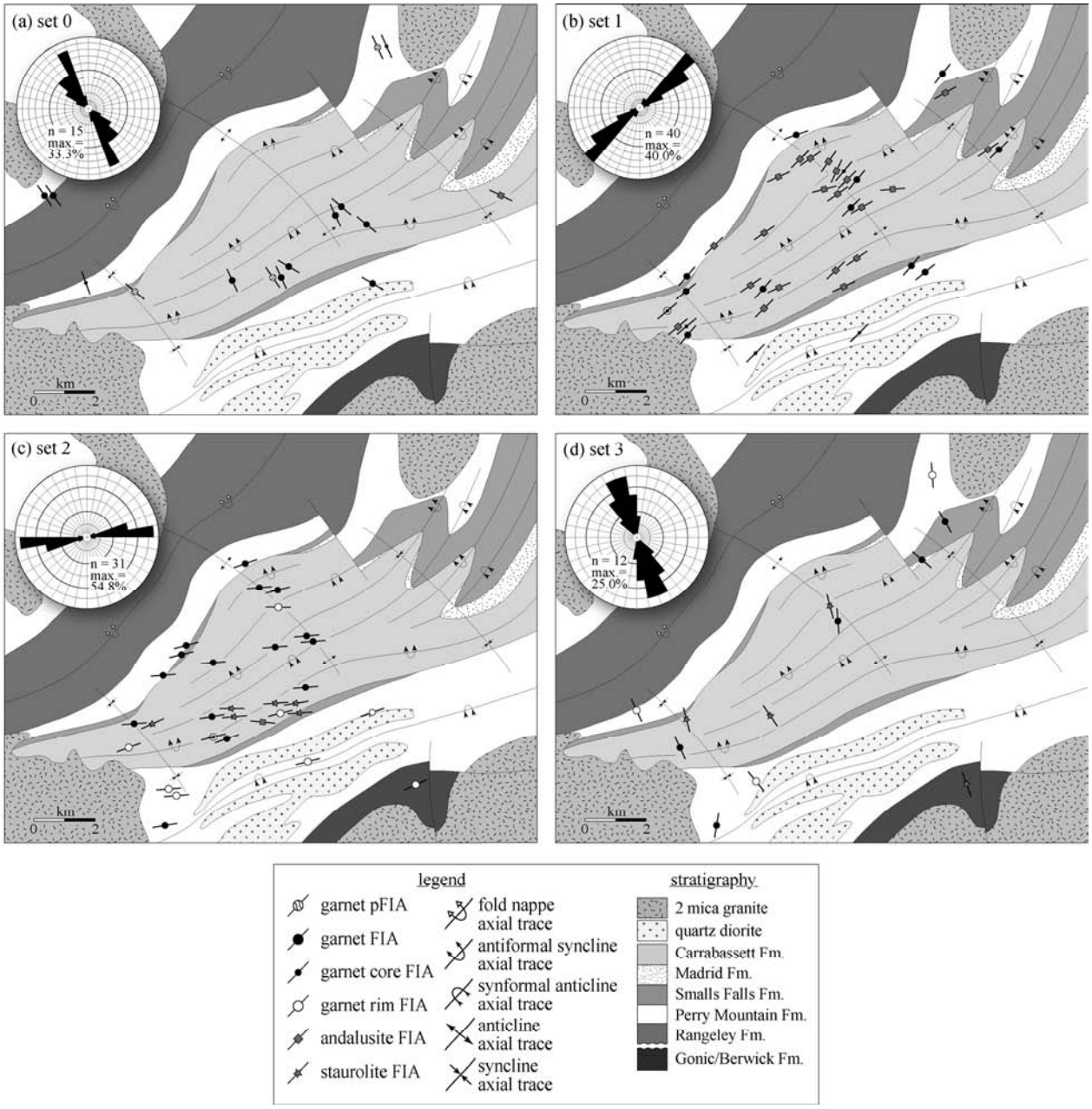

Figure 8. Maps and equal area rose diagrams of the 4 successive FIA sets for samples collected from the Lebanon Antiformal Syncline, New Hampshire. (a) FIA set 0 trends. (b) FIA set 1 trends. (c) FIA set 2 trends. (d) FIA set 3 trends.

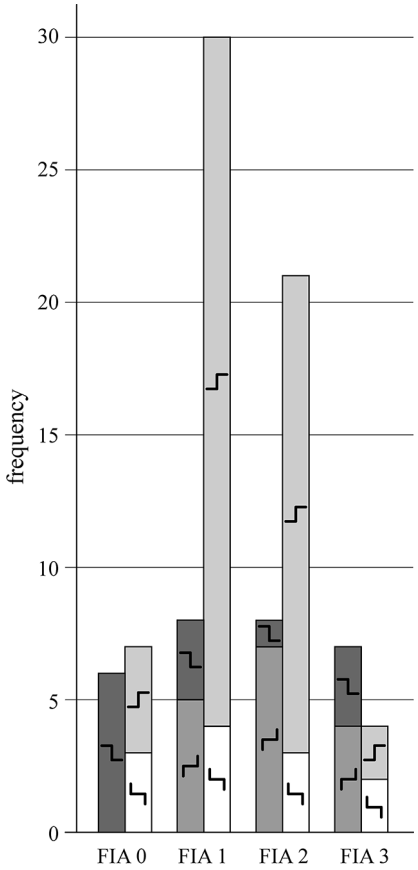

Figure 9. Histograms showing the asymmetry of inclusion trails preserved within porphyroblasts separated according to FIA sets and whether the geometry can be interpreted as resulting from a flat-to-steep or steep-to-flat transition of successive foliations. The inclusion trail asymmetry is recorded as it would project onto a SW-NE section looking NW for FIA sets 0 and 3, and looking NE in a section oriented NW-SE for FIA sets 1 and 2.

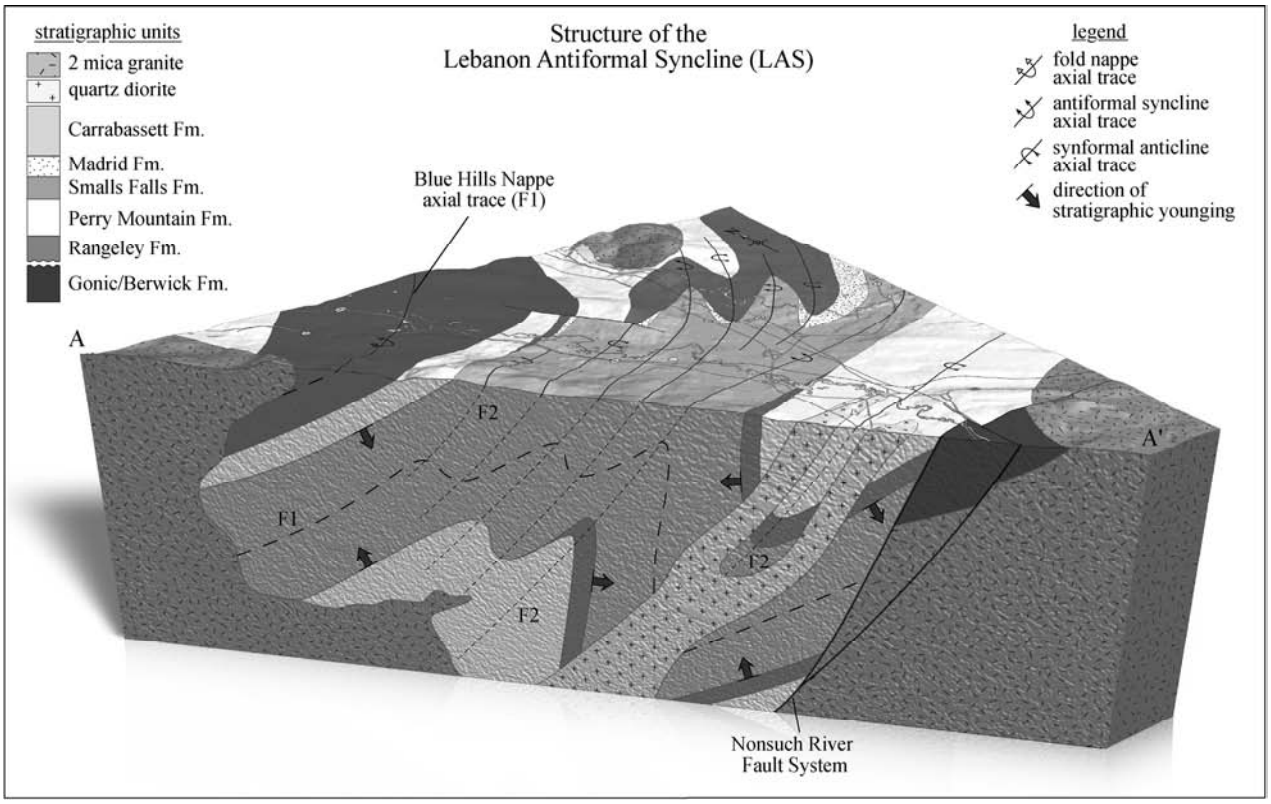

Figure 10. Block diagram illustrating the major structural and stratigraphic features of the Lebanon Antiformal Syncline as viewed looking NE. The line of section is indicated in Figure 2.

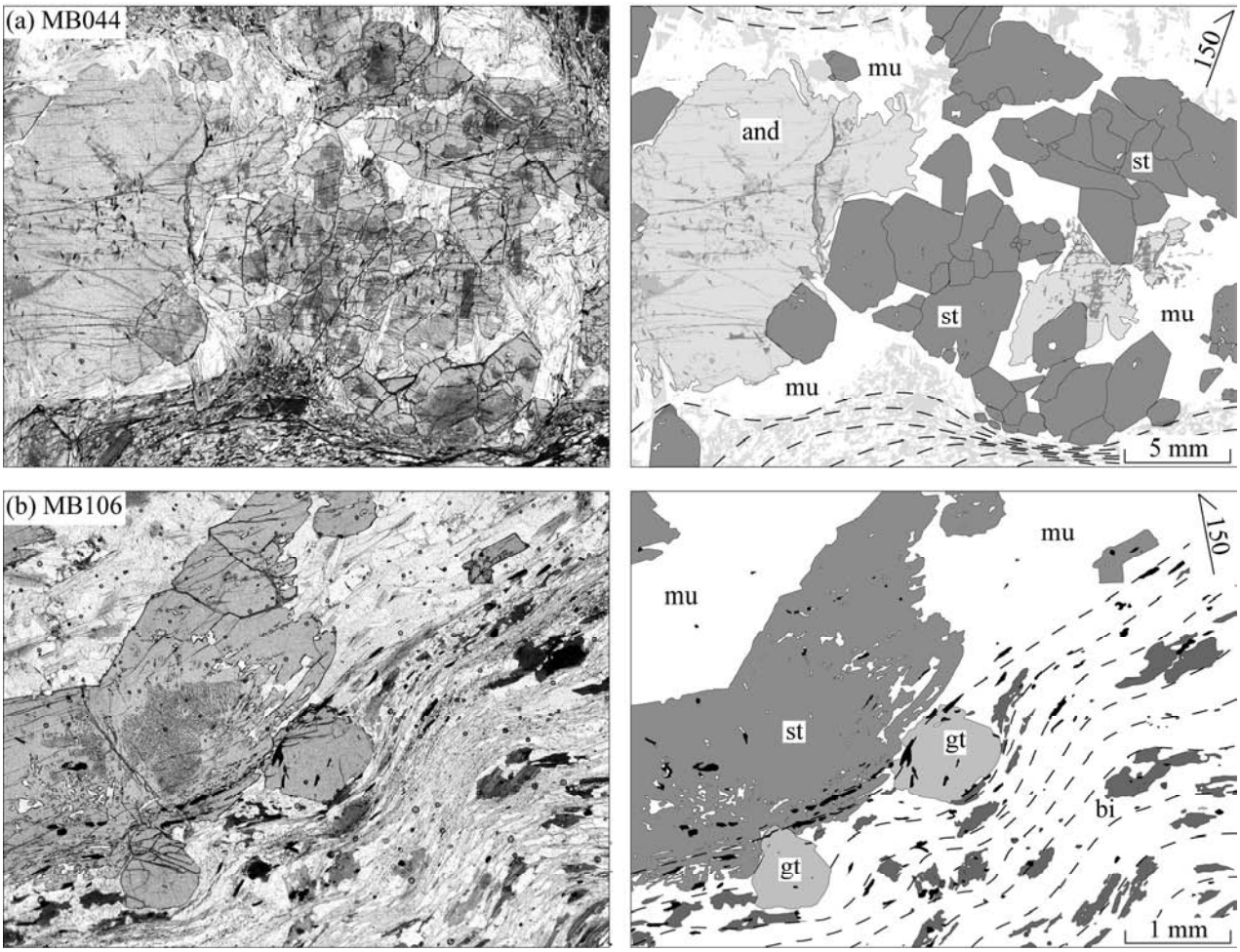

Figure 11. Photomicrographs and interpretive sketches illustrating pseudomorphs of staurolite and muscovite after andalusite. The pseudomorphs are interpreted as interpreted as forming during early M_2 metamorphism. Plane polarized light. Scale bars in lower right corners. (a) Sample MB044. Partial pseudomorph of andalusite by coarse-grained muscovite and idioblastic to subidioblastic staurolite with quartz-rich symplectitic cores. (b) Sample MB106. Staurolite replacing andalusite and extending into the matrix, overgrowing the foliation developed against the andalusite rim.

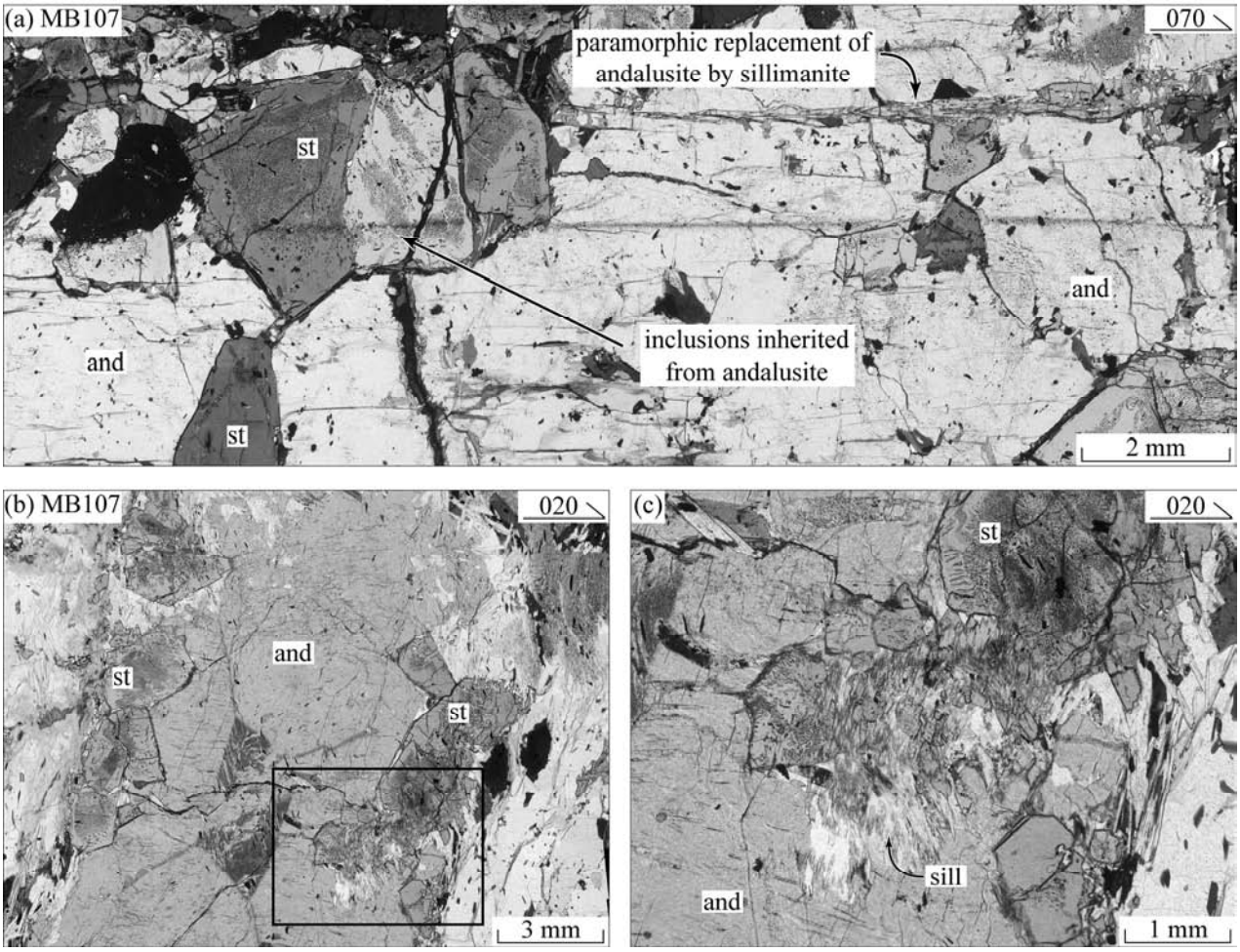

Figure 12. Photomicrographs illustrating the relationship between andalusite, staurolite and sillimanite. Scale bars in lower right corners. (a) Sample MB107. Crossed polarized light. The staurolite (upper left) replaced andalusite and incorporated the latter's inclusion trails. Sillimanite paramorphically replaced andalusite and staurolite (upper right) during the late D_2 high temperature contact metamorphic event. (b) Sample MB107. Plane polarized light and (c) enlargement of inset shown in (b). Fibrolitic sillimanite replacing andalusite and staurolite as a result of the thermal pulse that accompanied the waning stages of D_2. Staurolite maintains its euhedral crystal faces only where it is protected by andalusite.

	MB019	**MB063**
	wt.% oxides	
SiO_2	70.30	61.80
TiO_2	0.72	0.88
Al_2O_3	14.50	19.60
MnO	0.12	0.07
MgO	1.73	2.11
CaO	0.12	0.40
Na_2O	0.83	0.83
K_2O	3.64	4.64
P_2O_5	0.04	0.14
SO_3	0.01	0.01
FeO*	6.46	6.30
loi	*1.57*	*2.79*
Sum	100.76	100.20

* All Fe as FeO

Table 2. Major element analyses (shown as weight % oxide) of bulk compositions used in the calculation of pseudosections.

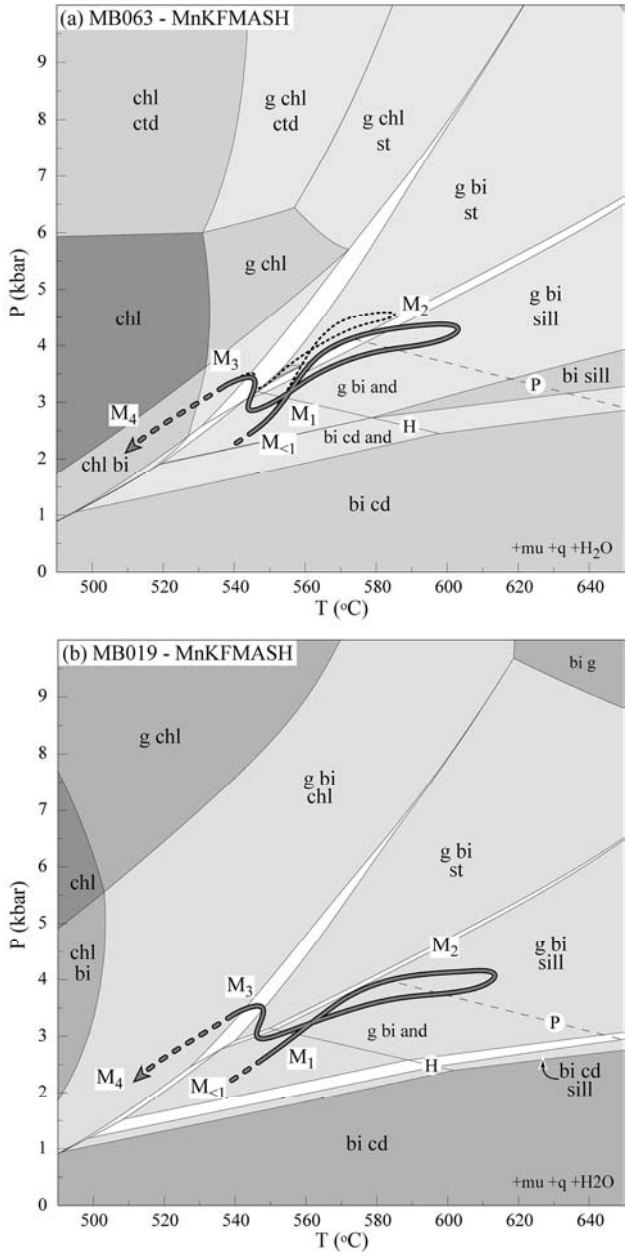

Figure 13. Pseudosections showing approximate P-T paths for rocks in (a) the transition zone (solid line) and staurolite zone (dotted line) (b) sillimanite zone. The stable M_2 mineral assemblage is governed by the pressure and temperature conditions relative to the g-bi-st-sill divariant field. The andalusite-sillimanite reaction curves of Holdaway (1971; solid line) and Pattison (1992; dashed line) are both shown. Mineral abbreviations used are as follows: chl = chlorite, ctd = chloritoid, cd = cordierite, g = garnet, st = staurolite, bi = biotite, and = andalusite, sill = sillimanite, q = quartz, mu = muscovite.

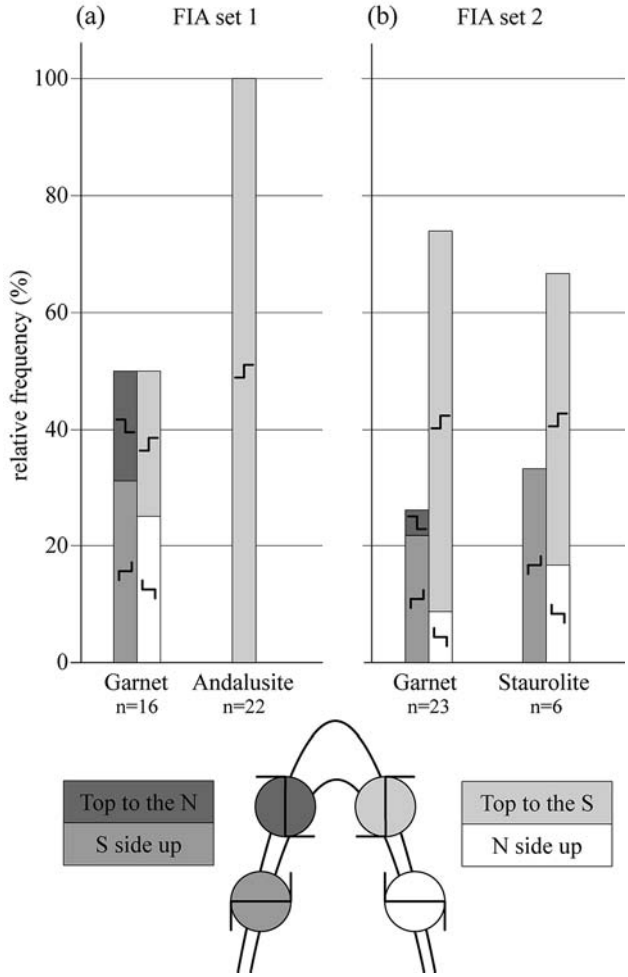

Figure 14. Histograms showing the relative frequency of inclusion trail asymmetries preserved within porphyroblasts separated according to whether the geometry can be interpreted as resulting from a flat-to-steep or steep-to-flat transition of successive foliations. The inclusion trail asymmetry is recorded as it would project onto a NW-SE section looking NE. (a) FIA set 1 asymmetry data plotted separately for garnet and andalusite porphyroblasts. (b) FIA set 2 data plotted separately for garnet and staurolite porphyroblasts.

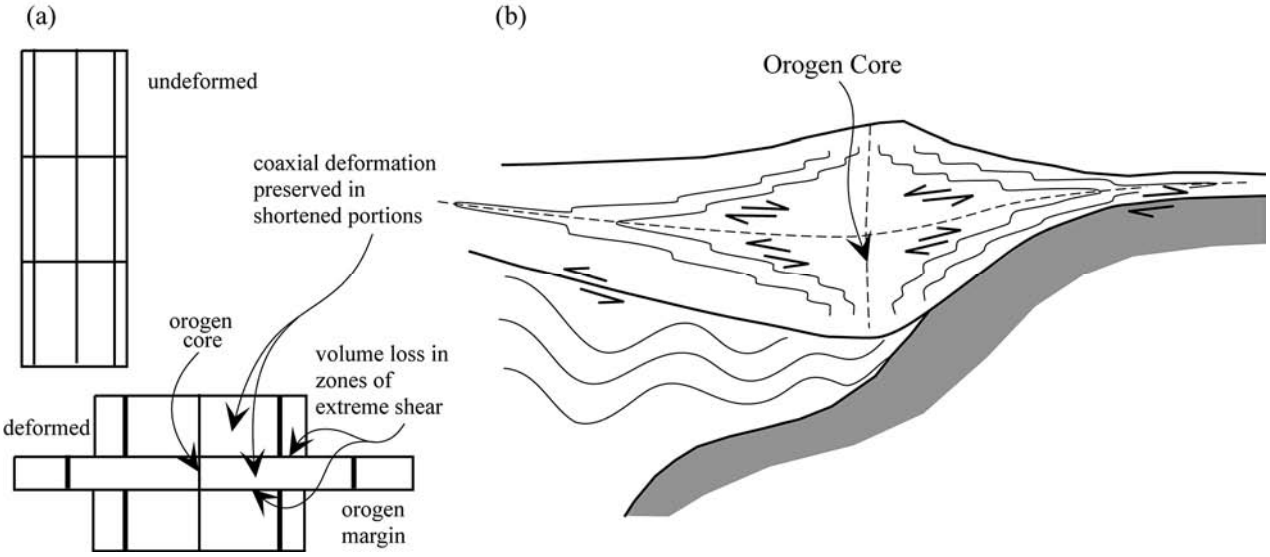

Figure 15. (a) Demonstration of the principle that the accumulation of displacement during gravitational collapse and spreading results in an increase in the degree of shearing with distance from the core to the margins of an orogen when partitioning of the amount of bulk shortening occurs vertically through the crust. (b) The same principle in a more geologically significant context, where the zones of progressive shearing contain portions of the progressive shortening history and the zones of progressive shortening contain some effects of the progressive shearing history and faults do not lie on their boundaries. After Bell and Newman (2006).

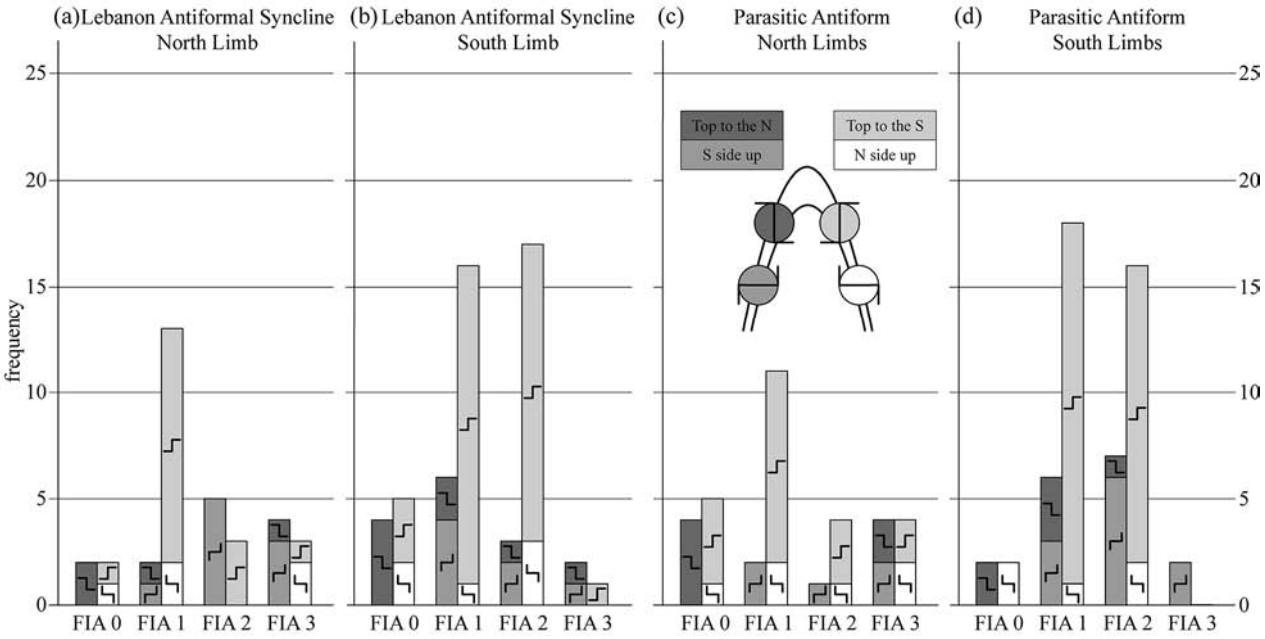

Figure 16. Histograms of inclusion trail asymmetries divided into FIA sets and plotted separately for (a) the northern and (b) the southern limb of the Lebanon Antiformal Syncline. The data is also divided into that from (c) the northern and (d) the southern limbs of the second order antiforms that are parasitic to the Lebanon Antiformal Syncline. The inclusion trail asymmetry is recorded as it would project onto a SW-NE section looking NW for FIA sets 0 and 3, and looking NE in a section oriented NW-SE for FIA sets 1 and 2. It can be seen that most of the porphyroblast growth occurred on the southern limbs of both the Lebanon Antiformal Syncline and the smaller scale parasitic antiforms during horizontal bulk shortening.

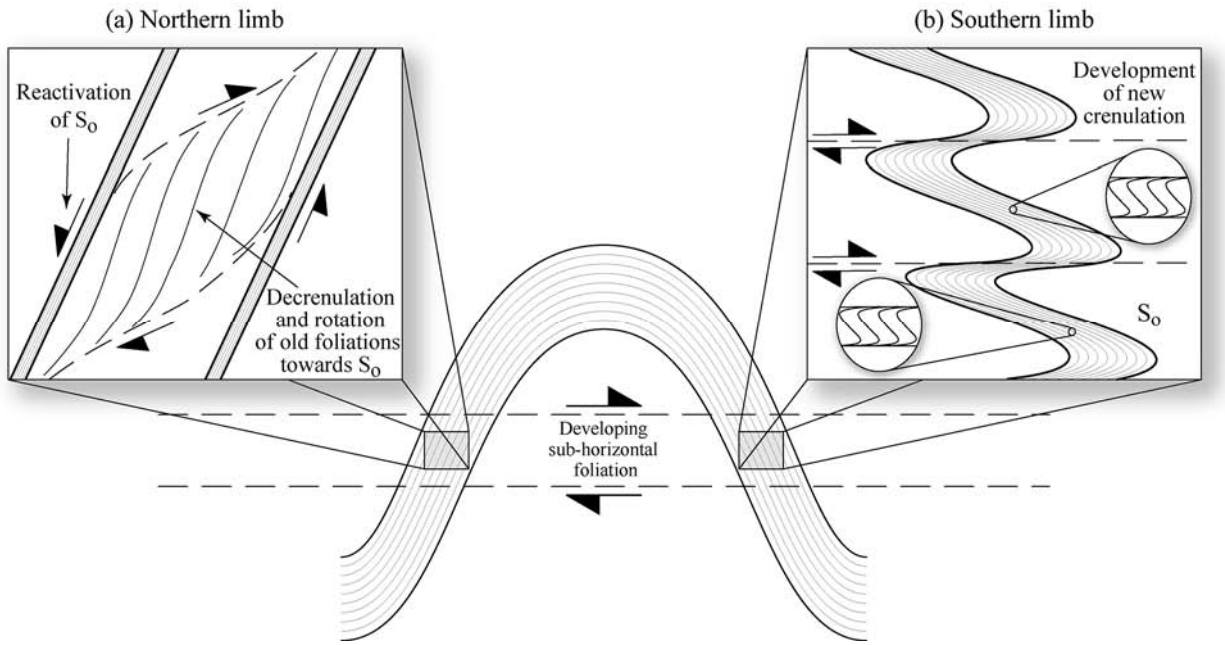

Figure 17. Schematic cross-sectional sketch looking towards the east, showing the effects of a developing sub-horizontal foliation with a clockwise differentiation asymmetry (shown by single barbed arrows) on each limb of an upright fold. (a) Anticlockwise reactivation of bedding (S_0) can occur on the northern limb and will accommodate some of the effects of clockwise shearing on the developing foliation. This reactivation results in decrenulation of the newly developed crenulations and unfolding and rotation of earlier foliations towards S_0. The remains of the developing foliation are also rotated towards S_0. (b) Reactivation on the southern limb is not possible and a new crenulation cleavage continues to develop. Modified from Bell *et al*., 2003.

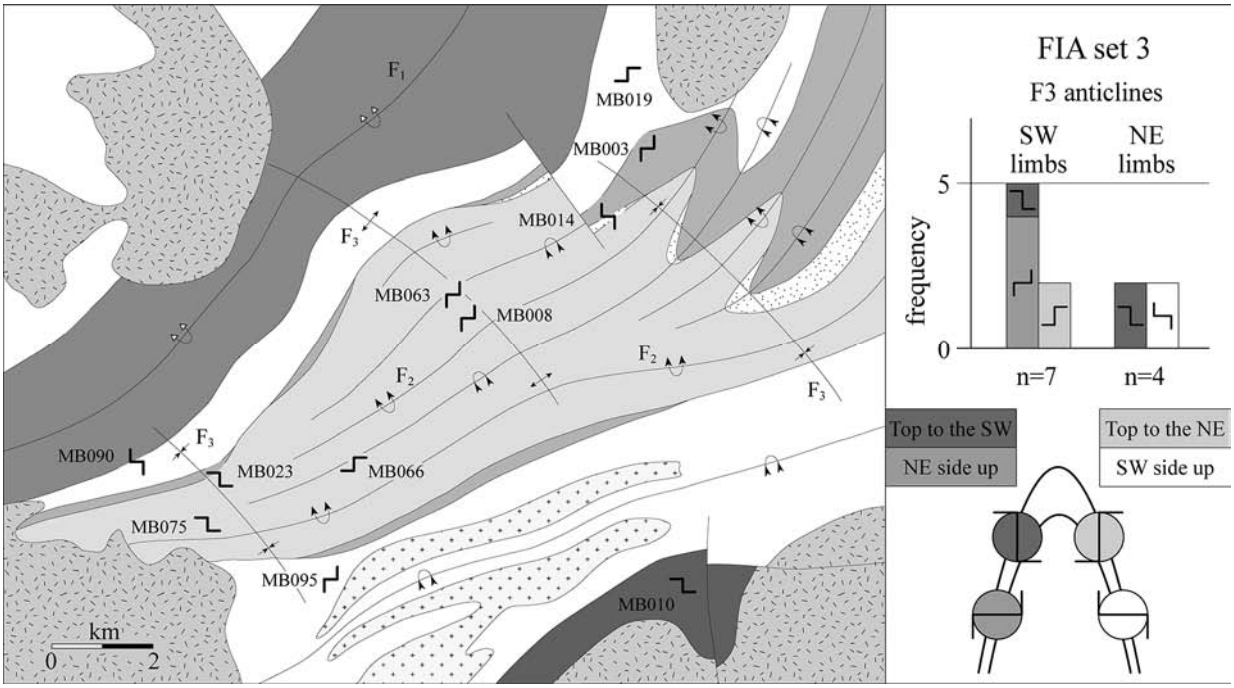

Figure 18. FIA set 3 is most commonly preserved in samples that were collected close to the axis of F_3 folds. The garnet and staurolite porphyroblasts that grew during the formation of the steeply dipping S_3 crenulation cleavage display exclusively clockwise inclusion trail asymmetries on the NE limbs and anticlockwise asymmetries on the SW limbs of F_3 antiforms, indicating that FIA set 3 is related to the gentle folds that result in a broad scale change in trend of the F_2 fold axes from E-W in the south-west of the mapped area to nearly N-S in the north-east.

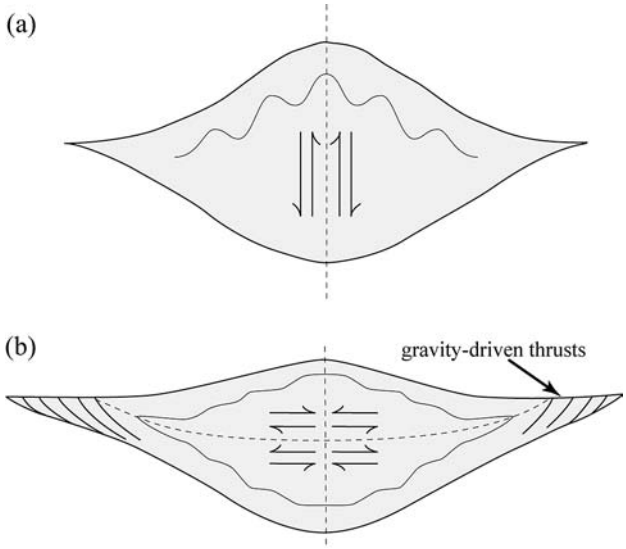

Figure 19. Schematic representation of the upper 50-60 km of the lithosphere during (a) uplift and (b) gravity induced collapse phases of orogenesis as proposed by Bell and Johnson (1989). The dominant sense of shear in each sector is indicated by the single barbed arrows.

Deformation Event	Metamorphism	FIA	
D<1: NE-SW directed bulk shortening. Coarsely partitioned foliation development	M<1: Garnet, randomly oriented biotite	FIA set 0 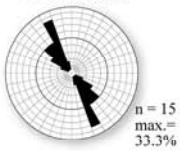	
D1: NW-SE directed bulk shortening. Development of strong, penetrative, steeply dipping foliation axial planar to up-right F_1 folds. Late stage re-orientation of folds and foliation due to gravitational collapse and spreading away from the orogen core. Emplacement of the Blue Hills Nappe.	M1: Low pressure event involving early garnet growth during the coaxial phase of sub-vertical foliation development followed by garnet and andalusite porphyroblast growth, commonly preserving top to the SE differentiation asymmetries as inclusion trails.	FIA set 1 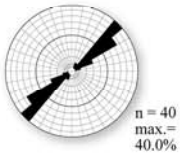	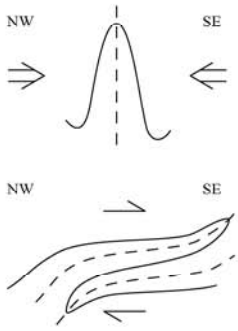
D2: Refolding of overturned limb of nappe resulting in folds with steeply dipping axial planes. Development of a distinctive, spaced crenulation cleavage (S_2). Further gravitationally induced collapse and spreading away from the orogen core and flattening of earlier formed folds and foliations.	M2: Higher pressure event due to overturning and refolding of the stratigraphic sequence and possibly due to loading of allochthonous material moving away from the orogen core. Late heat and fluid pulse associated with the intrusion of granitic melts. Growth of garnet and staurolite porphyroblastic phases as well as tourmaline and both fibrolitic and tabular sillimanite.	FIA set 2 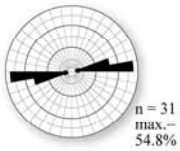	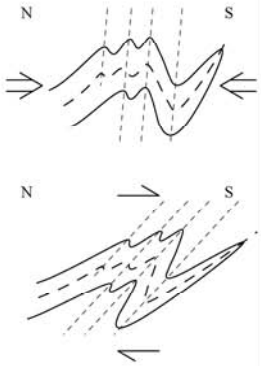
D3: Faulting (?) and gentle (F_3) folding resulting in the curvature of F_2 fold axes and the development of a weak crenulation cleavage.	M3: Growth of garnet and staurolite porphyroblasts and prograde chlorite.	FIA set 3 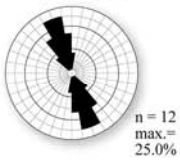	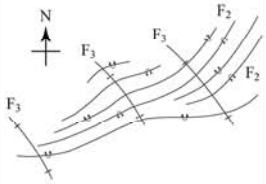
	M4: Sericitisation of aluminosilicates and chlorite pseudomorphs of biotite and garnet.		

Figure 20. Schematic diagram showing the relationship between deformation, metamorphism and porphyroblast growth. The relative succession of FIA sets is shown on equal area rose diagrams with a 10° class interval.

Appendix A:

FitPitch data

MB018 Inclusion Trail Pitch/Strike

Section Orientation	Garnet Core	Garnet Rim	Section Orientation	Garnet Core	Garnet Rim
000	114	171	060	23	147
000	100	04	060	21	150
000	116	10	090	52	144
000	106	06	090	60	147
000	125	175	090	73	160
000	135	177	090	65	145
000	122	01	090	70	146
000	133	00	090	69	144
000	127	01	090	63	147
000	125	05	090		143
000	134	00	120	60	144
000	122	177	120	57	136
000	129	178	120	66	138
000	125	176	120	60	150
000		178	120	68	148
000		174	150	54	175
000		03	150	74	145
000		179	150	61	155
030	151	157	150	61	170
030	136	161	150	94	165
030	143	158	150	59	160
030	138	157	150	70	159
030	142	159	150	67	
030	137	162	150	62	
030	144	167	150	55	
030	141	160	horizontal	054	006
030	139	150	horizontal	054	005
030		155	horizontal	043	176
060	34	151	horizontal	030	170
060	32	153	horizontal	050	165
060	20	150	horizontal	055	170
060	21	144			

MB019 Inclusion Trail Pitch/Strike

Section Orientation	Crenulated Cleavage	Differentiated Crenulation	Garnet Rim
000	54	6	14
000	58	170	8
000	59	168	16
000	54		170
000	53		
030	59	109	147
030	61	122	148
030	51	124	154
050	67	110	136
050	60	115	140
050	59	99	134
050			133
060	59	94	126
060	67	99	
060	53	108	
060	48	118	
060	61		
090	50	105	124
090	38	111	123
090	42	104	124
090	38	95	119
090	46		
120	30	100	128
120	12	109	126
120	27	112	123
120		108	
130	178	113	115
130	6	115	120
130	7	117	130
130	2	114	
130		111	
140	167	118	125
140	170	120	129
140	178	116	
150	163	103	136
150	159	108	135
150	146	116	130
150	149	120	130
150	144	123	127
150		125	
horizontal	312	350	10
horizontal	330	4	14
horizontal	310	5	10
horizontal	320	8	12
horizontal	309	348	11
horizontal	321	355	8
horizontal	310		9
horizontal	318		14
horizontal	312		

MB022 Inclusion Trail Pitch/Strike

Section Orientation	Coticule Garnets	Section Orientation	Coticule Garnets	Section Orientation	Coticule Garnets	Section Orientation	Coticule Garnets
000	151	000	0	030	63	070	102
000	153	000	38	030	136	070	145
000	81	000	31	030	165	070	124
000	176	000	158	030	168	070	105
000	16	000	25	030	94	070	120
000	155	000	34	030	5	070	144
000	170	000	21	030	100	070	111
000	158	000	153	030	133	070	130
000	57	000	41	030	134	070	105
000	10	000	150	030	78	070	98
000	51	000	171	030	160	070	134
000	154	000	30	030	169	070	137
000	57	000	31	030	125	070	149
000	22	000	68	030	142	070	116
000	152	000	4	030	122	070	81
000	148	000	29	030	132	070	80
000	133	000	144	060	69	070	2
000	52	000	35	060	95	070	105
000	150	000	18	060	175	070	103
000	51	000	20	060	66	070	104
000	154	000	135	060	161	070	118
000	156	000	48	060	68	070	85
000	164	000	26	060	60	070	113
000	16	000	31	060	172	070	89
000	165	000	40	060	112	070	98
000	48	000	166	060	104	070	144
000	163	030	163	060	160	070	10
000	44	030	158	060	132	070	146
000	153	030	113	060	144	070	116
000	16	030	93	060	102	070	130
000	20	030	167	060	94	070	117
000	2	030	122	060	72	070	115
000	19	030	164	060	96	080	96
000	52	030	71	060	110	080	116
000	14	030	43	060	114	080	104
000	53	030	92	060	159	080	102
000	47	030	155	060	114	080	118
000	8	030	150	060	116	080	137
000	153	030	71	060	134	080	92
000	134	030	39	060	135	080	118
000	42	030	150	060	114	080	115
000	162	030	73	060	85	080	129
000	25	030	76	060	128	080	80
000	42	030	55	060	128	080	100
000	176	030	62	060	122	080	129
000	38	030	124	060	137	080	105
000	167	030	152	060	90	080	99
000	163	030	148	060	114	080	111
000	154	030	104	060	115	080	155
000	147	030	120	060	97	080	64
000	154	030	178	060	140	080	109
000	17	030	179	060	159	080	114

MB022 Inclusion Trail Pitch/Strike continued

Section Orientation	Coticule Garnets	Section Orientation	Coticule Garnets	Section Orientation	Coticule Garnets	Section Orientation	Coticule Garnets
080	89	090	87	120	92	150	166
080	151	090	85	120	159	150	162
080	120	090	104	120	160	150	100
080	116	090	111	120	122	150	163
080	109	090	89	120	138	150	61
080	115	090	109	120	162	150	36
080	101	090	137	120	117	150	43
080	115	090	125	120	163	150	122
080	143	090	144	120	134	150	145
080	136	090	104	150	48	150	26
080	92	090	172	150	164	150	120
080	107	090	120	150	130	150	158
080	134	090	117	150	52	horizontal	9
080	115	090	123	150	143	horizontal	339
080	133	090	105	150	159	horizontal	329
080	109	120	143	150	160	horizontal	312
080	140	120	39	150	165	horizontal	350
080	148	120	70	150	156	horizontal	344
080	125	120	78	150	143	horizontal	295
080	130	120	160	150	158	horizontal	320
080	142	120	165	150	168	horizontal	320
080	84	120	101	150	157	horizontal	58
080	72	120	144	150	167	horizontal	318
080	84	120	100	150	147	horizontal	338
080	80	120	146	150	164	horizontal	30
090	140	120	128	150	115	horizontal	20
090	130	120	178	150	32	horizontal	35
090	121	120	120	150	156	horizontal	312
090	104	120	88	150	144	horizontal	327
090	105	120	96	150	2	horizontal	347
090	119	120	137	150	173	horizontal	27
090	125	120	138	150	161	horizontal	349
090	133	120	140	150	56	horizontal	16
090	102	120	133	150	96	horizontal	19
090	120	120	114	150	0	horizontal	352
090	121	120	87	150	171	horizontal	330
090	121	120	139	150	112	horizontal	6
090	74	120	82	150	149	horizontal	4
090	104	120	90	150	140	horizontal	352
090	128	120	102	150	130	horizontal	354
090	151	120	90	150	7	horizontal	348
090	100	120	134	150	108	horizontal	18
090	128	120	158	150	125	horizontal	2
090	86	120	144	150	158	horizontal	4
090	75	120	131	150	142	horizontal	10
090	148	120	145	150	121	horizontal	3
090	133	120	134	150	133	horizontal	2
090	119	120	125	150	89	horizontal	340
090	111	120	98	150	147		
090	89	120	111	150	130		

MB028 Inclusion Trail Pitch/Strike

Section Orientation	Coticule Garnets	Section Orientation	Coticule Garnets	Section Orientation	Coticule Garnets
000	48	000	132	000	51
000	50	000	66	000	65
000	72	000	70	030	54
000	62	000	51	030	53
000	150	000	32	030	68
000	56	000	47	030	49
000	124	000	53	030	109
000	54	000	36	030	104
000	58	000	51	030	110
000	56	000	134	030	115
000	68	000	68	030	116
000	131	000	95	030	58
000	67	000	54	030	56
000	74	000	62	030	48
000	69	000	49	030	72
000	67	000	131	030	98
000	48	000	133	030	71
000	127	000	51	030	56
000	72	000	89	030	68
000	108	000	51	030	112
000	59	000	68	030	32
000	69	000	68	030	88
000	116	000	50	030	115
000	119	000	60	030	111
000	50	000	63	030	55
000	65	000	93	030	110
000	64	000	44	030	76
000	48	000	63	030	55
000	52	000	72	030	54
000	130	000	41	030	110
000	114	000	134	030	108
000	65	000	132	030	113
000	54	000	54	030	174
000	64	000	49	030	72
000	63	000	66	030	55
000	42	000	39	030	51
000	51	000	67	030	114
000	119	000	83	030	57
000	126	000	145	030	68
000	132	000	54	030	108
000	124	000	41	030	56
000	18	000	53	030	73
000	44	000	65	030	156
000	56	000	58	030	114
000	57	000	52	030	139
000	55	000	128	030	17
000	38	000	124	030	54
000	52	000	65	030	45
000	25	000	46	030	53
000	37	000	112	030	73
000	130	000	130	030	2

MB028 Inclusion Trail Pitch/Strike continued

Section Orientation	Coticule Garnets	Section Orientation	Coticule Garnets	Section Orientation	Coticule Garnets
030	53	060	136	090	150
030	56	060	90	090	43
030	55	060	98	090	30
030	46	060	72	090	67
030	116	060	110	090	52
030	19	060	50	090	35
030	114	060	119	090	27
030	135	060	49	090	114
030	48	060	116	090	29
030	71	060	114	090	37
030	72	060	98	090	55
030	54	060	50	090	110
030	62	060	59	090	114
030	112	060	108	090	123
030	54	060	67	090	31
030	76	060	70	090	108
030	54	060	75	090	115
030	40	060	51	090	111
030	75	060	35	090	74
030	118	060	10	090	67
030	112	060	105	090	32
030	113	060	44	090	155
030	70	060	49	090	164
030	120	060	34	090	91
030	53	060	73	090	64
030	135	060	70	090	36
030	56	060	77	090	64
030	72	060	48	090	59
030	49	060	49	090	112
030	108	060	91	090	69
030	71	060	51	090	60
030	54	060	49	090	104
030	54	060	86	090	60
030	100	060	71	090	68
030	113	060	98	090	30
030	55	060	69	090	19
030	57	060	53	090	54
030	29	090	112	090	104
030	53	090	105	090	112
030	119	090	65	090	32
030	58	090	34	090	67
060	54	090	30	090	32
060	50	090	95	090	101
060	49	090	60	090	32
060	70	090	56	090	44
060	51	090	29	090	65
060	117	090	75	090	163
060	74	090	28	090	109

MB028 Inclusion Trail Pitch/Strike continued

Section Orientation	Coticule Garnets	Section Orientation	Coticule Garnets	Section Orientation	Coticule Garnets
090	65	120	40	150	163
090	67	120	117	150	140
090	110	120	4	150	138
090	71	120	164	150	137
090	29	120	178	150	145
090	29	120	174	150	95
090	65	120	48	150	162
090	34	120	170	150	142
090	108	120	125	150	93
090	65	120	121	150	153
090	39	120	148	150	129
090	110	120	40	150	143
090	157	120	172	150	134
090	109	120	37	150	56
090	30	120	36	150	38
090	105	120	175	150	35
090	66	120	176	150	87
090	61	120	39	150	135
090	60	120	127	150	159
090	29	150	77	150	42
090	68	150	164	150	163
090	169	150	160	150	129
090	60	150	132	horizontal	121
120	130	150	69	horizontal	122
120	38	150	109	horizontal	39
120	168	150	170	horizontal	110
120	39	150	65	horizontal	135
120	171	150	110	horizontal	160
120	58	150	130	horizontal	134
120	122	150	142	horizontal	120
120	125	150	158	horizontal	115
120	68	150	160	horizontal	152
120	40	150	169	horizontal	110
120	119	150	160	horizontal	115
120	39	150	149	horizontal	134
120	165	150	135	horizontal	24
120	26	150	142	horizontal	109
120	20	150	138	horizontal	119
120	173	150	117	horizontal	114
120	158	150	165	horizontal	59
120	123	150	27	horizontal	128
120	125	150	44	horizontal	113
120	38	150	99	horizontal	6
120	149	150	21	horizontal	154
120	170	150	106	horizontal	100
120	169	150	158	horizontal	114
120	173	150	166	horizontal	154
120	157	150	93		

MB030 Inclusion Trail Pitch/Strike

Section Orientation	Garnet Core	Garnet Rim	Section Orientation	Garnet Core	Garnet Rim
000	28	45	080	43	167
000	23	42	080	52	164
000	19	47	080	53	167
000	41	44	080	58	1
000	29	49	080	61	6
000	20	35	080	63	
000	14	51	080	55	
000	29	47	090	32	153
000	41	48	100	44	160
000	14	45	100	40	159
000	42	45	100	64	163
000	35		100	43	158
000	27		100	49	157
000	23		100	42	161
000	32		100		159
000	175		110	63	153
000	33		110	38	149
030	24	23	110	100	148
030	24	32	110	51	156
030	32	43	110	61	150
030	62	36	110		160
030	16	29	120	39	153
030	39	37	120	155	150
030	17		120	144	
030	23		150	6	140
060	61	21	150	4	135
060	45	11	150	124	138
060	43	16	150	14	104
060	38	19	150	154	156
060	35	12	150	149	121
060	55	14	150	156	139
060	74	11	150	100	144
060	50	16	150	121	147
060	47		150	113	146
060	44		150	46	148
060	50		horizontal	35	75
060	67		horizontal	21	70
080	62	24	horizontal	31	70
080	54	19	horizontal	20	72
080	72	152	horizontal	16	78
080	35	148	horizontal	40	90
080	32	159	horizontal	20	68
080	41	165	horizontal	28	
080	51	158	horizontal	20	
080	53	169	horizontal	14	
080	44	171			

MB051 Inclusion Trail Pitch/Strike

Section Orientation	Crenulated Cleavage	Differentiated Crenulation	Garnet Rim	Section Orientation	Crenulated Cleavage	Differentiated Crenulation	Garnet Rim
000	110	72	160	090	158	128	162
000	115	74	141	090	175	110	
000	114	70	143	090	162		
000	108	75	144	120	61	110	10
000	102	70	152	120	61	102	5
000	114	48	140	120	70	102	2
000	108	70		120	54	120	4
000	114	74		120	58	103	
000	104	76		120	62		
000	108			150	68	104	25
030	114	56	140	150	71	90	21
030	113	55	143	150	67	93	19
030	105	70	140	150	50	102	24
030	103	65	144	150		110	22
030		64	136	150		107	
030		52		150		110	
030		53		150		114	
030		55		horizontal	81	49	115
060	122	117	153	horizontal	90	50	127
060	126	115	147	horizontal	85	55	109
060	122	87	146	horizontal	108	54	136
060	124	115	142	horizontal	105	45	
060	128	112	138	horizontal	100	56	
060	125	119	139	horizontal	120	39	
060	125	120	149	horizontal	102		
060		112		horizontal	101		
090	165	103	160	horizontal	125		
090	143	115	172	horizontal	95		

MB105 Inclusion Trail Pitch/Strike

Section Orientation	Garnet Core	Garnet Rim	Section Orientation	Garnet Core	Garnet Rim
000	110	36	120	114	136
000	70	43	120	20	133
000	68		120	90	144
000	54		120	25	130
030	30	17	120		137
030	72	12	150	96	150
030	100	10	150	140	140
030	89	113	150	80	137
030	63	15	150	92	138
030	102		150	104	139
060	58	175	150	102	138
060	96	162	150	94	120
060	40	161	150	125	
060		167	horizontal	54	40
090	58	153	horizontal	61	42
090	11	158	horizontal	8	44
090	70	145	horizontal	57	42
090	58	148	horizontal	61	43
090	118	151	horizontal	75	44
090	18	157	horizontal	109	42
090	20	149	horizontal	73	41
090	50	148	horizontal	88	38

Appendix B:

Sample localities and mineralogical data

Sample #	Unit	Eastings	Northings	% qtz/ k-feldspar	% plag	% bt	% mu	% chl	prograde/ retrograde	% and	% alteration of andalusite	% sill	fibrolitic/ tabular	% st	% gt	% tourm	% opaques
MB003	3	338889	4802880	70	1	2	18	1	retro	2	99				1	1	3
MB006	4	337182	4799613	40	2	15	10			15	10			5	1	<1	1
MB007	4	336208	4798899	45	1	15	25	3	pro+retro	2	90			3	2	1	1
MB008	4	335330	4799605	55	5	10	5	7	retro		100				3		1
MB010	5	339325	4794007	70	1	10	5	1	pro+retro					2	6	1	3
MB012	4	338159	4800187	50	1	8	25	8	retro	2	90			2		<1	1
MB013	4	338095	4801180	45	1	26	18	2	pro+retro	1	90			1	2		1
MB014	3	338174	4801614	52	1	5	20	2	retro		100				2	1	15
MB018	2	338888	4803527	55	1	20	15	2	retro	3	95	1	fibrolitic		2	<1	1
MB019	2	338447	4804397	50	3	20	18					2	fibrolitic		3	<1	<1
MB021	4	340536	4800854	40	1	25	18	5	pro+retro	6	55				2	1	3
MB022	2	331167	4792741	45	1	15	20	1	pro+retro			1	fibrolitic		15	<1	1
MB023	4	330214	4796434	53	1	15	20	1	retro	2	80	1	fibrolitic	3	2	<1	1
MB024	2	337663	4797061	55	1	10	10	15	retro			2	fibrolitic		3	1	2
MB028	1	327392	4799770	50	3	5	20					2	fibrolitic		18	1	1
MB030	2	338069	4796421	65	2	15	10	1	retro			2	fibrolitic	1	2	1	1
MB031	4	335808	4797366	57	2	10	15	10	retro		100				3	1	1
MB033	4	335173	4796967	55	2	10	14	12	retro		100				4	1	1
MB035	2	335885	4794840	40	3	17	25	5	retro		100	1	fibrolitic	<1	6		1
MB037	2	331977	4798718	55	2	5	25	5	retro		100	<1	fibrolitic		3	<1	3
MB038	2	331396	4799335	35	8	5	24	15	retro			8	fibrolitic		3		1
MB039	2	332475	4799888	55	2	15	18	2	retro		100	1	fibrolitic			2	3
MB040	4	332452	4796476	50	2	20	22	<1	retro							<1	2
MB041	3	338072	4797288	60	8	5	13	7	retro		100				2	<1	1
MB042	4	335055	4796900	45	2	12	20	1	retro	2	95	2	fib + tab	8	3	<1	2
MB043	4	334423	4796253	45	1	12	15	8	retro	6	80	3	fib + tab	3	2	<1	2
MB044	4	334822	4798789	50	1	12	18	2	retro	4	70			8	2	<1	1
MB045	2	331175	4797911	42	3	15	20	3	retro			1	fibrolitic		2	12	1
MB048	2	333705	4802040	45	15	10	20	5	retro		100	3	fibrolitic			<1	1
MB049	4	335826	4799092	50	1	20	10	2	retro	8	45			2	3	<1	2
MB050	4	334392	4800748	55	3	22	5	2	retro	6	65	2	fib + tab		1	1	1
MB051	2	333999	4801564	50	4	15	20	2	retro		100	2	fib + tab		4	<1	1
MB053	4	334551	4800307	50	2	16	14	1	retro	6	80	2	fibrolitic	2	3	<1	1

Sample #	Unit	Eastings	Northings	% qtz/ k-feldspar	% plag	% bt	% mu	% chl	prograde/ retrograde	% and	% alteration of andalusite	% sill	fibrolitic/ tabular	% st	% gt	% tourm	% opaques
MB054	4	334099	4800715	56	6	12	12	3	retro	3	80	2	fibrolitic	<1	<1	<1	1
MB055	4	335103	4799690	45	1	15	30	5	retro		100	<1	fibrolitic			<1	1
MB057	4	335920	4799072	50	1	15	15	10	retro	2	95			1	1	<1	1
MB058	4	337870	4798394	55	1	15	18	2	retro		100			1	4	<1	1
MB060	3	337052	4799102	45	1	17	27	3	pro+retro		100				3	1	2
MB061	3	336836	4798813	60	2	18	12	2	retro						1	1	2
MB063	4	335086	4800082	30	2	22	24	2	pro+retro	5	70	2	fib + tab	6	3	1	2
MB065	4	335302	4799984	46	2	20	10	1	retro	12	20	1	fib + tab	1	2	<1	1
MB066	4	332957	4796484	55	2	18	15	1	retro		100			3	3	1	1
MB067	4	332781	4796502	50	6	10	25	3	retro		100				3	<1	1
MB068	2	331563	4793822	40	7	15	15	7	pro+retro		100	5	fib + tab	3	4	1	2
MB069	2	331367	4794011	45	7	15	20	2	pro+retro		100	3	fibrolitic	1	4	<1	2
MB070	2	330863	4794566	45	15	15	17	<1	retro			<1	fibrolitic		2	1	1
MB071	4	330179	4794984	46	3	19	20	2	pro+retro		100	4	fib + tab		2	1	1
MB072	4	329324	4796069	40	2	18	30	1	retro		100	2	fibrolitic		3	1	2
MB074	4	330236	4795224	46	7	15	20	6	pro+retro		100	1	fibrolitic		2	1	1
MB075	4	329987	4795483	50	3	15	20	3	retro		100	<1	fibrolitic	2	2	<1	1
MB076	4	329595	4795761	60	3	5	20	4	pro+retro		100	3	fibrolitic		2	1	1
MB077	4	329506	4795924	60	3	10	16	5	pro+retro		100	1	fibrolitic		2	1	1
MB078	2	328889	4796491	40	10	18	22	3	retro		100	1	fibrolitic		2	1	2
MB079	4	329691	4795963	50	5	14	10	12	retro		100	1	fibrolitic		2	2	3
MB080	4	332761	4795763	60	6	10	12	2	retro		100	<1	fibrolitic		3	1	4
MB081	4	333075	4795786	40	10	20	20	1	retro		100	<1	fibrolitic		3	1	2
MB082	4	342372	4799296	50	1	8	15	23	pro+retro		100					<1	1
MB083	4	342715	4799705	50	1	9	12	20	pro+retro		100					<1	3
MB084	4	332888	4798337	55	6	12	16	5	retro		100				2	<1	1
MB085	4	332884	4798502	50	4	10	20	10	retro		100				2	<1	2
MB087	4	332031	4796861	55	2	16	9	14	pro+retro		100				1	1	1
MB090	2	328614	4796717	50	20	8	14	3	retro			1	fibrolitic		1	1	1
MB092	2	338173	4795772	65	6	8	7	4	retro			3	fibrolitic	<1	2	1	2
MB093	4	333382	4800199	40	5	22	15	1	retro	8	75	5	fib + tab	<1		<1	2
MB094	4	333562	4799818	50	2	17	23	5	retro		100					1	1
MB095	2	332415	4794270	56	5	15	14	1	pro+retro		100	3	fibrolitic	<1	3	<1	1

Sample #	Unit	Eastings	Northings	% qtz/ k-feldspar	% plag	% bt	% mu	% chl	prograde/ retrograde	% and	% alteration of andalusite	% sill	fibrolitic/ tabular	% st	% gt	% tourm	% opaques
MB096	4	330476	4796384	55	8	10	10	10	retro			1	fibrolitic		2	1	1
MB097	4	330322	4796616	40	10	15	20	8	retro		100				2	1	2
MB099	2	338102	4796775	45	10	12	25	3	pro+retro							1	2
MB101	3	330335	4796838	65	4	12	7	3	retro		100	2	fibrolitic		3		3
MB103	4	330613	4796739	55	4	12	7	3	retro						3	<1	2
MB104	4	331186	4797784	50	8	15	20	3	retro		100	<1	fibrolitic	<1		1	1
MB105	2	331861	4798655	45	10	12	15	9	retro			3	fib + tab		2	<1	1
MB106	4	333420	4796712	40	2	8	27			<1	99	2	fib + tab	14	2	<1	2
MB107	4	335242	4796426	50	5	10	14	<1	retro	5	55	4	fib + tab	6	2		2
MB108	2	335937	4796212	45	4	4	35	3	retro		100	1	fib + tab	1	2	1	3
MB109	4	335744	4801581	48	15	12	10	2	retro	1	85	8	fibrolitic		1	1	1
MB110	4	335004	4800663	50	1	15	12	1	retro	12	55	1	fib + tab	3	2	1	1

1 Coarse grained migmatite (Perry Mt/ Rangely Fms).
2 Non-rusty, coticule bearing Perry Mt Fm.
3 Rusty weathering Smalls Falls Fm.
4 Grey metaturbidites (Carrabassett Fm)
5 Poorly bedded Gonic and Berwick Fms.

Mineral abbreviations used are as follows: qtz = quartz, k-felds = K feldspar, plag = plagioclase, bt = biotite, mu = muscovite, chl = chlorite, and = andalusite, sill = sillimanite, st = staurolite, gt = garnet, tourm = tourmaline.

Appendix C:

JCU collection numbers

Sample Number	JCU Collection Number	Sample Number	JCU Collection Number
MB001	74151	MB061	74192
MB003	74152	MB063	74193
MB004	74153	MB065	74194
MB006	74154	MB066	74195
MB007	74155	MB067	74196
MB008	74156	MB068	74197
MB010	74157	MB069	74198
MB012	74158	MB070	74199
MB013	74159	MB071	74200
MB014	74160	MB074	74201
MB014	74161	MB075	74202
MB018	74162	MB076	74203
MB019	74163	MB077	74204
MB021	74164	MB078	74205
MB022	74165	MB079	74206
MB023	74166	MB080	74207
MB024	74167	MB081	74208
MB028	74168	MB082	74209
MB030	74169	MB083	74210
MB031	74170	MB084	74211
MB033	74171	MB085	74212
MB035	74172	MB086	74213
MB037	74173	MB087	74214
MB038	74174	MB090	74215
MB039	74175	MB092	74216
MB040	74176	MB093	74217
MB041	74177	MB094	74218
MB042	74178	MB095	74219
MB043	74179	MB096	74220
MB044	74180	MB097	74221
MB045	74181	MB099	74222
MB048	74182	MB100	74223
MB049	74183	MB101	74224
MB050	74184	MB103	74225
MB051	74185	MB104	74226
MB053	74186	MB105	74227
MB054	74187	MB106	74228
MB055	74188	MB107	74229
MB057	74189	MB108	74230
MB058	74190	MB109	74231
MB060	74191	MB110	74232

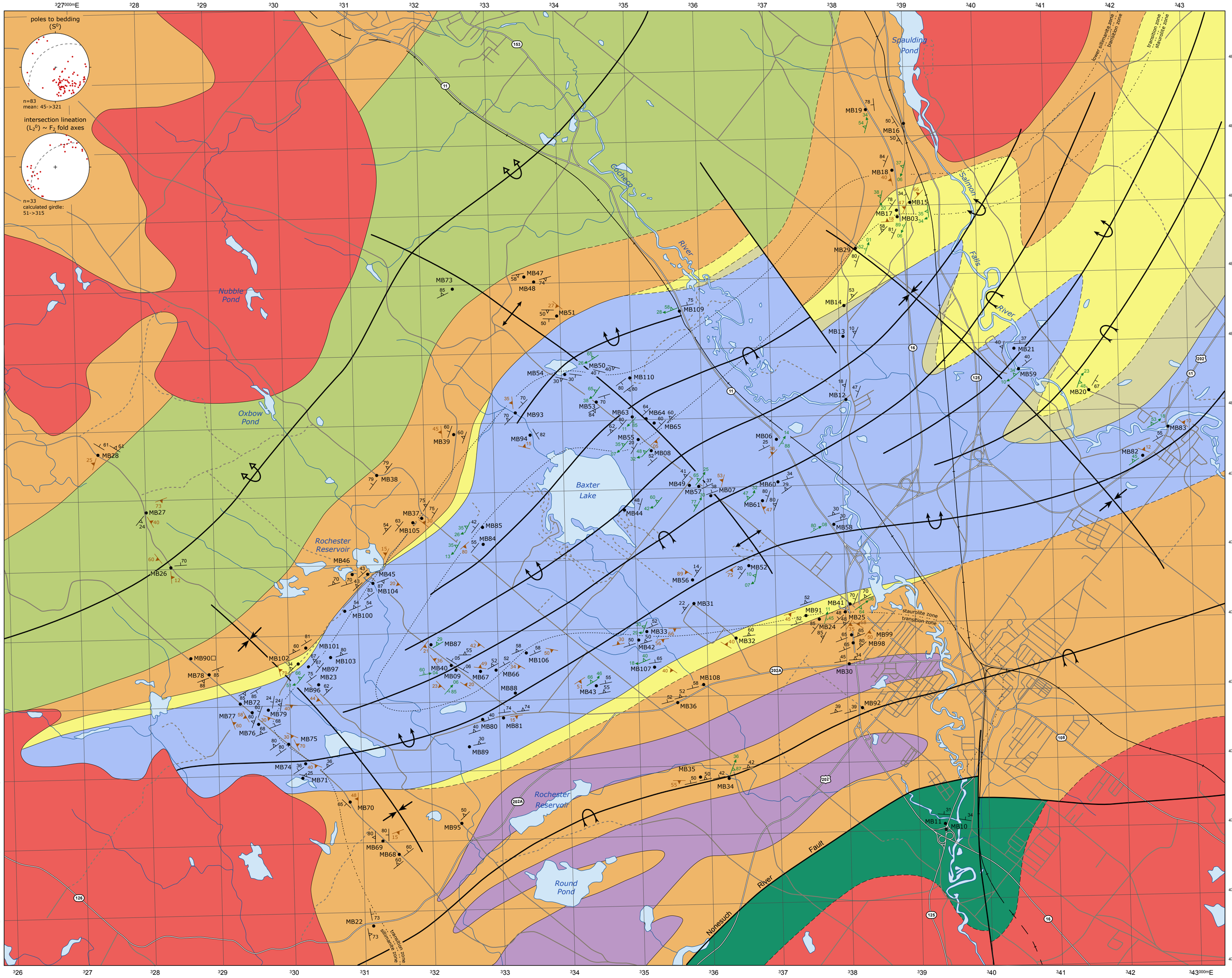

Appendix D: Structure and Stratigraphy of the Lebanon Antiformal Syncline, New Hampshire, USA

Scale 1:36000

1 .5 0 kilometres 1 2

1 .5 0 miles 1 2

		unit name	brief lithological description
377±? Ma[2] 363±? Ma[2]		2 mica granite	weakly foliated to non-foliated grey 2 mica granite
393±5 Ma[3,4]		quartz diorite	weakly foliated to non-foliated biotite quartz diorite/granodiorite
age of deposition[1] (based on regional correlation): Devonian, lower		Carrabassett Fm.☐	Grey/silver rhythmically bedded meta-turbidite with occasional lenses of rusty weathering schist. The transitions from quartzite to schist in the well preserved graded beds are gradual (slow-graded) and provide excellent control on direction of "younging". The schistose layers are commonly composed almost entirely of coarse andalusite.
Silurian, upper		Madrid Fm.	Light grey, massive laminated, calcareous metasandstone.
Silurian, upper		Smalls Falls Fm.	Rusty weathering, red-brown to black, sulphidic and, in places, graphitic schist. Coarse pyrite and/or pyrrhotite occur in some areas.
Silurian, middle		Perry Mountain Fm.	Grey, well-bedded, meta-turbidite with stringers or pods of pink "coticule" parallel to bedding, near the base of many of the metasandstone layers. The transitions from quartzite to schist are sharp (fast-graded), making determination of younging direction problematic.
Silurian, lower		Rangeley Fm.	Migmatitic gneiss with swirly foliation, composed of leucocratic quartzofeldspathic and dark biotite-rich layers. Rusty weathering in part, with minor to abundant calcareous lenses.
Pre-Cambrian (?)		Gonic/Berwick Fm.	Dark purple biotite-quartz-feldspar granofels or schist with interbedded calc-silicate granofels and minor metapelites.

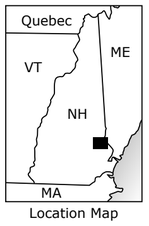

Location Map

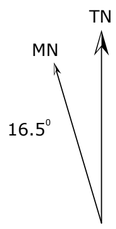

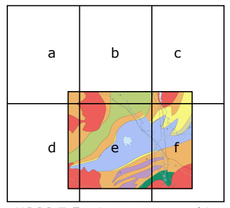

a Alton
b Farmington
c Milton
d Parker Mountain
e Baxter Lake
f Rochester

USGS 7.5 minute topographic maps covering mapped area

Grid: 1000-metre Universal Transverse Mercator, Zone 19
UTM grid declination 1.5° West at map centre
1987 magnetic North declination 16.5° West at map centre
1927 North American Datum

Geology modified from base map of Eusden *et al.*, 1984[5].
Hydrology and culture from USGS 7.5 minute topographic maps.

Submitted by M.D. Bruce as part of a Ph. D. thesis in the School of Earth and Environmental Sciences, James Cook University, Australia.

Last modified 22nd Jul., 2007

geologic symbols

- MB34 ● sample location and number
- metamorphic isograd known/ inferred
- 48 dip and strike of bedding/compositional layering (S_0)
- 39 dip and strike of dominant foliatiion (S_m)
- 50 dip and strike of matrix crenulation (S_{m+1}, S_{m+2}, etc.)
- 66 S_1 dip and strike of mesoscale F_2 fold axial plane (including axial plunge)
- fold nappe axial trace
- antiformal syncline axial trace
- synformal anticline axial trace
- antiform axial trace
- synform axial trace

roads and rivers

- U.S. route
- state route
- road
- track/trail
- railway line
- disused railway line
- stream
- lake/river

1. Eusden, J.D.,Jr., Bothner, W.A. and Hussey, A.M., 1987. The Kearsarge-Central Maine Synclinorium of southeastern New Hampshire and southwestern Maine: stratigraphic and structural relations of an inverted section, American Journal of Science, v. 287, p. 242-264.

2. Eusden, J.D.,Jr.and Barreiro, B., 1988. The timing of peak high-grade metamorphism in central-eastern New England. Maritime Sediments and Atlantic Geology, v. 24, p. 241-255.

3. Lyons, J.B. and Livingston, D.E., 1977, Rb-Sr age of the New Hampshire Plutonic Series, Geological Society of America Bulletin, v.88, p. 1808-1812.

4. Steiger, R.H. and Jager, E, 1977, Subcommision on Geochronology; convention on decay constants in geo- and cosmochronology, Earth and Planetary Science Letters, v. 36, p. 359-363.

5. Eusden, J.D., Jr., Bothner, W.A. and Hussey, A.M., Laird, J., 1984. Silurian and Devonian rocks in the Alton and Berwick quadrangles, New Hampshire and Maine, In Hanson, L.S. (ed.) Geology of the coastal lowlands, Boston, MA to Kennebunk, ME: New England Intercollegiate Geologic Conference, 1984, Trip C5, 325-351.